UNIVERSITY OF CALIFORNIA

Los Angeles

Development of Hematopoietic Stem Cell-Engineered Invariant Natural Killer T Cells for Cancer Immunotherapy

A dissertation submitted in partial satisfaction of the

requirements for the degree Doctor of Philosophy

in Molecular Biology

by

Yanruide Li

2021

ABSRACT OF THE DISSERTATION

Development of Hematopoietic Stem Cell-Engineered
Invariant Natural Killer T Cells for Cancer Immunotherapy

by

Yanruide Li
Doctor of Philosophy in Molecular Biology
University of California, Los Angeles, 2021
Professor Lili Yang, Chair

Cell-based immunotherapy has become the new-generation cancer medicine. Invariant natural killer T (iNKT) cells are potent immune cells for targeting cancer; however, healthy donor blood contains extremely low numbers of endogenous iNKT cells, making it exceedingly challenging to generate adequate iNKT cells for cell therapy. In this study, we aim to develop both autologous and allogeneic hematopoietic stem cell-engineered iNKT (HSC-iNKT) cell therapy that has potential to provide patients with therapeutic levels of iNKT cells for the treatment of cancers. Through combining hematopoietic stem cell (HSC) gene engineering and HSC differentiation, we achieved the generation of human HSC-iNKT cells at high yield and purity. The first generation of HSC-iNKT cells were generated using a bone marrow-liver-thymus (BLT) humanized mouse model, the second generation of HSC-iNKT cells were generated using an Artificial Thymic Organoid (ATO) culture system, and the third generation of HSC-iNKT cells were developed using an *Ex Vivo* Feeder-Free culture system. These HSC-

iNKT cells closely resembled endogenous iNKT cells, effectively targeted tumor cells using multiple mechanisms *in vitro* and *in vivo*, and most attractively, exhibited high safety and low immunogenicity. These cells could be further engineered with chimeric antigen receptor (CAR) to enhance tumor targeting, or/and gene-edited to ablate surface HLA molecules and further reduce immunogenicity. Collectively, these preclinical studies demonstrated the feasibility, safety, and cancer therapy potential of HSC-iNKT cell products and laid a foundation for their future translational and clinical development.

The dissertation of Yanruide Li is approved.

Andrew Goldstein

Arnold I. Chin

Dinesh Subba Rao

Sanaz Memarzadeh

Lili Yang, Committee Chair

University of California, Los Angeles

2021

Dedication

This dissertation is wholeheartedly dedicated to our beloved parents, who have been my source of inspiration and gave me strength whenever I encountered difficulties; to our mentor, friends, and labmates who shared their words of advice and encouragement during my Ph.D. life; and to my committee, for their guidance throughout my graduate work.

Table of Contents

List of Figures

Acknowledgement

I would like to thank my advisor, Dr. Lili Yang, for her unwavering support and encouragement of me and this project, it wouldn't have been possible without her, A big thank you to the lab members of Lili's lab, as well as my thesis committee, who assisted me with advice and research during my Ph.D. life at UCLA. Lastly, I would like to acknowledge my parents, without whose hard work and sacrifice I wound not have been able to pursue and succeed in my education.

Chapter 1 includes, with permission, material from a published review: Li YR, Zhou Y, Kramer A, Yang L. Engineering stem cells for cancer immunotherapy. Trends Cancer. 2021 Aug 31:S2405-8033(21)00171-0. doi: 10.1016/j.trecan.2021.08.004. Epub ahead of print. PMID: 34479851.

Chapter 2 is adapted from a published manuscript: Zhu Y, Smith DJ, Zhou Y, Li YR, Yu J, Lee D, Wang YC, Di Biase S, Wang X, Hardoy C, Ku J, Tsao T, Lin LJ, Pham AT, Moon H, McLaughlin J, Cheng D, Hollis RP, Campo-Fernandez B, Urbinati F, Wei L, Pang L, Rezek V, Berent-Maoz B, Macabali MH, Gjertson D, Wang X, Galic Z, Kitchen SG, An DS, Hu-Lieskovan S, Kaplan-Lefko PJ, De Oliveira SN, Seet CS, Larson SM, Forman SJ, Heath JR, Zack JA, Crooks GM, Radu CG, Ribas A, Kohn DB, Witte ON, Yang L. Development of Hematopoietic Stem Cell-Engineered Invariant Natural Killer T Cell Therapy for Cancer. Cell Stem Cell. 2019 Oct 3;25(4):542-557.e9. doi: 10.1016/j.stem.2019.08.004. Epub 2019 Sep 5. PMID: 31495780; PMCID: PMC7018522. We gratefully thank D. Baltimore (California Institute of Technology) and J. Economou (UCLA) for advising this study. We thank the University of California, Los Angeles (UCLA) animal facility for providing animal support; the UCLA Translational Pathology Core Laboratory (TPCL) for providing histology support; the UCLA AIDS Institute/CFAR Virology Core/Gene and Cell Therapy Core/Humanized Mouse Core for providing human cells and tissues and humanized mice services; the UCLA

BSCRC Flow Cytometry Core Facility for cell sorting support; the US National Institutes of Health Tetramer Core Facility for providing the hCD1d/PBS-57 tetramer reagents; N. Rozengurt (UCLA) for providing pathology analysis support; P. Wang (University of Southern California, USC) for critical reading of this manuscript; and E.L. Siegler for editing the manuscript. This work was supported by a Director's New Innovator Award from the National Institutes of Health (NIH DP2 CA196335, to L.Y.), a Partnering Opportunity for Translational Research Projects Award from the California Institute for Regenerative Medicine (CIRM TRAN1–08533, to L.Y.), a Stem Cell Research Award from the Concern Foundation (to L.Y.), a Research Career Development Award from the STOP CANCER Foundation (to L.Y.), and a BSCRC-RHF Research Award from the Rose Hills Research Foundation (to L.Y.). D.J.S. is a predoctoral fellow supported by the UCLA Tumor Immunology Training Grant (USHHS Ruth L. Kirschstein Institutional National Research Service Award # T32 CA009056). J.Y. is a predoctoral fellow supported by the UCLA Broad Stem Cell Center (BSCRC) Predoctoral Fellowship.

Chapter 3 is adapted from a published manuscript: Li YR, Zhou Y, Kim YJ, Zhu Y, Ma F, Yu J, Wang YC, Chen X, Li Z, Zeng S, Wang X, Lee D, Ku J, Tsao T, Hardoy C, Huang J, Cheng D, Montel-Hagen A, Seet C, Crooks GM, Larson SM, Sasine JP, Pellegrini M, Ribas A, Kohn DB, Witte O, Wang P, and Yang L. Development of Allogeneic HSC-Engineered iNKT Cells for Off-The-Shelf Cancer Immunotherapy. Cell Reports Medicine. In Press. We thank the University of California, Los Angeles (UCLA) animal facility for providing animal support; the UCLA Translational Pathology Core Laboratory (TPCL) for providing histology support; the UCLA Technology Center for Genomics & Bioinformatics (TCGB) facility for providing RNAseq services; the UCLA CFAR Virology Core for providing human cells; and the UCLA BSCRC Flow Cytometry Core Facility for cell sorting support. This work was supported by a Director's New Innovator Award from the NIH (DP2 CA196335, to L.Y.), a

Partnering Opportunity for Translational Research Projects Award and a Partnering Opportunity for Discovery Stage Award from the California Institute for Regenerative Medicine (CIRM TRAN1-08533 and DISC2-11157, to L.Y.), a Stem Cell Research Award from the Concern Foundation (to L.Y.), a Research Career Development Award from the STOP CANCER Foundation (to L.Y.), a BSCRC-RHF Research Award from the Rose Hills Research Foundation (to L.Y.), and an Ablon Scholars Award (to L.Y.). Y-R.L. is a predoctoral fellow supported by the UCLA Whitcome Predoctoral Fellowship in Molecular Biology. J.Y. is a predoctoral fellow supported by the UCLA Broad Stem Cell Research Center (BSCRC) Predoctoral Fellowship. D.L. is a predoctoral fellow supported by T32 Microbial Pathogenesis Training Grant (Ruth L. Kirschstein National Research Service Award, T32-AI007323). Z.L. is a postdoctoral fellow supported by the UCLA Tumor Immunology Training Grant (USHHS Ruth L. Kirschstein Institutional National Research Service Award, T32-CA009120). S.Z is a predoctoral fellow supported by the UCLA Medical Scientist Training Program Grant (T32-GM008042).

Chapter 4 is adapted from a manuscript that is in preparation: Li YR, Li Z, Zhou Y, Kim YJ, Yu J, Lee D, Kramer A, Hon R, Crooks GM, Ribas A, Kohn DB, Witte O, Wang P, and Yang L. Combating Ovarian Cancer Using Stem Cell-Engineered Off-The-Shelf CAR-iNKT Cells. We thank the University of California, Los Angeles (UCLA) animal facility for providing animal support; the UCLA Translational Pathology Core Laboratory (TPCL) for providing histology support; the UCLA Technology Center for Genomics & Bioinformatics (TCGB) facility for providing RNAseq services; the UCLA CFAR Virology Core for providing human cells; and the UCLA BSCRC Flow Cytometry Core Facility for cell sorting support. This work was supported by a Director's New Innovator Award from the NIH (DP2 CA196335, to L.Y.), a Partnering Opportunity for Translational Research Projects Award and two Partnering Opportunity for Discovery Stage Awards from the California Institute for

Regenerative Medicine (CIRM TRAN1-08533, DISC2-11157, and DISCCOVID19-12020 to L.Y.), a Stem Cell Research Award from the Concern Foundation (to L.Y.), a Research Career Development Award from the STOP CANCER Foundation (to L.Y.), a BSCRC-RHF Research Award from the Rose Hills Research Foundation (to L.Y.), and an Ablon Scholars Award (to L.Y.). Y-R.L. is a predoctoral fellow supported by the UCLA Whitcome Predoctoral Fellowship in Molecular Biology. Z.L. is a postdoctoral fellow supported by the UCLA Tumor Immunology Training Grant (USHHS Ruth L. Kirschstein Institutional National Research Service Award, T32-CA009120). J.Y. is a predoctoral fellow supported by the UCLA Broad Stem Cell Research Center (BSCRC) Predoctoral Fellowship. D.L. is a predoctoral fellow supported by T32 Microbial Pathogenesis Training Grant (Ruth L. Kirschstein National Research Service Award, T32-AI007323).

BIOGRAPHICAL SKETCH

NAME: **Yanruide (Charlie) Li**

POSITION TITLE: **Graduate Student Research Assistant**

EDUCATION/TRAINING

INSTITUTION AND LOCATION	DEGREE	Start Date	Completion Date	FIELD OF STUDY
Zhejiang University, China	B.S.	09/2013	06/2017	Biological Science
University of California Los Angeles	Ph.D.	09/2017	In Progress	Immunity, Microbes, and Molecular Pathogenesis

A. Personal Statement

My general scientific interests are in understanding the molecular mechanisms controlling antitumor immunity and developing them into the next generation of therapeutics. I received an undergraduate education at Zhejiang University where I was highly motivated to pursue an academic, translational research path. The research experience of assisting in the fighting against cancer led me to UCLA under the home area of Immunity, Microbes, and Molecular Pathogenesis. Currently, I am working in Dr. Lili Yang 's Lab focusing on the genetic engineering of invariant natural killer T (iNKT) cells for the treatment of cancer including solid tumors and hematologic malignancies. A multitude of strategies are used, including providing the immune cells with tumor-recognition specificity, as well as enhancing their tumor-fighting capacity. Now I am leading several promising projects aiming to generate allogeneic hematopoietic stem cell-derived CAR-engineered iNKT cells for cancer immunotherapy.

B. Positions and Honors

Positions and Employment

2017-Current Graduate student researcher, University of California, Los Angeles
2018-2019 Teaching Assistant, University of California, Los Angeles,
2016-2017 Research Assistant, Harvard Medical School, Sichen Shao Lab
2013-2016 Research Assistant, Zhejiang University, Wanxi Yang Lab

Honors

2021 Sydney C. Rittenberg Award, Department of MIMG, UCLA
2021 Summer Mentored Research Fellowship, UCLA
2021 2nd Place within the **Cancer Category** in Pearl Cohen Poster Award, UCLA
2020 Whitcome Pre-Doctoral Training Fellowship in Molecular Biology, UCLA
2019 Whitcome Pre-Doctoral Training Fellowship in Molecular Biology, UCLA

C. Contributions to Science

1. The functions of myosin Va during tumorigenesis: The majority of my undergraduate career focused on the myosin superfamily and testicular cancer. We demonstrated the irreplaceable roles of the myosin superfamily during tumorigenesis, and I found that myosin Va was an important factor in the functioning of organelle motility, spindle formation, and cell motility. I detected myosin Va in testicular tumor tissues using sqRT-PCR, western blot, and immunofluorescence. Tumor samples showed an increased expression of myosin Va, abnormal actin and myosin Va distribution. In addition, multi-nucleation and aberrant nuclear morphology were observed in myosin Va-knockdown cells. Wounding assay and CCK-8-based cell counting were conducted to verify myosin Va roles in enhancing cell migration, viability and proliferation. In light of these, we published two reviews and one research article to demonstrate that myosin Va is a potential therapeutic target of testicular cancer.

a. **Yan-Ruide Li**, Wan-Xi Yang. Myosin superfamily: The multi-functional and irreplaceable factors in spermatogenesis and testicular tumors. *Gene*. 2016, 576:195-207.

b. **Yan-Ruide Li**, Wan-Xi Yang. Myosins as the fundamental components during tumorigenesis: diverse and indispensable. *Oncotarget*. 2016, 7:46785-46812.
c. **Yan-Ruide Li**, Zhong Ai, Dong Han, Lu-Han Ni, Fu-Qing Tan, Wan-Xi Yang. Myosin Va plays essential roles in maintaining normal mitosis, enhancing tumor cell motility and viability. *Oncotarget*. 2017, 8:54654-54671.

2. **Hematopoietic stem cell-engineered invariant natural killer T cells for cancer immunotherapy**: After joining Dr. Lili Yang's Lab, I started working on iNKT cells-based immunotherapy. We used a bone marrow-liver-thymus (BLT) humanized mouse model and generated HSC-engineered human iNKT cells *in vivo*. In this project, I detected the phenotype and functionality of BLT-iNKT cells, explored multiple iNKT cell tumor-attacking mechanisms, and established two tumor killing models for both blood cancer and solid tumor in humanized mice.
d. Yanni Zhu, Drake J. Smith, Yang Zhou, **Yan-Ruide Li**, Jiaji Yu et al. Hematopoietic stem cell-engineered invariant natural killer T cells for cancer immunotherapy. *Cell Stem Cell.* 2019, 3;25(4):542-557.
e. **Yan-Ruide Li**, Yang Zhou, Samual Zeng, Lili Yang. Methods for studying mouse and human invariant natural killer T cells. *Methods in Molecular Biology.* 2021;2388:35-57.
f. **Yan-Ruide Li**, Yang Zhou, Adam Kramer, Lili Yang., Engineering Stem Cells for Cancer Immunotherapy. *Trends in Cancer.* 2021 Aug 31;S2405-8033(21)00171-0.
g. **Yan-Ruide Li**, Zach Dunn, Derek Lee, Lili Yang, Stem Cells and "Off-the-Shelf" cancer therapy. *Cells*. In Press.

3. Universal Hematopoietic Stem Cell-engineered CAR iNKT for Off-the-shelf Cancer Immunotherapy. Now I am leading a project generating allogeneic off-the-shelf iNKT in *in vitro* culture systems. To work towards translating this iNKT-based therapy into clinics and boosting immunotherapy responses, we engineer the iNKT cells to express CARs by transducing with a retrovector encoding CAR gene, and knocking out the beta 2-microglobulin (B2M) and CIITA genes to avoid host-versus-graft (HvG) depletion by a CRISPR-Cas9 gene-editing system.
h. **Yan-Ruide Li**, Yang Zhou, Yu Jeong Kim et al. Generation of allogeneic hematopoietic stem cell-engineered invariant natural killer T cells for off-the-shelf immunotherapy. *Cell Reports Medicine*. In Press.
i. **Yan-Ruide Li,** Samuel Zeng, Lili Yang. Hematopoietic stem cell-engineered invariant natural killer T cells for allogeneic Graft-Versus-Host disease prevention. In Preparation.
j. **Yan-Ruide Li,** Derek Lee, Jocelyn Lin, Lili Yang. Generation of Allogeneic Hematopoietic Stem Cell-Engineered Invariant Natural Killer T cells for COVID-19 Therapeutic Intervention. *Stem Cell Research & Therapy*. In Press.
k. **Yan-Ruide Li,** Zhe Li, Adam Kramer, Noah Cook, Lili Yang. Development of HSC-derived mesothelin CAR-engineered iNKT cells for treating ovarian cancers. In Preparation.
l. Yu Jeong Kim, Jiaji Yu, **Yan-Ruide Li**, Zhe Li et al. A Next-Generation, Off-The-Shelf Hematopoietic Stem Cell-based CAR-iNKT Cell Therapy for Cancer. In Preparation.
m. Jiaji Yu, Yu Jeong Kim, **Yan-Ruide Li**, Yu-Chen Wang et al. Off-the-shelf Hematopoietic Stem Cell-based NY-ESO-1-specific T cells for Immunotherapy. In Preparation.

4. Deciphering molecular control of antitumor immunity: Another training in Dr. Lili Yang lab involves fundamental and translational study of tumor immunology. In particular, the identification of new immune checkpoints and the development of new immunotherapies are a major focus of my research. In a recent study, we have identified creatine as an important metabolic regulator controlling antitumor T cell immunity, underscoring the potential of creatine supplementation to improve T cell-based cancer immunotherapies.
n. Yu-Chen Wang, Xi Wang, Jiaji Yu, Feiyang Ma, Yang Zhou, Samuel Zeng, Xiaoya Ma, **Yan-Ruide Li**, and Lili Yang. Targeting monoamine oxidase A-regulated TAM polarization for cancer immunotherapy. *Nature Communications* (in press); 2021.
o. Xi Wang, Bo Li, Yu Jeong Kim, Yu-Chen Wang, Zhe Li, Jiaji Yu,Samuel Zeng, XiaoYa Ma, **Yan-Ruide Li**, and Lili Yang. Targeting monoamine oxidase A for T cell-based cancer immunotherapy. *Science Immunology* (in press); 2021.

Chapter 1 - Introduction

Cell-Based Cancer Immunotherapy

Over the past decade, cell-based immunotherapy has shown great promise as the new-generation cancer medicine [1]. Genetic engineering of T, natural killer (NK), invariant natural killer T (iNKT), and other immune cells have yielded encouraging results for cancer immunotherapy [2,3]. A series of clinical trials using engineered immune cells with chimeric antigen receptors (CARs) or T cell receptors (TCRs) have been conducted to treat various forms of cancer, ranging from solid tumors to hematologic malignancies [4–9]. Despite the remarkable successes in the clinic, most of the current FDA-approved CAR T cell products are manufactured using autologous T cells obtained from the intended recipient patient. Such as approach is costly, labor intensive, and difficult to broadly deliver to all patients in need. Allogeneic immune cellular products that can circumvent the manufacturing issues of inadequate cell numbers, suboptimal T cell states and delays in treatment therefore are in great demand [10].

Two major categories of such allogeneic cell products are based on engineering healthy donor-derived conventional αβ T cells or NK cells [11–14]. The treatment of patients with B cell malignancies following allogeneic hematopoietic stem cell transplantation (HSCT) using donor-derived CD19 CAR-engineered leukocytes achieved complete or partial remissions [15–17]; however, graft-versus-host disease (GvHD) has developed in a subset of patients in a few of these studies [15,16]. Therefore, these allogeneic T cells need to be gene-edited to ablate endogenous TCR expression, usually through disrupting the *TRAC* or/and *TRBC* gene loci, to make them suitable for allogeneic cell therapy [18–21]. Notably, none of these techniques enables 100% TCR knockout in CAR-T cells, thus requiring further purification of the T cell products prior to use in patients [22]. On the other hand, NK-based allogeneic cell products are considered of low GvHD risk and thereby do not require additional gene-editing, but *in vivo* clonal

expansion, antitumor performance, and long-term cryopreservation of NK-based cellular products may be limited compared to that of conventional αβ T cells [12]. Two such allogeneic cell products, a conventional αβ T cell-based universal CD19-CAR engineered T cells (UCART19) and an NK cell-based CB-derived CD19-CAR engineered NK cells, were recently performed in phase I clinical trials treating $CD19^+$ B cell malignancies [19,23]. These studies reported the feasibility, antileukemic activity, and manageable safety of the two allogeneic cell products, revealing an encouraging step forward for the field of allogeneic cell therapy [19,23].

Engineering stem cells provides another attractive approach for cell-based cancer immunotherapy. On the one hand, for hematopoietic stem cell transplantation (HSCT), genetic engineered stem cells provide a persistent and stable source for long-term generation of immune cells with specific tumor targeting. In addition, CAR-engineered stem cells may generate CAR-NK or CAR-myeloid cells in addition to CAR-T cells, resulting in broader anti-tumor activity that arises quickly post-transplantation and does not solely require *de novo* thymopoiesis [24,25]. On the other hand, engineering stem cell could provide an "off-the-shelf" cellular product, obviating the need for a personalized and patient-specific product. Performing gene engineering or gene editing on stem cells requiring a small starting number could save on the use of gene-engineering/editing materials (e.g., lentivector and CRISPR-Cas9/gRNA) that can be cost-limiting, and also enable the maximal gene engineering/editing efficiency that can be carried on into the final cell products. Furthermore, the development of stem cell-engineered cellular therapy will provide opportunities for upscaling the manufacturing and banking of the products (**Figure 1-1**).

Invariant Natural Killer T (iNKT) Cells

Invariant natural killer T (iNKT) cells are a small population of αβ T lymphocytes [26,27]. These cells have several unique features, making them ideal for developing off-the-shelf cellular therapy for cancer:

1) iNKT cells have the remarkable capacity to target multiple types of cancer independent of tumor antigen- and MHC-restrictions [28]. iNKT cells recognize glycolipid antigens presented by non-polymorphic CD1d, which frees them from MHC-restriction. Although the natural ligands of iNKT cells remain to be identified, it is suggested that iNKT cells can recognize certain conserved glycolipid antigens derived from many tumor tissues. iNKT cells can be stimulated through recognizing these glycolipid antigens that are either directly presented by $CD1d^+$ tumor cells, or indirectly cross-presented by tumor infiltrating antigen-presenting cells (APCs) like macrophages or dendritic cells (DCs) in case of $CD1d^-$ tumors. Thus, iNKT cells can respond to both $CD1d^+$ and $CD1d^-$ tumors.

2) iNKT cells can employ multiple mechanisms to attack tumor cells [28,29]. iNKT cells can directly kill $CD1d^+$ tumor cells through cytotoxicity, but their most potent anti-tumor activities come from their immune adjuvant effects. iNKT cells remain quiescent prior to stimulation, but after stimulation, they immediately produce large amounts of cytokines, including IFN-γ. IFN-γ activates NK cells to kill MHC-negative tumor target cells. Meanwhile, iNKT cells also activate DCs that then stimulate CTLs to kill MHC-positive tumor target cells. Therefore, iNKT cell-induced anti-tumor immunity can effectively target multiple types of cancer independent of tumor antigen-and MHC-restrictions, thereby effectively blocking tumor immune escape and minimizing the chance of tumor recurrence.

3) iNKT cells do not cause graft-versus-host disease (GvHD). Because iNKT cells do not recognize mismatched MHC molecules and protein autoantigens, these cells are not expected to cause GvHD. This notion is strongly supported by clinical data analyzing donor-derived iNKT cells in blood cancer patients receiving allogeneic bone marrow or peripheral

blood stem cell transplantation. These clinical data showed that the levels of engrafted allogenic iNKT cells in patients correlated positively with graft-versus-leukemia effects and negatively with GvHD [30,31].

4) iNKT cells can be engineered to avoid host-versus-graft (HvG) depletion. The availability of powerful gene-editing tools like the CRISPR-Cas9 system make it possible to genetically modify iNKT cells to make them resistant to host immune cell-targeted depletion: knockout of beta 2-microglobulin (B2M) gene will ablate HLA-I molecule expression on iNKT cells to avoid host $CD8^+$ T cell-mediated killing [14]; knockout of CIITA gene will ablate HLA-II molecule expression on iNKT cells to avoid $CD4^+$ T cell-mediated killing [32]. Both B2M and CIITA genes are approved good targets for the CRISPR-Cas9 system in human primary cells [14,33]. Ablation of HLA-I expression on iNKT cells may make them targets of host NK cells. However, iNKT cells seem naturally resistant to allogenic NK cell killing. Nonetheless, if necessary, the concern can be addressed by delivering into iNKT cells an NK-inhibitory gene like HLA-E.

5) iNKT cells have strong relevance to cancer. There is compelling evidence to suggest a significant role of iNKT cells in tumor surveillance in mice, in which iNKT cell defects predispose them to cancer and the adoptive transfer or stimulation of iNKT cells can provide protection against cancer [29,34]. In humans, iNKT cell frequency is decreased in patients with solid tumors (including melanoma, colon, lung, breast, and head and neck cancers) and blood cancers (including leukemia, multiple myeloma, and myelodysplastic syndromes), while increased iNKT cell numbers are associated with a better prognosis. There are also instances wherein the administration of α-GalCer-loaded DCs and *ex vivo* expanded autologous iNKT cells has led to promising clinical benefits in patients with lung cancer and head and neck cancer, although the increases of iNKT cells have been transient and the clinical benefits have been short-term, likely due to the limited number of iNKT cells used for transfer and the

depletion of these cells thereafter [28,35]. Therefore, it is plausible to propose that an "off-the-shelf" iNKT cellular product enabling the transfer into patients' sufficient numbers of iNKT cells at multiple doses may provide patients with the best chance to exploit the full potential of iNKT cells to battle their diseases.

Engineering Stem Cells for iNKT Cell-Based Cancer Immunotherapy

In addition to conventional T and NK cells, new cell carriers have been explored for cancer immunotherapy, particularly unconventional T cells, such as invariant natural killer T (iNKT) cell, gamma delta T (γδ T) cell and mucosal associated invariant T (MAIT) cell. These cells serve as great candidates for off-the-shelf cancer therapy.

iNKT cells are a unique T cell subpopulation specialized with CD1d-restriction that can recognize lipid antigens [26,36]. Activated iNKT cells lead to the activation of both innate and adaptive immune cells impelling the development of iNKT-based immunotherapy. In addition, iNKT cells have limited capacity to induce GvHD. It has been approved that adoptive iNKT transfer is associated with reduced GvHD in multiple clinical trials [26,37–40]. However, the application of iNKT cell-based immunotherapy is restricted by its extremely low number in the peripheral blood. Yang laboratory developed a new approach that to increase the number of circulating iNKT cells through iNKT TCR-engineering of HSCs [41,42]. It has been demonstrated that both mouse and human HSCs engineered with iNKT TCR can successfully differentiate into mouse and human iNKT cells *in vivo*. The HSC-derived iNKT cells resembled the characters of endogenous PBMC-derived iNKT cells, deploying anti-tumor efficacy and no toxicity [41,42]. Alternatively, Kaneko et al and Fujii Group reported the generation of human iNKT cells from iPSCs. The iPSC-derived iNKT cells showed rapid proliferation in response to α-GalCer stimulation and possessed strong anti-tumor activity to the K562 leukemia cell line [28,43–45].

In conclusion, engineering unconventional innate-type T cells (e.g., iNKT cells) that have powerful antitumor capacity while free of GvHD risk represents an attractive direction for developing allogeneic cell therapy for cancer especially for solid tumors [37,46–48]. Yang lab has successfully developed HSC-engineered iNKT cell therapy for cancer, using either *in vivo* BLT mouse model or *in vitro* "off-the-shelf" culture systems [41,42]. These approaches demonstrate the feasibility, safety, and cancer therapy potential of the proposed HSC-iNKT, cell therapy and laid a foundation for future translational and clinical development (**Figure 1-2**).

Figures

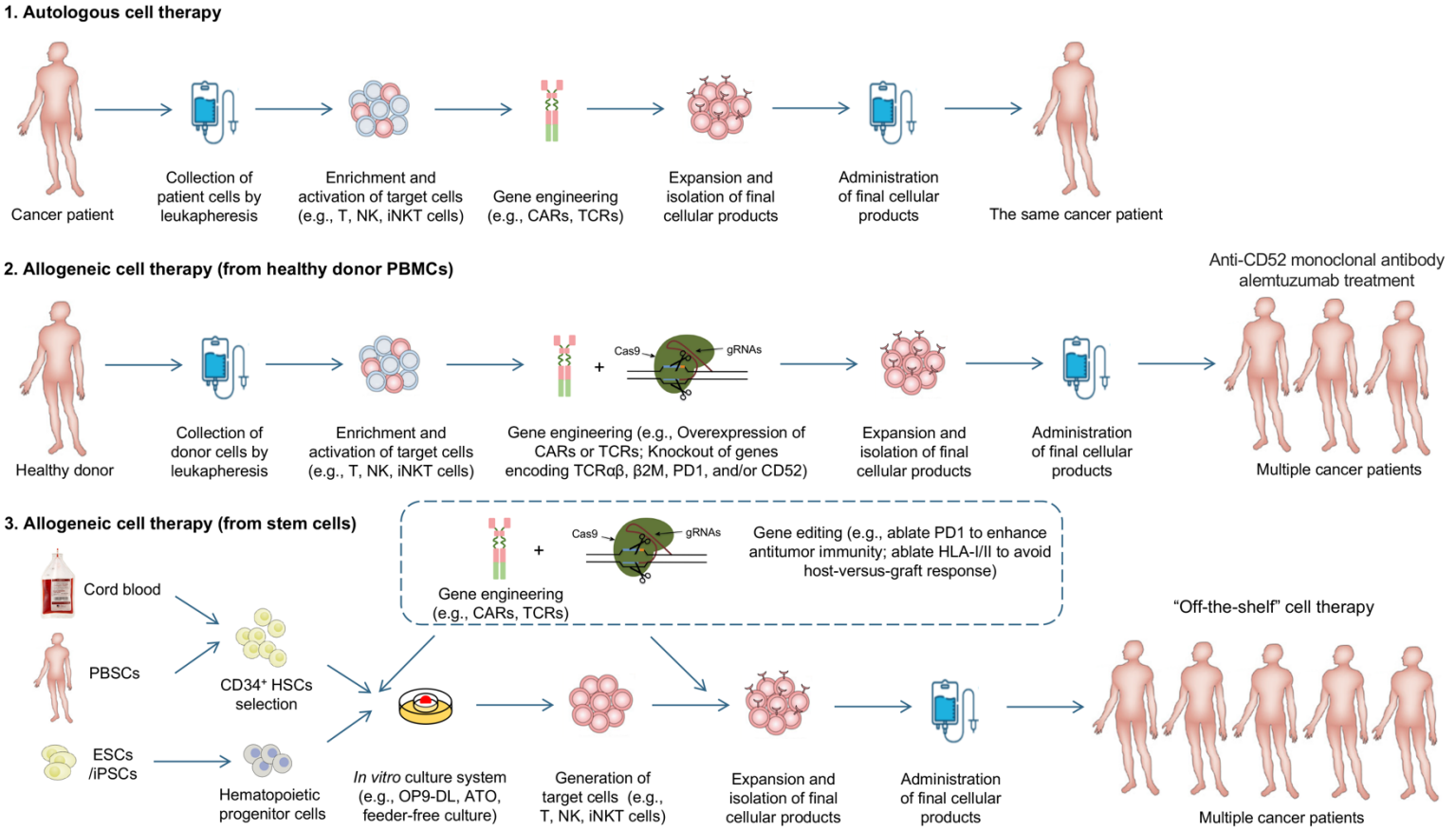

Figure 1-1. Schematics of current autologous and allogeneic cell-based cancer immunotherapies. 1. Schematics of autologous cellular product manufacturing. Target cells (e.g., T, NK, or iNKT cells) are collected from patients by leukapheresis and are then genetically engineered. The engineered cells are expanded *ex vivo* while the patient undergoes bridging and/or lymphodepleting chemotherapy. The engineered cellular products are then infused into the same patient. 2. Schematics of healthy donor PBMC-derived allogeneic cellular product manufacturing. Healthy donors for banking are selected and their PBMCs are used to generate genetically engineered immune cells. Notably, because conventional αβ T cells risk inducing GvHD in allogeneic hosts due to HLA incompatibility, these T cells need to be gene-edited to ablate endogenous TCR expression, usually through disrupting the *TRAC* or/and *TRBC* gene loci, to make them suitable for allogeneic cell therapy. Meanwhile *CD52* gene is also disrupted in order to generate allogeneic cells resistant to the anti-CD52 monoclonal antibody alemtuzumab, which can be used to eliminate host T cells expressing CD52 and avoid allorejection. 3. Schematics of stem cell-derived allogeneic cellular product manufacturing. Human $CD34^+$ HSCs are collected from either cord blood or from granulocyte-colony stimulating factor (G-CSF)-mobilized human periphery blood. These HSCs are genetic engineered and then cultured in "off-the-shelf" *in vitro* culture system (e.g., OP9-DL, ATO, or feeder-free culture) to generate mature effector immune cells. The immune cells could also be derived from ESCs/iPSCs using culture conditions that first promote hematopoietic

differentiation and then target cell differentiation, followed by target cell maturation and activation. Of note, the gene engineering and editing could be performed on stem cells or differentiated immune cells. Performing both gene-engineering and gene-editing on the small numbers of starting stem cells upfront of the *in vitro* culture could save on the use of gene-engineering/editing materials (e.g., lentivector and CRISPR-Cas9/gRNA) that can be cost-limiting, and also enable the maximal gene engineering/editing efficiency that can be carried on into the final cell products.

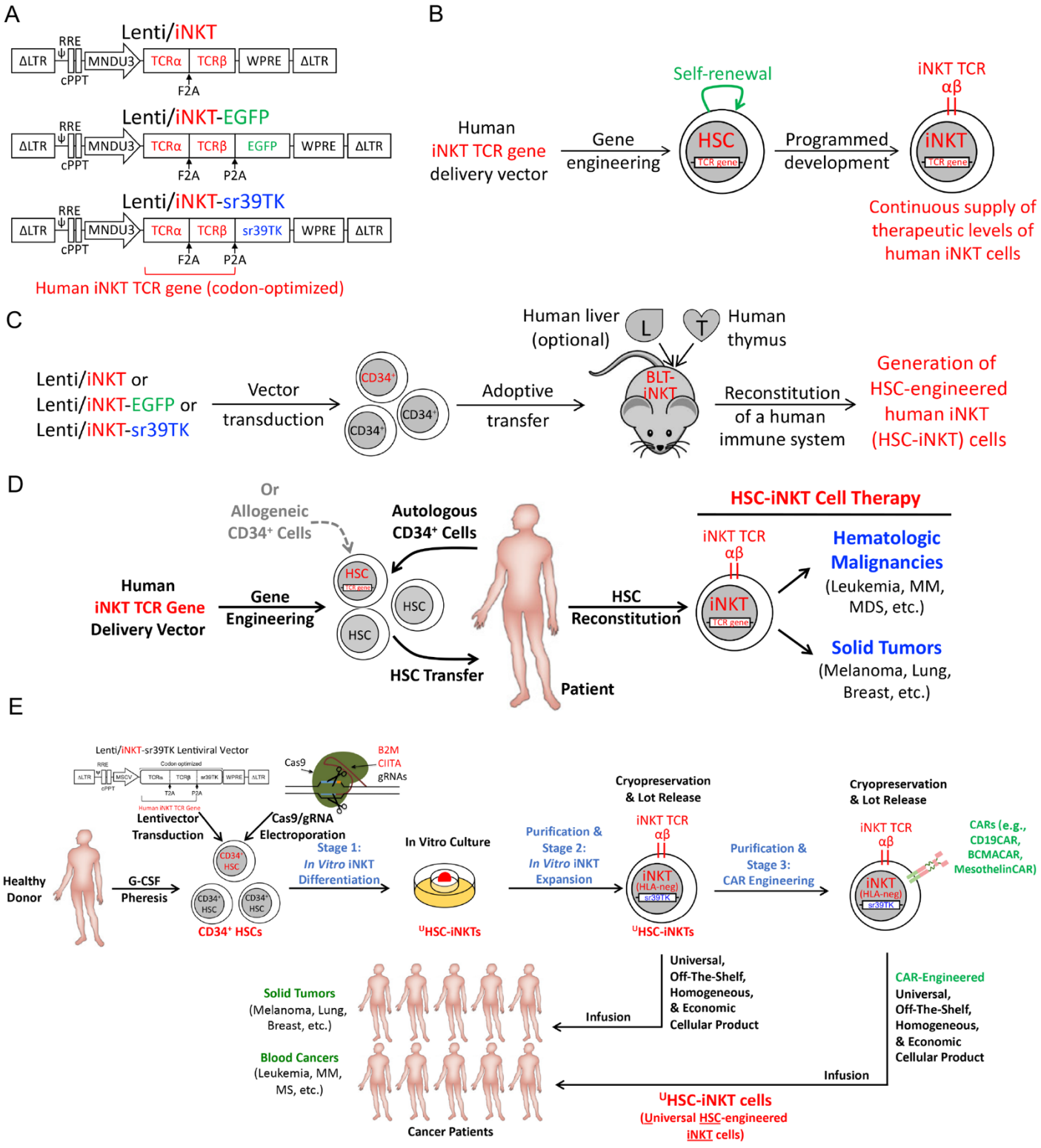

Figure 1-2. HSC-engineered iNKT cell therapy for cancer.

The same strategies could be applied to generate HSC-engineered γδ T, MAIT, and TCR-specific αβ T (e.g., NY-ESO-1-T) cells.

(A) Schematics of the Lenti/iNKT vectors.

(B) Generation of HSC-engineered iNKT cells.
(C) Experimental design to generate HSC-iNKT cells in a BLT humanized mouse model.
(D) Proposed HSC-iNKT cell therapy. Autologous or allogeneic human HSCs could be collected and engineered with Lenti/iNKT vectors, followed by adoptive transfer into cancer patients.
(E) Proposed allogeneic "off-the-shelf" HSC-iNKT cell therapy. G-CSF-mobilized $CD34^+$ HSCs could be collected from healthy donors, engineered with Lenti/iNKT vectors and a CRISPR-Cas9/B2M-CIITA-gRNAs complex, then be differentiated into iNKT cells in an *in vitro* culture (e.g., ATO and feeder-free culture). The iNKT cells will then be purified and further expanded *in vitro*, followed by cryopreservation and lot release. CAR engineering could also be incorporated into HSC-iNKT cells to enhance the antitumor capacity of these cells. Note that knockout of *B2M* and *CIITA* genes could efficiently ablate HLA-I/II expression on HSC-iNKT cells to avoid HvG responses following the autologous transfer of iNKT cells.

Chapter 2 - Development of Autologous Hematopoietic Stem Cell-Engineered Invariant Natural Killer T Cell Therapy for Cancer

Abstract

Invariant natural killer T (iNKT) cells are potent immune cells for targeting cancer; however, their clinical application has been greatly hindered by their extremely low numbers in cancer patients. In this study, we aim to develop a hematopoietic stem cell-engineered iNKT (HSC-iNKT) cell therapy that has the potential to provide patients with therapeutic levels of iNKT cells for a lifetime. Using a bone marrow-liver-thymus (BLT) humanized mouse model, we demonstrated the efficient and long-term generation of HSC-iNKT cells in vivo. These HSC-iNKT cells closely resembled endogenous human iNKT cells, could deploy multiple mechanisms to attack tumor cells, and effectively suppressed tumor growth in vivo in multiple human tumor xenograft mouse models. Preclinical safety studies showed no toxicity or tumorigenicity of the intended HSC-iNKT cell therapy. Collectively, these results demonstrated the feasibility, safety, and cancer therapy potential of the proposed HSC-iNKT cell therapy and laid a foundation for future clinical development.

Introduction

Invariant natural killer T (iNKT) cells are a small population of αβ T lymphocytes highly conserved from mice to humans [36,49]. These cells have several unique features, making them exceedingly attractive agents for developing cancer immunotherapy [50–52]. First, iNKT cells have a strong relevance to cancer. There is compelling evidence suggesting a significant role of iNKT cells in tumor surveillance in mice [34,53]. In humans, iNKT cell frequencies are decreased in patients with solid tumors (including melanoma, colon, lung, breast, and head and neck cancers) and hematologic malignancies (including leukemia, multiple myeloma, and myelodysplastic syndromes), while increased iNKT cell numbers are associated with a better

prognosis [34,52,54]. Second, iNKT cells have the remarkable capacity to target multiple types of cancer independent of tumor antigen and major histocompatibility complex (MHC) restrictions [28]. iNKT cells recognize glycolipid antigens presented by non-polymorphic CD1d, which frees them from MHC restriction [36]. Many tumor tissues express conserved glycolipid antigens that can be recognized by iNKT cells, although the nature of these glycolipids remain to be identified [26,49]. Third, iNKT cells can deploy multiple mechanisms to attack tumor cells, including direct killing of $CD1d^+$ tumors and immune adjuvant effects such as activating NK cells, activating DCs and thereby stimulating cytotoxic T lymphocytes (CTLs), and inhibiting tumor-associated macrophages (TAMs) [28,29,51].

Attracted by the potent and broad anticancer functions of iNKT cells, researchers have conducted a series of clinical trials utilizing iNKT cells to treat various forms of cancer, ranging from solid tumors to hematologic malignancies [55,56]. These clinical trials have utilized α-galactosylceramide (αGC, a synthetic glycolipid ligand specifically stimulating iNKT cells) alone, or αGC-pulsed DCs alone or in combination with ex vivo-expanded patient iNKT cells and have shown these treatments to be safe and well tolerated. Several recent trials reported encouraging antitumor immunity in patients with melanoma, non-small cell lung cancer, and head and neck squamous cell carcinomas, attesting to the therapeutic potential of iNKT cell-based immunotherapies [35,38,43,57,58]. However, most other trials yielded unsatisfactory results. Overall, these trials have all worked through the direct stimulation or ex vivo-expansion of patients' endogenous iNKT cells, thus yielding only short-term, limited clinical benefits to a small number of patients. The extremely low frequencies of iNKT cells in cancer patients (~0.001-0.1% in blood), as well as the rapid depletion of these cells post-stimulation, are considered the major factors limiting the success of these trials [51]. In order to unleash the full potential of iNKT cells for cancer immunotherapy, innovative therapies that can overcome these limitations are in high demand.

In this study, we aim to overcome the current limitations by genetic engineering of human hematopoietic stem cells (HSCs) to produce iNKT cells targeting cancer. Because of the longevity and self-renewal of HSCs, by adoptively transferring iNKT T cell receptor (TCR) gene-engineered HSCs into cancer patients, this new therapy has the potential to provide patients with therapeutic levels of iNKT cells for a lifetime [59]. This TCR-engineered HSC transfer approach takes advantage of two molecular mechanisms governing T cell development, TCR allelic exclusion and TCR instruction, to genetically program HSCs to produce T cells of designated antigen specificity and T cell subtype identity [60]. Previously, we and others have successfully utilized this strategy to generate tumor antigen-specific CD4 helper and CD8 cytotoxic T cells of both mouse and human origins [60–62]. Human clinical trials are ongoing, testing NY-ESO-1 TCR-engineered HSC adoptive therapy for treating multiple cancers [63,64]. Recently, we successfully generated iNKT cells in mice through iNKT TCR-engineered bone marrow transfer and proved the cancer therapy potential of the engineered iNKT cells in a mouse melanoma lung metastasis model [42]. Based on these previous works, as well as the scientific rationale that human iNKT cells also follow a "TCR-instructed" developmental path similar to that of the mouse iNKT cells [34], we hypothesized that it would be possible to engineer human HSCs with a human iNKT TCR gene to produce human iNKT cells targeting cancer. Here, we report the preclinical development of the proposed HSC-engineered iNKT cell therapy, demonstrating its feasibility, safety, and cancer therapy potential. Our study also established a humanized BLT-iNKT mouse model that can be utilized as a valuable tool to study human iNKT cell biology and iNKT cell-based immunotherapy.

Materials and Methods

Mice

NOD.Cg-PrkdcSCIDIl2rgtm1Wjl/SzJ (NOD/SCID/IL-2Rγ-/-, NSG) mice were maintained in the animal facilities at the University of California, Los Angeles (UCLA). Six- to ten-week-old females were used for all experiments unless otherwise indicated. All animal experiments were approved by the Institutional Animal Care and Use Committee of UCLA.

Human Tumor Cell Lines

Human multiple myeloma (MM) cell line MM.1S, human chronic myelogenous leukemia cancer cell line K562, and human melanoma cell line A375 were all purchased from the American Type Culture Collection (ATCC). MM.1S and K562 cells were cultured in R10 medium. A375 cells were cultured in D10 medium.

To make stable tumor cell lines overexpressing human CD1d, human HLA-A2.1, human NY-ESO-1, human IL-15, and/or firefly luciferase and enhanced green fluorescence protein (Fluc-EGFP) dual-reporters, the parental tumor cell lines were transduced with lentiviral vectors encoding the intended gene(s). 72h post lentivector transduction, cells were subjected to flow cytometry sorting to isolate gene-engineered cells for making stable cell lines. Six stable tumor cell lines were generated for this study, including MM.1S-FG, MM.1S-hCD1d-FG, A375-hIL-15-FG, A375-hIL-15-hCD1d-FG, A375-A2-ESO-FG, and K562-FG.

Human PBMCs, CD34$^+$ HSCs, and Thymus Tissues

Human peripheral blood mononuclear cells (PBMCs), human fetal liver or cord blood CD34+ hematopoietic stem and progenitor cells (referred to as HSCs), and fetal thymus tissues were obtained from the CFAR Gene and Cellular Therapy Core Laboratory at UCLA, without identification information under federal and state regulations. Postnatal human thymus was obtained under IRB exemption as anonymized, discarded waste from patients undergoing cardiac surgery at Children's Hospital Los Angeles (CHLA). G-CSF-mobilized healthy donor

peripheral blood units were purchased from HemaCare or Cincinnati Children's Hospital Medical Center (CCHMC), followed by isolation of CD34+ HSCs through magnetic-activated cell sorting using a CliniMACS (Miltenyi Biotec) according to the manufacturer's instructions. For all isolates, the purity of CD34+ cells were more than 97% as evaluated by flow cytometry.

Materials and Reagents

α-Galactosylceramide (αGC, KRN7000) was purchased from Avanti Polar Lipids. Fluorochrome-conjugated hCD1d/PBS-57 tetramer reagents were provided by the NIH Tetramer Core Facility (Emory University, Atlanta, GA). Recombinant human IL-2, IL-3, IL-4, IL-7, IL-15, Flt3-Ligand, Stem Cell Factor (SCF), Thrombopoietin (TPO), and Granulocyte-Macrophage Colony-Stimulating Factor (GM-CSF) were purchased from Peprotech.

X-VIVO™ 15 Serum-free Hematopoietic Cell Medium was purchased from Lonza. RPMI1640 and DMEM cell culture medium were purchased from Corning Cellgro. Fetal bovine serum (FBS) was purchased from Sigma. Medium supplements, including Penicillin-Streptomycine-Glutamine (P/S/G), MEM non-essential amino acids (NEAA), HEPES Buffer Solution, and Sodium Pyruvate, were purchased from Gibco. Beta-Mercaptoethanol (β-ME) was purchased from Sigma. Normocin was purchased from InvivoGen. Complete lymphocyte culture medium (denoted as C10 medium) was made of RPMI 1640 supplemented with FBS (10% vol/vol), P/S/G (1% vol/vol), MEM NEAA (1% vol/vol), HEPES (10 mM), Sodium Pyruvate (1 mM), β-ME (50 uM), and Normocin (100 ug/ml). Medium for culturing monocyte-derived dendritic cells (MoDC) and non-adherent tumor cells (denoted as R10 medium) was made of RPMI 1640 supplemented with FBS (10% vol/vol) and P/S/G (1% vol/vol). Adherent cell culture medium (denoted as D10 medium) was made of DMEM supplemented with FBS (10% vol/vol) and P/S/G (1% vol/vol).

Lentiviral Vectors

Lentiviral vectors used in this study were all constructed from a parental lentivector pMNDW, that contains the MND retroviral LTR U2 region as an internal promoter and contains an additional Woodchuck Responsive Element (WPRE) to stabilize viral mRNA (Giannoni et al., 2013; Smith et al., 2016). The Lenti/iNKT vector was constructed by inserting into pMNDW a synthetic bicistronic gene encoding human iNKT TCRα-F2A-TCRβ; the Lenti/iNKT-EGFP vector was constructed by inserting into pMNDW a synthetic tricistronic gene encoding human iNKT TCRα-F2A-TCRβ-P2A-EGFP; the Lenti/iNKT-sr39TK vector was constructed by inserting into pMNDW a synthetic tricistronic gene encoding human iNKT TCRα-F2A-TCRβ-P2A-sr39TK; the Lenti/FG vector was constructed by inserting into pMNDW a synthetic bicistronic gene encoding Fluc-P2A-EGFP; the Lenti/CD1d vector was constructed by inserting into pMNDW a synthetic gene encoding human CD1d; the Lenti/IL-15-FG vector was constructed by inserting into pMNDW a synthetic tricistronic gene encoding human IL-15-F2A-Fluc-P2A-EGFP; the Lenti/ESO-sr39TK vector was constructed by inserting into pMNDW a synthetic tricistronic gene encoding human NY-ESO-1-specific TCRα-F2A-TCRβ-P2A-sr39TK; the Lenti/HLA-A2 vector was constructed by inserting into pMNDW a synthetic gene encoding human HLA-A2.1; and the Lenti/NY-ESO-1 vector was constructed by inserting into pMNDW a synthetic gene encoding human NY-ESO-1. The synthetic gene fragments were obtained from GenScript and IDT. Lentiviruses were produced using 293T cells, following a standard calcium precipitation protocol and an ultracentrifigation concentration protocol or a tandem tangential flow filtration concentration protocol as previously described [42]. Lentivector titers were measured by transducing HT29 cells with serial dilutions and performing Droplet Digital PCR (ddPCR), following established protocols [42].

Antibodies and Flow Cytometry

Fluorochrome-conjugated antibodies specific for human CD45 (clone H130), TCRαβ (clone I26), CD4 (clone OKT4), CD8 (clone SK1), CD45RO (clone UCHL1), CD45RA (clone HI100), CD161 (clone HP-3G10), CD69 (clone FN50), CD56 (clone HCD56), CD62L (clone DREG-56), CD14 (clone HCD14), CD11b (clone ICRF44), CD11c (clone N418), CD20 (clone 2H7), HLA-A2 (clone BB7.2), CD1d (clone 51.1), PD-1 (clone EH12.2H7), CCR4 (clone L291H4), CCR5 (clone HEK/1/85a), CXCR3 (clone G025H7), NKG2D (clone 1D11), IFN-γ (clone B27), Granzyme B (clone QA16A02), Perforin (clone dG9), TNF-□ (clone Mab11), IL-2 (clone MQ1-17H12), IL-4 (clone MP4-25D2) and IL-17 (clone BL168) were purchased from BioLegend; fluorochrome-conjugated antibodies specific for human CD34 (clone 581), TCR Vα24-Jα18 (clone 6B11) were purchased from BD Biosciences; fluorochrome-conjugated antibodies specific for human PLZF (alone 9E12), T-bet (clone 4B10), and CD1d (clone 1B1) were purchased from eBioscience. A fluorochrome-conjugated antibody specific for human Vβ11 was purchased from Beckman-Coulter. Human Fc Receptor Blocking Solution (TruStain FcX™) was purchased from BioLegend, while mouse Fc Block (anti-mouse CD16/32) was purchased from BD Biosciences. Fixable Viability Dye eFluor506 (e506) were purchased from affymetrix eBioscience. Cells were stained as previously described (Yang and Baltimore, 2005). Intracellular cytokines were measured using a Cell Fixation/Permeabilization Kit (BD Biosciences) according to the manufacturer's instructions. Stained cells were analyzed using a MACSQuant Analyzer 10 flow cytometer (Miltenyi Biotec). FlowJo software was used to analyze the data.

Human iNKT Cell TCR Vβ Repertoire Analysis

Human iNKT cell TCR Vβ repertoire was analyzed through flow cytometry using an IOTest® Beta Mark TCR V beta Repertoire Kit (Beckman-Coulter), following the manufacturer's instructions. Tube G was not used in staining because it included an antibody for Vβ11, which

was stained separately. All other combined hTCR Vβs (FITC) and hTCR Vβs (PE) antibodies collectively stained for human TCR Vβ 1, 2, 3, 4, 5.1, 5.2, 5.3, 7.1, 7.2, 8, 9, 12, 13.1, 13.2, 13.6, 16, 17, 18, 20, 21.3, and 23.

ELISA

The ELISAs for detecting human cytokines were performed following a standard protocol from BD Biosciences. The capture and biotinylated antibody pairs for detecting human IFN-□, IL-4, and IL-17 were purchased from BD Biosciences. The streptavidin-HRP conjugate was purchased from Invitrogen. Human IFN-γ, IL-4 and IL-17 standards were purchased from eBioscience. The tetramethylbenzidine (TMB) substrate was purchased from KPL. The samples were analyzed for absorbance at 450 nm using an Infinite M1000 microplate reader (Tecan).

Ganciclovir (GCV) In Vitro Killing Assay

Healthy donor PBMC T cells were cultured in vitro in C10 medium for 8 days, in the presence of 1 μg/ml anti-human CD3 (Clone HIT3a; LEAFTM purified; Biolegend), 1 μg/ml anti-human CD28 (Clone CD28.2; LEAFTM purified; Biolegend), and 10 ng/ml recombinant human IL-2. On days 2 and 3, concentrated Lenti/iNKT-sr39TK vectors were added into the cell culture. On day 4, titrated amounts of GCV (0-50 μM) were added into the cell culture. On day 8, selective killing of lentivector-transduced T cells (identified as hCD1d/PBS-57+ cells among total T cells) were analyzed using flow cytometry.

Single-Cell Human iNKT TCR Cloning

The single-cell iNKT TCR RT-PCR was performed based on an established protocol, with certain modifications [42]. Single human iNKT cells were sorted from healthy donor PBMCs

based on a stringent forum of surface markers (hTCRαβ^{+}hTCR Vα24-Jα18^{+}hTCR Vβ11^{+}CD161^{+}) using a FACSAria II flow cytometer (BD Biosciences). Single cells were sorted directly into PCR plates containing cell lysis buffer. The plates were then immediately flash frozen and stored at -80 C until use. Upon thawing, the cell lysate from each cell was split in half on the same PCR plate and processed directly into iNKT TCR cloning for both α and β chain genes using a OneStep RT-PCR kit (QIAGEN), following the manufacturer's instructions and using the human iNKT TCR gene-specific primers. These primers were designed to amplify the ~200-300 bps spanning the CDR3 regions of the iNKT TCR α and β chain cDNAs and were customer-synthesized by IDT: for TCRα (FW primer: 5′- GCT CTC TGC ACA TCA CAG CCT CCC AG -3′; BW primer: 5′- CGG TGA ATA GGC AGA CAG ACT TGT CAC TG -3′) and for TCRβ (FW: 5′- CCA CAG AGA AGG GAG ATC TTT CCT CTG AGT C -3′; BW: 5′- CCT GTG GCC AGG CAC ACC AGT G -3′). Verified sequences (productive germline Vα24-Jα18-Cα assembly for TCRα and Vβ11-D/J/N-Cβ assembly for TCRβ) were used to construct the complete cDNA sequences encoding the TCR α and β chains from a single cell, based on information about human TCR genomic segments [the international ImMuno-GeneTics information system (IMGT), www.imgt.org]. The selected iNKT TCR α and β pair cDNAs were then synthesized as a single bicistonic gene, with codon optimization and an F2A sequence linking the TCRα and TCRβ cDNAs to enable their co-expression (GenScript).

Generation of BLT and BLT-iNKT Humanized Mice

BLT (human bone marrow-liver-thymus engrafted NSG mice) and BLT-iNKT (human iNKT TCR gene-engineered BLT mice) humanized mice were generated as previously described, with some modifications [42,65,66]. In brief, human CD34^{+} HSCs were cultured for no more than

48 hours in X-VIVO™ 15 Serum-free Hematopoietic Cell Medium (Lonza) containing recombinant human Flt3 ligand (50 ng/mL), SCF (50 ng/mL), TPO (50 ng/mL), and IL-3 (20 ng/mL) in non-tissue culture-treated plates coated with Retronectin (20 μg/ml) (Takara). Viral transduction, when applicable, was performed at 24 hours by adding concentrated lentivectors (Lenti/iNKT, Lenti/iNKT-EGFP, or Lenti/iNKT-sr39TK) directly to the culture medium. At around 48 hours, $CD34^+$ cells were collected and i.v. injected into NSG mice (~0.5-1 x 106 cells per recipient) that had received 270 rads of total body irradiation. 1-2 fragments of human fetal or postnatal thymus (~1 mm^3) were implanted under the kidney capsule of each recipient NSG mouse. The mice were maintained on trimethoprim/sulfmethoxazole (TMS) chow in a sterile environment for 8-12 weeks until analysis or use for further experiments.

Generation of Secondary BLT-iNKT Humanized Mice

Secondary BLT-iNKT mice were generated through harvesting total bone marrow cells and human thymus implants from primary BLT-iNKT mice followed by adoptive transfer into NSG recipient mice. Recipient NSG mice were pre-conditioned with 270 rads of total body irradiation. 10 x 10^6 primary BLT-iNKT mice bone marrow cells were i.v. injected into each NSG recipient mouse. Human thymus implants were dissected from the kidney capsule of primary BLT-iNKT mice, cut into fragments (~1 mm^3), then surgically implanted under the kidney capsule of the NSG recipient mice (1-2 fragments per recipient). The mice were maintained on TMS chow in a sterile environment for 8-12 weeks until analysis or further experiments.

Safety Study of HSC-iNKT Cell Therapy in BLT-iNKT Mice

BLT-iNKT mice and control BLT mice were monitored for body weight and survival rate over a period of 5 months after HSC transfer. At the end of 5 months, mice were terminated, and

various tissues were collected, including bone marrow, spleen, Ileum, pancreas, kidney, lung, liver, heart, and brain. Tissues were fixed with 10% neutral-buffered formalin and embedded in paraffin for sectioning (5 μm thickness), followed by hematoxylin and eosin staining using standard procedures (UCLA Translational Pathology Core Laboratory). The sections were examined by a mouse pathologist (N.R.) who was blinded to the sample group assignments during initial scoring. Scores were assigned on the basis of a combination of criteria, including inflammation, hematopoietic neoplasm, and non-hematopoietic neoplasm. An ordinal scale scoring system was used: 0, no abnormal findings; 1, mild; 2, moderate; and 3, severe.

In another set of longer-term experiments, BLT-iNKT mice and control BLT mice were maintained for a period of over 8 months, to monitor graft-versus-host (GvH) reactions in these animals. Over time, mouse survival rates were recorded. At 6 months post-HSC transfer, a subset of animals were terminated and their tissues (e.g. liver) were collected and processed for flow cytometry analysis following established protocols [42]. Activation status of engrafted human conventional αβ T cells (identified as $hCD45^{+}hTCR\ \alpha\beta\ ^{+}6B11^{-}$ cells) was assessed through measuring T cell expression of CD45RA and CD45RO surface markers ($CD45RA^{lo}CD45RO^{hi}$ indicating T cell activation).

Biodistribution and Controlled Depletion of HSC-iNKT Cells in BLT-iNKT Humanized Mice Visualized by PET/CT Imaging

BLT-iNKTTK mice (BLT-iNKT mice generated using Lenti/iNKT-sr39TK vector-transduced PBSCs) were utilized for this study. Regular BLT mice were included as imaging controls. To study controlled depletion of vector-engineered human HSCs and their progeny immune cells, experimental animals received i.p. injection of nucleoside prodrug ganciclovir (GCV) for five consecutive days (50 mg/kg per injection per day). PET/CT imaging data were collected one day prior to GCV treatment, and 7 days post GCV treatment. PET/CT scans were performed

using a microPET/CT system Genisys 8 (Sofie Bioscience). Mice were anesthetized using 1.5-2% isoflurane. 20 μCi of 18F-FHBG probes was administrated via tail vein. Acquisition of static PET images was started 60 min after probe injection. Maximum-likelihood expectation maximization with 60 iterations was used for PET image reconstruction. All images were corrected for photon attenuation. The CT acquisition parameters were 40 kVp, 190 mA, and 720 projections with an exposure time of 55 ms at each projection. For image analysis, PET/CT images were analyzed using OsiriX Imaging Software (Version 3.9.3; Pixmeo SARL).

HSC-iNKT Cell Phenotype and Functional Study

HSC-engineered human iNKT cells (denoted as HSC-iNKT cells) were isolated from the spleen of BLT-iNKT mice. Phenotype of HSC-iNKT cells was studied using flow cytometry, through analyzing cell surface markers, including co-receptors (CD4 and CD8), NK cell markers (CD161 and NKG2D), memory/effector T cell markers (CD45RO and CD69), and homing markers (CD62L, CCR4, CCR5, and CXCR3). Native human iNKT cells and conventional T cells isolated from healthy donor PBMCs (denoted as PBMC-iNKT and PBMC-Tc cells, respectively) were included as FACS analysis controls.

Response of HSC-iNKT cells to antigen stimulation was studied by culturing BLT-iNKT spleen cells in vitro in C10 medium for 7 days, in the presence or absence of αGC (100 ng/ml). Proliferation of HSC-iNKT cells (identified as $hCD45^{+}hTCR\ \alpha\beta^{+}6B11^{+}$ cells of total cell culture) was measured by cell counting and flow cytometry over time. Cytokine production was assessed by ELISA analysis of cell culture supernatants collected on day 7 (for human IFN-γ, IL-4, and IL-17).

Capacity of HSC-iNKT cells to produce effector molecules was studied in comparison with that of native PBMC-iNKT cells and PBMC-Tc cells. BLT-iNKT spleen cells and healthy donor PBMCs were cultured in vitro in C10 medium for 7 days with αGC stimulation (100

ng/ml). On day 7, cells were collected and analyzed for intracellular production of various pro-inflammatory cytokines (IFN-γ, TNF-α, and IL-2) and cytotoxic molecules (Perforin and Granzyme B) using a Cytofix/Cytoperm Fixation/Permeabilization Kit (BD Biosciences) (Smith et al., 2015). The CD4/CD8 co-receptor expression patterns on HSC-iNKT cells and PBMC-iNKT cells pre- and post-αGC stimulation were studied using flow cytometry.

HSC-iNKT Cell In Vitro Expansion

Various tissues (spleen, lymph nodes, liver, bone marrow) were collected from BLT-iNKT mice, processed into single mononuclear cells, and pooled together for in vitro culture. Healthy donor PBMCs were loaded with αGC (by culturing 1 x 108 PBMCs in 5 ml C10 medium containing 5 ug/ml αGC for 1 hour), irradiated at 6,000 rads, then used to stimulate HSC-iNKT cells (denoted as αGC/PBMCs). To expand HSC-iNKT cells, pooled BLT-iNKT mouse tissue cells were mixed with αGC/PBMCs (ratio 1:1 or 1:1.5) and cultured in C10 medium for 7 days. Recombinant human IL-7 (10 ng/ml) and IL-15 (10 ng/ml) were added to cell cultures from day 2. On day 7, cell cultures were collected and HSC-iNKT cells were sorted out using flow cytometry (identified as $hCD45^{+}hTCR\alpha\beta^{+}6B11^{+}$ cells). The sorted HSC-iNKT cells (>99% purify based on flow cytometry analysis) were expanded further with αGC/APCs and IL-7/IL-15 for another 7 to 14 days, then were aliquoted and frozen in LN2 storage tanks. For mechanistic and efficacy studies, HSC-iNKT cells were thawed from frozen stock and utilized for the intended assays.

HSC-iNKT Cell Tumor-Attacking Mechanism Study: In Vitro Direct Tumor Cell Killing Assay

MM.1S-FG or MM.1S-hCD1d-FG tumor cells (5-10 x 10^3 cells per well) were co-cultured with HSC-iNKT cells (ratio 1:10, unless otherwise indicated) in Corning 96-well clear bottom black plates for 24-48 hours, in X-VIVOTM 15 medium with or without the addition of αGC

(100 ng/ml). At the end of culture, live tumor cells were quantified by adding D-Luciferin (150 ug/ml) (Caliper Life Science) to cell cultures and reading out luciferase activities using an Infinite M1000 microplate reader (Tecan) according to the manufacturer's instructions. In tumor cell killing assays involving blocking CD1d, 10 ug/ml LEAFTM purified anti-human CD1d antibody (Clone 51.1, Biolegend) or LEAFTM purified mouse IgG2b isotype control antibody (Clone MG2b-57, Biolegend) was added to tumor cell cultures one hour prior to adding HSC-iNKT cells.

HSC-iNKT Cell Tumor-Attacking Mechanism Study: In Vitro NK Adjuvant Effect Assay

Primary human NK cells were isolated from healthy donor PBMCs through magnetic-activated cell sorting (MACS sorting), using an NK Cell Isolation Kit (Miltenyi Biotec) according to the manufacturer's instructions. K562-FG cells (5 x 104 cells per well) were co-cultured with NK cells and HSC-iNKT cells (ratio 1:2:2) in Corning 96-well clear bottom black plates for 24 hours, in C10 medium with or without the addition of αGC-loaded irradiated PBMCs as antigen presenting cells (APCs). Live tumor cells were quantified by adding D-Luciferin (150 ug/ml) (Caliper Life Science) to the cell cultures and reading out luciferase activities using an Infinite M1000 microplate reader (Tecan). NK cell activation status was monitored through measuring NK cell expression of CD69 using flow cytometry. Cytokine production from co-cultured NK and HSC-iNKT cells was analyzed through collecting cell culture supernatants and assaying cytokines (IFN-γ and IL-2) using ELISA.

HSC-iNKT Cell Tumor-Attacking Mechanism Study: In Vitro DC/CTL Adjuvant Effect Assay

$CD1d^+$/HLA-$A2^+$ human monocyte-derived dendritic cells (MoDCs) were generated by isolating $CD14^+$ monocytes from HLA-$A2^+$ healthy donor PBMCs using MACS sorting, followed by culturing monocytes in R10 medium supplemented with recombinant human GM-

CSF (100 ng/ml) and IL-4 (20 ng/ml) for 4 days. NY-ESO-1 specific CD8+ human cytotoxic T lymphocytes (CTLs, or ESO-T cells) were generated through engineering human CD34+ HSCs with a TCR gene encoding a 1G4 TCR (HLA-A2-restricted, NY-ESO-1 tumor antigen-specific) and differentiating the TCR gene-engineered HSCs into CD8+ CTLs in an Artificial Thymic Organoid (ATO) culture, following an established protocol (Bethune et al., 2018; Seet et al., 2017). The resulting ESO-T CTLs were co-cultured with CD1d+/HLA-A2+ MoDCs in C10 medium for 3 days, with or without the addition of HSC-iNKT cells (cell ratio 1:1:1) and αGC (100 ng/ml). Activation of MoDCs was analyzed at 24 hours through measuring MoDC surface expression of CD86 using flow cytometry. Expansion of ESO-T cells was quantified at 72 hours through cell counting and flow cytometry analysis (ESO-T cells were gated as hTCRαβ$^+$hTCR Vα13.1$^+$ cells of the total cell cultures). Tumor-killing potential of ESO-T cells was measured by adding A375-A2-ESO-FG tumor cells (1:1 ratio to input ESO-T cells) to the ESO-T/MoDC co-culture 24 hours post co-culture setup, and quantifying live tumor cells via luciferase activity reading in another 24 hours.

HSC-iNKT Cell Tumor-Attacking Mechanism Study: In Vitro Macrophage Inhibition Assay

CD14$^+$ monocytes were isolated from healthy donor PBMCs through MACS sorting, followed by co-culturing with HSC-iNKT cells (ratio 1:1) for 24-48 hours in C10 medium with or without the addition of αGC (100 ng/ml). At the end of culture, cells were collected for flow cytometry analysis, to assess the activation of HSC-iNKT cells (gated as hTCRαβ$^+$6B11$^+$ cells of total cell culture) by measuring their expression of CD69, and to assess the viability of monocytes (gated as CD14$^+$ cells of total cell culture) with the eBioscience Fixable Viability Dye eFluor 506 (e506).

Bioluminescence Live Animal Imaging (BLI)

BLI was performed using an IVIS 100 imaging system (Xenogen/PerkinElmer). Live animal imaging was acquired 5 minutes after intraperitoneal injection of D-Luciferin (1 mg per mouse). Imaging results were analyzed using a Living Imaging 2.50 software (Xenogen/PerkinElmer).

HSC-iNKT Cell In Vivo Antitumor Efficacy Study: MM.1S Human Multiple Myeloma Xenograft NSG Mouse Model

NSG mice were inoculated with 0.5-1 x 10^6 MM.1S-hCD1d-FG or MM.1S-FG cells intravenously (day 0) and were allowed to develop MM over the course of about 3 weeks. Prior to tumor inoculation (day 0), mice were pre-conditioned with 175 rads of total body irradiation. Three days post-tumor inoculation (day 3), mice received i.v. injection of vehicle (PBS) or 1 x 10^7 HSC-iNKT cells. Recombinant human IL-15 was supplemented to experimental animals through i.p injection to support the peripheral maintenance of HSC-iNKT cells twice per week starting from day 3 (500 ng per animal per injection). Over time, tumor loads in experimental animals were monitored using BLI, twice per week starting from day 2. At around week 3, mice were terminated. Various mouse tissues (blood, spleen, liver, and bone marrow) were harvested and processed for flow cytometry analysis to detect tissue-residing tumor cells (identified as GFP^+ cells) and HSC-iNKT cells (identified as $hCD45^+6B11^+$ cells), following established protocols (Smith et al., 2016). Activation status of HSC-iNKT cells was monitored through measuring cell surface expression of CD62L and CD69 markers using flow cytometry.

HSC-iNKT Cell In Vivo Antitumor Efficacy Study: A375 Human Melanoma Xenograft NSG Mouse Model

NSG mice were inoculated with 1 x 10^6 αGC-loaded A375-hIL-15-hCD1d-FG cells or 1 x 106 αGC-loaded A375-hIL-15-FG cells subcutaneously (day 0) and were allowed to grow solid tumors over the course of approximately 4 weeks. Three days post-tumor inoculation (day 3),

mice received 100 rads of total body irradiation followed by i.v. injection of vehicle (PBS) or 1 x 10^7 HSC-iNKT cells. Note that inclusion of a human IL-15 gene in the tumor cells aimed to provide human IL-15 within solid tumors in vivo, because the on-site presence of IL-15 has been indicated to be critical in maintaining iNKT cell survival in the hypoxic solid tumor microenvironment. Recombinant human IL-15 was also supplemented to experimental animals through i.p injection to support the peripheral maintenance of HSC-iNKT cells twice per week starting from day 3 (500 ng per animal per injection). Over time, tumor loads in experimental animals were monitored twice per week starting from day 2 by measuring total body luminescence using BLI (shown as TBL p/s), and by measuring tumor size using a FisherbrandTM TraceableTM digital caliper (Thermo Fisher Scientific) (tumor volume calculated as (W(2) x L)/2 mm3). At approximately week 4, mice were terminated. Solid tumors were retrived, weighted using a PA84 precision balance (Ohaus), then processed for flow cytometry analysis to detect tumor-infiltrating HSC-iNKT cells (identified as $hCD45^+6B11^+$ cells). Various mouse tissues (blood, spleen, and liver) were also collected and processed for flow cytometry analysis to detect tissue-residing HSC-iNKT cells (identified as $hCD45^+6B11^+$ cells), following established protocols (Smith et al., 2016). Activation status of HSC-iNKT cells was monitored through measuring cell surface expression of CD62L and CD69 markers using flow cytometry.

RESULTS

Cloning of Human iNKT TCR Genes

Single human iNKT cells were sorted from healthy donor peripheral blood mononuclear cells (PBMCs) using flow cytometry based on a stringent combination of surface markers, gated as $hTCR\alpha\beta^+6B11^+hTCRV\beta11^+hCD161^{hi}$ (**Figure 2-1A**). 6B11 is a monoclonal antibody that specifically recognizes the human iNKT TCR invariant alpha chain (hTCR Vα24-Jα18) [67]. We

included hTCR Vβ11 staining to focus on the dominant Vβ11$^+$ population of human iNKT cells [36]. The sorted single human iNKT cells were then subjected to TCR cloning using an established single-cell TCR cloning technology (**Figure 2-1B**) [42]. A validated pair of iNKT TCR α and β chain genes (thereafter collectively referred to as the human iNKT TCR gene) were selected for further development.

Construction of Human iNKT TCR Gene Delivery Vectors

A clinical lentiviral vector designated for HSC-based gene therapy was chosen to deliver the iNKT TCR gene (**Figure 2-1C**) [68]. The lentivector contains an MNDU3 promoter that mediates high and stable expression of transgene in human HSCs and their progeny human immune cells [68]. Three vectors were constructed: 1) a Lenti/iNKT vector encoding the iNKT TCR gene, which is intended for eventual clinical usage; 2) a Lenti/iNKT-EGFP vector encoding the iNKT TCR gene together with an enhanced green fluorescent protein (EGFP) reporter gene, which allows for convenient tracking of vector-engineered HSCs and their progeny cells using flow cytometry and thus is valuable for preclinical studies; and 3) a Lenti/iNKT-sr39TK vector encoding the iNKT TCR gene together with an sr39TK suicide/PET imaging reporter gene, which allows for monitoring vector-engineered HSCs and their progeny cells using PET imaging and for depleting engineered cells through ganciclovir (GCV) administration in case of an adverse side effect, and thus is valuable for early clinical development (**Figure 2-1C**) [69]. The gene-delivery capacity of these lentivectors, as well as the functionality of the encoded human iNKT TCR gene and EGFP and sr39TK reporter genes, were studied by transducing 293T cells (**Figure 2-1D**) and primary human PBMC T cells (**Figures 2-1E-2-1G**) with individual lentivectors followed by functional tests. Notably, all three lentivectors mediated efficient expression of the human iNKT TCR gene (**Figure 2-1D**); the resulting transgenic

human iNKT TCRs recognized αGC and responded to αGC stimulation, as evidenced by hCD1d/PBS-57 tetramer binding and induced IFN-γ production (**Figures 2-1E and 2-1F**); and the encoded sr39TK enabled efficient GCV-induced depletion of gene-engineered cells (**Figure 2-1G**). In the present study, these three lentivectors were utilized simultaneously or individually, depending on the purpose of a given experiment.

iNKT TCR Gene-Engineering of Human HSCs

iNKT TCR gene-delivery lentivectors were of high titer, and transduced human $CD34^+$ hematopoietic stem and progenitor cells (referred to as HSCs thereafter) of various donors robustly and efficiently (**Figures 2-2B-2-2D**). Gene-engineering rate of HSCs could be conveniently adjusted through titrating lentivectors utilized for transduction, resulting in 0-50% iNKT TCR^+ cells with an average Vector Copy Number (VCN) of 0-3 per cell (**Figure 2-2E**).

Production of BLT-iNKT Humanized Mice

We utilized a BLT (human bone marrow-liver-thymus engrafted NOD/SCID/$\gamma c^{-/-}$ mice) humanized mouse model, that supports the engraftment of human HSCs and supports the development of human T cells, to study the *in vivo* generation of HSC-engineered human iNKT cells [42,65,66]. Human HSCs, either mock-transduced or transduced with human iNKT TCR gene-delivery vectors, were adoptively transferred into NOD/SCID/$\gamma c^{-/-}$ (NSG) mice engrafted with human thymus to produce standard BLT mice or iNKT TCR gene-engineered BLT mice (denoted as BLT or BLT-iNKT mice, respectively) (**Figure 2-3A**). These BLT and BLT-iNKT humanized mice were then utilized for further study.

Generation of HSC-iNKT Cells in BLT-iNKT Humanized Mice

We detected efficient and comparable reconstitution of human immune cells, in particular human αβ T cells, in both BLT and BLT-iNKT mice (**Figure 2-3B**). BLT mice contained minimal numbers of endogenous human iNKT cells below detection level (**Figure 2-3B**). Numbers of human iNKT cells were greatly increased in BLT-iNKT mice; these iNKT cells started to appear in the peripheral blood of BLT-iNKT mice around 2 months post-HSC transfer, then peaked and stabilized around 3 months, indicating that they were derived from the iNKT TCR gene-engineered HSCs (**Figure 2-3B**). Analysis of BLT-iNKT mice revealed a tissue distribution of HSC-engineered human iNKT cells (referred to as HSC-iNKT cells thereafter) that was typical of human iNKT cells: besides circulating in blood, HSC-iNKT cells homed to lymphoid organs such as the bone marrow and spleen, as well as other peripheral organs such as the liver (**Figures 2-3C and 2-3D**) [34]. The *in vivo* production of HSC-iNKT cells was stable and long-lasting, evident in the persistence of high levels of iNKT cells in the primary BLT-iNKT mice for over 5 months after the initial HSC transfer (**Figure 2-3B**), and in the secondary BLT-iNKT mice after the secondary HSC transfer (**Figures 2-3E-2-3G**). These results indicate that the iNKT TCR gene-engineered HSCs retain their longevity and self-renewal capacity and are able to produce iNKT cells over time, highlighting the long-term therapeutic potential of the HSC-engineered iNKT cell approach. Moreover, by titrating the iNKT TCR gene-engineering rate of HSCs used for adoptive transfer, we could generate BLT-iNKT mice that contained gradient levels of human iNKT cells ranging from 5% to over 60% of total human αβ T cells (**Figures 2-3H and 2-2E**). The capacity to control the outputs of engineered human iNKT cells could be very valuable for the clinical application of HSC-iNKT cell therapy, allowing dosing the engineered iNKT cells in cancer patients according to their therapeutic needs.

The method of generating human iNKT cells through TCR gene-engineering of HSCs is highly robust. In our experiments, we have succeeded in generating HSC-iNKT cells in BLT-iNKT mice engineered with all three iNKT TCR gene delivery lentivectors (Lenti/iNKT, Lenti/iNKT-EGFP, and Lenti/iNKT-sr39TK), using human $CD34^+$ HSCs isolated from various cell sources from multiple donors (cord blood, fetal liver, and G-CSF-mobilized peripheral blood), and using human thymus implants collected from various tissue sources and multiple donors (fetal thymus and post-natal thymus) (**Figure 2-3I**). Notably, there was no need to match human $CD34^+$ HSCs with human thymus implants for donors, or tissue sources, or human leukocytes antigens (HLAs), making the generation of BLT-iNKT mice highly adaptable (**Figure 2-3I**). The BLT-iNKT humanized mouse model therefore can be utilized as a powerful and versatile tool for the preclinical development of HSC-iNKT cell therapy, and for the study of human iNKT cell biology and other human iNKT cell-based immunotherapies. Importantly, the success of generating human iNKT cells through TCR gene engineering of G-CSF-mobilized peripheral blood $CD34^+$ HSCs (referred to as PBSCs thereafter) from multiple human donors directly indicates the robustness and translational potential of the proposed HSC-iNKT cell therapy (**Figures 2-3I and 2-2A**). Because of their possible relevance to early clinical development, in this report, we focused on studying HSC- iNKT cells generated in BLT-iNKT mice produced with Lenti/iNKT-sr39TK vector-transduced PBSCs (and implanted with human fetal thymus), unless otherwise indicated.

Safety Study of HSC-iNKT Cell Therapy in BLT-iNKT Humanized Mice

Safety of the HSC-iNKT cell therapy was evaluated by long-term monitoring and terminal pathology analysis of the BLT-iNKT humanized mice in comparison with the control BLT mice (**Figure 2-5**). Over a period of 5 months, BLT-iNKT mice showed a steady body weight increase and a survival rate comparable to that of the control BLT mice (**Figures 2-5A and 2-**

5B). Pathological analysis of the various tissues of the BLT-iNKT mice collected at the end of 5 months showed no increase of tissue inflammation, hematopoietic neoplasm, or non-hematopoietic neoplasm, comparable to that of the control BLT mice (**Figure 2-5C**). 5 months after HSC transfer, BLT mice gradually developed graft-versus-host disease (GvHD) and eventually died of this disease due to the xenoreactive nature of the engrafted human conventional αβ T cells. Intriguingly, compared to the control BLT mice, BLT-iNKT mice were significantly protected from GvHD, evidenced by the reduced auto-activation of engrafted human conventional αβ T cells in BLT-iNKT mice (**Figures 2-5D-2-5F**) and the resulting elongated survival of these mice (**Figure 2-5G**). This phenomenon agreed with the clinical observation that in leukemia patients who received allogenic HSC transfer, levels of donor-derived iNKT cells positively correlated with the therapeutic effects of graft-versus-leukemia (GvL) and negatively correlated with the incidences and severity of GvHD, presumably attributed to the regulatory function of human iNKT cells [30,31,39]. Reduced GvHD in BLT-iNKT mice suggest that, like native human iNKT cells, HSC-iNKT cells promote a favorable balance of GvL compared to GvHD. Therefore, the HSC-iNKT cell therapy was demonstrated to be safe, with additional anti-GvHD benefits, in the BLT-iNKT pre-clinical animal model.

Biodistribution and Controlled Depletion of HSC-iNKT Cells in BLT-iNKT Humanized Mice Visualized by PET Imaging

Incorporation of an sr39TK suicide/PET imaging reporter gene in the human iNKT TCR gene delivery vector provides an additional safety control for HSC-iNKT cell therapy, allowing the depletion of gene-engineered human immune cells through GCV treatment in case the therapy needs to be terminated due to safety concerns (**Figure 2-4A**). It also provides an opportunity to visualize the biodistribution and *in vivo* dynamics of the gene-engineered human HSCs and

their progeny cells in Lenti/iNKT-sr39TK vector-engineered BLT-iNKT mice (denoted as BLT-iNKT^{TK} mice) using non-invasive PET imaging, a clinically applicable technology (**Figure 2-4A**). Using PET imaging combined with CT scan, we detected the distribution of gene-engineered human immune cells across the lymphoid tissues of BLT-iNKT^{TK} mice, particularly in the bone marrow and spleen (**Figure 2-4B**). Treating BLT-iNKT^{TK} mice with GCV effectively depleted gene-engineered human cells across the body (**Figures 2-4C-2-4D and 2-6A-2-6B**). The depletion of gene-engineered human cells in bone marrow was confirmed by droplet digital PCR (**Figure 2-4G**). Importantly, the GCV-induced depletion was specific, evidenced by the selective depletion of HSC-iNKT cells but not the overall human immune cells in BLT-iNKT^{TK} mice as measured by flow cytometry (**Figures 2-4E-2-4F and 2-6C-2-6D**).

Development of HSC-iNKT Cells in BLT-iNKT Humanized Mice

Utilizing the BLT-iNKT mouse model, we set out to study the *in vivo* development of HSC-iNKT cells. Like conventional αβ T cells, iNKT cells originate from HSCs and develop in the thymus [34]. Analysis of the human thymus implants in BLT-iNKT mice detected the presence of developing HSC-iNKT cells (**Figures 2-7A and 2-8A**). These cells appeared as $CD4^-CD8^-$ double-negative (denoted as DN), $CD4^+CD8^+$ double-positive (denoted as DP), $CD4^+CD8^-$ single-positive (denoted as CD4 SP), and $CD4^-CD8^+$ single-positive (denoted as CD8 SP), corresponding with a human iNKT development path from DN to DP, then to CD4/CD8 SP or back to DN cells (**Figure 2-7A**) [34]. In addition to their development in the thymus to gain TCR expression (Control Point 1), iNKT cells differ from conventional αβ T cells in that they undergo an additional maturation step in the periphery to upregulate the expression of memory T cell and NK cell markers (CD45RO and CD161, respectively) [34]. Indeed, CD45RO and CD161 markers were upregulated further on HSC-iNKT cells detected in the periphery of

BLT-iNKT mice (**Figures 2-7A-2-7B and 2-8A-2-8B**). Overall, mature HSC-iNKT cells detected in the periphery of BLT-iNKT mice displayed a collection of surface developmental markers closely resembling that of endogenous human iNKT cells detected in the peripheral blood of healthy human donors: they expressed the CD4/CD8 co-receptors of a mixed pattern (DN, CD4 SP, and CD8 SP); and they expressed high levels of memory T cell and NK cell markers ($CD45RO^{hi}$ and $CD161^{hi}$) (**Figures 2-7B and 2-7C**). Interestingly, previous mouse studies indicated that during their development in the thymus [34], iNKT cells were selected by DP thymocytes expressing CD1d, unlike that for conventional αβ T cells. We found that in the human thymus implants of BLT-iNKT mice, the DP cells (of both developing HSC-iNKT cells and developing conventional αβ T cells) expressed high levels of human CD1d, suggesting that HSC-iNKT cells could also be selected on DP human thymocytes (**Figure 2-7A**).

We have previously shown that overexpression of a transgenic mouse iNKT TCR gene in mouse HSCs induced allelic exclusion and blocked the rearrangement of endogenous TCR genes in the resulting HSC-engineered mouse iNKT cells [42]. Study of the human HSC-iNKT cells generated in BLT-iNKT mice revealed that these cells expressed the transgenic human iNKT TCRs (hTCR $Vβ11^{+}$), but not the other human TCR Vβ chains analyzed in our experiments, indicating that allelic exclusion also occurred during the development of human HSC-iNKT cells (**Figures 2-7D and 2-7E**). Utilizing BLT-iNKT mice engineered with the Lenti/iNKT-EGFP vector (denoted as BLT-$iNKT^{GFP}$ mice), we studied the lineage differentiation of iNKT TCR-engineered human HSCs by tracking GFP^{+} human HSCs and their progeny human immune cells. Analysis of human αβ T cell population in the periphery of these BLT-$iNKT^{GFP}$ mice revealed that GFP^{+} cells were exclusively human iNKT cells (**Figures 2-8C and 2-8D**). Analysis of bone marrow cells of these BLT-$iNKT^{GFP}$ mice showed that GFP^{+} and GFP^{-} cells comprised a similar composition of all lineages of human immune cells analyzed, including HSCs, T cells, B cells, myeloid cells, monocytes, dendritic cells, and

NK cells (**Figures 2-8E and 2-8F**). Taken together, these results indicate that iNKT TCR-engineered human HSCs have the full potential to remain as long-term HSCs or to differentiate into various lineages of human immune cells; however, once going down the path of T cell development, the engineered T cell progenitor cells will commit to become iNKT cells following a TCR-instruction mechanism [42]. Notably, because only T cells express the CD3 molecules that are required to support the surface display of TCRs and the downstream TCR signaling events, the expression of transgenic human iNKT TCRs is functionally restricted to the therapeutic HSC-iNKT cells without interfering with the activities of other lineages of human immune cells, which is a desirable feature for gene- and cell-based therapies.

Phenotype and Functionality of HSC-iNKT Cells

Next, we studied the phenotype and functionality of HSC-iNKT cells, in comparison with that of endogenous human iNKT cells and conventional αβ T cells isolated from the peripheral blood of healthy human donors (denoted as PBMC-iNKT and PBMC-Tc cells, respectively). HSC-iNKT cells displayed a surface phenotype closely resembling PBMC-iNKT cells but distinct from PBMC-Tc cells: they expressed a mixed pattern of CD4/CD8 co-receptors (DN, CD4 SP, and CD8 SP); they expressed high levels of NK cell markers (CD161 and NKG2D); they upregulated T cell memory and activation markers (CD45RO and CD69); and they down-regulated lymphoid organ homing marker (CD62L) and upregulated peripheral tissue and inflammatory site homing markers (CCR4, CCR5, and CXCR3) (**Figure 2-7F**). When stimulated with αGC, HSC-iNKT cells proliferated vigorously (**Figure 2-7G**). They secreted high levels of T_H0/T_H1 cytokines such as IFN-γ, limited amounts of T_H2 cytokines such as IL-4, and minimal amounts of T_H17 cytokines such as IL-17, indicating a T_H0/T_H1-prone effector function of these cells (**Figure 2-7H**). Intracellular staining showed that at the single-cell level, HSC-iNKT cells produced excess amounts of effector molecules, in particular pro-

inflammatory cytokines (IFN-γ, TNF-α, and IL-2) and cytotoxic molecules (Perforin and Granzyme B), at levels comparable to that produced by the native PBMC-iNKT cells (**Figure 2-7I**). The capacity to produce excess amounts of pro-inflammatory and cytotoxic effector molecules is a signature of iNKT cells which is attractive to cancer therapy [50–52]. Analysis of transcription factor expression pattern revealed that HSC-iNKT cells expressed high levels of PLZF, the "master" transcription factor regulating iNKT cell development and functionality, resembling that of native iNKT cells while differing from that of native conventional αβ T cells and γδ T cells isolated from healthy donor peripheral blood (**Figure 2-8G**) [70,71].

Tumor-Attacking Mechanisms of HSC-iNKT Cells

One of the most attractive features of iNKT cells is that they can attack tumors through multiple mechanisms. We therefore studied HSC-iNKT cells for their capacity to deploy these various tumor-attacking mechanisms [26,28,42,72], including: 1) direct killing of $CD1d^+$ tumor cells, 2) adjuvant effects on enhancing NK-mediated killing of tumor cells, 3) adjuvant effects on boosting dendritic cell and cytotoxic T lymphocyte (DC/CTL) antitumor activities, and 4) inhibition of tumor-associated macrophages (TAMs) (**Figure 2-9A**).

We utilized an *in vitro* tumor cell killing assay to study the direct killing of $CD1d^+$ tumor cells, wherein HSC-iNKT cells were co-cultured with $CD1d^+$ target tumor cells. A human multiple myeloma (MM) cell line, MM.1S, was chosen as the model tumor target, because MM has a strong clinical relevance to iNKT cells, and because primary human MM tumor cells are $CD1d^+$ and are proven targets of native human iNKT cell killing [73,74]. Notably, most MM cell lines, including MM.1S, have lost CD1d expression. We therefore engineered MM.1S cells to overexpress CD1d. We also engineered these cells to overexpress the firefly luciferase (Fluc) and EGFP reporters to enable the sensitive measurement of tumor killing using luminescence

reading or flow cytometry. The resulting MM.1S-FG and MM.1S-hCD1d-FG cell lines were then used for the *in vitro* tumor cell killing assay (**Figures 2-10A and 2-10B**). In the presence of αGC, HSC-iNKT cells killed tumor cells aggressively in an CD1d-dependant manner, attesting to the strong tumor-killing potency of HSC-iNKT cells triggered by CD1d/antigen recognition (**Figures 2-9B-2-9C and 2-10C-2-10D**). Importantly, even without the addition of αGC, HSC-iNKT cells could still effectively kill MM.1S-hCD1d-FG tumor cells, although tumor killing was less aggressive and required the addition of IL-15 (**Figures 2-9D and 2-9E**). Besides its role as an essential homeostatic cytokine in supporting the peripheral maintenance of iNKT cells, IL-15 is critical in supporting the function of iNKT cells, especially when iNKT cells respond to sub-optimal antigen stimulations [75]. The direct killing of MM.1S-hCD1d-FG tumor cells by HSC-iNKT cells was dependent on the presence of CD1d on tumor cells (**Figures 2-9E**), indicating that HSC-iNKT cells can directly kill $CD1d^+$ tumor cells by recognizing tumor cell-derived lipid antigens presented by CD1d.

Next, we studied the capacity of HSC-iNKT cells for enhancing NK cell-mediated killing of tumor cells, utilizing an *in vitro* NK adjuvant effect assay (**Figure 2-9F**). A K562 human myelogenous leukemia cell line, which did not express HLA-I or CD1d, was engineered to express Fluc and EGFP and utilized as the model tumor target to assess NK cell-mediated killing (**Figures 2-10E-2-10G**). αGC was used as a surrogate tumor-derived lipid antigen to stimulate HSC-iNKT cells. Antigen-stimulated HSC-iNKT cells significantly enhanced the activation and tumor cell-killing efficacy of NK cells (**Figures 2-9G-2-9I**), likely through secreting NK cell-activation cytokines, including IFN-γ and IL-2 (**Figure 2-10H**). Therefore, HSC-iNKT cells can function as an effective cellular adjuvant to enhance NK cell-mediated killing of tumor cells.

Subsequently, we evaluated the ability of HSC-iNKT cells for boosting DC- and CTL-mediated antitumor activities, using an *in vitro* DC/CTL adjuvant effect assay (**Figure 2-9J**).

DC-stimulated CTL response to NY-ESO-1, a well-studied tumor antigen common in many cancers, was analyzed [76]. Monocyte-derived dendritic cells (MoDCs) were generated from HLA-A2$^+$ healthy donor PBMCs (Figures S6A and S6B); these MoDCs expressed CD1d as well as HLA-A2 and thus could present αGC to stimulate HSC-iNKT cells, and also present NY-ESO-1 peptide (ESOp) to activate ESO-specific CD8$^+$ CTLs (denoted as ESO-T cells) (**Figures 2-11C and 2-11D**). ESO-T cells were derived *in vitro* from ESO TCR gene-engineered human CD34$^+$ HSCs by growing these HSCs in an Artificial Thymic Organoid (ATO) culture followed by antigen expansion (**Figures 2-11E and 2-11F**) [77]. In the presence of αGC, HSC-iNKT cells efficiently promoted the maturation of MoDCs as evidenced by the upregulation of co-stimulatory marker CD86 on MoDCs (**Figures 2-9K and 2-9L**). MoDCs matured by HSC-iNKT cells showed significantly enhanced capacity to present ESOp tumor antigens, thereby inducing greatly increased activation and expansion of ESO-T cells and resulting in enhanced ESO-T cell mediated killing of target tumor cells (**Figures 2-12M-2-12N and 2-11G-2-11H**). Therefore, HSC-iNKT cells can function as an effective cellular adjuvant to boost DC/CTL antitumor activities.

Lastly, we evaluated the potential of HSC-iNKT cells in inhibiting tumor-associated macrophages (TAMs), utilizing an *in vitro* macrophage inhibition assay (**Figure 2-9O**). Human CD14$^+$ monocytes isolated from healthy donor PBMCs were used in this study (**Figure 2-11I**). These monocytes expressed CD1d (**Figure 2-11J**); when loaded with αGC as a surrogate tumor-derived lipid antigen, these monocytes stimulated HSC-iNKT cells (evidenced by upregulation of CD69 on HSC-iNKT cells; **Figures 2-12P and 2-12Q**) and were quickly killed by HSC-iNKT cells (**Figures 2-12R and 2-12S**). Therefore, HSC-iNKT cells have the potential to inhibit TAMs in a CD1d/antigen-dependent manner.

Taken together, these results indicate that HSC-iNKT cells are capable of deploying multiple mechanisms to attack tumor cells, attesting to their multifaceted cancer therapy potential.

In Vivo Antitumor Efficacy of HSC-iNKT Cells Against Hematologic Malignancies in a Human Multiple Myeloma Xenograft Mouse Model

In vivo antitumor efficacy of HSC-iNKT cells against hematologic malignancies was studied using a human multiple myeloma (MM) xenograft NSG mouse model (**Figure 2-12A**). The pre-established MM.1S-hCD1d-FG human MM cell line was utilized for this study (**Figure 2-10A**). MM.1S-hCD1d-FG cells were inoculated intravenously (i.v.) into NSG mice to establish disease, followed by i.v. injection of HSC-iNKT cells and monitoring of HSC-iNKT cell therapeutic effects (**Figure 2-12A**). This tumor model allowed the *in vivo* study of direct killing of $CD1d^+$ blood cancer cells by HSC-iNKT cells (**Figure 2-10E**). HSC-iNKT cells showed a robust suppression of MM, as evidenced by a significant decrease of total body luminescence measured by BLI (**Figures 2-12B and 2-12C**). Terminal tissue collection and flow cytometry analysis confirmed a significant reduction of GFP^+ tumor cells in multiple tissues, particularly in the bone marrow, which is the primary site of MM, and in the liver, which is another major MM site in this model (**Figures 2-12D and 2-12E**). Correspondingly, flow cytometry analysis detected the presence of HSC-iNKT cells in various tumor-residing tissues (**Figure 2-12F**). In particular, high numbers of HSC-iNKT cells homed to the areas of MM involvement, including bone marrow and liver (**Figure 2-12F**), where these HSC-iNKT cells displayed an activated phenotype ($CD62L^{lo}CD69^{hi}$) correlating with their antitumor function (**Figures 2-12G-2-12I**). The antitumor efficacy of HSC-iNKT cells was robust and consistent for all three donors that we studied (**Figure 2-12A**). The suppression of MM in the MM.1S-CD1d-FG model was mediated by HSC-iNKT cells through a CD1d-dependent tumor recognition and suppression mechanism, because HSC-iNKT cells did not exhibit tumor suppression effects and were not enriched at tumor sites in the control MM.1S-FG model which lacked the expression of CD1d

(**Figures 2-12J-2-12L**). These data demonstrated the *in vivo* antitumor efficacy of HSC-iNKT cells and support their therapeutic potential against hematologic malignancies.

In Vivo Antitumor Efficacy of HSC-iNKT Cells Against Solid Tumors in a Human Melanoma Xenograft Mouse Model

To evaluate the *in vivo* antitumor efficacy of HSC-iNKT cells against solid tumors, we developed a human melanoma xenograft NSG mouse model that supports the study of *in vivo* direct killing of $CD1d^{+}$ solid tumor cells by HSC-iNKT cells (**Figure 2-13A**). An A375-hCD1d-hIL-15-FG human melanoma cell line and a control A375-hIL-15-FG melanoma cell line were generated for this study (**Figures 2-14A and 2-14B**). When co-cultured *in vitro*, HSC-iNKT cells effectively killed the A375-hCD1d-hIL-15-FG cells in a CD1d/antigen dependent manner (**Figures 2-14C-2-14F**). For the *in vivo* study, A375-hIL-15-hCD1d-FG cells loaded with αGC were subcutaneously inoculated into NSG mice to form solid tumors, followed by i.v. injection of HSC-iNKT cells and monitoring of tumor growth (**Figure 2-13A**). We detected a significant suppression of tumor growth by HSC-iNKT cells, analyzed by time-course BLI (**Figures 2-13B and 2-13C**), measurement of tumor size over time (Figure 7D), and terminal tumor weight assessment (**Figure 2-13E**). Terminal tissue collection and flow cytometry analysis revealed a highly efficient infiltration of HSC-iNKT cells into solid tumors (**Figure 2-13F**). The targeted homing of HSC-iNKT cells to the tumor sites was impressive, as much smaller numbers of HSC-iNKT cells were detected in all other tissues examined (blood, spleen, and liver), likely due to the expression of inflammatory site-homing markers on HSC-iNKT cells (e.g. $CD62L^{lo}CXCR3^{hi}$) (**Figures 2-13F and 2-7F**). The capacity of human iNKT cells to effectively home to and infiltrate solid tumors is considered one of the most attractive features of iNKT cells for cancer immunotherapy. HSC-iNKT cells isolated from tumors displayed a highly active phenotype ($CD62L^{lo}CD69^{hi}$) compared to HSC-iNKT cells isolated

from non-tumor tissues like the liver, corresponding with their antitumor activities (**Figures 2-13G-2-13I**). The suppression of solid tumor growth in the A375-hIL-15-hCD1d-FG model was mediated by HSC-iNKT cells through a CD1d-dependent direct killing mechanism, because HSC-iNKT cells did not induce tumor suppression in the control A375-hIL-15-FG model which lacked the expression of CD1d (**Figures 2-13J-2-13L and 2-14G-2-14H**). Taken together, these *in vivo* results demonstrated the therapeutic potential of HSC-iNKT cells for treating solid tumors. In particular, the capacity of HSC-iNKT cells to effectively traffic to the tumor sites and infiltrate solid tumors is highly desirable for cancer immunotherapy.

DISCUSSION

HSC transplantation (HSCT) has a history of over half a century and has been utilized routinely to treat a variety of malignant and non-malignant hematopoietic disorders. Over the last decade, gene-engineered HSCT has undergone rapid development and has shown great promise for treating diseases like monogene-related immunodeficiencies [78]. Safe and efficient gene delivery vectors have been developed, and robust HSC gene modification protocols have been established. In 2016, the first gene-engineered HSCT therapy product received marketing authorization from the European Medicines Agency, marking a major milestone and paving the way for this new class of cell therapy drugs [78]. Therefore, both the technology and clinical platforms are ready to translate the intended HSC-iNKT cell therapy.

HSCT for treating hematologic malignancies can be performed using patients' autologous HSCs (referred to as auto-HSCT), or using allogeneic HSCs from HLA-matched or HLA-haploidentical donors and cord blood units (referred to as allo-HSCT) [78]. Because HSC-iNKT cells are selected by non-polymorphic CD1d molecule, HSC-iNKT therapy can be utilized in both auto-HSCT and allo-HSCT settings (**Figure 2-3I**). Interestingly, it has been reported that

in allo-HSCT recipients with various hematologic malignancies, the occurrences and levels of donor-derived iNKT cells positively correlated with cancer remission and overall survival while negatively correlated with GvHD [30,31,39]. In our experiments, we observed a significant reduction of GvHD symptoms in BLT-iNKT mice compared to those in control BLT mice, supporting the anti-GvHD effects of HSC-iNKT cells (**Figures 2-5D-2-5G**). Overall, it is plausible to propose that HSC-iNKT cell therapy performed in an allo-HSCT setting may provide cancer patients with dual benefits of cancer suppression and GvHD prevention. HSCT are routinely performed in the US and around the world at well-established clinical centers. In 2016 in the US alone, about 15,000 cases of auto-HSCT and 8,000 cases of allo-HSCT were performed, predominantly for treating MM, MDS, and acute leukemia. These existing therapeutic needs and clinic resources can greatly facilitate the clinical development and possible future application of HSC-iNKT cell therapy for treating hematologic malignancies, which if successful, can be extended to treat solid tumors [55,56].

Generation of HSC-engineered iNKT cells requires a functional thymus. Aging-related degeneration of human thymus in many cancer patients therefore may be a concern [79]. Clinical studies of adult cancer patients receiving HSC transfer were reported previously, showing the reconstitution of iNKT cells in these patients [30,80]. These clinical data support the likelihood that HSC-iNKT therapy can benefit aged cancer patients.

Increasing iNKT cells in cancer patients may have certain risks, including possible toxicity and interference of immune surveillance. The levels of iNKT cells achievable in cancer patients may also be limited by the availability of host supporting factors such as homeostatic cytokines. These concerns can be greatly alleviated through controlling the iNKT cell outputs via controlling the HSC gene-engineering rates (**Figures 2-3H and 2-2E**). iNKT cell levels range widely in human population; the high end can reach ~5% of iNKT cells in blood of healthy individuals. For clinical trial design, an initial dose targeting ~5% iNKT cells in blood may be

a rational starting point: 1) this level exists in healthy individuals and therefore should be physiological safe and possible to achieve, and 2) this level represents over 100-1,000 folds increase of iNKT cells in cancer patients and likely can exhibit certain therapeutic effects. After the 5% initial dose proven to be possible and tolerable, dose escalation (up or down) may follow. Of course, all need to be tested clinically. Notably, besides the dosage design, we have engineered an additional safety control for the intended HSC-iNKT therapy, by incorporating an sr39TK suicide gene in the iNKT TCR gene delivery vector (**Figures 2-1C and 2-1G**). This engineered safety control will allow the effective depletion of engineered iNKT cells (and their engineered progenitor HSCs) through GCV administration in case of a safety need (**Figures 2-4 and 2-6**).

In our study, HSC-iNKT cells suppressed tumor growth but did not eliminate tumor cells, suggesting that the efficacy of HSC-iNKT therapy may be further improved through combining with other therapeutic modalities. For instance, adoptive transfer of αGC-loaded DCs into cancer patients has been demonstrated to be safe and effective in stimulating human iNKT cells *in vivo;* therefore, it is plausible to propose that a combination of HSC-iNKT cell therapy with DC/αGC vaccination would maximize the therapeutic potential of the engineered HSC-iNKT cells [55,56]. Alternatively, iNKT cells in cancer patients have been shown to express high levels of T cell-exhaustion marker PD-1[81]. In our *in vivo* study, we detected the upregulation of PD-1 on HSC-iNKT cells isolated from tumor sites in both the human MM and melanoma xenograft models. It is therefore conceivable that a combination of HSC-iNKT cell therapy with the PD-1/PD-L1 blockade therapy may also produce synergistic therapeutic effects [82]. Moreover, recent studies showed promising cancer therapy potential of chimeric antigen receptor (CAR)-engineered iNKT cells; therefore further engineering HSC-iNKT cells to express CAR to enhance their tumor-targeting effectiveness may represent another attractive approach [37,47,83].

One of the most attractive features of iNKT cells is their capacity to attack tumors through multiple mechanisms (**Figure 2-9**). Notably, compared to the direct killing mechanism, other indirect adjuvant/regulatory mechanisms of HSC-iNKT cells could be even more powerful and more valuable for cancer therapy, especially for treating solid tumors that largely do not express CD1d or only express low levels of CD1d. Because of the limitation of current human tumor xenograft models, which are primarily designed to study the direct killing of tumor cells, we only examined the direct tumor-killing effect of HSC-iNKT cells *in vivo* (**Figures 2-12 and 2-13**). A complete study and full appreciation of the potential of HSC-iNKT cells *in vivo* requires an animal model supporting the engraftment of various human effector immune cells (NK, DC, CTL, TAM) and supporting the *in vivo* function of these human immune cells, and ideally also supporting the engraftment of primary human tumor cells rather than just human tumor cell lines, which remains a challenging task [84]. The development of next-generation humanized mouse models, that are based on NSG (NOD/SCID/$\gamma c^{-/-}$) or BRG (BALB/cA/$RAG2^{-/-}\gamma c^{-/-}$) mice engineered to express human immune cell-supporting cytokines/molecules (e.g. SIRPα, TPO, IL-3, GM-CSF, M-CSF), may provide new opportunities to incorporate various human immune cells in a human tumor xenograft model and allow for *in vivo* study of the multifaceted antitumor mechanisms of human iNKT cells [85]. Nonetheless, in our previous mouse study using immune-competent animals, we proved that HSC-engineered mouse iNKT cells effectively suppressed tumor growth in a syngeneic B16 melanoma mouse model. Because the B16 tumor cells utilized in that study do not express CD1d, antitumor effects in that mouse study were considered to be mediated by the adjuvant and TAM suppression effects of HSC-iNKT cells [42,86].

In summary, here we report the pre-clinical development of an HSC-iNKT cell therapy that has the potential to treat a broad range of hematologic malignancies and solid tumors and that is ready to translate into clinical development. Our study also established a humanized BLT-

iNKT mouse model that can be utilized as a valuable tool to study human iNKT cell biology and human iNKT cell-based immunotherapy. Interestingly, compared to native human iNKT cells expanded from healthy donor peripheral blood, HSC-iNKT cells generated in BLT-iNKT mice were more prone to differentiate into DN/$CD8^+$ subtype producing T_H1 cytokines (such as IFN-γ) post-antigen stimulation. It could be an interesting topic for future study to find out whether this is a special phenomenon of the BLT-iNKT mouse model or a common feature of HSC-engineered human iNKT cells. The latter may suggest a unique advantage of HSC-iNKT therapy because DN/$CD8^+$ and T_H1-like human iNKT cells are generally considered most valuable for cancer therapy.

Acknowledgements

We gratefully thank D. Baltimore (California Institute of Technology) and J. Economou (UCLA) for advising this study. We thank the University of California, Los Angeles (UCLA) animal facility for providing animal support; the UCLA Translational Pathology Core Laboratory (TPCL) for providing histology support; the UCLA AIDS Institute/CFAR Virology Core/Gene and Cell Therapy Core/Humanized Mouse Core for providing human cells and tissues and humanized mice services; the UCLA BSCRC Flow Cytometry Core Facility for cell sorting support; the US National Institutes of Health Tetramer Core Facility for providing the hCD1d/PBS-57 tetramer reagents; N. Rozengurt (UCLA) for providing pathology analysis support; P. Wang (University of Southern California, USC) for critical reading of this manuscript; and E.L. Siegler for editing the manuscript. This work was supported by a Director's New Innovator Award from the National Institutes of Health (NIH DP2 CA196335, to L.Y.), a Partnering Opportunity for Translational Research Projects Award from the California Institute for Regenerative Medicine (CIRM TRAN1-08533, to L.Y.), a Stem Cell Research Award from the Concern Foundation (to L.Y.), a Research Career Development

Award from the STOP CANCER Foundation (to L.Y.), and a BSCRC-RHF Research Award from the Rose Hills Research Foundation (to L.Y.). D.J.S. is a predoctoral fellow supported by the UCLA Tumor Immunology Training Grant (USHHS Ruth L. Kirschstein Institutional National Research Service Award # T32 CA009056). J.Y. is a predoctoral fellow supported by the UCLA Broad Stem Cell Center (BSCRC) Predoctoral Fellowship.

Author contributions

Y.Z., D.J.S. and L.Y. designed the experiments, analyzed the data, and wrote the manuscript. L.Y. conceived and oversaw the study, with the assistance from Y.Z., and with suggestions from S.K., D.S.A., S.H, P.K., S.D.O., C.S., S.L., S.F., J.H., J.E., J.Z., G.C., C.R., A.R., D.B.K., and O.W.. Y.Z. and D.J.S. performed all experiments, with the assistance from Y.Z., Y.L., J.Y., D.L., Y.W., S.D.B., C.H., J.K., T.T., L.J.L., A.T.P., and H.M.. J.M. assisted with TCR cloning. D.C. performed cell sorting. R.H. helped with lentivirus production. B.C.F. and F.U. helped with vector copy analysis. B.B.M. and M.M. helped with PBSC isolation. L.W. and L.P. performed PET/CT imaging and analyzed data. V.R. performed BLT surgeries. D.J. and X.W. helped with the statistical analysis of data.

Figures

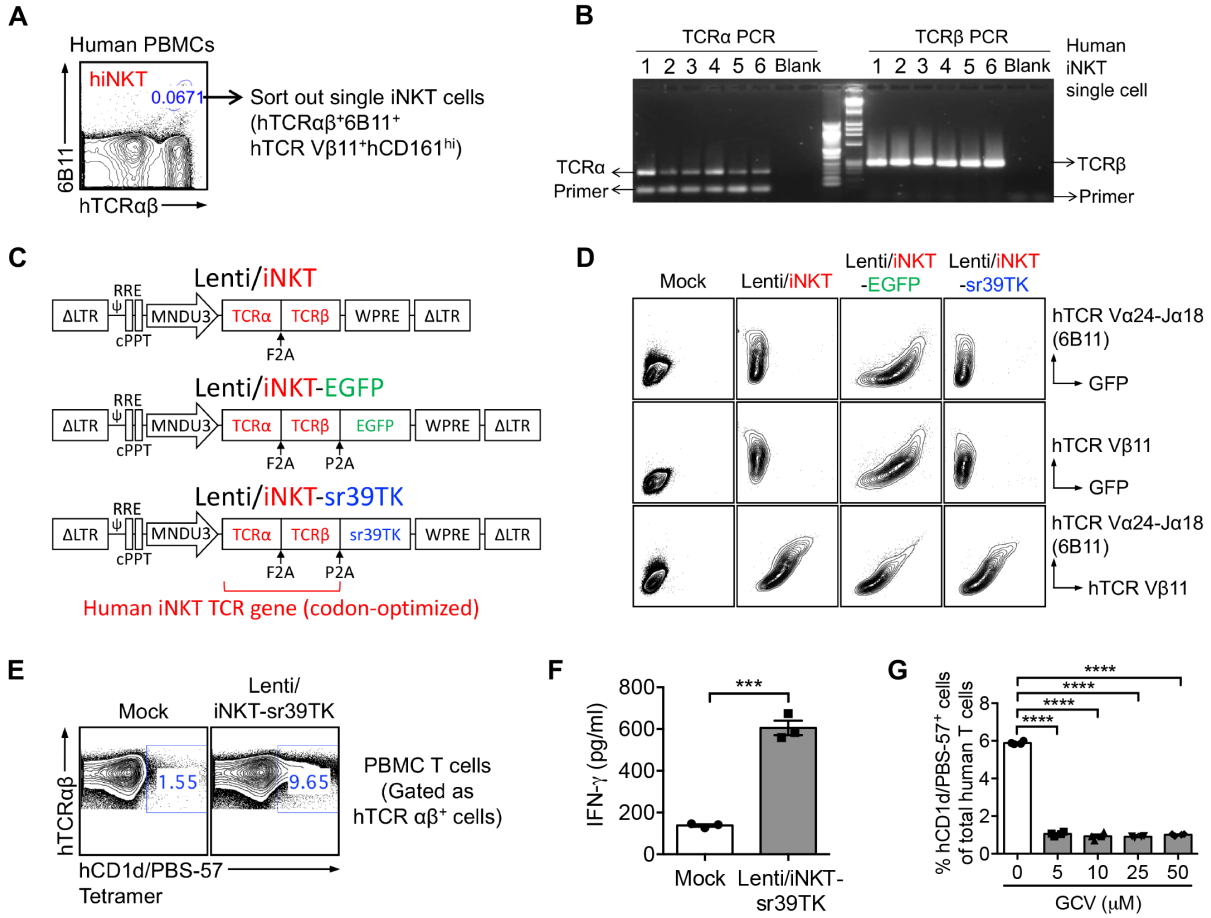

Figure 2-1. Cloning of Human Invariant Natural Killer T Cell Receptor (iNKT TCR) Genes and Construction of Lentiviral Gene Delivery Vectors.

(A-B) Cloning of human iNKT TCR genes using a single-cell RT-PCR approach. (A) FACS sorting of single human iNKT cells. (B) Representative DNA gel image showing the human TCR α and β chain PCR products from six sorted single iNKT cells.

(C) Schematic of the Lenti/iNKT, Lenti/iNKT-EGFP, and Lenti/iNKT-sr39TK vectors.

(D) FACS detection of intracellular expression of iNKT TCRs (identified as hTCR Vβ11$^+$6B11$^+$) in 293T cells transduced with the indicated iNKT TCR gene delivery lentivectors.

(E-G) Functional characterization of the Lenti/iNKT-sr39TK vector. Human PBMC T cells were transduced with the Lenti/iNKT-sr39TK vector, then subjected to functional tests. (E) FACS detection of surface iNKT TCR expression on vector-transduced PBMC T cells. (F) ELISA analysis of IFN-γ production by vector-transduced PBMC T cells one day post-αGC stimulation (n = 3). (G) FACS quantification of the depletion of vector-transduced PBMC T cells (gated as hCD1d/PBS-57$^+$ cells among total hTCRαβ$^+$ cells) at day 4 post GCV treatment (n = 4).

Representative of 2 experiments. Data are presented as the mean ± SEM. ***P < 0.001, ****P < 0.0001, by Student's *t* test.

A

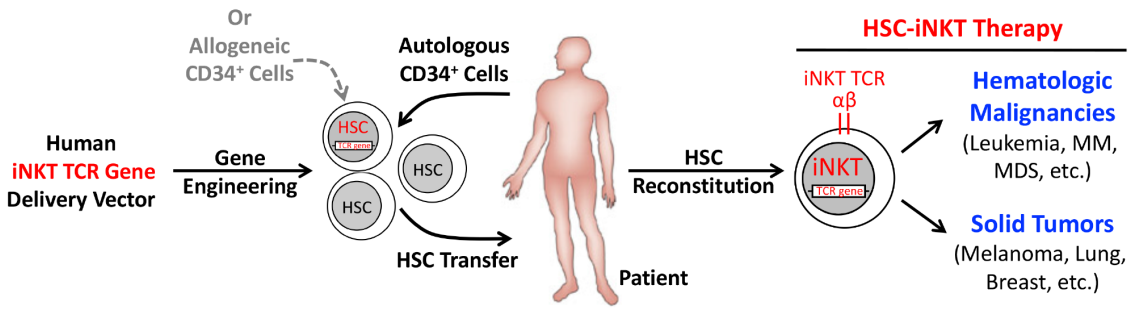

B

Vector Titer (Lenti/iNKT-sr39TK)			
Titer (TU/ml)	**Average**	**STDEV**	**%CV**
Un-Concentrated Supernatant	8.27×10^5	6.40×10^4	7.73%
Concentrated Supernatant (2000x fold)	5.30×10^9	2.55×10^8	4.90%

C

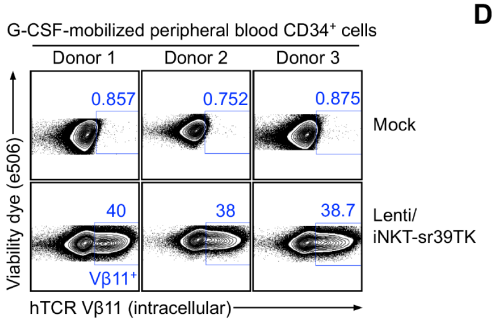

D

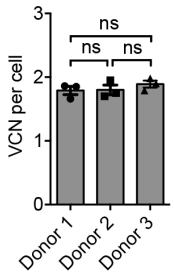

E

Transduction of G-CSF mobilized CD34⁺ HSCs (1 x 10^6)				
Lenti/iNKT-sr39TK (TU)	0	1 x 10^8	2 x 10^8	4 x 10^8
% Vβ11⁺	0	19%	39%	51%
VCN	0	1.28	1.73	1.98

Figure 2-2. Development of a hematopoietic stem cell-engineered invariant natural killer T (HSC-iNKT) cell therapy.

(A) Schematic representation of the concept of HSC-iNKT cell therapy. Autologous or allogeneic human CD34⁺ HSCs will be collected and engineered *in vitro* with a human iNKT TCR gene, followed by adoptive transfer into cancer patients. Post-HSC reconstitution, iNKT TCR gene-engineered HSCs will continuously produce human iNKT cells. This therapy has the potential to provide cancer patients with therapeutic levels of iNKT cells for a life time. HSC-iNKT cell therapy may benefit patients with a broad range of cancers, including various hematologic malignancies and solid tumors. MM, multiple myeloma; MDS, myelodysplastic syndromes.

(B) Titer of the Lenti/iNKT-sr39TK vector. A 4-liter batch of Lenti/iNKT-sr39TK lentiviral vector was produced using a 293T virus packaging cell line transient transfection method, followed by concentration to 2 ml (2000x fold) using an established tandem tangential filtration method. Vector titers prior to and post-concentration were measured by transducing HT29 cells with serial dilutions and performing Droplet Digital PCR (ddPCR) (n = 3). TU, transduction unit.

(C-D) Transduction of HSCs with the Lenti/iNKT-sr39TK vector. G-CSF-mobilized peripheral blood CD34⁺ HSCs from three healthy donors were studied. Concentrated Lenti/iNKT-sr39TK vector were added to HSC cultures (2 x 10^8 TU per 1 x 10^6 HSCs). Three days later, HSCs were collected and analyzed for intracellular expression of iNKT TCR

(identified as hTCR Vβ11$^+$) using flow cytometry. (C) Representative FACS plots. (D) Quantification of C (n = 3).

(E) Titrated transduction of HSCs with the Lenti/iNKT-sr39TK vector. Representative data studying G-CSF-mobilized peripheral blood CD34$^+$ HSCs from a selected donor were presented. Titrated amount of concentrated Lenti/iNKT-sr39TK vector were added to HSC cultures. Three days later, a portion of HSCs were collected and analyzed for intracellular expression of iNKT TCR (identified as hTCR Vβ11$^+$) using flow cytometry. 14 days later, the remaining HSCs were collected and analyzed for vector copy number (VCN) using droplet digital PCR (ddPCR). Note the correlation between vector titers and transduction rates. Average VCN per cell at all transduction rates remained between 1-3, which is considered to be a relative safe range for lentivector-mediated gene therapy.

Representative of 2 experiments. Data were presented as the mean ± SEM. ns, not significant, by 1-way ANOVA (D).

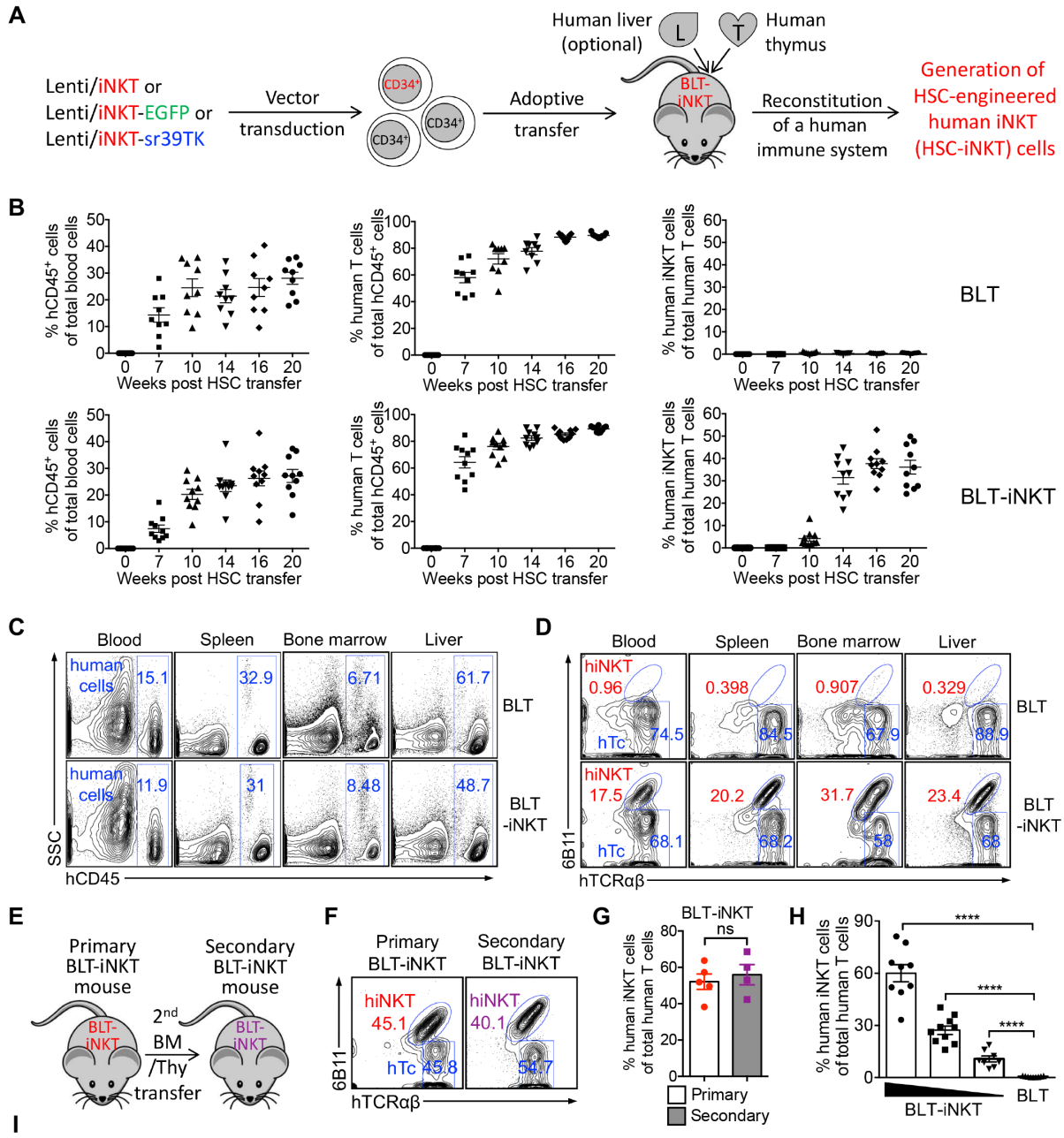

Successful generation of HSC-engineered human iNKT cells in a BLT humanized mouse model	
Human iNKT TCR vectors	Lenti/iNKT; Lenti/iNKT-EGFP; Lenti/iNKT-sr39TK
Human CD34$^+$ HSCs	cord blood CD34$^+$ cells (one donor); fetal liver CD34$^+$ cells (> 3 donors); healthy donor G-CSF-mobilized peripheral blood CD34$^+$ cells (> 3 donors)
Human thymus	fetal thymus (> 20 donors); postnatal thymus (one donor, 14 years old)

Note: Human CD34$^+$ HSCs and human thymus do no need to be donor- or HLA-matched.

Figure 2-3. Generation of Hematopoietic Stem Cell-Engineered Human iNKT (HSC-iNKT) Cells in BLT-iNKT Humanized Mice.

(A) Experimental design to generate HSC-iNKT cells in a BLT humanized mouse model.

(B-D) Generation of HSC-iNKT cells in BLT-iNKT mice (produced using human fetal thymus and Lenti/iNKT-sr39TK vector-transduced PBSCs). (B) Time-course FACS monitoring of human immune cells (gated as hCD45$^+$ cells of total mononuclear cells), human αβ T cells (gated as hTCRαβ$^+$ cells of total hCD45$^+$ cells), and human iNKT cells (gated as 6B11$^+$ cells

of total hTCR$\alpha\beta^+$ cells) in the peripheral blood of BLT-iNKT mice and control BLT mice post-HSC transfer (n = 9-10). (C) FACS detection of human immune cells (gated as $hCD45^+$ cells) in various tissues of BLT-iNKT and control BLT mice, at week 20 post HSC transfer. (D) FACS detection of HSC-iNKT cells in various tissues of BLT-iNKT mice, at week 20 post-HSC transfer. hiNKT, human iNKT cells (gated as hTCR$\alpha\beta^+6B11^+$ cells of total $hCD45^+$ cells); hTc, conventional human αβ T cells (gated as hTCR$\alpha\beta^+6B11^-$ cells of total $hCD45^+$ cells).

(E-G) Long-term production of HSC-iNKT cells in BLT-iNKT mice. Data from a representative secondary HSC transfer experiment were presented, wherein the primary BLT-iNKT mice were generated using human fetal thymus and Lenti/iNKT vector-transduced PBSCs. (E) Experimental design. BM, total bone marrow cells harvested from the primary BLT-iNKT mice; Thy, human thymus implants collected from the primary BLT-iNKT mice. (F) FACS detection of HSC-iNKT cells in the peripheral blood of the secondary BLT-iNKT mice at week 16 after the secondary BM/Thy transfer. (G) Quantification of F (n = 4-5).

(H) Controlled production of HSC-iNKT cells in BLT-iNKT mice. PBSCs were transduced with titrated amounts of Lenti/iNKT-sr39TK vector (4×10^8, 2×10^8, or 1×10^8 TU per 1×10^6 PBSCs), followed by adoptive transfer into NSG mice together with human fetal thymus implants to produce BLT-iNKT mice. FACS quantification of human iNKT cells in the blood of indicated BLT-iNKT mice at week 16 post-HSC transfer (n = 8-10).

(I) Table summarizing experiments that have successfully generated HSC-iNKT cells in the BLT human mouse model. HLA, human leukocyte antigen.

Representative of 2 (E-G, H) and over 10 (B-D) experiments, respectively. Data are presented as the mean ± SEM. ns, not significant, ****$P < 0.0001$, by Student's *t* test.

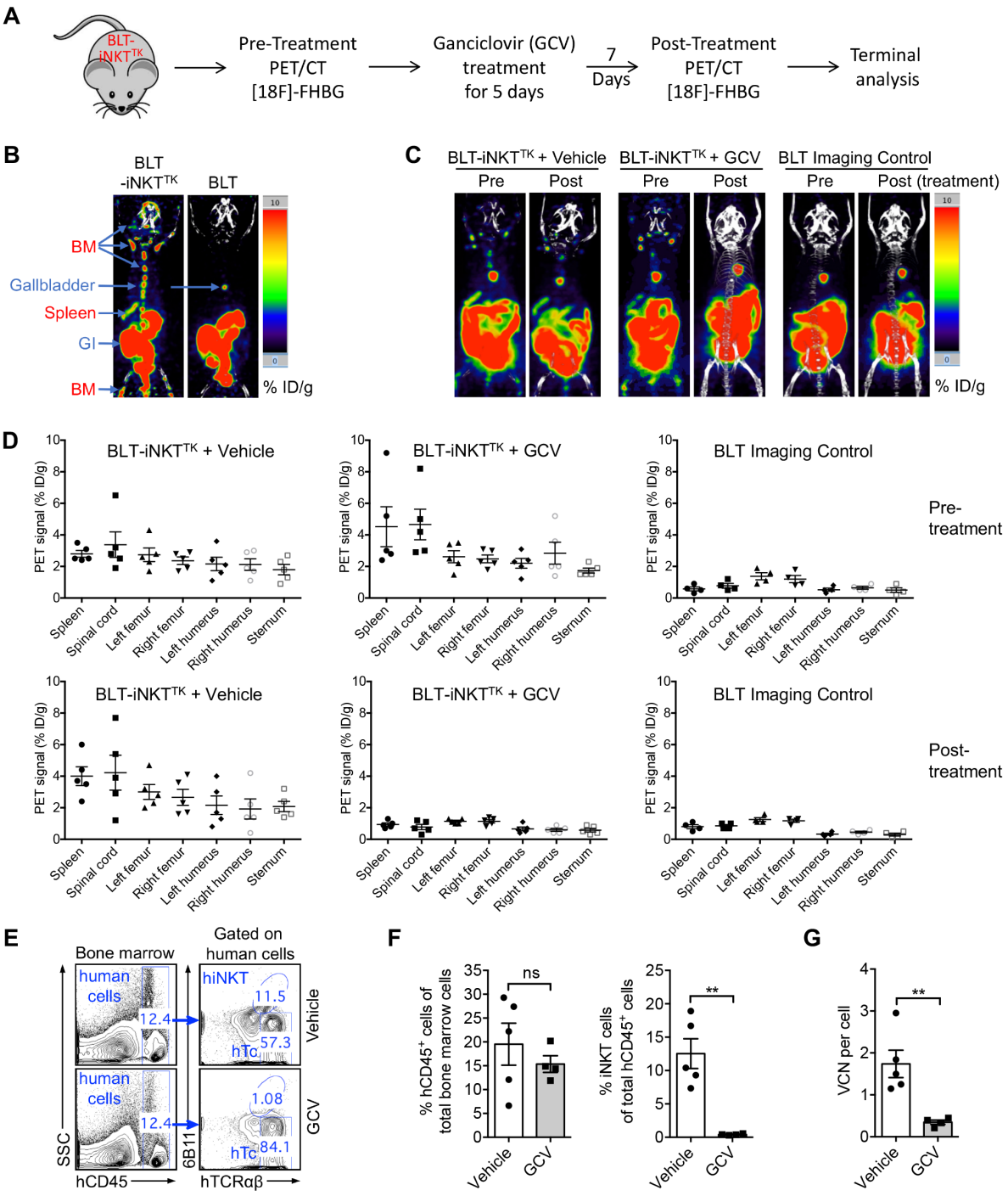

Figure 2-4. Biodistribution and Controlled Depletion of HSC-iNKT Cells in BLT-iNKT Humanized Mice Visualized by PET Imaging.

(A) Experimental design. BLT-iNKT^{TK}, BLT-iNKT mice generated with Lenti/iNKT-sr39TK vector-transduced PBSCs; PET/CT, positron emission tomography-computed tomography;

[18F]-FHBG, a PET reporter probe for imaging sr39TK gene-engineered cells; Ganciclovir (GCV), a drug which selectively ablates sr39TK gene-engineered cells.

(B) Biodistribution of vector-engineered human immune cells. Representative PET/CT images were presented. Note that there were background signals in the gastrointestinal tract (GI) and gallbladder of all mice. BM, bone marrow.

(C-D) PET/CT analysis of controlled depletion of vector-engineered human immune cells in BLT-iNKT^{TK} mice via GCV treatment. (C) Representative PET/CT images. (D) Quantification of C (n = 4-5).

(E-F) FACS validation of controlled depletion of HSC-engineered human iNKT (HSC-iNKT) cells in BLT-iNKT^{TK} mice via GCV treatment. (E) Representative FACS plots of bone marrow cells. (F) Quantification of E (n= 4-5).

(G) Droplet Digital PCR (ddPCR) validation of controlled depletion of vector-engineered human immune cells in BLT-iNKT^{TK} mice via GCV treatment (n = 4-5).

Representative of 2 experiments. Data are presented as the mean ± SEM. ns, not significant, **P < 0.01, by Student's *t* test (F, G).

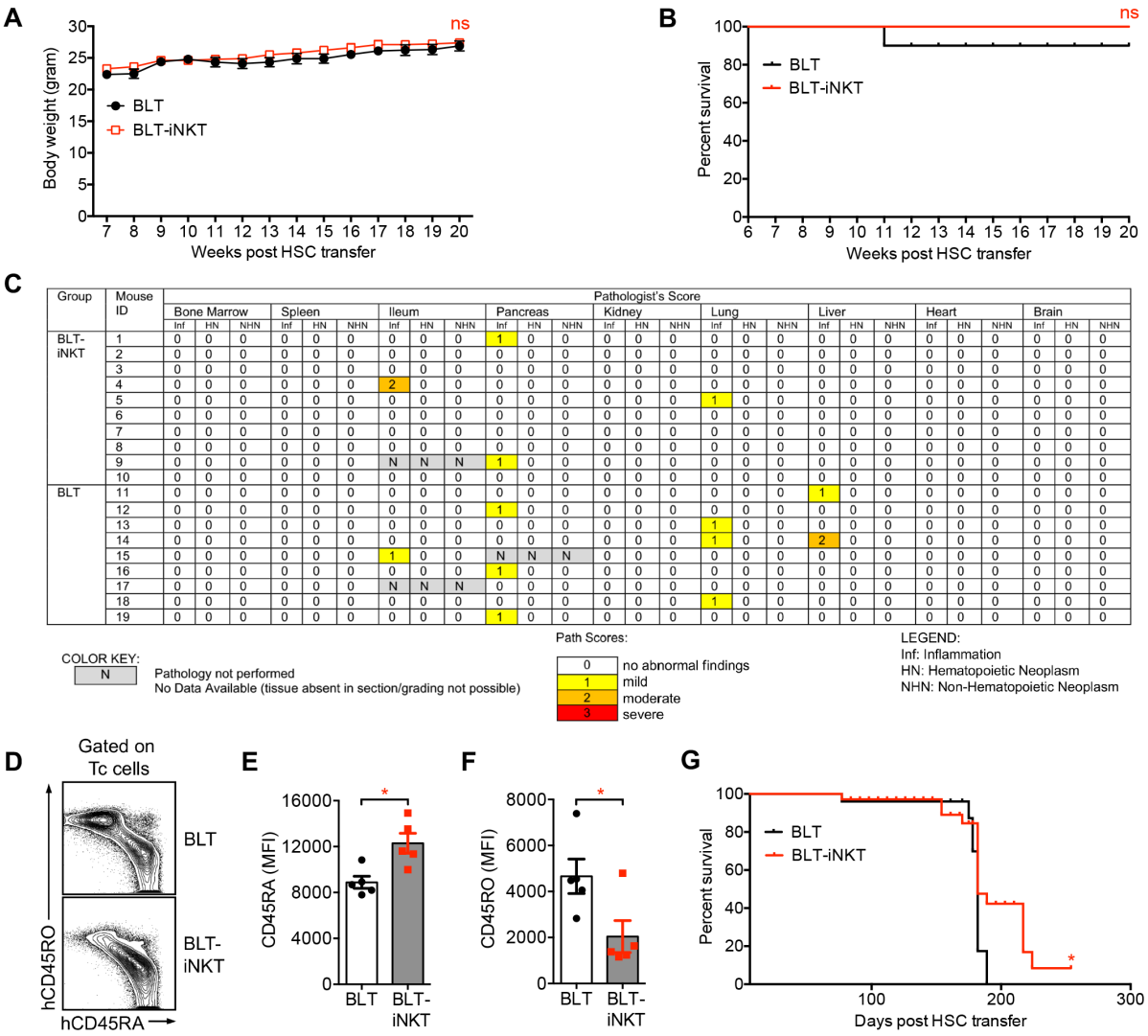

Figure 2-5. Safety study of HSC-iNKT cell therapy in BLT-iNKT humanized mice.

Representative data were presented, studying BLT-iNKT mice produced with human fetal thymus and Lenti/iNKT-sr39TK vector-transduced PBSCs. BLT mice generated in parallel using the same fetal thymus and PBSCs (mock-transduced) were included as a control.

(A-C) Monitoring of BLT-iNKT mice and control BLT mice over a period of 5 months post-HSC transfer, followed by tissue collection and pathological analysis. (A) Mouse body weight (n = 9-10). (B) Kaplan-Meier analysis of mouse survival rate (n = 9-10). (C) Mouse pathology. Various tissues were collected and analyzed by the UCLA Pathology Core. Tissues were analyzed for inflammation (Inf), hematopoietic neoplasm (HN), and non-hematopoietic neoplasm (NHN). Data were presented as pathologist's scores of individual mouse tissues (n = 9-10). 0, no abnormal findings; 1, mild; 2, moderate; 3, severe.

(D-F) Analysis of the auto-activation of human conventional T cells in BLT-iNKT and control BLT mice at 6 months post-HSC transfer. (D) FACS plots showing the expression of CD45RA and CD45RO markers on human T cells isolated from the liver of experimental mice. Tc, human conventional αβ T cells (gated as $hCD45^+hTCR\alpha\beta^+6B11^-$ cells). (E-F) Quantification of E (n = 5). Note that compared to Tc cells isolated from the control BLT mice, Tc cells isolated from the BLT-iNKT mice displayed a less antigen-experienced phenotype (marked as

hCD45RA^{lo}hCD45RO^{hi}), indicating their reduced graft-versus-host (GvH) responses in BLT-iNKT mice.

(G) Kaplan-Meier survival curves of BLT-iNKT mice and control BLT mice over a period of 8 months post-HSC transfer. N = 14-19. Mice were combined from 2 independent experiments.

Representative of 2 experiments. Data are presented as the mean ± SEM. ns, not significant, *P < 0.05, by Student's *t* test (A, E, F) or by log rank (Mantel-Cox) test adjusted for multiple comparisons (B, G).

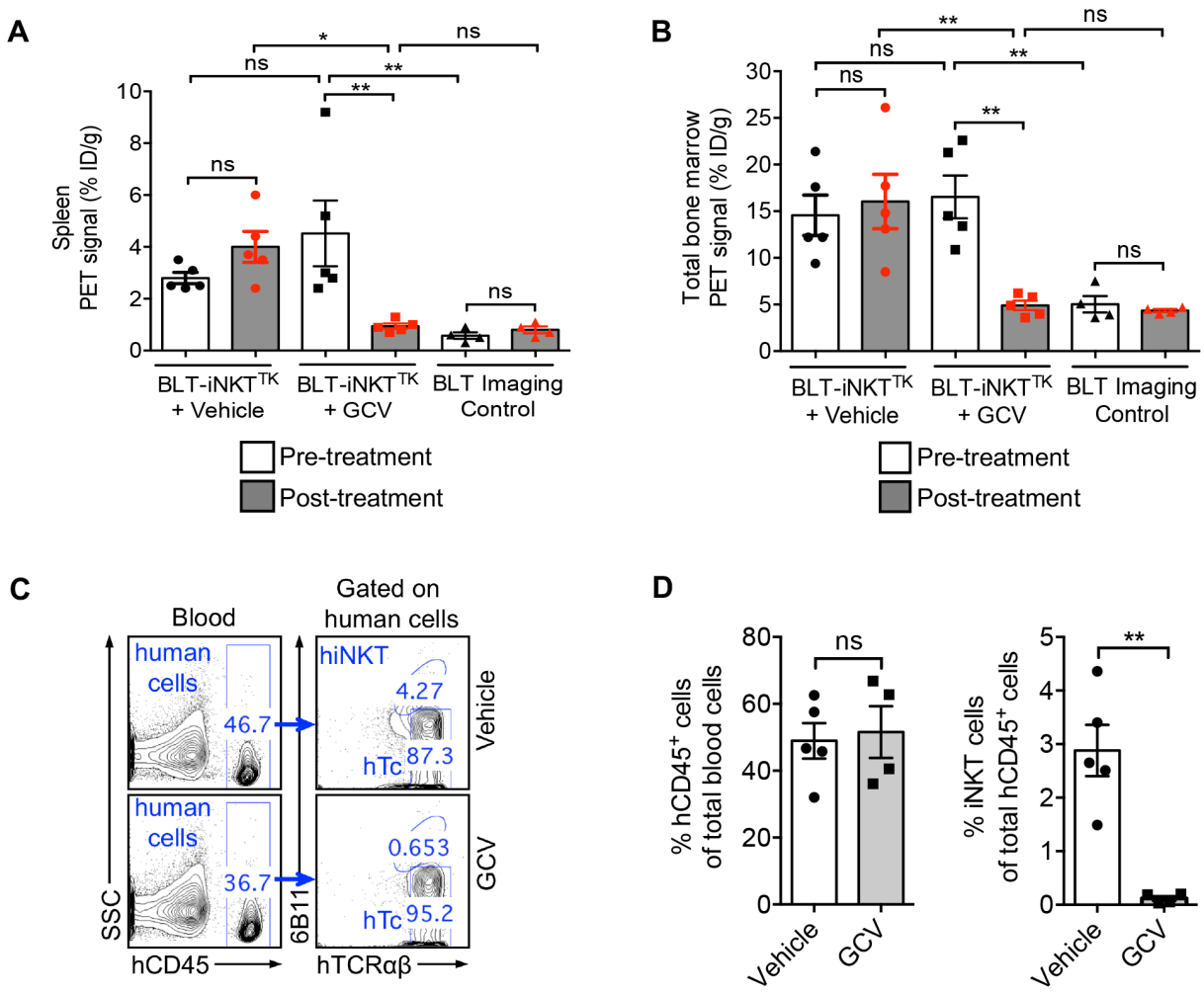

Figure 2-6. Controlled depletion of HSC-iNKT cells in BLT-iNKT humanized mice.

Representative data were presented, studying BLT-iNKT^{TK} mice produced with human fetal thymus and Lenti/iNKT-sr39TK vector-transduced PBSCs. BLT mice generated in parallel using the same fetal thymus and PBSCs (mock-transduced) were included as a control.

(A) Statistical analysis of PET/CT signals in the spleen of BLT-iNKT^{TK} and control BLT mice pre- and post-GCV treatment (n= 4-5).

(B) Statistical analysis of PET/CT signals in the bone marrow of BLT-iNKT^{TK} and control BLT mice pre- and post-GCV treatment (n = 4-5).

(C-D) FACS validation of controlled depletion of HSC-engineered human iNKT (HSC-iNKT) cells in BLT-iNKT^{TK} mice via GCV treatment. (C) Representative FACS plots of blood cells. (D) Quantification of C (n= 4-5). Note the selective depletion of HSC-iNKT cells (gated as hCD45$^+$ hTCRαβ$^+$6B11$^+$ cells) but not the overall human immune cells (gated as total hCD45$^+$ cells) in BLT-iNKT^{TK} mice post-GCV treatment.

Representative of 2 experiments. Data are presented as the mean ± SEM. ns, not significant, *P < 0.05, **P < 0.01, by 1-way ANOVA (A, B) or by Student's *t* test (D).

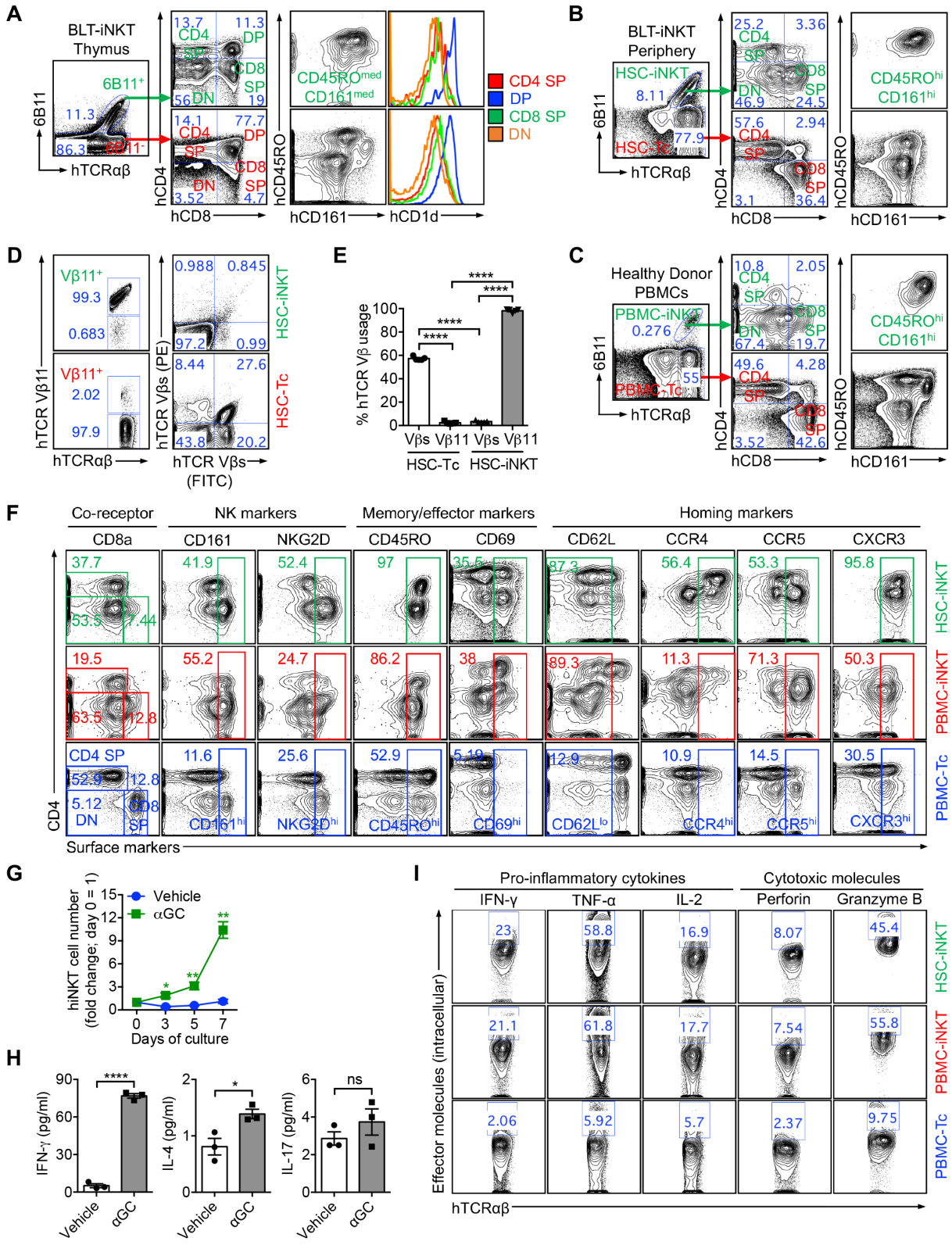

Figure 2-7. Development, Phenotype, and Functionality of HSC-iNKT Cells.

(**A-C**) Development of HSC-iNKT cells. (A) FACS analysis of cells harvested from the human thymus implants of BLT-iNKT mice, showing the detection of developing HSC-iNKT cells (gated as 6B11$^+$ cells; pre-gated on hCD45$^+$ cells) and their surface markers. (B) FACS analysis of cells harvested from the periphery (blood) of BLT-iNKT mice, showing the detection of

mature HSC-iNKT cells (gated as hTCRαβ$^+$6B11$^+$ cells; pre-gated on hCD45$^+$ cells) and their surface markers. (C) FACS analysis of control PBMCs collected from a representative healthy human donor, showing the presence of endogenous human iNKT (PBMC-iNKT) cells (gated as hTCRαβ$^+$6B11$^+$ cells; pre-gated on hCD45$^+$ cells) and their surface markers.

(**D-E**) Allelic exclusion of endogenous TCRs in HSC-iNKT cells. (D) FACS plots showing the TCR Vβ usage by HSC-iNKT cells (pre-gated as hCD45$^+$hTCRαβ$^+$6B11$^+$ cells) and HSC-T$_C$ cells (pre-gated as hCD45$^+$hTCRαβ$^+$6B11$^-$ cells) harvested from the liver of BLT-iNKT mice. hTCR Vβs (FITC) and hTCR Vβs (PE) staining antibodies collectively stained human TCR Vβ 1, 2, 3, 4, 5.1, 5.2, 5.3, 7.1, 7.2, 8, 9, 12, 13.1, 13.2, 13.6, 16, 17, 18, 20, 21.3, and 23. (E) Quantification of D (n = 5).

(**F**) Phenotype of HSC-iNKT cells. FACS plots are presented, showing the surface markers of HSC-iNKT cells isolated from the spleen of BLT-iNKT mice (identified as hCD45$^+$hTCRαβ$^+$6B11$^+$ cells), compared to those of native human iNKT cells and conventional αβ T cells isolated from healthy donor peripheral blood (identified as hCD45$^+$hTCRαβ$^+$6B11$^+$ or hCD45$^+$hTCRαβ$^+$6B11$^-$ cells, denoted as PBMC-iNKT and PBMC-Tc cells, respectively).

(**G-H**) Antigen responses of HSC-iNKT cells. Spleen cells of BLT-iNKT mice were cultured *in vitro* in the presence or absence of αGC (denoted as αGC or Vehicle, respectively) for 7 days. (G) FACS quantification of HSC-iNKT cell expansion over time (n = 3). (H) ELISA analysis of cytokine (IFN-γ, IL-4, IL-17) production at day 7 (n = 3).

(**I**) Production of effector molecules by HSC-iNKT cells. BLT-iNKT mice spleen cells and healthy donor PBMCs were stimulated *in vitro* with αGC for 7 days, followed by flow cytometry analysis of intracellular production of effector cytokines (IFN-γ, TNF-α, and IL-2) and cytotoxic molecules (Perforin and Granzyme B) in HSC-iNKT cells compared to that of the PBMC-iNKT and PBMC-Tc cells.

Representative of 2 experiments. Data are presented as the mean ± SEM. ns, not significant, *P < 0.05, **P < 0.01, ****P < 0.0001, by Student's *t* test.

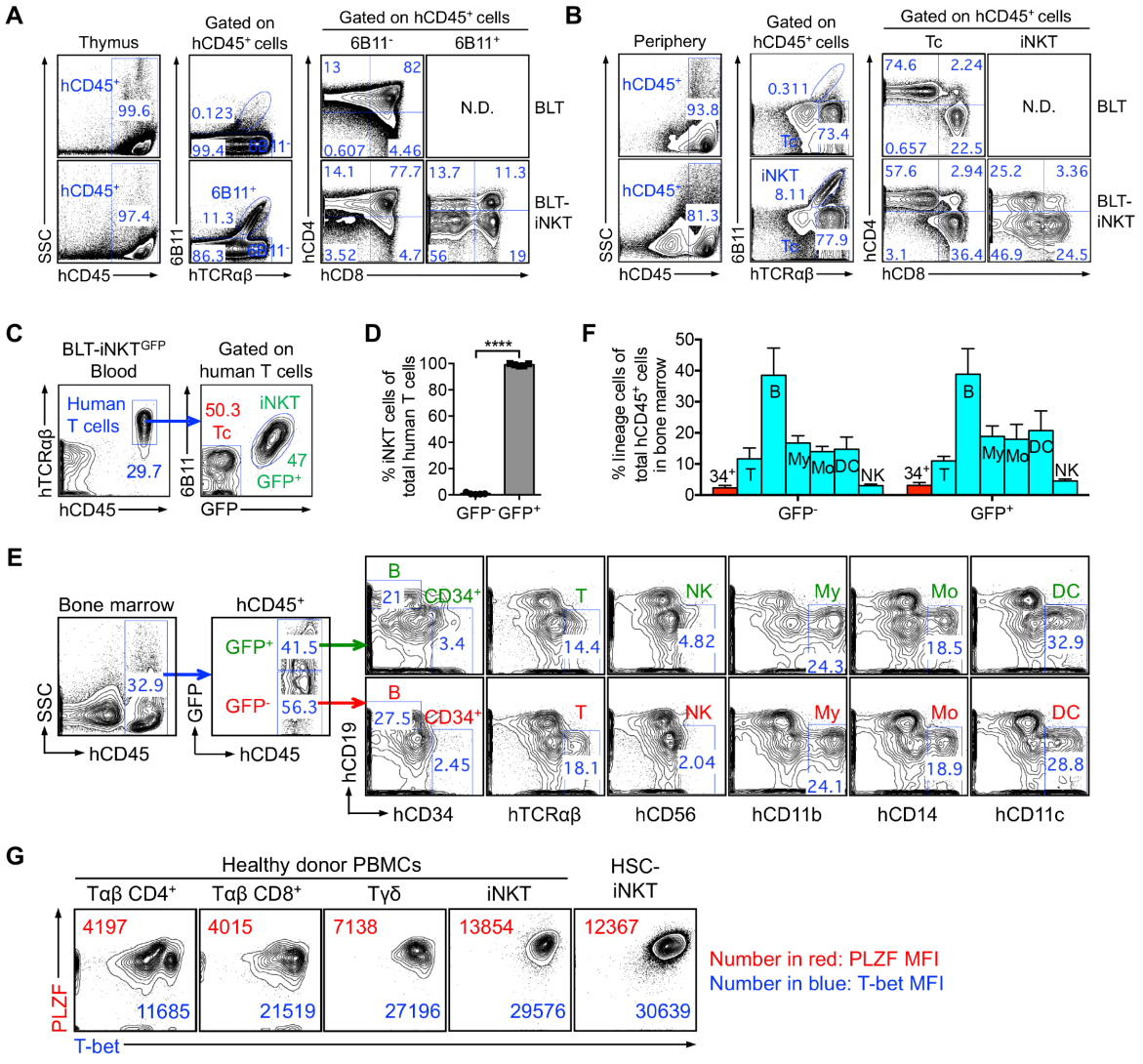

Figure 2-8. Development, phenotype, and functionality of HSC-iNKT cells.

Representative data were presented, studying HSC-iNKT cells generated from BLT-iNKT mice produced with Lenti/iNKT-sr39TK vector (A-B, G) or Lenti/iNKT-EGFP vector (C-F) transduced PBSCs.

(A) FACS plots showing the analysis of cells isolated from the human thymus implants of BLT-iNKT mice and control BLT mice. Note the detection of developing HSC-iNKT cells (gated as $hCD45^{+}hTCR\alpha\beta^{+}6B11^{+}$) in BLT-iNKT mice but not in control BLT mice. N.D., not detected.

(B) FACS plots showing the analysis of cells isolated from the periphery (blood) of BLT-iNKT mice and of control BLT mice. Note the detection of mature HSC-iNKT cells (gated as $hCD45^{+}hTCR\alpha\beta^{+}6B11^{+}$) in BLT-iNKT mice but not in control BLT mice. N.D., not detected.

(C-F) Lineage commitment of iNKT TCR gene-engineered human HSCs. BLT-iNKT mice generated with Lenti/iNKT-EGFP vector-transduced PBSCs were studied (denoted as BLT-iNKT^{GFP} mice). (C) FACS plots showing the analysis of human αβ T cells (pre-gated as hTCR45$^+$hTCRαβ$^+$ cells) present in the blood of BLT-iNKT^{GFP} mice, studying the correlation of GFP expression and iNKT cell (gated as 6B11$^+$) commitment. (D) Quantification of F (n = 5). (E) FACS plots showing the analysis of bone marrow cells of BLT-iNKT^{GFP} mice. (F) Quantification of E, showing the quantification of various lineages of human immune cells within the GFP$^-$ and GFP$^+$ subpopulations (pre-gated as hCD45$^+$GFP$^-$ and hCD45$^+$GFP$^+$, respectively) (n = 5). CD34$^+$ (34$^+$), CD34$^+$ hematopoietic stem and progenitor cells (gated as Lin$^-$hCD34$^+$); T, T cells (gated as hTCRαβ$^+$); B, B cells (gated as hCD19$^+$); My, myeloid cells (gated as hCD11b$^+$); Mo, monocytes/macrophages (gated as hCD14$^+$); DC, dendritic cells (gated as hCD11c$^+$); NK, natural killer cells (gated as hCD56$^+$).

(G) FACS plots showing the intracellular expression of master transcription factors PLZF and T-bet in HSC-iNKT cells. Various lineages of native human T cells isolated from healthy donor peripheral blood were studied as controls, including iNKT cells (identified as hTCRαβ$^+$6B11$^+$ cells), conventional CD4$^+$ αβ T cells (Tαβ CD4$^+$; identified as hTCRαβ$^+$6B11$^-$CD4$^+$CD8$^-$ cells), conventional CD8$^+$ αβ T cells (Tαβ CD4$^+$; identified as hTCRαβ$^+$6B11$^-$CD4$^-$CD8$^+$ cells), and gamma-delta T cells (Tγδ; identified as hTCRγδ$^+$ cells).

Representative of 2 experiments. Data were presented as the mean ± SEM. ****P < 0.0001, by Student's *t* test.

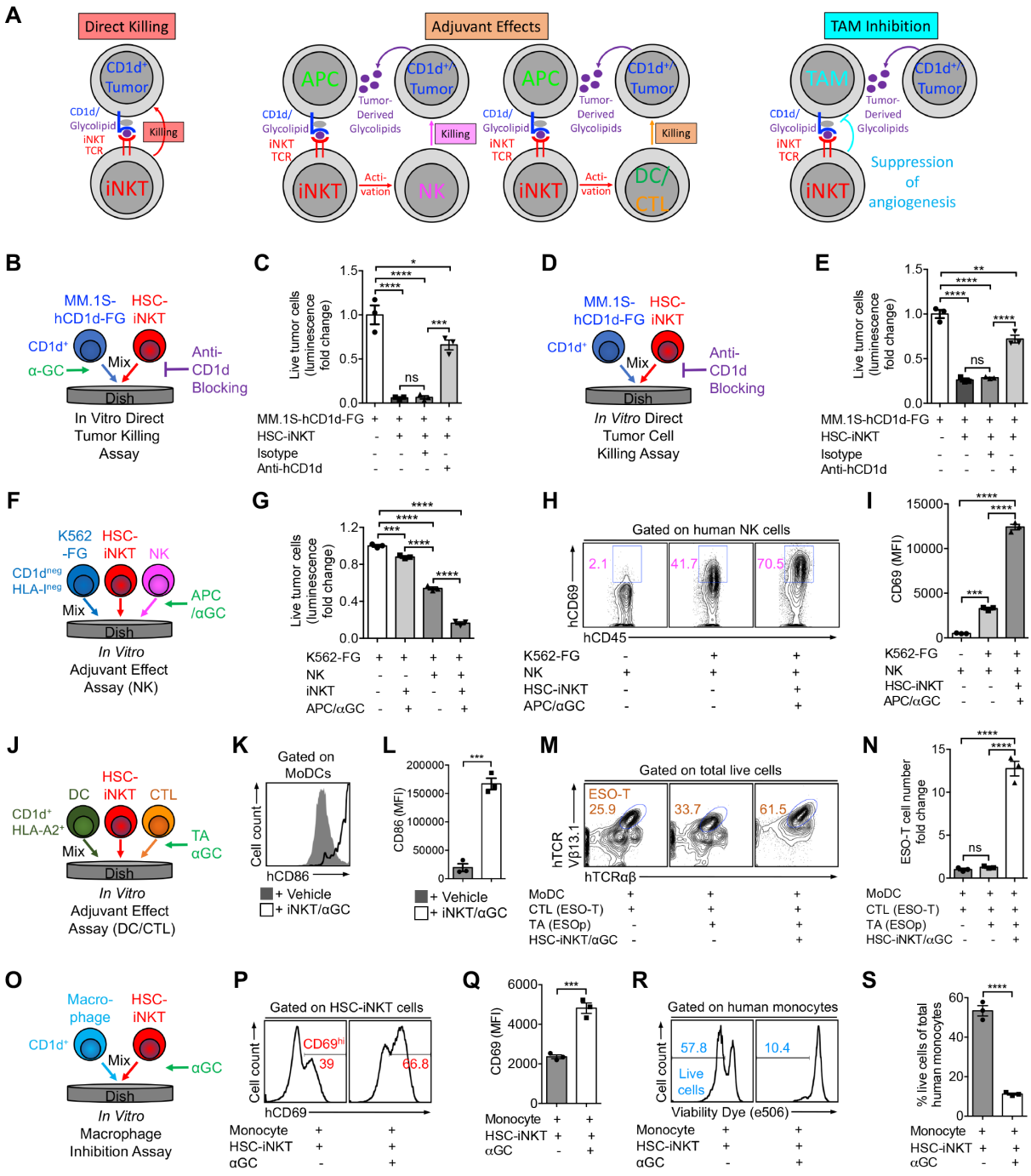

Figure 2-9. Tumor-Attacking Mechanisms of HSC-iNKT Cells.

(A) Diagram showing the possible mechanisms utilized by human iNKT cells to attack tumors. APC, antigen presenting cell; NK, natural killer cell; DC, dendritic cell; CTL, cytotoxic T lymphocyte; TAM, tumor-associated macrophage.

(B-E) Studying the direct killing of CD1d$^+$ tumor cells by HSC-iNKT cells (tumor:iNKT ratio 1:10). (B) Experimental design to study CD1d-dependent killing of MM.1S-hCD1d-FG cells in the presence of αGC. (C) Tumor killing data from B (n = 3). (D) Experimental design to study CD1d-dependent killing of MM.1S-hCD1d-FG cells in the absence of αGC. (E) Tumor killing data from D (n = 3). MM.1S-hCD1d-FG, MM.1S human multiple myeloma cell line

engineered to express human CD1d, firefly luciferase (Fluc), and enhanced green fluorescent protein (EGFP).

(F-I) Studying the adjuvant effects of HSC-iNKT cells on enhancing NK cell-mediated killing of tumor cells (tumor:NK:iNKT ratio 1:2:2). NK cells were isolated from healthy donor PBMCs. (F) Experimental design. (G) Tumor killing (n = 3). (H) FACS plots showing CD69 expression on NK cells (pre-gated as $hCD56^+$ cells) as a measurement of NK cell activation status. (I) Quantification of H (n = 3). K562-FG, K562 human myelogenous leukemia cell line engineered to express Fluc and EGFP.

(J-N) Studying the adjuvant effects of HSC-iNKT cells on boosting DC/CTL antitumor reactions (DC:CTL:iNKT ratio 1:1:1). Human monocyte-derived dendritic cells (MoDCs) and NY-ESO-1 TCR transgenic human CD8 cytotoxic T (ESO-T) cells were studied. NY-ESO-1 peptide (ESOp) was utilized as the tumor antigen (TA). Irradiated healthy donor PBMCs were utilized as antigen presenting cells (APCs). (J) Experimental design. (K) FACS plots showing CD86 expression on MoDCs (pre-gated as $hCD11c^+$ cells) as a measurement of MoDC maturation status. (L) Quantification of K (n = 3). (M) FACS plots showing the detection of ESO-T cells (gated as $hTCR\alpha\beta^+V\beta13.1^+$ cells) in the mixed cell culture. (N) Quantification of M (n = 3).

(O-S) Studying the inhibition of macrophages by HSC-iNKT cells (macrophage:iNKT ratio 1:1). Monocytes isolated from healthy donor PBMCs were studied. (O) Experimental design. (P) FACS plots showing CD69 expression on HSC-iNKT cells (pre-gated as $hTCR\alpha\beta^+6B11^+$ cells). (Q) Quantification of P (n = 3). (R) FACS plots showing the viability of monocytes (pre-gated as $hCD14^+$). Live cells were identified as $e506^-$. (S) Quantification of R (n = 3).

Representative of 2 experiments. Data are presented as the mean ± SEM. ns, not significant, *P < 0.05, **P < 0.01, ***P < 0.001, ****P < 0.0001, by 1-way ANOVA (C, E, G, I, N) or by Student's *t* test (L, Q, S).

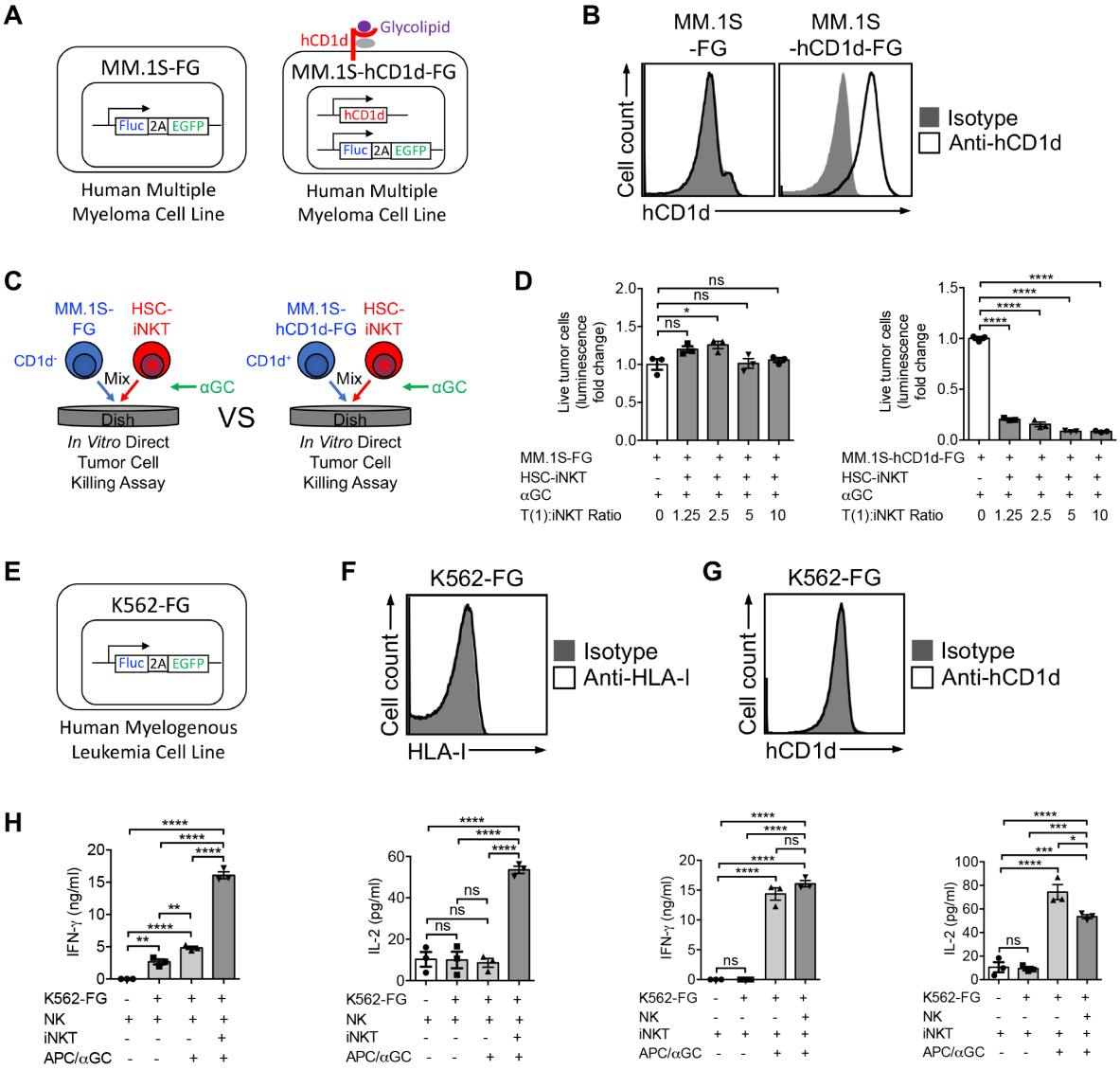

Figure 2-10. Tumor-attacking mechanisms of HSC-iNKT cells; direct killing of CD1d$^+$ tumor cells and NK adjuvant effects.

(A-D) Schematics showing the engineered MM.1S-FG and MM.1S-hCD1d-FG cell lines. MM.1S is a human multiple myeloma cell line. MM.1S-FG cell line was generated by stably transducing the parental MM.1S cell line with a Lenti/FG lentiviral vector encoding a firefly luciferase (Fluc) reporter gene and an enhanced green fluorescent protein (EGFP) reporter gene. MM.1S-hCD1d-FG cell line was generated by stably transducing the MM.1S-FG cell line with another Lenti/CD1d lentiviral vector encoding the human CD1d gene.

(B) FACS plots showing the detection of CD1d on MM.1S-hCD1d-FG cells, but not on MM.1S-FG cells.

(C-D) Studying the CD1d/αGC-mediated killing of tumor cells by HSC-iNKT cells. (C) Experimental design. (D) Tumor killing data from C (n = 3). Note the aggressive killing of tumor cells in a CD1d-dependant manner in the presence of αGC.

(E) Schematic of the K562-FG cell line. K562 is a human myelogenous leukemia cell line that is sensitive to NK cell-mediated tumor killing. The K562-FG cell line was generated by stably

transducing the parental K562 cell line with a Lenti/FG lentiviral vector encoding Fluc and EGFP dual reporter genes.

(F) FACS plot showing the absence of expression of MHC class I (HLA-I) on K562-FG cells.

(G) FACS plot showing the absence of expression of CD1d on K562-FG cells.

(H) ELISA analysis of IFN-γ and IL-2 in the supernatants of various mixed cell cultures (tumor:NK:iNKT ratio 1:2:2), showing the massive production of these cytokines by HSC-iNKT cells post-APC/αGC stimulation (n = 3).

Representative of 2 experiments. Data were presented as the mean ± SEM. ns, not significant, *P < 0.05, **, P<0.01, ***P < 0.001, ****P < 0.0001, by 1-way ANOVA.

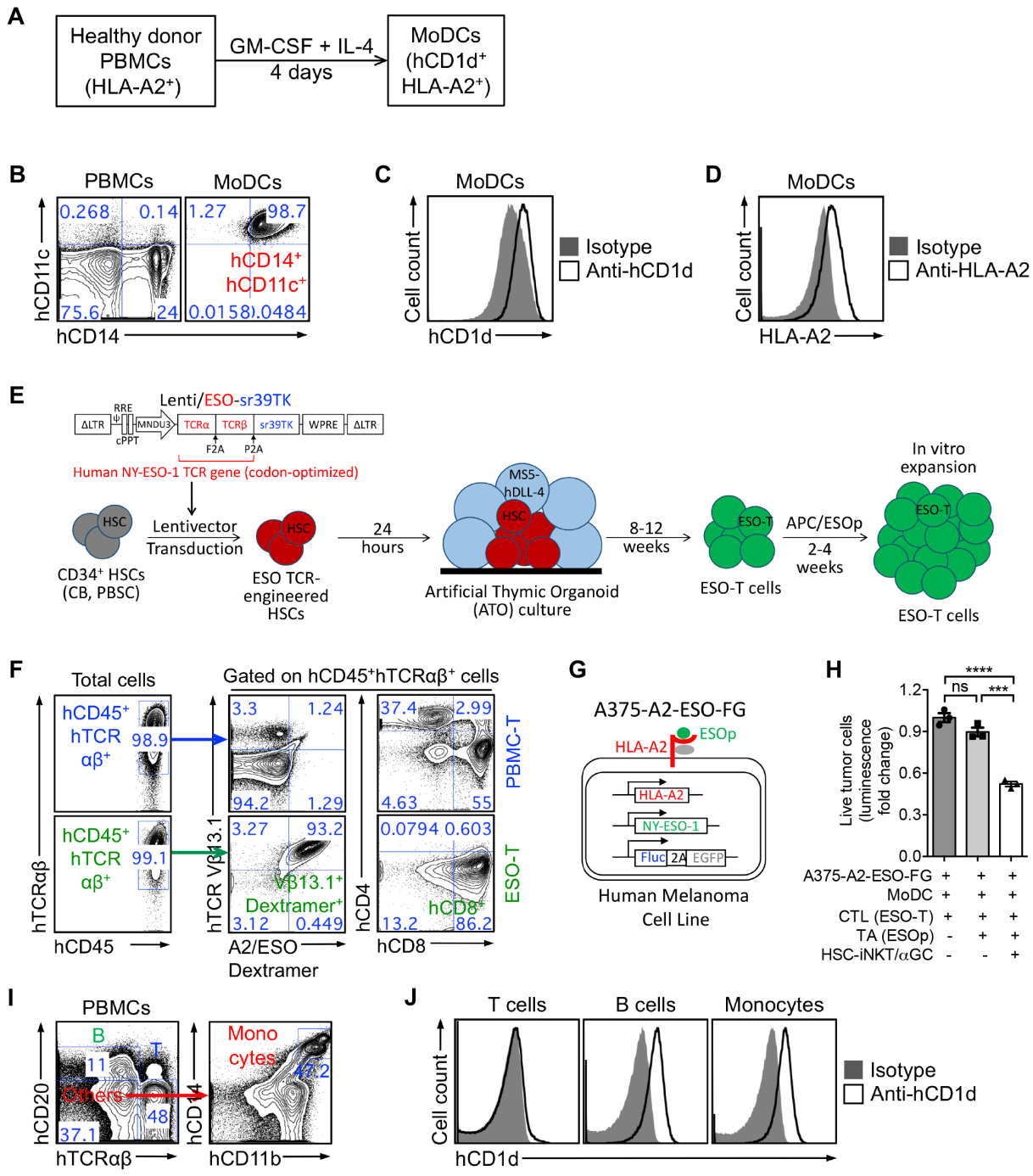

Figure 2-11. Tumor-attacking mechanisms of HSC-iNKT cells; adjuvant effects of HSC-iNKT cells on boosting DC/CTL antitumor reactions and inhibiting TAMs.

(A) Diagram showing the experimental design to generate HLA-A2$^+$hCD1d$^+$ human MoDCs. PBMCs, peripheral blood mononuclear cells; MoDCs, monocyte-derived dendritic cells.

(B) FACS plots showing the lineage verification of MoDCs (identified as $hCD14^{+}hCD11c^{+}$). PBMCs were included as a staining control.

(C) FACS plot showing the detection of CD1d on MoDCs.

(D) FACS plot showing the detection of HLA-A2 on MoDCs.

(E) Diagram showing the experimental design to generate NY-ESO-1-specific human CD8 cytotoxic T lymphocytes (denoted as ESO-T cells). Human $CD34^{+}$ HSCs were transduced with a Lenti/ESO-sr39TK vector, then differentiated into ESO-T cells in an artificial thymic organoid (ATO) culture, following by *in vitro* expansion of ESO-T cells with APC/ESOp stimulation. Human $CD34^{+}$ HSCs were isolated from cord blood (CB) or G-CSF-mobilized peripheral blood (denoted as peripheral blood stem cells, PBSCs). Lenti/ESO-sr39TK, lentivector encoding a human NY-ESO-1 TCR gene as well as an sr39TK suicide/PET imaging reporter gene; MS5-hDLL4, MS5 murine bone marrow stromal cell line engineered to express human Delta Like Canonical Notch Ligand 4; APC/ESOp, antigen-presenting cell (irradiated $HLA\text{-}A2^{+}$ healthy donor PBMCs) loaded with NY-ESO-$1_{157\text{-}165}$ peptide (ESOp). The transgenic NY-ESO-1 TCR recognizes NY-ESO-1 peptide presented by HLA-A2.1, and comprises a $V\beta\ 13.1^{+}$ beta chain.

(F) FACS plots showing the phenotype of ESO-T cells (characterized as $hCD45^{+}hTCR\alpha\beta^{+}$hTCR $V\beta13.1^{+}$A2/ESO $Dextramer^{+}hCD4^{-}hCD8^{+}$). Human T cells expanded from healthy donor PBMCs through CD3/CD28 Dynabeads stimulation were included as a staining control (denoted as PBMC-T cells). HLA-A2.1/NY-ESO-$1_{157\text{-}165}$ (A2/ESO) dextramer is a FACS staining reagent that detects HLA-A2.1-restricted and NY-ESO-1-specific human TCRs.

(G) Schematic showing the engineered A375-A2-ESO-FG cell line. A375 is a human melanoma cell line. A375-A2-ESO-FG cell line was generated by stably transducing the parental A375 cell line with lentivectors encoding an HLA-A2.1 gene, a NY-ESO-1 gene, and the Fluc and EGFP dual reporter genes.

(H) Tumor killing by ESO-T cells (n = 3). ESO-T cells were stimulated with MoDC/ESOp in the presence or absence of HSC-iNKT/αGC, followed by co-culture with A375-A2-ESO-FG tumor cells and analysis of tumor killing (tumor:DC:CTL:iNKT ratio 1:1:1:0.5).

(I) FACS plots showing the identification of T cells (gated as $hTCR\alpha\beta^{+}$ cells), B cells (gated as $hCD20^{+}$ cells), and monocytes (gated as $hCD14^{+}$ cells) from healthy donor peripheral blood mononuclear cells (PBMCs).

(J) FACS plots showing the measurement of CD1d expression on PBMC T cells, B cells, and monocytes gated from A. Note CD1d was highly expressed on antigen presenting cells (APCs) like B cells and monocytes, but not on T cells.

Representative of 2 experiments. Data were presented as the mean ± SEM. ns, not significant, ***P < 0.001, ****P < 0.0001, by 1-way ANOVA (H).

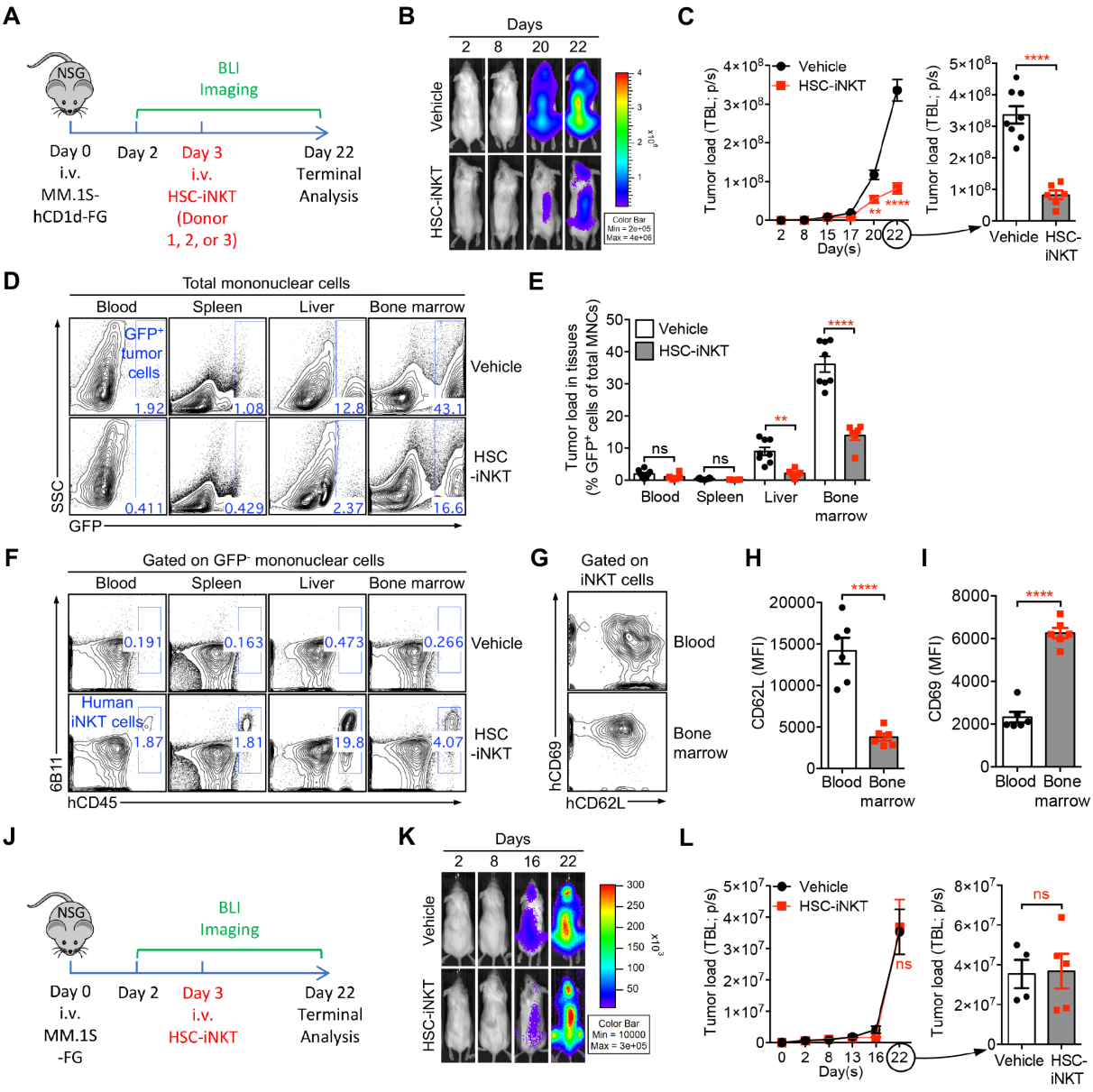

Figure 2-12. *In Vivo* Antitumor Efficacy of HSC-iNKT Cells Against Hematologic Malignancies in a Human Multiple Myeloma (MM) Xenograft Mouse Model.

(A-I) *In vivo* antitumor efficacy of HSC-iNKT cells was studied using an MM.1S-hCD1d-FG human MM xenograft NSG mouse model. HSC-iNKT cells derived from PBSCs of three different donors were studied, to verify the robustness of the HSC-iNKT cell therapy. Data from one representative donor were presented. (A) Experimental design. BLI, live animal bioluminescence imaging. (B) BLI images showing tumor loads in experimental mice over time. (C) Quantification of B (n = 6-8). TBL, total body luminescence. (D) FACS plots showing the detection of tumor cells (gated as GFP^+ cells) in various tissues of experimental mice. (E) Quantification of D (n = 6-8). MNCs, mononuclear cells. (F) FACS plots showing the detection of HSC-iNKT cells (gated as $hCD45^+hTCR\alpha\beta^+6B11^+$ cells) in various tissues of experimental mice. (G) FACS plots showing the expression of CD62L and CD69 on HSC-iNKT cells isolated from the blood and bone marrow of tumor-bearing mice. (H-I) Quantification of G (n = 6).

(J-L) *In vivo* antitumor efficacy of HSC-iNKT cells was studied using a control MM.1S-FG human MM xenograft NSG mouse model. HSC-iNKT cells derived from PBSCs of a representative donor were studied. (J) Experimental design. (K) BLI images showing tumor loads in experimental mice over time. (L) Quantification of K (n = 4-5).

Representative of 3 (A-I) and 2 (J-L) experiments. Data are presented as the mean ± SEM. ns, not significant, *P < 0.05, **P < 0.01, ****P < 0.0001, by Student's *t* test (C, E, H, I, L).

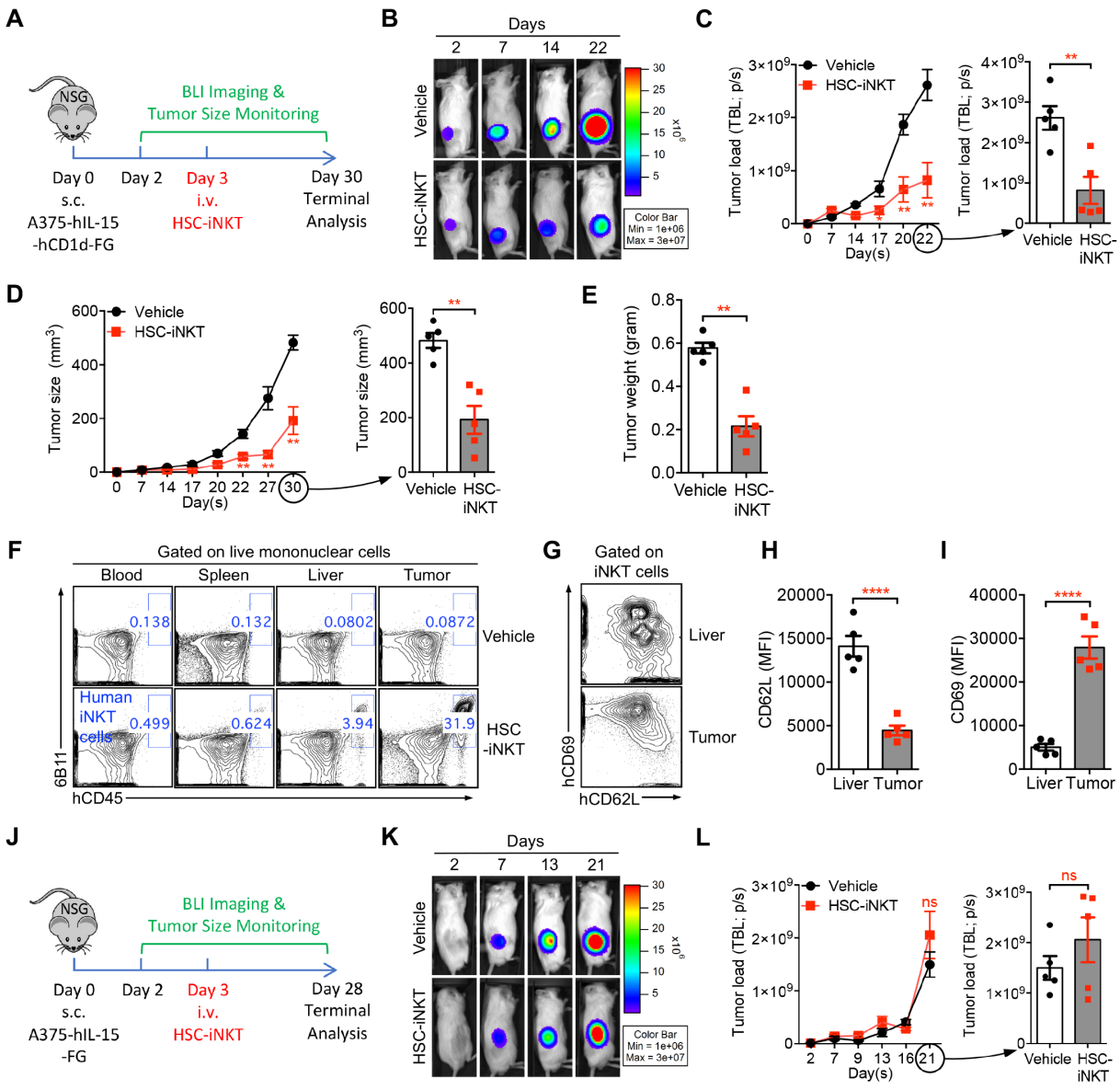

Figure 2-13. *In Vivo* Antitumor Efficacy of HSC-iNKT Cells Against Solid Tumors in a Human Melanoma Xenograft Mouse Model.

(A-I) *In vivo* antitumor efficacy of HSC-iNKT cells was studied using an A375-hIL-15-hCD1d-FG human melanoma xenograft NSG mouse model. (A) Experimental design. (B) BLI images showing tumor loads in experimental mice over time. Note that beyond day 22, BLI signals were saturated and thus were not included for quantification. (C) Quantification of B (n = 5). (D) Measurements of tumor size over time (n = 5). (E) Measurements of tumor weight at the terminal harvest on day 30 (n = 5). (F) FACS plots showing the detection of HSC-iNKT cells (gated as $hCD45^{+}hTCR\alpha\beta^{+}6B11^{+}$ cells) in various tissues of experimental mice. (G) FACS plots showing the expression of CD62L and CD69 on HSC-iNKT cells isolated from the livers and tumors of tumor-bearing mice. (H-I) Quantification of G (n = 5).

(J-L) *In vivo* antitumor efficacy of HSC-iNKT cells was studied using a control A375-hIL-15-FG human melanoma xenograft NSG mouse model. (J) Experimental design. (K) BLI images showing tumor loads in experimental mice over time. Note that beyond day 21, BLI signals were saturated and thus were not included for quantification. (L) Quantification of K (n = 5).

Representative of 2 experiments. Data are presented as the mean ± SEM. ns, not significant, **P < 0.01, ****P < 0.0001, by Student's *t* test (C, D, E, H, I, L).

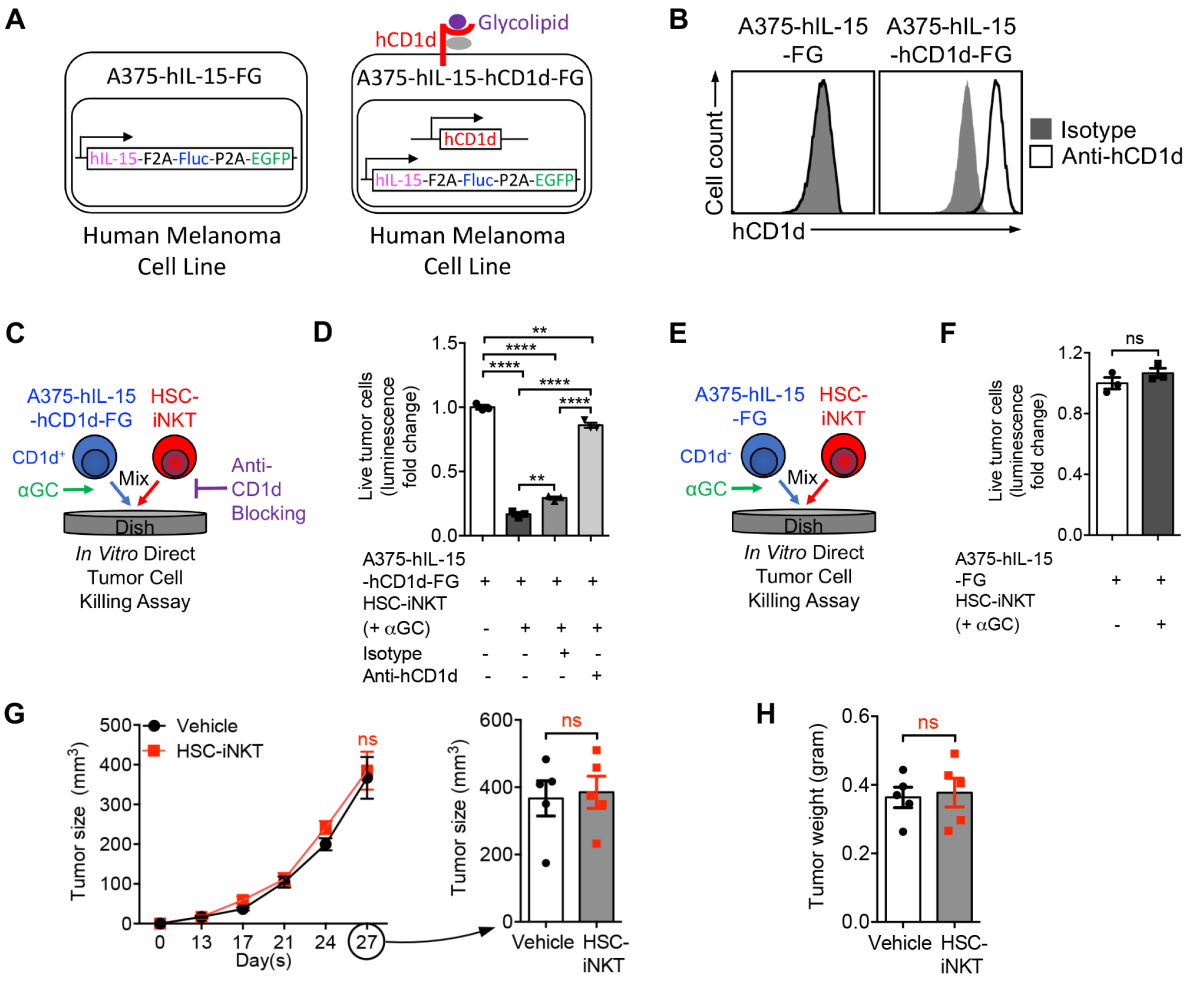

Figure 2-14. *In vivo* antitumor efficacy of HSC-iNKT cells against solid tumors in a human melanoma xenograft mouse model.

(A) Schematics showing the engineered A375-hIL-15-FG and A375-hIL-15-hCD1d-FG cell lines. A375 is a human melanoma cell line. A375-hIL-15-FG cell line was engineered by stably transducing the parental A375 cell line with a Lenti/hIL-15-FG lentiviral vector encoding a human IL-15 gene, a Fluc reporter gene, and an EGFP reporter gene. A375-hIL-15-hCD1d-FG cell line was generated by stably transducing the A375-hIL-15-FG cell line with another Lenti/CD1d lentiviral vector encoding the human CD1d gene.

(B) FACS plots showing the detection of CD1d on A375-hIL-15-hCD1d-FG cells, but not on A375-hIL-15-FG cells.

(C-D) Studying the *in vitro* direct killing of A375-hIL-15-hCD1d-FG cells by HSC-iNKT cells in the presence of αGC (tumor:iNKT ratio 1:2). (C) Experimental design. (D) Tumor killing (n = 3). Note that tumor killing was dependent on CD1d.

(E-F) Studying the *in vitro* direct killing of A375-hIL-15-FG cells by HSC-iNKT cells in the presence of αGC (tumor:iNKT ratio 1:2). (E) Experimental design. (F) Tumor killing (n = 3). Note the lack of tumor killing.

(G-H) Studying the *in vivo* antitumor efficacy of HSC-iNKT cells in the control A375-hIL-15-FG human melanoma xenograft NSG mouse model (related to main Figures 7J-7L). (G)

Measurements of tumor size over time (n = 5). (H) Measurements of tumor weight at the terminal harvest on day 28 (n = 5).

Representative of 2 experiments. Data were presented as the mean ± SEM. ns, not significant, **P < 0.01, ****P < 0.0001, by 1-way ANOVA (D) or by Student's *t* test (F, G, H).

Chapter 3 - Development of Allogeneic HSC-Engineered iNKT Cells for Off-The-Shelf Cancer Immunotherapy

Abstract

Cell-based immunotherapy has become the new-generation cancer medicine; "off-the-shelf" allogenic cell products that can be manufactured at large-scale and distributed readily to treat cancer patients are in great demand. Invariant natural killer T (iNKT) cells are ideal cell carriers for developing allogeneic cell therapy because they are powerful immune cells targeting cancers without graft-versus-host disease (GvHD) risk. However, healthy donor blood contains extremely low numbers of endogenous iNKT cells, making it exceedingly challenging to generate adequate iNKT cells for allogeneic cell therapy. Here, we report a technology breakthrough to overcome this critical limitation. Through combining hematopoietic stem cell (HSC) gene engineering and *in vitro* HSC differentiation, we achieved the generation of human allogeneic HSC-engineered iNKT (^{Allo}HSC-iNKT) cells at high yield and purity; these cells closely resembled endogenous iNKT cells, effectively targeted tumor cells using multiple mechanisms *in vitro* and *in vivo*, and most attractively, exhibited high safety and low immunogenicity. These cells could be further engineered with chimeric antigen receptor (CAR) to enhance tumor targeting, or/and gene-edited to ablate surface HLA molecules and further reduce immunogenicity. Collectively, these preclinical studies demonstrated the feasibility and cancer therapy potential of ^{Allo}HSC-iNKT cell products and laid a foundation for their future translational and clinical development.

Introduction

Over the past decade, immunotherapy has become the new-generation cancer medicine [1,87,88]. In particular, T cell-based cancer therapy has shown great promise [89]. An outstanding example is the chimeric antigen receptor (CAR)-engineered T (CAR-T) cell adoptive therapy, which

targets certain blood cancers at impressive efficacy, and has been approved by FDA to treat $CD19^+$ B cell malignancies [89–91]. Adoptive transfer of *in vitro* expanded tumor-infiltrating T lymphocytes (TILs) and TCR-engineered T cells also show promises in treating some blood cancers and solid tumors in clinics [92,93]. However, most of the current T cell therapies fall in the category of autologous cell therapy, wherein T cells collected from a patient are manufactured and used to treat that single patient. Such an approach is time consuming, logistically challenging, and costly; furthermore, for the patients with heavily lymphopenic pretreatment or rapidly proliferative disease, it might not always be possible to produce autologous cell products [90,94]. Allogenic cell products that can be manufactured at large-scale and distributed readily to treat a broad range of cancer patients therefore are in great demand. Conventional αβ T cells have been utilized for generating allogeneic cell products; however, these T cells risk inducing graft-versus-host disease (GvHD) in allogeneic hosts due to HLA incompatibility, and thereby requiring additional gene-editing to ablate their endogenous TCR expression that may potentially increase manufacture complexity [18–21]. Innate immune cells such as natural killer (NK) cells that have no GvHD risk have been investigated; however, NK cells may have limited in vivo clonal expansion and antitumor performance compared to those of T cells [12,95].

Invariant natural killer T (iNKT) cells are a small population of αβ T lymphocytes [36]. iNKT cells have several unique features, making them ideal for developing off-the-shelf cellular therapy for cancer. Compared to conventional T cells, iNKT cells can attack tumor cells using multiple mechanisms and at higher efficacy; can more effectively traffic to and infiltrate solid tumors; can alter solid tumor immunosuppressive microenvironment; and most importantly, do not induce GvHD [26,28,30,31,37–40,45]. However, human blood contains extremely low numbers of iNKT cells (0.001-1%), making it very difficult to reliably grow large numbers of allogeneic iNKT cells for cell therapies [51]. Moreover, allogeneic iNKT products expanded from blood

may contain bystander allogeneic conventional αβ T cells and thus risk inducing GvHD. Technology breakthroughs are needed to exploit the allogeneic cell therapy potential of iNKT cells.

Previously, we have established a method to generate large numbers of iNKT cells through TCR gene engineering of hematopoietic stem cells (HSCs) followed by *in vivo* reconstitution; using this method, we have successfully generated both mouse and human HSC-engineered iNKT (HSC-iNKT) cells [41,42]. However, such an *in vivo* approach cannot be used to produce off-the-shelf mature allogeneic iNKT cells [41,42]. Here, we intended to build on the HSC-iNKT engineering approach and develop an *in vitro* culture method to produce large numbers of off-the-shelf human iNKT cells for allogeneic cell therapy applications. Here we report the preclinical development of the proposed allogeneic HSC-iNKT cell therapy, demonstrating its manufacture feasibility, cancer therapy potential, and high safety profile.

Materials and Methods

Mice

NOD.Cg-Prkdc^{SCID}Il2rg^{tm1Wjl}/SzJ (NOD/SCID/IL-2Rγ$^{-/-}$, NSG) mice were maintained in the animal facilities of the University of California, Los Angeles (UCLA). 6-10 weeks old mice were used for all experiments unless otherwise indicated. All animal experiments were approved by the Institutional Animal Care and Use Committee of UCLA.

Cell Lines

The MS5-DLL4 murine bone marrow derived stromal cell line was obtained from Dr. Gay Crooks' lab (UCLA). Human multiple myeloma cancer cell line MM.1S, chronic myelogenous leukemia cancer cell line K562, melanoma cell line A375, lung carcinoma cell line H292, and prostate cancer cell line PC3 were purchased from the American Type Culture Collection

(ATCC). MM.1S cells were cultured in R10 medium. K562 cells were cultured in C10 medium. A375, H292, and PC3 were cultured in D10 medium.

To make stable tumor cell lines overexpressing human CD1d, and/or firefly luciferase and enhanced green fluorescence protein (Fluc-EGFP) dual-reporters, the parental tumor cell lines were transduced with lentiviral vectors encoding the intended gene(s) [41]. 72h post lentivector transduction, cells were subjected to flow cytometry sorting to isolate gene-engineered cells for making stable cell lines. Six stable tumor cell lines were generated for this study, including MM.1S-FG, MM.1S-CD1d-FG, A375-FG, PC3-FG, H292-FG, and K562-FG.

Human CD34$^+$ Hematopoietic Stem Cells (HSCs) and Periphery Blood Mononuclear Cells (PBMCs)

Cord blood cells were purchased from HemaCare. G-CSF-mobilized healthy donor peripheral blood cells were purchased from HemaCare or Cincinnati Children's Hospital Medical Center (CCHMC). Human CD34$^+$ HSCs were isolated through magnetic-activated cell sorting using ClinMACs CD34$^+$ microbeads (Miltenyi Biotech). Cells were cryopreserved in Cryostor CS10 (Sigma) using CoolCell (BioCision) and were frozen in liquid nitrogen for all experiments and long-term storage. Healthy donor human PBMCs were obtained from the UCLA/CFAR Virology Core Laboratory, without identification information under federal and state regulations.

Media and Reagents

α-Galactosylceramide (αGC, KRN7000) was purchased from Avanti Polar Lipids. Recombinant human IL-2, IL-3, IL-4, IL-7, IL-15, Flt3-Ligand, Stem Cell Factor (SCF), Thrombopoietin (TPO), and Granulocyte-Macrophage Colony-Stimulating Factor (GM-CSF) were purchased from Peprotech. Ganciclovir (GCV) was purchased from Sigma.

X-VIVO 15 Serum-free Hematopoietic Cell Medium was purchased from Lonza. RPMI 1640 and DMEM cell culture medium were purchased from Corning Cellgro. Fetal bovine serum (FBS) was purchased from Sigma. Medium supplements, including Penicillin-Streptomycine-Glutamine (P/S/G), MEM non-essential amino acids (NEAA), HEPES Buffer Solution, and Sodium Pyruvate, were purchased from GIBCO. Beta-Mercaptoethanol (β-ME) was purchased from Sigma. Normocin was purchased from InvivoGen. Complete lymphocyte culture medium (denoted as C10 medium) was made of RPMI 1640 supplemented with FBS (10% vol/vol), P/S/G (1% vol/vol), MEM NEAA (1% vol/vol), HEPES (10 mM), Sodium Pyruvate (1 mM), β-ME (50 mM), and Normocin (100 mg/ml). Medium for culturing human MM.1S tumor cell line (denoted as R10 medium) was made of RPMI 1640 supplemented with FBS (10% vol/vol) and P/S/G (1% vol/vol). Adherent cell culture medium (denoted as D10 medium) was made of DMEM supplemented with FBS (10% vol/vol) and P/S/G (1% vol/vol).

Lentiviral and Retroviral Vectors

Lentiviral vectors used in this study were all constructed from a parental lentivector pMNDW as previously described [41]. The Lenti/iNKT-sr39TK vector was constructed by inserting into pMNDW vector a synthetic tricistronic gene encoding human iNKT TCRα-F2A-TCRβ-P2A-sr39TK; the Lenti/FG vector was constructed by inserting into pMNDW a synthetic bicistronic gene encoding Fluc-P2A-EGFP; the Lenti/CD1d vector was constructed by inserting into pMNDW a synthetic gene encoding human CD1d. The synthetic gene fragments were obtained from GenScript and IDT. Lentiviruses were produced using HEK 293T cells, following a standard calcium precipitation protocol and an ultracentrifigation concentration protocol as previously described [41,42]. Lentivector titers were measured by transducing HT29 cells with serial dilutions and performing digital qPCR, following established protocols [41,42].

The Retro/BCAR-tEGFR vector was constructed by inserting into the parental MP71 vector a synthetic gene encoding human BCMA scFV-41BB-CD3ζ-P2A-tEGFR. The synthetic gene fragments were obtained from IDT. Vsv-g-pseudotyped Retro/BCAR-tEGFR retroviruses were generated by transfecting HEK 293T cells following a standard calcium precipitation protocol [41,42]; the viruses were then used to transduce PG13 cells to generate a stable retroviral packaging cell line producing Retro/BCAR-tEGFR retroviruses (denoted as PG13-BCAR-tEGFR cell line). For retrovirus production, the PG13-BCAR-tEGFR cells were seeded at a density of 8 x 10^5 cells per ml in D10 medium and cultured in a 15 cm-dish (30 ml per dish) for 2 days; virus supernatants were then harvested and stored at -80 °C for future use.

Antibodies and Flow Cytometry

All flow cytometry stains were performed in PBS for 15 min at 4 °C. The samples were stained with Fixable Viability Dye eFluor506 (e506) mixed with Mouse Fc Block (anti-mouse CD16/32) or Human Fc Receptor Blocking Solution (TrueStain FcX) prior to antibody staining. Antibody staining was performed at a dilution according to the manufacturer's instructions. Fluorochrome-conjugated antibodies specific for human CD45 (Clone H130), TCRαβ (Clone I26), CD4 (Clone OKT4), CD8 (Clone SK1), CD45RO (Clone UCHL1), CD161 (Clone HP-3G10), CD69 (Clone FN50), CD56 (Clone HCD56), CD62L (Clone DREG-56), CD14 (Clone HCD14), CD11b (Clone ICRF44), CD11c (Clone N418), CD1d (Clone 51.1), CCR4 (Clone L291H4), CCR5 (Clone HEK/1/85a), CXCR3 (Clone G025H7), NKG2D (Clone 1D11), DNAM-1 (Clone 11A8), CD158 (KIR2DL1/S1/S3/S5) (Clone HP-MA4), IFN-γ (Clone B27), granzyme B (Clone QA16A02), perforin (Clone dG9), TNF-α (Clone Mab11), IL-2 (Clone MQ1-17H12), HLAE (Clone 3D12), β2-microglobulin (B2M) (Clone 2M2), HLA-DR (Clone L243), TCR Vδ2 (Clone B6) were purchased from BioLegend; Fluorochrome-conjugated antibodies specific for human CD34 (Clone 581) and TCR Vα24-Jβ18 (Clone 6B11) were

purchased from BD Biosciences; Fluorochrome-conjugated antibodies specific for human Vβ11 was purchased from Beckman-Coulter; Fluorochrome-conjugated antibodies specific for human ULBP-2,5,6 (Clone 165903) was purchased from R&D Systems. Human Fc Receptor Blocking Solution (TrueStain FcX) was purchased from Biolegend, and Mouse Fc Block (anti-mouse CD16/32) was purchased from BD Biosciences. Fixable Viability Dye e506 were purchased from Affymetrix eBioscience. Intracellular cytokines were stained using a Cell Fixation/Permeabilization Kit (BD Biosciences). Stained cells were analyzed using a MACSQuant Analyzer 10 flow cytometer (Miltenyi Biotech). FlowJo software was utilized to analyze the data.

Enzyme-Linked Immunosorbent Cytokine Assays (ELISA)

The ELISAs for detecting human cytokines were performed following a standard protocol from BD Biosciences. Supernatants from co-culture assays were collected and assayed to quantify IFN-γ, TNF-α, IL-2, IL-4, and IL-17. The capture and biotinylated pairs for detecting cytokines were purchased from BD Biosciences. The streptavidin-HRP conjugate was purchased from Invitrogen. Human cytokine standards were purchased from eBioscience. Tetramethylbenzidine (TMB) substrate was purchased from KPL. The samples were analyzed for absorbance at 450 nm using an Infinite M1000 microplate reader (Tecan).

In Vitro Generation of Allogeneic HSC-Engineered iNKT (^{Allo}HSC-iNKT) Cells

Frozen-thawed human $CD34^+$ HSCs were revived in HSC-culture medium composed of X-VIVO 15 Serum-free Hematopoietic Cell Medium supplemented with SCF (50 ng/ml), FLT3-L (50 ng/ml), TPO (50 ng/ml), and IL-3 (10 ng/ml) for 24 hours; the cells were then transduced with Lenti/iNKT-sr39TK viruses for another 24 hours following an established protocol (Zhu

et al., 2019). The transduced HSCs were then collected and put into a 2-Stage *in vitro* HSC-iNKT culture.

At Stage 1, gene-engineered HSCs were differentiated into iNKT cells in an artificial thymic organoid (ATO) culture over 8 weeks. ATO was generated following a previously established protocol, with certain modifications [77,96]. Briefly, MS5-DLL4 cells were harvested by trypsinization and resuspended in serum free ATO culture medium (‘‘RB27’’) composed of RPMI 1640 (Corning), 4% B27 supplement (ThermoFisher Scientific), 30 mM L-ascorbic acid 2-phosphate sesquimagnesium salt hydrate (Sigma-Aldrich) reconstituted in PBS, 1% penicillin/streptomycin (Gemini Bio-Products), 1% Glutamax (ThermoFisher Scientific), 5 ng/ml rhFLT3L and 5 ng/ml rhIL-7 (Peprotech). RB27 was made fresh weekly. 1.5-6 x 10^5 MS5-DLL4 cells were combined with 0.3-10 x 10^4 transduced HSCs per ATO in 1.5 mL Eppendorf tubes (up to 12 ATOs per tube) and centrifuged at 300 g for 5 min at 4 °C in a swinging bucket centrifuge. Supernatants were carefully removed, and the cell pellet was resuspended in 6 ml RB27 per ATO and mixed by brief vortexing. ATOs were plated on a 0.4 mm Millicell transwell insert (EMD Millipore; Cat. PICM0RG50) placed in a 6-well plate containing 1 mL RB27 per well. Medium was changed completely every 3-4 days by aspiration from around the cell insert followed by replacement with 1 ml fresh RB27/cytokines. ATO cells were harvested by adding FACS buffer (PBS/0.5% bovine serum album/2mM EDTA) to each well and briefly disaggregating the ATO by pipetting with a 1 ml ‘‘P1000’’ pipet, followed by passage through a 50 mm nylon strainer.

At Stage 2, isolated ATO cells comprising ^{Allo}HSC-iNKT cells were expanded with αGC-loaded PBMCs (αGC-PBMCs). αGC-PBMCs were prepared by incubating 10^7-10^8 PBMCs in 5 ml C10 medium containing 5 μg/ml αGC for 1 hour, followed by irradiation at 6,000 rads. ATO cells were mixed with irradiated αGC-PBMCs at ratio 1:1, followed by culturing in C10 medium supplemented with human IL-7 (10 ng/ml) and IL-15 (10 ng/ml) for

2 weeks; cell cultures were split and fresh media/cytokines were added if needed. The Stage 2 expansion culture could be extended to 3 weeks by adding additional αGC-PBMCs at ratio 1:1 at the end of week 2. At the end of Stage 2 culture, the resulting ^{Allo}HSC-iNKT cell products were collected and cryopreserved for future use.

In Vitro Generation of BCMA CAR-Engineered ^{Allo}HSC-iNKT (^{Allo}BCAR-iNKT) Cells

^{Allo}HSC-iNKT cells were generated in the 2-Stage HSC-iNKT culture as described above, followed by an additional Stage 3 CAR engineering culture. At one week into Stage 2 culture, ^{Allo}HSC-iNKT cells were collected and stimulated with CD3/CD28 T-activator beads (ThermoFisher Scientific) in the presence of recombinant human IL-15 (10 ng/ml) and human IL-7 (10 ng/ml) for two days; the cells were then spin-infected with frozen-thawed Retro/BCAR-tEGFR retroviral supernatants supplemented with polybrene (10 μg/ml, Sigma-Aldrich) at 660 g at 30 °C for 90 min. Retronectin (Takara) could be pre-coated on plate to increase transduction efficiency. After transduction, the resulting ^{Allo}BCAR-iNKT cells were expanded for another 1-2 weeks in C10 medium supplemented with recombinant human IL-15 (10 ng/ml) and IL-7 (10 ng/ml), and then were collected and cryopreserved for future use.

In Vitro Generation of HLA-Ablated Universal HSC-iNKT (^{U}HSC-iNKT) Cells

^{U}HSC-iNKT cells were generated following the protocol of generating ^{Allo}HSC-iNKT cells, with one additional gene-editing step. $CD34^+$ HSCs were revived in HSC-culture medium on day 1, transduced with Lenti/iNKT-sr39TK viruses on day 2, and then were electroporated with a CRISPR-Cas9/B2M-CIITA-gRNAs complex on day 3, followed by entering the 2-Stage HSC-iNKT culture to generate ^{U}HSC-iNKT cells.

^{U}BCAR-iNKT cells were generated following the protocol of generating ^{Allo}BCAR-iNKT cells, with the same additional gene-editing step. $CD34^+$ HSCs were revived in HSC-culture medium

on day 1, transduced with Lenti/iNKT-sr39TK viruses on day 2, and then were electroporated with a CRISPR-Cas9/B2M-CIITA-gRNAs complex on day 3, followed by entering the 3-Stage BCAR-iNKT culture to generate ^{U}BCAR-iNKT cells.

For electroporation, 2×10^5 HSCs per condition were pelleted at 90 x g for 10 mins at room temperature (RT), resuspended in 20 µl P3 solution (Lonza), mixed with pre-aliquoted B2M and CIITA gRNAs (1 µl of each gRNA at 100 µM) and Cas9 (4 µl at 6.5 mg/ml), and pulsed once at 250 V for 5 milliseconds in an Amaxa 4D Nucleofector X Unit (Lonza). After electroporation, HSCs were rested at RT for 10 minutes, and then transferred to a 24-well tissue culture treated plate overnight before entering the 2-Stage HSC-iNKT or 3-Stage BCAR-iNKT culture.

If necessary, the resulting ^{U}HSC-iNKT or ^{U}BCAR-iNKT cell products collected at the end of the *in vitro* culture could be purified using Magnetic-Activate Cell Sorting (MACS) via B2M (Santa Cruz Biotechnology) and HLA-II magnetic beads labeling (Miltenyi Biotec), to enrich the HLA-I/II double negative cells in the final ^{U}HSC-iNKT or ^{U}BCAR-iNKT cell products.

Generation of PBMC-Derived Conventional αβT, iNKT, γδT, and NK Cells

Healthy donor PBMCs were obtained from the UCLA/CFAR Virology Core Laboratory, and were used to generate the PBMC-Tc, PBMC-iNKT, PBMC-γδT, and PBMC-NK cells.

To generate PBMC-Tc cells, PBMCs were stimulated with CD3/CD28 T-activator beads (ThermoFisher Scientific) and cultured in C10 medium supplemented with human IL-2 (20 ng/mL) for 2-3 weeks, following the manufacturer's instructions.

To generate PBMC-iNKT cells, PBMCs were MACS-sorted via anti-iNKT microbeads (Miltenyi Biotech) labeling to enrich iNKT cells, which were then stimulated with donor-matched irradiated αGC-PBMCs at the ratio of 1:1, and cultured in C10 medium supplemented

with human IL-7 (10 ng/ml) and IL-15 (10 ng/ml) for 2-3 weeks. If needed, the resulting PBMC-iNKT cells could be further purified using Fluorescence-Activated Cell Sorting (FACS) via human iNKT TCR antibody (Clone 6B11; BD Biosciences) staining.

To generate PBMC-γδT cells, PBMCs were stimulated with Zoledronate (5 μM; Sigma-Aldrich) and cultured in C10 medium supplemented with human IL-2 (20 ng/ml) for 2 weeks. If needed, the resulting PBMC-γδT cells could be further purified using FACS via human TCR Vδ2 antibody (Clone B6; Biolegend) staining or via MACS using a human TCRγ/δ T Cell Isolation Kit (Miltenyi Biotech).

To generate PBMC-NK cells, PBMCs were FACS-sorted via human CD56 antibody (Clone HCD56; Biolegend) labeling or MACS-sorted using a human NK Cell Isolation Kit (Miltenyi Biotech).

Generation of BCMA CAR-Engineered PBMC T (BCAR-T) cells

Healthy donor PBMCs were stimulated with CD3/CD28 T-activator beads (ThermoFisher Scientific) in the presence of recombinant human IL-2 (30 ng/ml), following the manufacturer's instructions. On day 2, cells were spin-infected with frozen-thawed Retro/BCAR-tEGFR retroviral supernatants supplemented with polybrene (10 μg/ml, Sigma-Aldrich) at 660 g at 30 °C for 90 min. Retronectin (Takara) could be pre-coated on plate to increase transduction efficiency. The resulting BCAR-T cells were expanded for another 7-10 days, and then were cryopreserved for future use.

Single Cell TCR Sequencing

^{Allo}HSC-iNKT ($6B11^{+}TCR\alpha\beta^{+}$), PBMC-iNKT ($6B11^{+}TCR\alpha\beta^{+}$), and PBMC-Tc ($6B11^{-}TCR\alpha\beta^{+}$) cells were sorted using a FACSAria II flow cytometer. Sorted cells were immediately delivered to the UCLA TCGB (Technology Center for Genomics and Bioinformatics) Core to

perform single cell TCR sequencing using a 10X Genomics Chromium™ Controller Single Cell Sequencing System (10X Genomics), following the manufacturer's instructions and the TCGB Core's standard protocol. Libraries were constructed using an Illumina TruSeq RNA Sample Prep Kit (Cat#FC-122-1001) and sequenced with 150 bp paired end reads (5,000 reads/cell) on an Illumina NovaSeq. The reads were mapped to the human T cell receptor reference genome (hg38) using Cell Ranger VDJ. The frequencies of the α or β chain recombination were plotted.

Deep RNA Sequencing (Deep RNAseq) and Data Analysis

A total of 25 cell samples were analyzed, as described in the following table:

Sample name	Number of replicates (from different donors)	FACS sorting markers	Description
^{Allo}HSC-iNKT (from PBSC)	3	6B11^{+}TCRαβ^{+}	^{Allo}HSC-iNKT cells derived from G-CSF mobilized peripheral blood CD34^{+} HSCs
^{Allo}HSC-iNKT (from CB)	3	6B11^{+}TCRαβ^{+}	^{Allo}HSC-iNKT cells derived from cord blood CD34^{+} HSCs
PBMC-iNKT (CD4^{-})	3	6B11^{+}TCRαβ^{+}CD4^{-}	PBMC-iNKT cells derived from healthy donor PBMCs (CD4^{-} cells were analyzed)
PBMC-αβTc (CD4^{-})	8	6B11^{-} TCRαβ^{+}CD4^{-}	PBMC-αβTc cells derived from healthy donor PBMCs (CD4^{-} cells were analyzed)
PBMC-NK	2	CD56^{+}TCRαβ^{-}	PBMC-NK cells derived from healthy donor PBMCs
PBMC-γδT	6	TCRγδ^{+}TCR αβ^{-}	PBMC-γδT cells derived from healthy donor PBMCs

Both ^{Allo}HSC-iNKT and PBMC-iNKT cells were activated *in vitro* with αGC, PBMC-αβTc cells were stimulated with CD3/CD28 T-activator beads, and PBMC-γδT cells were stimulated with Zoledronate. Cell samples were sorted using a FACSAria II flow cytometer. Total RNAs were isolated from each cell sample using an miRNeasy Mini Kit (QIAGEN) and delivered to the UCLA TCGB Core to perform Deep RNA sequencing using an Illumina HiSeq3000, following the manufacturer's instructions and the TCGB Core's standard protocol. cDNAs were synthesized using an iScript cDNA Synthesis Kit (1708890, BioRad). Libraries were constructed using an Illumina TruSeq Stranded Total RNA Sample Prep kit and sequenced with 50 bp single end reads (20 M reads/sample) on an Illumina HiSeq3000. The reads were mapped with STAR 2.5.3a to the human genome (hg38). The counts for each gene were obtained using --quantMode GeneCounts in STAR commands, and the other parameters during alignment were set to default. Data quality was checked using Illumina's proprietary software. Sequencing depth normalized counts were obtained from the differential expression analysis and were used for principal component analysis.

^{Allo}HSC-iNKT Cell Phenotype and Functional Study

^{Allo}HSC-iNKT cells and their derivatives (i.e., ^{Allo}BCAR-iNKT, ^{U}HSC-iNKT, and ^{U}BCAR-iNKT cells) were analyzed in comparison with PBMC-Tc, PBMC-NK, PBMC-iNKT, or/and BCAR-T cells. Phenotype of these cells was studied using flow cytometry, by analyzing cell surface markers including co-receptors (i.e., CD4 and CD8), NK cell receptors (i.e., CD161, NKG2D, DNAM-1, and KIR), memory T cell markers (i.e., CD45RO), and inflammatory tissue/tumor homing markers (i.e., CCR4, CCR5, and CXCR3). Capacity of these cells to produce cytokines (i.e., IFN-γ, TNF-α, and IL-2) and cytotoxic molecules (i.e., perforin and granzyme B) were studied using flow cytometry via intracellular staining.

Response of ^{Allo}HSC-iNKT cells to antigen stimulation was studied by culturing ^{Allo}HSC-iNKT cells *in vitro* in C10 medium for 7 days, in the presence or absence of αGC (100 ng/ml). Proliferation of ^{Allo}HSC-iNKT cells was measured by cell counting and flow cytometry (identified as $6B11^{+}TCR\alpha\beta^{+}$) over time. Cytokine production was assessed by ELISA analysis of cell culture supernatants collected on day 7 (for human IFN-γ. TNF-α, IL-2, IL-4, and IL-17).

In Vitro Tumor Cell Killing Assay

Tumor cells (1 x 10^4 cells per well) were co-cultured with effector cells (at ratios indicated in figure legends) in Corning 96-well clear bottom black plates for 8-24 hours, in C10 medium with or without the addition of αGC (100 ng/ml). At the end of culture, live tumor cells were quantified by adding D-luciferin (150 μg/ml; Caliper Life Science) to cell cultures and reading out luciferase activities using an Infinite M1000 microplate reader (Tecan).

In some experiments, 10 μg/ml of LEAF™ purified anti-human NKG2D (Clone 1D11, Biolegend), anti-human DNAM-1 antibody (Clone 11A8, Biolegend), or LEAF™ purified mouse lgG2bk isotype control antibody (Clone MG2B-57, Biolegend) was added to co-cultures, to study NK activating receptor-mediated tumor cell killing mechanism.

All the PBMC-derived cells and HSC-derived iNKT cells were cryopreserved before use. The cells for comparison (e.g., ^{Allo}HSC-iNKT and PBMC-NK cells in Figure 3) were cryopreserved and thawed for testing side-by-side using Mr. Frosty Freezing Container (Thermo Scientific Nalgene) following the manufacture's instructions.

In Vitro Mixed Lymphocyte Reaction (MLR) Assay: Studying Graft-Versus-Host (GvH) Response

PBMCs of multiple healthy donors were irradiated at 2,500 rads and used as stimulators, to study the GvH response of ^{Allo}HSC-iNKT cells and their derivatives (i.e., ^{Allo}BCAR-iNKT and ^{U}BCAR-iNKT cells) as responders. PBMC-Tc or BCAR-T cells were included as responder controls. Stimulators (5 x 10^5 cells/well) and responders (2 x 10^4 cells/well) were co-cultured in 96-well round bottom plates in C10 medium for 4 days; the cell culture supernatants were then collected to measure IFN-γ production using ELISA.

In Vitro MLR Assay: Studying Host-Versus-Graft (HvG) Response

PBMCs of multiple healthy donors were used as responders, to study the HvG response of ^{Allo}HSC-iNKT cells and their derivatives (i.e., ^{Allo}BCAR-iNKT and ^{U}BCAR-iNKT cells) as stimulators (irradiated at 2,500 rads). PBMC-Tc, PBMC-iNKT or BCAR-T cells were included as stimulator controls. Stimulators (5 x 10^5 cells/well) and responders (2 x 10^4 cells/well) were co-cultured in 96-well round bottom plates in C10 medium for 4 days; the cell culture supernatants were then collected to measure IFN-γ production using ELISA.

In Vitro MLR Assay: Studying NK Cell-Mediated Allorejection

PBMC-NK cells isolated from PBMCs of multiple healthy donors were used to study the NK cell-mediated allorejection of ^{Allo}HSC-iNKT cells and their derivatives (i.e., ^{Allo}BCAR-iNKT and ^{U}BCAR-iNKT cells). Allogeneic PBMC-Tc or PBMC-iNKT cells were included as controls. PBMC-NK cells (2 x 10^4 cells/well) and the corresponding allogeneic cells (2 x 10^4 cells/well) were co-cultured in 96-well round bottom plates in C10 medium for 24 hours; the cell cultures were then collected to quantify live cells using flow cytometry.

Bioluminescence Live Animal Imaging (BLI)

BLI was performed using an IVIS 100 imaging system (Xenogen/PerkinElmer) or a Spectral Advanced Molecular Imaging (AMI) HTX imaging system (Spectral instrument Imaging). Live animal imaging was acquired 5 minutes after intraperitoneal (i.p.) injection of D-Luciferin (1 mg per mouse). Imaging results were analyzed using a Living Imaging 2.50 software (Xenogen/ PerkinElmer) or an AURA imaging software (Spectral Instrument Imaging).

^{Allo}HSC-iNKT Cell In Vivo Antitumor Efficacy Study: A375 Human Melanoma Xenograft NSG Mouse Model

NSG mice were pre-conditioned with 100 rads of total body irradiation (day -1), followed by subcutaneous inoculation with 1 x 10^6 A375-FG cells (day 0). On day 3, the tumor-bearing experimental mice received intravenous (i.v.) injection of vehicle (PBS), 1.2 x 10^7 ^{Allo}HSC-iNKT cells, or 1.2 x 10^7 PBMC-NK cells. Over time, tumor loads were monitored by measuring total body luminescence using BLI and by measuring tumor size using a Fisherbrand™ Traceable™ digital caliper (Thermo Fisher Scientific). The tumor size was calculated as W x L mm^2. At around week 3, mice were terminated, and solid tumors were retrieved and weighted using a PA84 precision balance (Ohaus).

^{Allo}BCAR-iNKT Cell In Vivo Antitumor Efficacy Study: MM.1S Human MM Xenograft NSG Mouse Model

NSG mice were pre-conditioned with 175 rads of total body irradiation (day -1), followed by intravenous inoculation with 1 x 10^6 MM-CD1d-FGFP cells (day 0). To study antitumor efficacy under low tumor load condition, on day 3, the tumor-bearing experimental mice received i.v. injection of vehicle (PBS), ^{Allo}BCAR-iNKT cells (7 x 10^6 CAR^+ cells), or conventional BCAR-T cells (7 x 10^6 CAR^+ cells). To study antitumor efficacy under high tumor load condition, on day 15, the tumor-bearing experimental mice received i.v. injection

of vehicle (PBS), ^{Allo}BCAR-iNKT cells (5 x 10^6 CAR^+ cells), or conventional BCAR-T cells (5 x 10^6 CAR^+ cells). Over time, experimental mice were monitored for survival, and their tumor loads were measured using BLI.

^{U}BCAR-iNKT Cell In Vivo Antitumor Efficacy Study: MM.1S Human MM Xenograft NSG Mouse Model

NSG mice were pre-conditioned with 175 rads of total body irradiation (day -1), followed by intravenous inoculation with 5 x 10^5 MM-CD1d-FGFP cells (day 0). On day 3 the tumor-bearing experimental mice received i.v. injection of vehicle (PBS), ^{Allo}BCAR-iNKT cells (3 x 10^6 CAR^+ cells), or conventional BCAR-T cells (3 x 10^6 CAR^+ cells). Over time, experimental mice were monitored for survival, and their tumor loads were measured using BLI.

Ganciclovir (GCV) In Vitro and In Vivo Killing Assay

For GCV *in vitro* killing assay, ^{Allo}HSC-iNKT cells were cultured in C10 medium in the presence of titrated amount of GCV (0-50 μM) for 4 days; live ^{Allo}HSC-iNKT cells were then counted using a hematocytometer (VWR) via Trypan Blue staining (Fisher Scientific).

GCV *in vivo* killing assay was performed using an NSG xenograft mouse model. NSG mice received i.v. injection of 1 x 10^7 ^{Allo}HSC-iNKT cells on day 0, followed by i.p. injection of GCV for 5 consecutive days (50 mg/kg per injection per day). On day 5, mice were terminated. Multiple tissues (i.e., spleen, liver, and lung) were collected and processed for flow cytometry analysis to detect tissue-infiltrating ^{Allo}HSC-iNKT cells (identified as iNKT TCR^+CD45^+), following established protocols (Zhu et al., 2019).

Histological Analysis

Tissues (i.e., heart, liver, kidney, lung, and spleen) were collected from the experimental mice, fixed in 10% Neutral Buffered Formalin for up to 36 hours, then embedded in paraffin for sectioning (5 μm thickness). Tissue sections were prepared and stained with Hematoxylin and Eosin (H&E) by the UCLA Translational Pathology Core Laboratory, following the Core's standard protocols. Stained sections were imaged using an Olympus BX51 upright microscope equipped with an Optronics Macrofire CCD camera (AU Optronics) at 20 x and 40 x magnifications. The images were analyzed using Optronics PictureFrame software (AU Optronics).

Statistical Analysis

GraphPad Prism 6 (Graphpad Software) was used for statistical data analysis. Student's two-tailed *t* test was used for pairwise comparisons. Ordinary 1-way ANOVA followed by Tukey's or Dunnett's multiple comparisons test was used for multiple comparisons. Log rank (Mantel-Cox) test adjusted for multiple comparisons was used for Meier survival curves analysis. Data are presented as the mean ± SEM, unless otherwise indicated. In all figures and figure legends, "n" represents the number of samples or animals utilized in the indicated experiments. A P value of less than 0.05 was considered significant. ns, not significant; *P < 0.05; **P < 0.01; ***P < 0.001; ****P < 0.0001.

Results

Generation of Allogeneic HSC-Engineered iNKT (^{Allo}HSC-iNKT) Cells

Human CD34$^+$ hematopoietic stem and progenitor cells (referred to as HSCs in this study) collected from either cord blood (denoted as CB-HSCs) or from granulocyte-colony stimulating factor (G-CSF)-mobilized human periphery blood (denoted as PBSCs) were transduced with a Lenti/iNKT-sr39TK vector and then cultured *in vitro* in a 2-Stage artificial

thymic organoid (ATO)/α-galactosylceramide (αGC) culture system (**Figure 3-1A**). The Lenti/iNKT-sr39TK vector has been previously used to develop an autologous HSC-engineered iNKT cell therapy for cancer [41]; ATO is an *in vitro* 3D culture that supports the human HSC differentiation into T cells [77,96]; while αGC is a synthetic agonist glycolipid ligand that specifically stimulates iNKT cells [36]. We routinely achieved over 50% lentivector transduction rate of HSCs (**Figure 3-1B**). Transduced HSCs were then placed in the Stage 1 ATO culture, where they differentiated into human iNKT cells over a course of 8 weeks with over 100-fold expansion (**Figures 3-1A and 3-1C**). At the end of Stage 1 culture, ATOs were dissociated into single cells that were then placed in the Stage 2 αGC expansion culture for another 2-3 weeks, resulting in another 100-1000-fold expansion and an ^{Allo}HSC-iNKT cell product of high yield and purity (**Figures 3-1A and 3-1D**).

In the ATO/αGC culture, ^{Allo}HSC-iNKT cells followed a typical iNKT cell development path defined by CD4/CD8 co-receptor expression [34]. During Stage 1, ^{Allo}HSC-iNKT cells transited from $CD4^-CD8^-$ (DN) to $CD4^+CD8^+$ (DP), then toward $CD4^-CD8^{+/-}$ (**Figure 3-1E**). At the end of Stage 2, majority (> 99%) of ^{Allo}HSC-iNKT cells showed a $CD4^-CD8^{+/-}$ (CD8 SP/DN) phenotype (Figure 1E). Note that the end ^{Allo}HSC-iNKT cell product did not contain a $CD4^+CD8^-$ (CD4 SP) population that are present in the endogenous human iNKT cells (Figure 1E; [34]. In general, CD8 SP/DN human iNKT cells are considered to be proinflammatory and highly cytotoxic and thereby are desirable for cancer immunotherapy [34,45,97–100].

Flow cytometry analysis showed that the ^{Allo}HSC-iNKT cell product comprised high-purity transgenic iNKT cells (**Figure 3-1D**); single cell TCR sequencing analysis confirmed that these ^{Allo}HSC-iNKT cells uniformly expressed the transgenic iNKT TCRs while nearly undetectable randomly recombined endogenous αβ TCRs (**Figure 3-1F**). In sharp contrast to ^{Allo}HSC-iNKT cells, conventional αβ T cells isolated from health donor periphery blood

(denoted as PBMC-Tc cells) expressed highly diverse endogenously recombined αβ TCRs, whereas iNKT cells isolated from health donor periphery blood (denoted as PBMC-iNKT cells) expressed a conserved invariant TCR α chain (Vα24-Jα18) and limited diverse TCR β chains (dominantly Vβ11) (**Figure 3-1F**).

The manufacture of ^{Allo}HSC-iNKT cells was highly robust: we generated ^{Allo}HSC-iNKT cell products of high purity and yield from all 12 donors tested (4 CB-HSCs and 8 PBSCs) (**Figure 3-1G**). Based on our results, it was estimated that from one CB donor (comprising ~5 x 10^6 CB-HSCs), ~5 x 10^{11} ^{Allo}HSC-iNKT cells could be generated that can potentially be formulated into ~500-5,000 doses (~10^8-10^9 cells per dose based on the approved CAR-T cell therapy doses) [89]; from one PBSC donor (comprising ~5 x 10^8 PBSCs), ~3 x 10^{13} ^{Allo}HSC-iNKT cells could be generated that can potentially be formulated into ~30,000-300,000 doses (**Figure 3-1G**). The resulting ^{Allo}HSC-iNKT cell product contained pure transgenic iNKT cells and nearly undetectable bystander conventional αβ T cells, thereby lack of GvHD risk and suitable for "off-the-shelf" application.

Phenotype and Functionality of ^{Allo}HSC-iNKT Cells

Next, we analyzed the phenotype and functionality of ^{Allo}HSC-iNKT cells in comparison with endogenous human PBMC-iNKT and PBMC-Tc cells. ^{Allo}HSC-iNKT cells displayed a phenotype closely resembling PBMC-iNKT cells while distinct from PBMC-Tc cells: they expressed high levels of memory T cell markers (i.e., CD45RO), NK cell markers (i.e., CD161), as well as peripheral tissue and inflammatory site homing markers (i.e., CCR4, CCR5 and CXCR3) (**Figure 3-2A**). When stimulated with αGC, ^{Allo}HSC-iNKT cells proliferated vigorously (**Figure 3-2B**) and secreted high levels of Th0/Th1 cytokines (i.e., IFN-γ, TNF-α, and IL-2) while limited amounts of Th2 cytokines (i.e., IL-4) and Th17 cytokines (i.e., IL-17) (**Figure 3-2C**), indicating a Th0/Th1-prone functionality of ^{Allo}HSC-iNKT cells that agrees

with their CD8 SP/DN phenotype (**Figures 3-1E and 3-2A**) ([34,45,97,98]. Intracellular staining showed that at the single-cell level, ^{Allo}HSC-iNKT cells produced exceedingly high levels of effector cytokines (i.e., IFN-γ, TNF-α, and IL-2) and cytotoxic molecules (i.e., Perforin and Granzyme B) (**Figure 3-2D**). The ability to generate excess amounts of antitumor effector molecules is a promising signature of iNKT cells for cancer immunotherapy [51,52].

Transcriptome Profiling of ^{Allo}HSC-iNKT Cells

To fully characterize ^{Allo}HSC-iNKT cells, we performed deep RNAseq analysis of these cells; ^{Allo}HSC-iNKT cells generated from both CB and PBSC CD34$^+$ HSCs were studied. Healthy donor PBMC-derived endogenous iNKT (PBMC-iNKT), conventional αβ T (PBMC-αβTc), γδ T (PBMC-γδT), and NK (PBMC-NK) cells were included as controls. All cell types were prepared from multiple donors. Because ^{Allo}HSC-iNKT cells were dominantly CD4-negative (CD8 SP/DN), the CD4-negative subpopulations of PBMC-iNKT (CD8 SP/DN) and PBMC-αβTc (CD8$^+$) cells were analyzed in this experiment.

Principal component analysis (PCA) of the global gene expression profiles showed that ^{Allo}HSC-iNKT cells (both CB and PBSC-derived) were located the closest to PBMC-iNKT cells, next to PBMC-αβTc and PBMC-γδT cells, and the furthest from PBMC-NK cells, validating the iNKT cell nature of ^{Allo}HSC-iNKT cells (**Figure 3-2E**) [101].

"Master" transcription factor gene profiling analysis revealed a distinctive signature of ^{Allo}HSC-iNKT cells: they expressed high levels of *ZBTB16* that encodes PLZF, a signature transcription factor of innate T (e.g., iNKT and γδT) cells and NK cells [102]; they expressed high levels of *TBX21* that encodes T-bet, an essential transcription factor regulating Th1 polarization of T cells [103]; they expressed low levels of *GATA3* and *RORC* that respectively encodes GATA3 and RORγ, critical transcription factors regulating Th2 and Th17 polarization of T cells [104]; and they expressed high levels of *NFKB1* and *JUN* that respectively encodes NF-κB1 and c-

Jun, important transcription factors for TCR signaling (**Figure 3-2F**) [105,106]. These transcription factors have been indicated to play important roles in regulating iNKT cell development and functionality [70,107,108]. Of note, the *TBX21*^{high}*GATA3*^{low}*RORC*^{low} expression profile of ^{Allo}HSC-iNKT cells consists with their Th0/Th1-prone cytokine production profile (**Figure 3-2C**).

Further analysis of the various genes related to antitumor effector functions (e.g., genes encoding activation/homing markers, cytokines, and cytotoxic molecules) revealed ^{Allo}HSC-iNKT cells to be highly potent effector cells, in agreement with their *in vitro* phenotype and functionality characterization (**Figures 3-2A to 3-2D**). In addition, several interesting gene signatures stood out, which are highlighted below.

Typical iNKT cells exert NK function besides T cell function, via surface expression of NK receptors (Bendelac et al., 2007, Fujii et al., 2013; Vivier et al., 2012). Interestingly, compared to PBMC-iNKT and even PBMC-NK cells, ^{Allo}HSC-iNKT cells expressed exceedingly high levels of NK activating receptor genes (e.g., *NCAM1*, *NCR1*, *NCR2*, *KLR2*, and *KLR3*) while low levels of NK inhibitory receptor genes (e.g., *KIR3DL1*, *KIR3DL2*, *KIR2DL1*, and *KIR2DL2*), suggesting that ^{Allo}HSC-iNKT cells might exhibit a superior antitumor NK function (**Figure 3-2G**).

Tissue inflammatory homing markers expressed on effector immune cells enable them to access inflammatory tissues including tumor sites [97,109]. ^{Allo}HSC-iNKT cells expressed exceedingly high levels of multiple tissue inflammatory homing marker genes (e.g., *CCR1*, *CCR2*, *CCR3*, *CCR5*, *CCR6*, and *CXCR3*), comparable to those of endogenous innate T cells (i.e., PBMC-iNKT and PBMC-γδT cells) but significantly higher than those of endogenous conventional αβ T and NK cells (i.e., PBMC-αβTc and PBMC-NK cells), suggesting a strong capacity of ^{Allo}HSC-iNKT cells to home to and penetrate tumor sites (**Figure 3-2H**).

Human leukocyte antigen (HLA) incompatibility may trigger host T cell-mediated allorejection of adoptively transferred allogeneic cellular products, thereby limiting their

therapeutic efficacy [110,111]. Interestingly, compared to all the endogenous T cells (i.e., PBMC-iNKT, PBMC-αβTc, and PBMC-γδT cells) and NK cells (i.e., PBMC-NK cells) tested, ^{Allo}HSC-iNKT cells expressed much lower levels of HLA expression-related genes (e.g., genes encoding HLA-I molecules, B2M, HLA-II molecules, and HLA-II transactivators), suggesting that ^{Allo}HSC-iNKT cells might naturally resist allorejection and thereby have certain advantage over many PBMC-derived allogeneic cell products for "off-the-shelf" cell therapy (**Figure 3-2I**).

Tumor Targeting of ^{Allo}HSC-iNKT Cells Through Intrinsic NK Function

Following the NK lead of our RNAseq study (**Figure 3-2G**), we investigated the NK phenotype and antitumor function of ^{Allo}HSC-iNKT cells, in comparison with those of endogenous PBMC-NK cells. Flow cytometry analysis of cell surface markers showed that ^{Allo}HSC-iNKT cells expressed significantly higher levels of NK activating receptors (i.e., NKG2D and DNAM-1) while nearly undetectable NK inhibitory receptors (i.e., killer cell immunoglobulin-like receptors, KIRs) (**Figures 3-3A and 3-3B**). NK activating receptors recognize stress molecules (e.g., MIC-A/B and ULBP1-4 recognized by NKG2D, and CD112 and CD155 recognized by DNAM-1) upregulated on many tumor cells and trigger tumor targeting (Lee et al., 2017; Liu et al., 2019; Paul and Lal, 2017); while NK inhibitory receptors recognize matched "self" MHC molecules and suppress tumor killing [115,116]. Flow cytometry analysis of intracellular effector molecules showed that compared to PBMC-NK cells, ^{Allo}HSC-iNKT cells produced exceedingly higher levels of cytotoxic molecules (i.e., Perforin and Granzyme B) (**Figures 3-3A and 3-3B**). Collectively, these results confirmed a promising antitumor potential of ^{Allo}HSC-iNKT cells through their intrinsic NK function.

An attractive feature of NK cell-based cancer immunotherapy is its capacity to target a broad range of tumor cells independent of HLA and tumor antigen restrictions [112]. However,

NK cell-based therapy also confronts several significant challenges such as the limited *in vivo* efficacy of NK cells, as well as their intolerance to cryopreservation that poses a significant technical hurdle for their clinical and commercial applications [117,118]. Based on the "super active" NK phenotype of ^{Allo}HSC-iNKT cells, we wondered whether these cells might exhibit improved antitumor NK function. Moreover, unlike NK cells, iNKT cells can resist well to cryopreservation [119]; we therefore wondered whether ^{Allo}HSC-iNKT cells might also improve on this aspect.

Using an *in vitro* tumor cell killing assay, we evaluated the tumor killing efficacy of ^{Allo}HSC-iNKT cells in comparison with PBMC-NK cells (**Figure 3-3C**). Five human tumor cell lines were used as targets, including a leukemia cell line K562, a melanoma cell line A375, a lung cancer cell line H292, a prostate cancer cell line PC3, and a multiple myeloma cell line MM.1S. All five tumor cell lines were engineered to overexpress the firefly luciferase (Fluc) and enhanced green fluorescence protein (EGFP) dual-reporters, to enable the convenient monitoring of these tumor cells using either luciferase assay or flow cytometry (**Figure 3-4A**). Compared to PBMC-NK cells, ^{Allo}HSC-iNKT cells exhibited a significantly enhanced tumor killing efficacy across all five tumor cell lines (**Figures 3-3D, 3-3E, and 3-4B to 3-4D**). Interestingly, ^{Allo}HSC-iNKT cells sustained strong tumor killing efficacy after cryopreservation, whereas PBMC-NK cells were sensitive to freeze-thaw cycles and showed greatly reduced viability and antitumor capacity following cryopreservation (**Figures 3-3D, 3-3E, and 3-4B to 3-4D**). Blocking of NK activating receptors (i.e., NKG2D and DNAM-1) reduced tumor killing efficacy of ^{Allo}HSC-iNKT cells (**Figures 3-3F to 3-3H and 3-4E to 3-4G**), confirming their NK activating receptor-mediated tumor targeting function.

Next we evaluated the *in vivo* antitumor efficacy of ^{Allo}HSC-iNKT cells using a human melanoma xenograft NSG (NOD.Cg-Prkdc^{scid}Il2rg^{tm1Wjl}/SzJ) mouse model. A375-FG tumor cells were subcutaneously inoculated into NSG mice to form solid tumors, followed by a

paratumoral injection of ^{Allo}HSC-iNKT or PBMC-NK cells (**Figure 3-3I**). ^{Allo}HSC-iNKT cells effectively suppressed tumor growth at an efficacy higher than that of PBMC-NK cells, as evidenced by the time-course live animal bioluminescence imaging (BLI) monitoring (**Figures 3-3J and 3-4H**), tumor size measurement (**Figure 3-3K**), and terminal tumor weight assessment (**Figure 3-4I**).

Taken together, these studies support a cancer therapy potential of ^{Allo}HSC-iNKT cells through their intrinsic NK function, allowing these cells to target a board range of tumors independent of HLA and tumor antigen restrictions. Attractively, ^{Allo}HSC-iNKT cells may exhibit improved antitumor efficacy and cryopreservation resistance compared to NK cell-based allogeneic cell therapy products.

Tumor Targeting of ^{Allo}HSC-iNKT Cells Through Engineered Chimeric Antigen Receptors

Chimeric antigen receptor (CAR)-engineered cell therapy has great promise for treating cancer [89–91,120]; we therefore explored the potential of ^{Allo}HSC-iNKT cells as the allogeneic cell carriers for CAR-directed "off-the-shelf" cell therapy. A second-generation B-cell maturation antigen (BCMA)-targeting CAR (BCAR) was used for this study (**Figure 3-6A**); this BCAR contains 4-1BB and CD3ζ signaling domains and has shown clinical efficacy in treating human multiple myeloma (MM) [121].

^{Allo}HSC-iNKT cells were generated as previously described (**Figure 3-1A**); mature ^{Allo}HSC-iNKT cells were further transduced with a Retro/BCAR-tEGFR retroviral vector to produce the BCAR-engineered ^{Allo}HSC-iNKT cells (denoted as ^{Allo}BCAR-iNKT cells) (**Figure 3-5A**). The entire culture time (~10-11 weeks) and cell yield (~10^{11} per CB donor or ~10^{12} per PBSC donor) were similar to those of generating non-CAR engineered ^{Allo}HSC-iNKT cells (**Figures 3-1A and 3-1G**). The resulting ^{Allo}BCAR-iNKT cells were pure iNKT cells with high BCAR expression rate (> 98% iNKT TCR$^+$ and up to 80% BCAR$^+$; **Figure 3-5B**), and displayed a

typical human iNKT cell phenotype and functionality similar to those of ^{Allo}HSC-iNKT cells (**Figures 3-2A, 3-2D, 3-6C, and 3-6D**). Therefore, ^{Allo}HSC-iNKT cells can be effectively engineered to express CARs without compromising cell yield and quality.

To assess the antitumor capacity of ^{Allo}BCAR-iNKT cells, we used an established *in vitro* MM.1S-CD1d-FG tumor cell killing assay [41]; non-CAR engineered ^{Allo}HSC-iNKT cells, as well as healthy donor PBMC-derived conventional T cells with or without engineering with the same BCAR (denoted as PBMC-T or BCAR-T cells), were included as controls (**Figure 3-5C**). The MM.1S-CD1d-FG cell line was generated by engineering the parental BCMA-positive MM.1S human MM cell line to overexpress human CD1d and the Fluc-EGFP dual-reporters [41], mimicking a large portion of primary patient MM samples that are BCMA$^+$CD1d$^+$ (**Figure 3-6B**) [122]. This *in vitro* tumor cell killing assay allowed us to evaluate the tumor killing capacity of ^{Allo}BCAR-iNKT cells, as well as to investigate their possible NK/TCR/CAR triple-mechanisms for targeting MM (**Figure 3-5D**).

The ^{Allo}HSC-iNKT cells without BCAR engineering were able to kill MM.1S-CD1d-FG tumor cells while PBMC-T cells could not, indicating an intrinsic antitumor NK function of ^{Allo}HSC-iNKT cells (**Figures 3-5E, 3-4D, and 3-4G**); this intrinsic antitumor NK function was inherited by ^{Allo}BCAR-iNKT cells, confirmed by NK activating receptor (i.e., DNAM-1) blocking assay (**Figure 3-5F**). Meanwhile, the tumor cell killing efficacy of ^{Allo}HSC-iNKT cells was enhanced by the addition of αGC that did not happen to PBMC-T cells, indicating an iNKT TCR-mediated antitumor function of ^{Allo}HSC-iNKT cells; this TCR-mediated antitumor function was also inherited by ^{Allo}BCAR-iNKT cells (**Figure 3-5E**). Importantly, compared to ^{Allo}HSC-iNKT cells, ^{Allo}BCAR-iNKT cells showed stronger tumor cell killing, indicating a CAR-mediated antitumor function of ^{Allo}BCAR-iNKT cells (**Figure 3-5E**). Therefore, ^{Allo}BCAR-iNKT cells are able to target MM tumor cells using the NK/TCR/CAR triple-mechanisms, that may grant ^{Allo}BCAR-iNKT cells a higher tumor targeting efficacy and an enhanced capacity to

counteract tumor antigen escape compared to conventional BCAR-T cells (**Figures 3-5D-3-5F**) [37,123,124].

The *In vivo* antitumor efficacy of ^{Allo}BCAR-iNKT cells was studied using an established MM.1S-CD1d-FG xenograft NSG mouse model (Zhu et al., 2019); conventional BCAR-T cells were included as a control. At a low tumor load condition, ^{Allo}BCAR-iNKT cells eliminated MM tumor cells as effectively as BCAR-T cells (**Figures 3-5H and 3-5I**); however, experimental mice treated with BCAR-T cells eventually died of graft-versus-host disease (GvHD) despite being tumor-free, while experimental mice treated with ^{Allo}BCAR-iNKT cells lived long-term with tumor-free and GvHD-free (**Figures 3-5I and 3-5J**). Impressively, at a high tumor load condition, ^{Allo}BCAR-iNKT cells still managed to suppress tumor growth effectively and achieved tumor clearance in a fraction of experimental mice (2 out of 5 mice); conventional BCAR-T cells suppressed tumor growth less well and could not achieve tumor clearance (**Figures 3-5K-3-5N and 3-6E**).

Taken together, these studies support an attractive potential of ^{Allo}HSC-iNKT cells as "off-the-shelf" cell carriers for CAR-directed cancer immunotherapy. The high antitumor efficacy and multiple tumor-targeting mechanisms of CAR-engineered ^{Allo}HSC-iNKT cells may provide new opportunities to target hard-to-treat tumors and counteract tumor antigen escape.

Safety Study of ^{Allo}HSC-iNKT Cells

Graft-versus-host (GvH) response is the primary safety concern of an "off-the-shelf" allogeneic cell therapy [89]. Since iNKT cells do not react to mismatched HLA molecules and protein alloantigens, these cells are not expected to mount GvH responses [30,31]. To verify this safety feature of ^{Allo}HSC-iNKT cells, we performed both *in vitro* and *in vivo* studies. In an *in vitro* mixed lymphocyte reaction (MLR) assay, in sharp contrast to conventional PBMC-Tc cells,

^{Allo}HSC-iNKT cells did not react to all the mismatched healthy donor PBMCs tested, evidence by their lack of IFN-γ production (**Figures 3-7A and 3-7B**). In an *in vivo* NSG mouse xenograft model, unlike PBMC-Tc cells that induced GvHD and killed experimental mice around two months post PBMC-Tc cell transfer, ^{Allo}HSC-iNKT cells did not cause GvHD and sustained long-term survival of experimental mice (**Figures 3-7C and 3-7D**). The lack of GvHD in ^{Allo}HSC-iNKT cell engrafted experimental mice was confirmed by histology analysis showing healthy tissue structures without lymphocyte infiltrations; on the contrary, analyses of PBMC-Tc cell engrafted experimental mice showed severe tissue damages associated with heavy lymphocyte infiltrations (**Figures 3-7E and 3-7F**). To study the influence of CAR engineering, we analyzed the GvH response of ^{Allo}BCAR-iNKT cells; BCAR-T cells were included as a control. Distinct from BCAR-T cells, ^{Allo}BCAR-iNKT cells showed no response in the *in vitro* MLR assay (**Figures 3-8A and 3-8B**) and induced no GvHD in the human MM xenograft NSG mouse model (**Figures 3-8C and 3-8D**), indicating that CAR engineering and tumor encountering do not change the GvH-free safety feature of ^{Allo}HSC-iNKT cells.

Besides GvHD risk, allogeneic cell therapy may confer other safety risks, including those common to cell-based cancer immunotherapy such as cytokine release syndrome (CRS) and neurotoxicity [125]. Although we did not observe that ^{Allo}HSC-iNKT cells induced tissue toxicity in our NSG xenograft mouse models (**Figures 3-7E and 3-7F**), these safety studies may be limited by the utilized preclinical animal models [125]. Additional safety control may be necessary, especially for the initial clinical development. We therefore have engineered a "safety switch" in ^{Allo}HSC-iNKT cell products by incorporating a suicide gene (i.e., sr39TK) in the human iNKT TCR gene delivery vector, resulting in ^{Allo}HSC-iNKT cells that are 100% labeled with the suicide gene (**Figure 3-1A**). In cell culture, addition of guanosine analog (GCV) effectively killed ^{Allo}HSC-iNKT cells (**Figure 3-8E**); in an NSG mouse xenograft model, administration of GCV effectively depleted ^{Allo}HSC-iNKT cells from all tissues

examined (e.g., liver, spleen, and lung; **Figures 3-7G-3-7I**). Of note, GCV has been used clinically as a prodrug to induce sr39TK-mediated suicide effect in cellular products [126]. Other alternative suicide switch systems (e.g., inducible Cas9 and truncated EGFR) can certainly be utilized [89,127–129].

Taken together, ^{Allo}HSC-iNKT cells are free of GvHD risk and can be equipped with an additional "safety switch", making them suitable for "off-the-shelf" allogeneic cell therapy.

Immunogenicity Study of ^{Allo}HSC-iNKT Cells

For allogeneic cell therapies, immunogenicity can be a concern because allorejection by host T and NK cells may greatly limit the efficacy of therapeutic allogeneic cells [13]. Host conventional CD8 and CD4 αβ T cells reject allogeneic cells through recognizing mismatched HLA-I and HLA-II molecules, respectively [14,32]. In a classical *in vitro* MLR assay studying T cell-mediated host-versus-graft (HvG) response via IFN-γ secretion reading, compared to endogenous conventional T and iNKT (i.e., PBMC-Tc and PBMC-iNKT) cells, ^{Allo}HSC-iNKT cells triggered a significantly reduced HvG response (**Figures 3-9A, 3-9C, and 3-10A**). Our previous RNAseq study made an interesting observation that compared to endogenous immune cells (i.e., conventional αβT, iNKT, γδT, and NK cells), ^{Allo}HSC-iNKT cells globally downregulated the expression of many genes controlling cell surface display of HLA-I and HLA-II molecules (**Figure 3-2I**). Flow cytometry analysis confirmed that compared to PBMC-Tc and PBMC-iNKT cells, ^{Allo}HSC-iNKT cells expressed significantly reduced levels of HLA-I molecules and nearly undetectable HLA-II molecules (**Figures 3-9B and 3-10B**), which may account for their resistance to T cell-mediated HvG response (**Figures 3-9C and 3-10A**). Because interferons can upregulate HLA-I expression (Axelrod et al., 2019), we studied HLA-I expression on ^{Allo}HSC-iNKT cells under IFN-γ stimulation (**Figure 3-11A**). ^{Allo}HSC-iNKT cells slightly upregulated surface HLA-I expression post IFN-γ stimulation; however, their

overall surface HLA-I level still remained significantly lower than those of PBMC-Tc and PBMC-iNKT cells (**Figures 3-11B and 3-11C**). Because an *in vivo* inflammatory tumor microenvironment may upregulate the expression of HLA molecules on tumor-infiltrating immune cells (e.g., via IFN-γ) [132], we also assessed HLA expression on ^{Allo}HSC-iNKT cells in an A375-FG human melanoma xenograft NSG mouse model adapted from a previous study (**Figures 3-3I**). A375-FG melanoma cells were subcutaneously inoculated in NSG mice to form solid tumors followed by injection of ^{Allo}HSC-iNKT cells; PBMC-Tc and PBMC-iNKT cells were included as controls (**Figure 3-9D**). Flow cytometry analysis of tumor-infiltrating ^{Allo}HSC-iNKT cells showed that these cells maintained low expressions of HLA-I and HLA-II molecules, at levels significantly lower than those of tumor-infiltrating PBMC-Tc and PBMC-iNKT cells (**Figures 3-9E and 3-9F**).

Next, we studied NK cell–mediated allorejection. Host NK cells reject allogeneic cells through a double-trigger mechanism: 1) "missing self" (i.e., missing of matching HLA-I molecules on allogeneic cells) triggers the release of KIR inhibition, and 2) "stress signal" (i.e., upregulated stress molecules on allogeneic cells) triggers the activation of NK activating receptors such as NKG2D [114,133,134]. Because ^{Allo}HSC-iNKT cells expressed low levels of HLA-I molecules, we wondered whether this might make ^{Allo}HSC-iNKT cells susceptible to host NK rejection. Surprisingly, in an *in vitro* MLR assay studying NK cell-mediated allorejection, compared to endogenous conventional T and iNKT (i.e., PBMC-Tc and PBMC-iNKT) cells, ^{Allo}HSC-iNKT cells survived rejection by mismatched healthy donor PBMC-derived NK cells significantly better (**Figures 3-9G-3-9I**); correspondingly, NK cells co-cultured with ^{Allo}HSC-iNKT cells exhibited less upregulation of NK activation markers (i.e., CD107a) (**Figures 3-10D and 3-10E**). Flow cytometry analysis revealed that compared to PBMC-Tc and PBMC-iNKT cells, ^{Allo}HSC-iNKT cells expressed much reduced and nearly undetectable levels of NKG2D ligands

(i.e., ULBP; **Figures 3-9J and 3-10C**) [135], which may be one of the possible mechanisms accounting for their resistance to NK cell-mediated allorejection.

Collectively, these studies revealed a stable HLA-I/II^{low} phenotype of ^{Allo}HSC-iNKT cells that may grant them advantage to resist host T cell-mediated rejection, compared to other healthy donor PBMC-derived allogeneic cell products; meanwhile, ^{Allo}HSC-iNKT cells also expressed low levels of stress molecules such as NKG2D ligands, making them also resistant to host NK cell-mediated allorejection. These "low immunogenicity" features of ^{Allo}HSC-iNKT cells support their application for "off-the-shelf" cell therapy.

Development of HLA-Ablated Universal HSC-iNKT (^{U}HSC-iNKT) Cells and Derivatives

Although ^{Allo}HSC-iNKT cells display a stable HLA-I/II^{low} phenotype (**Figures 3-2I, 3-9B, 3-9E, 3-9F, and 3-10B**), their residual HLA-I/II molecules may still make them susceptible to certain levels of host T cell-mediated allorejection. We therefore explored further engineering of the ^{Allo}HSC-iNKT cell products to achieve total ablation of their surface HLA-I/II molecules. Interestingly, this task can be accomplished by ablation of only two genes: 1) a *B2M* gene encoding the beta 2-microglobulin (B2M) that is required for the surface display of all types of HLA-I molecules [14], and 2) a *CIITA* gene encoding the class II transactivator (CIITA) that is required for the transcription of all types of HLA-II molecules [32]. Ablation of *B2M* and *CIITA* genes can be achieved by using the powerful gene-editing tools like the CRISPR-Cas9/gRNA system [33]. We postulated that by combining iNKT TCR gene-engineering and B2M/CIITA gene-editing, we would produce HLA-ablated "universal" HSC-iNKT (^{U}HSC-iNKT) cells totally resistant to host T cell-mediated allorejection. We intended to perform both gene-engineering and gene-editing on the small numbers of starting HSCs upfront of the HSC-iNKT cell culture; this manufacturing design would save on the use of gene-engineering/editing materials (i.e., lentivector and CRISPR-Cas9/gRNA) that can be cost-limiting, and also enable

the maximal gene engineering/editing efficiency that can be carried on into the final ^{U}HSC-iNKT cell products. Similar to the generation of ^{Allo}CAR-iNKT cell products (Figure 4A), a CAR engineering step can be incorporated after ^{U}HSC-iNKT cell differentiation, resulting in HLA-ablated universal CAR engineered HSC-iNKT (^{U}CAR-iNKT) cell products.

CB or PBSC-derived CD34^{+} HSCs were transduced with the Lenti/iNKT-sr39TK lentivector; 24 hours later, these HSCs were electroporated with a CRISPR-Cas9/B2M-CIITA-gRNAs complex (**Figure 3-12A**). The gene-engineering/editing efficiency was high; we routinely achieved over 50% lentivector transduction rate and over 50% HLA-I/II double-ablation rate (**Figure 3-12B**). The engineered HSCs were then put into the HSC-iNKT differentiation ATO culture for 8 weeks followed by 1 week of αGC expansion (**Figures 3-12A**); CRISPR-Cas9 gene editing did not interfere with HSC differentiation into iNKT cells and we obtained high yield of differentiated ^{U}HSC-iNKT cells similar to that of ^{Allo}HSC-iNKT cells (**Figures 3-1C and 3-12C**). CRISPR-Cas9 gene editing also did not interfere with the follow-up CAR engineering; we obtained an efficient BCMA-targeting CAR (BCAR) engineering rate similar to that of engineering PBMC-derived conventional BCAR-T cells (**Figure 3-12C**). The high HLA-I/II double-ablation rate of the starting HSCs was inherited by the resulting ^{U}BCAR-iNKT cells (i.e., ~50% of the resulting cells were HLA-I/II double-negative); if needed, the HLA-I/II double-negative cells could be further enriched (to over 97%) using Magnetic-Activated Cell Sorting (MACS) via B2M and HLA-II magnetic beads labeling (**Figures 3-12D**).

Despite HLA-I/II ablation, ^{U}BCAR-iNKT cells displayed a typical iNKT phenotype and a highly cytotoxic functionality similar to those of ^{Allo}BCAR-iNKT cells (**Figure 3-13A**). As expected, ^{U}BCAR-iNKT cells induced nearly undetectable T cell-mediated alloresponse when mixed with mismatched healthy donor PBMCs (**Figures 3-12E, 3-12F, and 3-13E**); meanwhile, ^{U}BCAR-iNKT cells maintained the resistance to NK cell-mediated allorejection

(**Figures 3-12G, 3-12H, and 3-13F**). Safety features of ^{U}BCAR-iNKT cells resembled those of ^{Allo}BCAR-iNKT cells: ^{U}BCAR-iNKT cells did not mount GvH response (**Figures 3-13B and 3-13C**) and they were sensitive to sr39TK/GCV-induced suicide control (**Figure 3-13D**). To study whether HLA ablation may impact the antitumor efficacy of ^{U}BCAR-iNKT cells, we performed *in vitro* and *in vivo* antitumor assays. In an established *in vitro* MM tumor cell killing assay (**Figure 3-5C**), ^{U}BCAR-iNKT cells effectively killed tumor cells at an efficacy comparable to that of ^{Allo}BCAR-iNKT cells (**Figures 3-5E, 3-13G, and 3-13H**). Similar to ^{Allo}BCAR-iNKT cells, ^{U}BCAR-iNKT cells could also utilize an NK/TCR/CAR triple-mechanisms targeting tumor cells (**Figures 3-5E, 3-5F, 3-13H, and 3-13I**), that may grant them advantage over conventional BCAR-T cells to gain additional antitumor efficacy (**Figure 3-13H**), as well as to counteract BCMA antigen escape that has been reported in conventional BCAR-T cell therapy clinical trials [37,123,124]. In an established *in vivo* human MM xenograft NSG mouse model (**Figure 3-5G**), ^{U}BCAR-iNKT cell treated animals achieved total tumor clearance and long-term survival; while BCAR-T cell treated animals only achieved partial tumor suppression that was followed by tumor relapse and GvHD development, leading to limited survival benefit (**Figures 3-12I-3-12L**).

Collectively, these studies support the generation of HLA-ablated universal HSC-iNKT cell products and derivatives (e.g., CAR-iNKT cell products), that are fully resistant to host T cell-mediated allorejection and thereby may have improved *in vivo* persistence and antitumor efficacy.

Discussion

Here we report the generation and characterization of allogeneic HSC-engineered iNKT cells and derivatives. Using an *in vitro* HSC-iNKT differentiation cell culture, we showed the generation of ^{Allo}HSC-iNKT cells that were of high yield and purity, high antitumor efficacy,

high safety profile (GvH-free and suicide control), and low immunogenicity (largely resistant to T and NK cell-mediated allorejection). These ^{Allo}HSC-iNKT cells could be further engineered to express CAR, thereby enhancing their tumor targeting capacity; these cells can also be further engineered to ablate their surface HLA molecules, thereby enhancing their resistance to host T cell-mediated allorejection. Collectively, our studies have generated ^{Allo}HSC-iNKT cells and demonstrated them as promising cell carriers for developing off-the-shelf cancer immunotherapy.

Development of allogeneic "off-the-shelf" cell therapies, many equipped with CARs, is becoming a fast-evolving frontier of cancer immunotherapy. Two major categories of such allogeneic cell products are based on engineering healthy donor-derived conventional αβ T cells or NK cells [11–14]. Because conventional αβ T cells risk inducing GvHD in allogeneic hosts due to HLA incompatibility, these T cells need to be gene-edited to ablate endogenous TCR expression, usually through disrupting the *TRAC* or/and *TRBC* gene loci, to make them suitable for allogeneic cell therapy but meanwhile may also potentially increase manufacture complexity [18–21]. On the other hand, NK-based allogeneic cell products are considered of low GvHD risk and thereby do not require additional gene-editing, but their *in vivo* clonal expansion and antitumor performance may be limited compared to that of conventional αβ T cells [12]. Two such allogeneic cell products, a conventional αβ T cell-based universal CD19-CAR engineered T cells (UCART19) and an NK cell-based CB-derived CD19-CAR engineered NK cells, were recently tested in phase I clinical trials treating CD19$^+$ B cell malignancies [19,23]. These studies reported the feasibility, certain antileukemic activity, and manageable safety profile of the two cell products, showing an encouraging step forward for the field of allogeneic cell therapy [19,23].

Engineering unconventional innate-type T cells (e.g., iNKT, γδ T, and MAIT cells) that have potent antitumor capacity while free of GvHD risk represents another promising direction for

developing allogeneic cell therapy for cancer especially for solid tumors [37,46,48,136]. In particular, iNKT cell-based cancer immunotherapy has attracted considerable attention. A preclinical study reported the enhanced anti-lymphoma activity of CAR19-engineered iNKT cells compared to conventional CAR19-T cells [37]. Another preclinical study reported the potent antitumor efficacy to neuroblastoma and no GvHD risk of CAR.GD2-engineered iNKT cells compared to conventional CAR.GD2-T cells [136]. A recent clinical trial testing autologous GD2.CAR-engineered iNKT cells also showed safety and certain efficacy in patients with relapsed or refractory neuroblastoma [48]. These studies suggest the therapeutical potential of iNKT-based cell products and support the development of such cell products for allogeneic cell therapy for cancer even solid tumors.

The *in vitro* HSC-iNKT differentiation cell culture was robust and of high yield (**Figure 3-1G**). The resulting ^{Allo}HSC-iNKT cell products were of high purity and nearly free of bystander conventional αβ T cells (**Figure 3-1D**), that may allow these cell products to be directly used for allogeneic cell therapy without an additional purification step; if necessary, commercially available human iNKT cell isolation reagents (e.g., human anti-iNKT microbeads from Miltenyi) can be used for further purification. Notably, we detected no expression of endogenous TCRs in ^{Allo}HSC-iNKT cells (**Figure 3-1F**), suggesting an induction of allelic exclusion by transgenic iNKT TCRs as previously reported [41,42]. The robustness, high yield, and high purity of ^{Allo}HSC-iNKT cell products will facilitate their next-stage translational and clinical development.

The antitumor efficacy of ^{Allo}HSC-iNKT cells was promising. These cells displayed a typical iNKT phenotype and functionality: they co-expressed memory T cell and NK cell markers, they expressed high levels of inflammatory tissue/tumor homing markers, and they produced high levels of cytokines and cytotoxic molecules outperforming T and NK cells (**Figures 3-2 and 3-3**). Interestingly, compared to endogenous cells (i.e., T, NK, and iNKT

cells), ^{Allo}HSC-iNKT cells expressed exceedingly high levels of NK activating receptors and low levels of NK inhibitory receptors (**Figure 3-2G**), that was associated with their superior antitumor NK function *in vitro* and *in vivo* (**Figure 3-3**). In addition, the NK/TCR/CAR tumor-targeting triple-mechanisms of ^{Allo}HSC-iNKT cells and their derivatives grant these cells a stronger antitumor efficacy (**Figures 3-5D-3-5F, 3-12I-3-12J, and 3-13G-3-13I**) and may enable them to counteract tumor antigen escape which has been observed in T cell-based cancer therapies [37,89,123,124]. Overall, in both a human blood cancer (i.e., MM) and a human solid tumor (i.e., melanoma) preclinical mouse xenograft models utilized in this study, ^{Allo}HSC-iNKT cells or their CAR-derivatives (i.e., ^{Allo}BCAR-iNKT and ^{U}BCAR-iNKT cells) showed an enhanced antitumor efficacy compared to healthy donor PBMC-derived NK or CAR-engineered conventional αβ T cells, highlighting their cancer therapy potential (**Figures 3-3I-3-3K, 3-4H-3-4I, 3-5G-3-5N, 3-6E, and 3-12I-3-12L**). Notably, a synthetic iNKT cell antagonist, αGC, has been demonstrated to specifically stimulate and expand iNKT cells in both preclinical and clinical studies; αGC is clinically available and may be used as a "designer stimulator" to enhance the *in vivo* performance of ^{Allo}HSC-iNKT cells [28,35,38,57,137].

The safety of ^{Allo}HSC-iNKT cells was appealing. In our studies, ^{Allo}HSC-iNKT cells showed no GvH responses against multiple random healthy donor PBMCs in an *in vitro* MLR assay (**Figures 3-7A, 3-7B, 3-8A, and 3-8B**), and showed no GvHD *in vivo* in multiple human tumor xenograft NSG mouse models (**Figures 3-7C-3-7F, and 3-8C-3-8D**), in consistent with their iNKT cell nature and high purity (**Figure 3-1**) [36]. A suicide switch (e.g., sr39TK/GCV) can also be incorporated into ^{Allo}HSC-iNKT cells to provide an additional safety control (**Figure 3-7G-3-7I, and 3-8E**). The high safety of ^{Allo}HSC-iNKT cells strongly support their allogeneic application.

A serendipity feature of ^{Allo}HSC-iNKT cells is their significantly lower immunogenicity compared to PBMC-derived endogenous immune cells (i.e., αβ T, iNKT, γδ

T, and NK cells). ^{Allo}HSC-iNKT cells expressed reduced levels of HLA-I molecules and nearly undetectable HLA-II molecules, that seemed to be genomically programmed (**Figure 3-2I**) and stable through the *in vitro* culture and *in vivo* persistence even within the tumor microenvironment (**Figures 3-9A-3-9F**); this feature may allow these cells to resist allorejection by host T cells and thereby alleviating the need of additional HLA gene editing or intense host T cell depletion preconditioning treatment (e.g., CD52 antibody treatment) [18,19]. Meanwhile, ^{Allo}HSC-iNKT cells also expressed reduced levels of NK activating receptor ligands (e.g., ULBP) (**Figure 3-9J**); this feature may allow these cells to also resist the allorejection by host NK cells and increase their suitability for allogeneic cell therapy (**Figures 3-9G-3-9I**). The biological regulations resulting in this low immunogenicity feature of ^{Allo}HSC-iNKT cells remain to be illustrated; nonetheless, such biological regulations seemed to interfere with neither the production nor the antitumor efficacy of ^{Allo}HSC-iNKT cells both *in vitro* and *in vivo* (**Figures 3-3, 3-5, and 3-12**).

Despite their promises, the current ^{Allo}HSC-iNKT cell products confront certain limitations that may be further improved: the manufacturing process can benefit from switching to a feeder-free culture system that will greatly simplify and accelerate the clinical and commercial development; the sr39TK/GCV suicide switch can be replaced with an alternative suicide switch system (e.g., inducible Cas9 or truncated EGFR) that are less immunogenic and cell-cycle dependent [89,127–129,138]; an *HLA-E* transgene can also be incorporated into the ^{Allo}HSC-iNKT cell products to further increase their resistance to host NK cell-mediated allorejection [133,139]; and pluripotent stem cells (i.e., ES cells and iPSCs) may be utilized as an alternative "unlimited" cell source to derive HSCs for the generation of ^{Allo}HSC-iNKT cells [45]. Further exploration of ^{Allo}HSC-iNKT cells as allogeneic cell carriers for developing off-the-shelf cell therapy treating cancer especially solid tumors will certain be interesting directions for future study.

Acknowledgements

We thank the University of California, Los Angeles (UCLA) animal facility for providing animal support; the UCLA Translational Pathology Core Laboratory (TPCL) for providing histology support; the UCLA Technology Center for Genomics & Bioinformatics (TCGB) facility for providing RNAseq services; the UCLA CFAR Virology Core for providing human cells; and the UCLA BSCRC Flow Cytometry Core Facility for cell sorting support. This work was supported by a Director's New Innovator Award from the NIH (DP2 CA196335, to L.Y.), a Partnering Opportunity for Translational Research Projects Award and a Partnering Opportunity for Discovery Stage Award from the California Institute for Regenerative Medicine (CIRM TRAN1-08533 and DISC2-11157, to L.Y.), a Stem Cell Research Award from the Concern Foundation (to L.Y.), a Research Career Development Award from the STOP CANCER Foundation (to L.Y.), a BSCRC-RHF Research Award from the Rose Hills Research Foundation (to L.Y.), and an Ablon Scholars Award (to L.Y.). Y-R.L. is a predoctoral fellow supported by the UCLA Whitcome Predoctoral Fellowship in Molecular Biology. J.Y. is a predoctoral fellow supported by the UCLA Broad Stem Cell Research Center (BSCRC) Predoctoral Fellowship. D.L. is a predoctoral fellow supported by T32 Microbial Pathogenesis Training Grant (Ruth L. Kirschstein National Research Service Award, T32-AI007323). Z.L. is a postdoctoral fellow supported by the UCLA Tumor Immunology Training Grant (USHHS Ruth L. Kirschstein Institutional National Research Service Award, T32-CA009120). S.Z is a predoctoral fellow supported by the UCLA Medical Scientist Training Program Grant (T32-GM008042).

Author contributions

Y-R.L., Y.Z, and L.Y. designed the experiments, analyzed the data, and wrote the manuscript. L.Y. conceived and oversaw the study, with assistance from Y-R.L. and Y.Z, and with suggestions from G.M.C., S.M.L., M.P., A.R., D.B.K., O.N.W., and P.W. Y-R.L. and Y.Z performed all experiments, with assistance from Y.J.K., Y.Zhu, F.M., J.Y., Y.-C.W., X.C., Z.L., Z.S., X.W., D.L., J.K., T.T., C.H., and J.H. D.C. performed cell sorting. A.M-H., and C.S. helped with ATO culture. J.S. provided MM patient BM samples. F.M. helped with analysis of RNAseq data. Xiaoyan Wang helped with the statistical analysis of data.

Figures

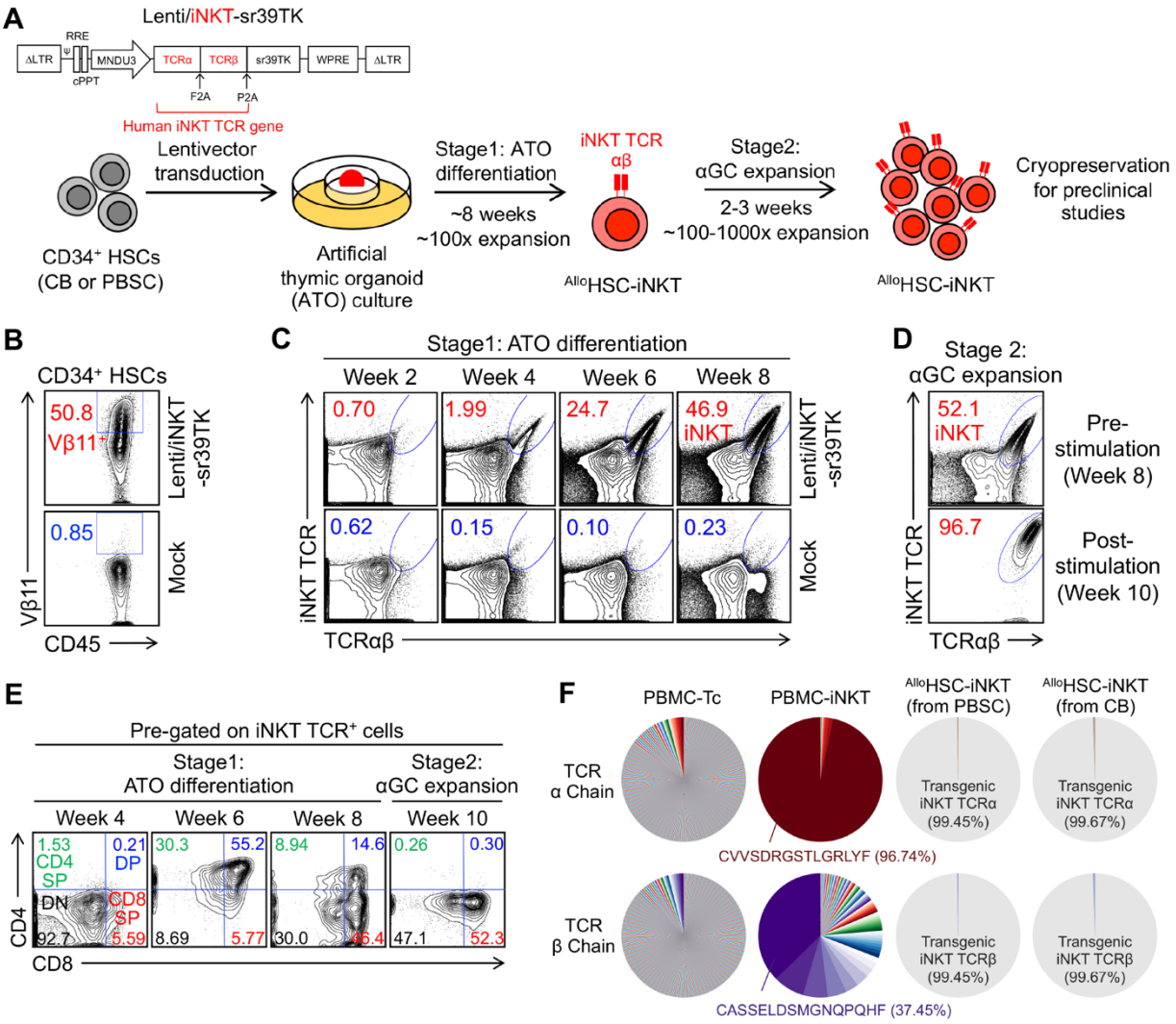

G

Input cells: Lenti/iNKT-sr39TK transduced human CD34⁺ HSCs (~50% lentivector transduction rate)	Estimated output AlloHSC-iNKT cells (per donor)	Estimated doses (per donor; 10^8-10^9 cells per dose)
CB-HSCs (4 donors were tested; ~5 x 10^6 HSCs per donor)	2.5-7.5 x 10^{11}	~500-5,000
PBSCs (8 donors were tested; ~5 x 10^8 HSCs per donor)	1.5-4.5 x 10^{13}	~30,000-300,000

Figure 3-1. *In Vitro* Generation of Allogenic HSC-Engineered iNKT (AlloHSC-iNKT) Cells
(A) Experimental design to generate AlloHSC-iNKT cells *in vitro*. HSC, hematopoietic stem cell; CB, cord blood; PBSC, periphery blood stem cell; αGC, α-galactosylceramide; Lenti/iNKT-sr39TK, lentiviral vector encoding an iNKT TCR gene and an sr39TK suicide/PET imaging gene.
(B-E) FACS monitoring of AlloHSC-iNKT cell generation. (B) Intracellular expression of iNKT TCR (identified as Vβ11⁺) in CD34⁺ HSCs at 72 hours post lentivector transduction. (C) Generation of iNKT cells (identified as iNKT TCR⁺TCRαβ⁺ cells) during Stage 1 ATO differentiation culture. A 6B11 monoclonal antibody was used to stain iNKT TCR. (D) Expansion of iNKT cells during Stage 2 αGC expansion culture. (E) Expression of CD4/CD8 co-receptors on AlloHSC-iNKT cells during Stage 1 and Stage 2 cultures. DN, CD4/CD8 double

negative; CD4 SP, CD4 single positive; DP, CD4/CD8 double positive; CD8 SP, CD8 single positive.
(F) Single cell TCR sequencing analysis of ^{Allo}HSC-iNKT cells. Healthy donor periphery blood mononuclear cell (PBMC)-derived conventional αβ T (PBMC-Tc) and iNKT (PBMC-iNKT) cells were included as controls. The relative abundance of each unique T cell receptor sequence among the total unique sequences identified for individual cells was represented by a pie slice.
(G) Table summarizing experiments that have successfully generated ^{Allo}HSC-iNKT cells.
Representative of 1 (F) and over 10 experiments (A-E).

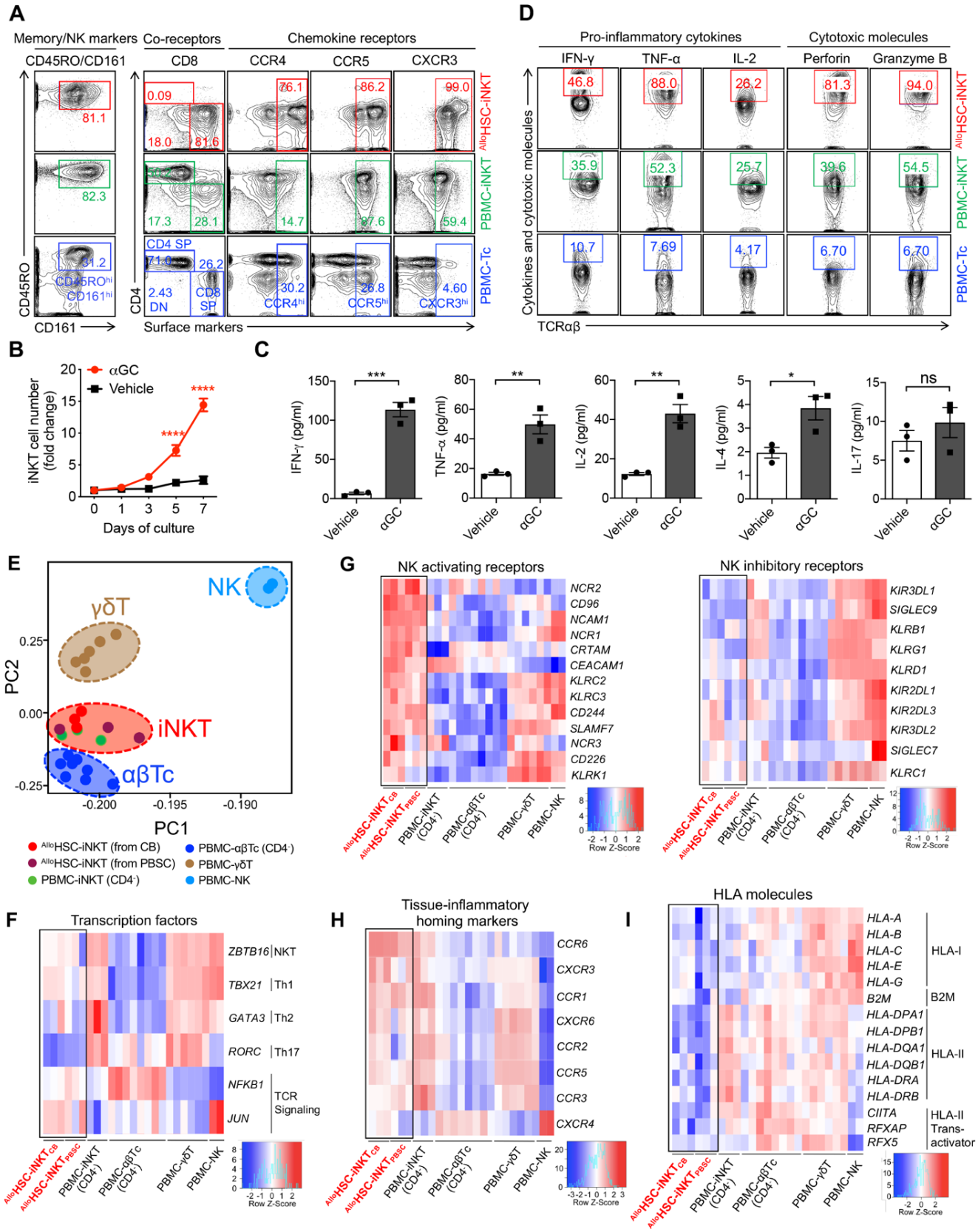

Figure 3-2. Characterization and Gene Profiling of ^{Allo}HSC-iNKT Cells

(A) FACS detection of surface markers on ^{Allo}HSC-iNKT cells. PBMC-iNKT and PBMC-Tc cells were included as controls.

(B-C) Antigen responses of ^{Allo}HSC-iNKT cells. ^{Allo}HSC-iNKT cells were cultured for 7 days, in the presence or absence of αGC (denoted as αGC or Vehicle, respectively). (B) Cell growth curve (n = 3). (C) ELISA analyses of cytokine (IFN-γ, TNF-α, IL-2, IL-4 and IL-17) production at day 7 post αGC stimulation (n = 3).
(D) FACS detection of intracellular cytokines and cytotoxic molecules in ^{Allo}HSC-iNKT cells. PBMC-iNKT and PBMC-Tc cells were included as controls.
(E-I) Deep RNAseq analysis of ^{Allo}HSC-iNKT cells generated from CB or PBSC-derived $CD34^+$ HSCs (n = 3 for each). Healthy donor PBMC-derived conventional $CD4^-$ αβ T (PBMC-αβTc; n = 8), $CD4^-$ iNKT (PBMC-iNKT; n = 3), γδ T (PBMC- γδT; n = 6), and NK (PBMC-NK; n = 2) cells were included as controls. N indicates different donors. (E) Principal component analysis (PCA) plot showing the ordination of all six cell types. (F-I) Heatmaps showing the expression of selected genes encoding transcription factors (F), NK activating and inhibitory receptors (G), tissue-inflammatory homing markers (H), and HLA molecules (I), for all six cell types.
Representative of 1 (E-I) and 3 (A-D) experiments. Data are presented as the mean ± SEM. ns, not significant, *P < 0.05, **P < 0.01, ***P < 0.001, ****P < 0.0001, by Student's *t* test.

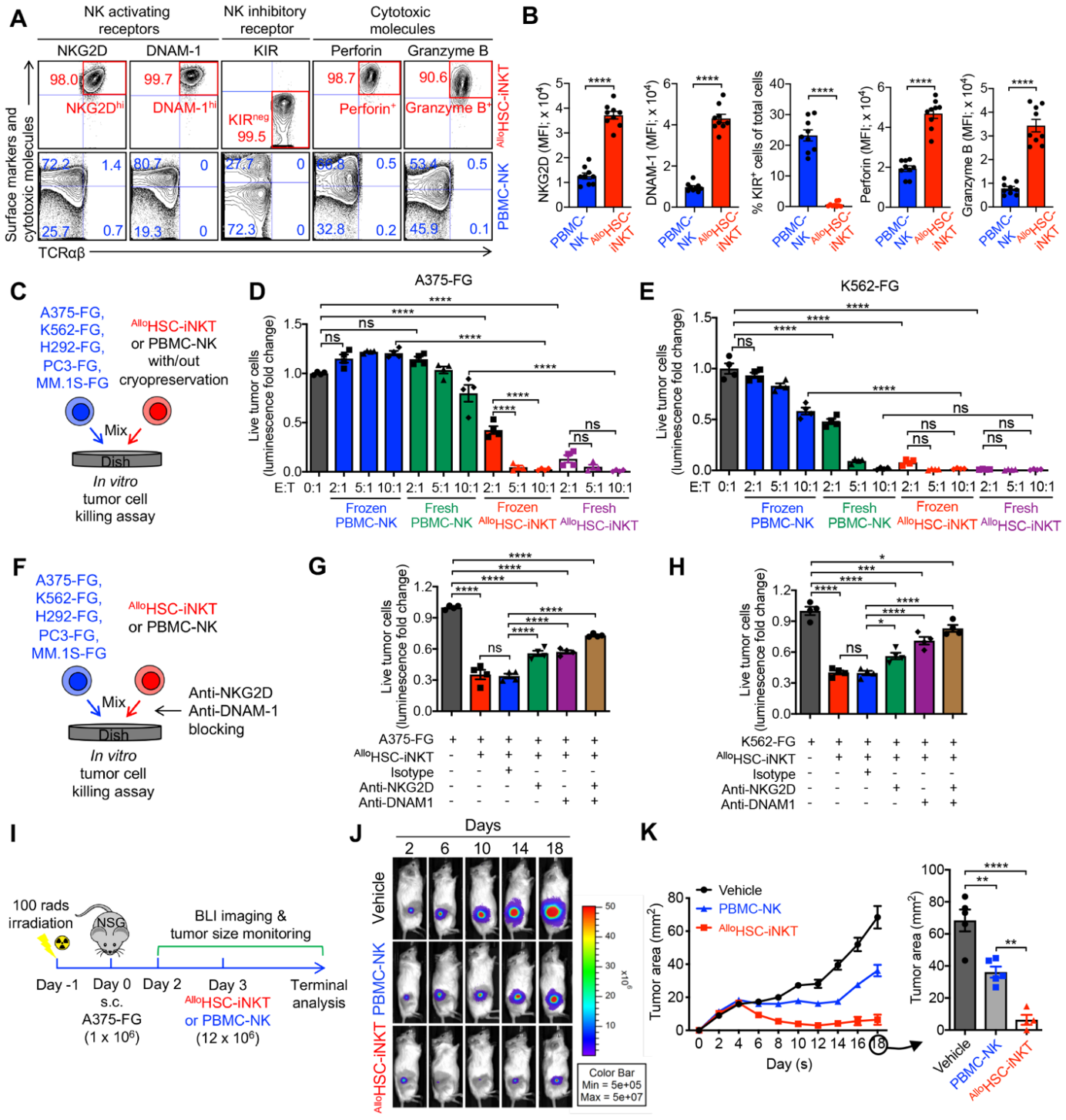

Figure 3-3. Tumor Targeting of ^{Allo}HSC-iNKT Cells Through Intrinsic NK Function

(A-B) FACS analyses of surface NK receptor expression and intracellular cytotoxic molecule production by ^{Allo}HSC-iNKT cells. PBMC-NK cells were included as a control. (A) Representative FACS plots. (B) Quantification of A (n = 9).

(C-E) *In vitro* direct killing of human tumor cells by ^{Allo}HSC-iNKT cells. PBMC-NK cells were included as a control. Both fresh and frozen-thawed cells were studied. Five human tumor cell lines were studied: A375 (melanoma), K562 (myelogenous leukemia), H292 (lung cancer), PC3 (prostate cancer), and MM.1S (multiple myeloma). All tumor cell lines were engineered

to express firefly luciferase and green fluorescence protein (FG) dual-reporters. (C) Experimental design. (D and E) Tumor killing data of A375-FG human melanoma cells (D) and K562-FG human myelogenous leukemia cells (E) at 24-hours (n = 4).
(F-H) Tumor killing mechanisms of ^{Allo}HSC-iNKT cells. NKG2D and DNAM-1 mediated pathways were studied. (F) Experimental design. (G) Tumor killing data of A375-FG human melanoma cells at 24-hours (tumor:iNKT ratio 1:2; n = 4). (H) Tumor killing data of K562-FG human myelogenous leukemia cells at 24-hours (tumor:iNKT ratio 1:1; n = 4).
(I-K) Studying the *in vivo* antitumor efficacy of ^{Allo}HSC-iNKT cells in an A375-FG human melanoma xenograft NSG mouse model. (I) Experimental design. BLI, live animal bioluminescence imaging. (J) BLI images showing tumor loads in experimental mice over time. (K) Tumor size measurements over time (n = 4-5).
Representative of 3 experiments. Data are presented as the mean ± SEM. ns, not significant, *P < 0.05, **P < 0.01, ***P < 0.001, ****P < 0.0001, by Student's *t* test (B) or by 1-way ANOVA (D, E, G, H, and K).

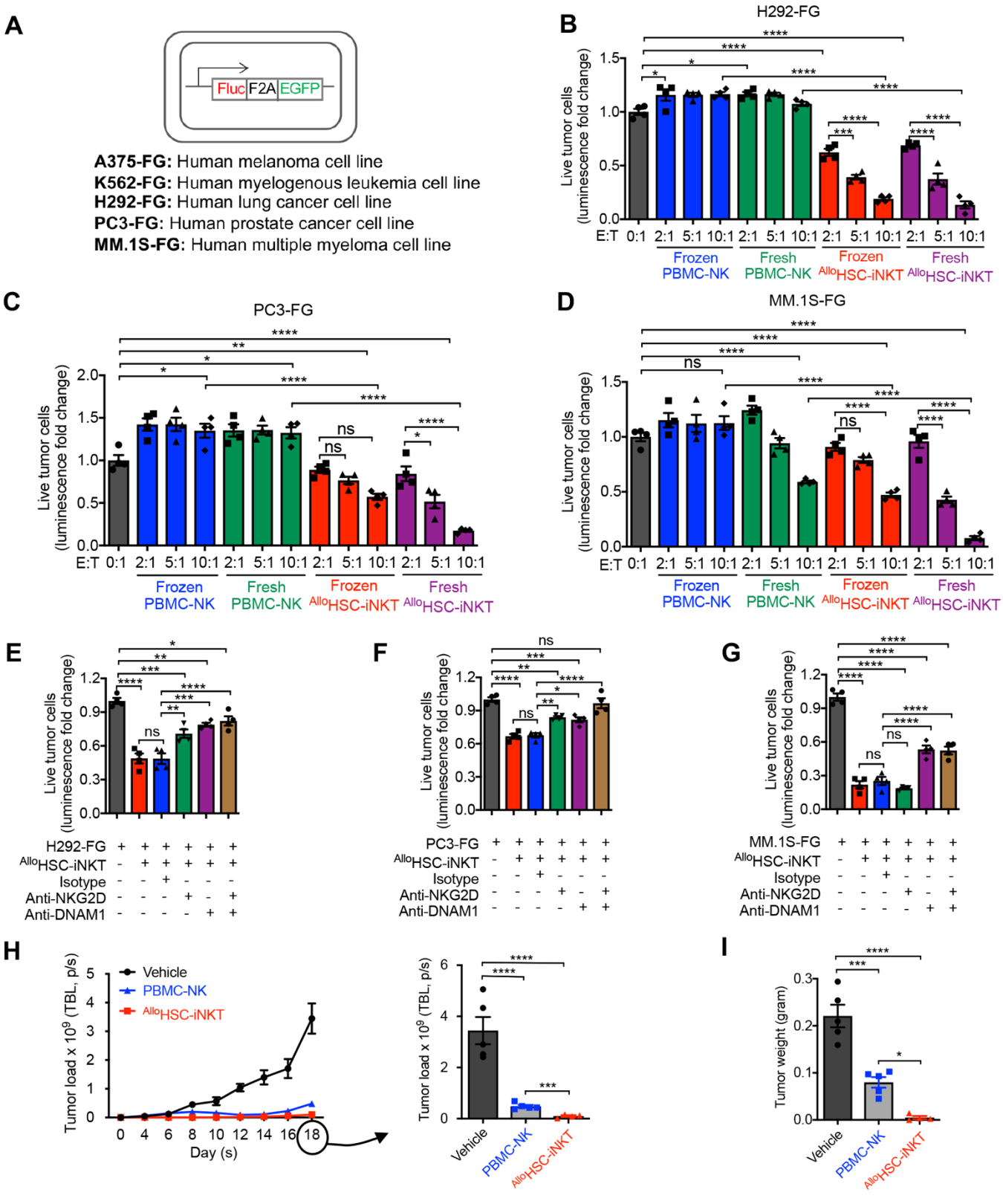

Figure 3-4. Tumor Targeting of ^{Allo}HSC-iNKT Cells Through NK Function
(A) Schematics showing the engineered A375-FG, K562-FG, H292-FG, PC3-FG, and MM.1S-FG cell lines. Fluc, firefly luciferase; EGFP, enhanced green fluorescent protein; F2A, foot-and-mouth disease virus 2A self-cleavage sequence.

(B-D) *In vitro* direct killing of human tumor cells by ^{Allo}HSC-iNKT cells. PBMC-NK cells were included as a control. Both fresh and frozen-thawed cells were studied. Tumor cell killing was analyzed at 24-hours post co-culture. Tumor killing data of H292-FG human lung cancer cells (B), PC3-FG human prostate cancer cells (C), and MM.1S-FG human multiple myeloma cells (D) were presented. N = 4.
(E-G) Tumor killing mechanisms of ^{Allo}HSC-iNKT cells. NKG2D and DNAM-1 mediated pathways were studied. Tumor cell killing was analyzed at 24-hours post co-culture. Tumor killing data of H292-FG (tumor:iNKT ratio 1:2), PC3-FG (tumor:iNKT ratio 1:10), and MM.1S-FG (tumor:iNKT ratio 1:15) were presented. N = 4. Related to main Figures 3F-3H.
(H-I) *In vivo* antitumor efficacy of ^{Allo}HSC-iNKT cells in an A375-FG human melanoma xenograft NSG mouse model. (H) BLI measurements of tumor loads over time (n = 4 or 5). (I) Tumor weight at the terminal harvest on day 18 (n = 4 or 5). Related to main Figures 3I-3K.
Representative of 3 experiments. Data are presented as the mean ± SEM. ns, not significant, *P<0.05, **P<0.01, ***P<0.001, ****P<0.0001, by 1-way ANOVA (B-G, I) or by Student's *t* test (H).

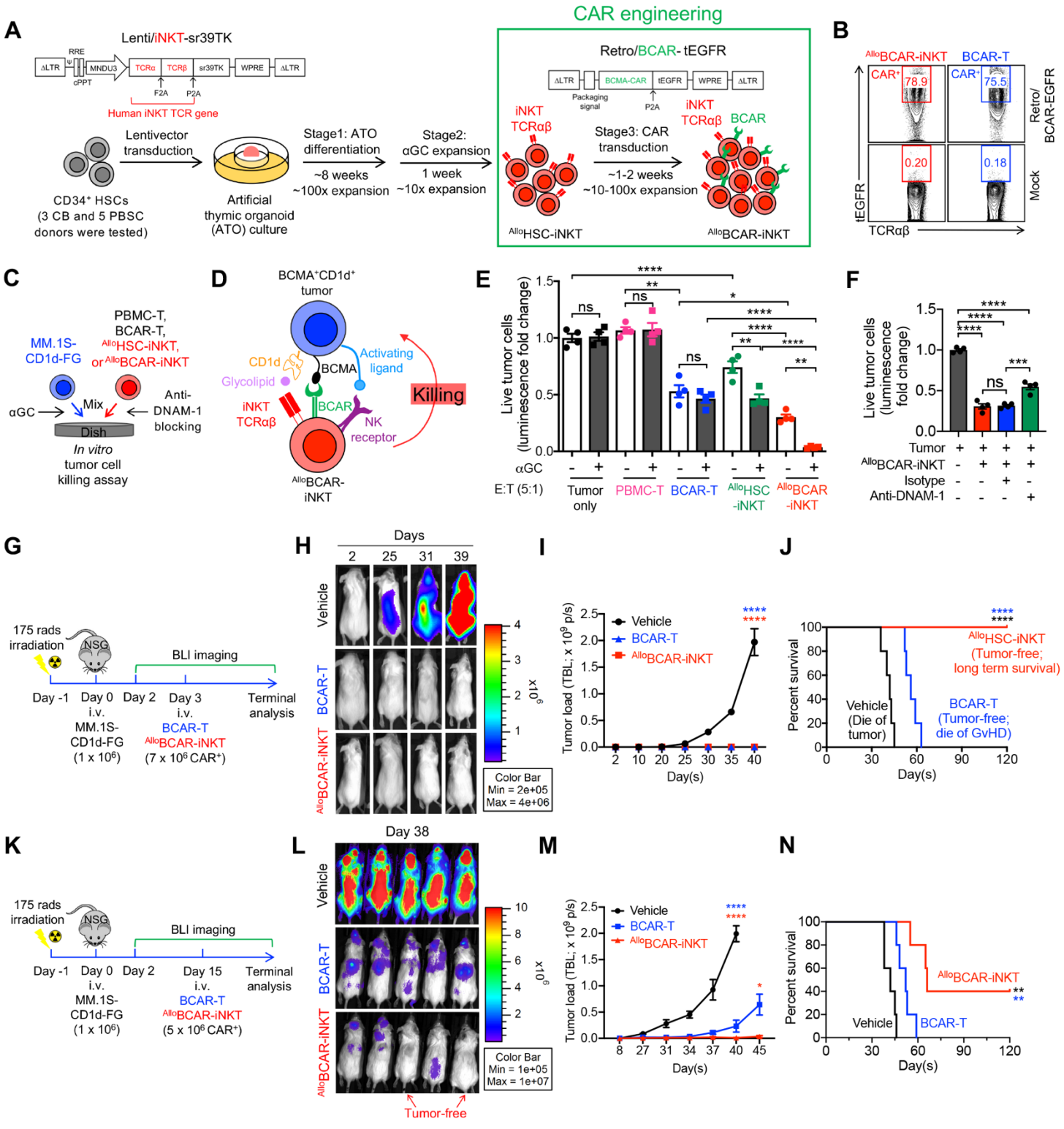

Figure 3-5. Tumor Targeting of ^{Allo}HSC-iNKT Cells Through Engineered Chimeric Antigen Receptors

(A) Experimental design to generate BCMA CAR-engineered ^{Allo}HSC-iNKT (^{Allo}BCAR-iNKT) cells *in vitro*. BCMA, B-cell maturation antigen; CAR, chimeric antigen receptor; BCAR, BCMA CAR; Retro/BCAR-tEGFR, retroviral vector encoding a BCMA CAR gene as well as a truncated epidermal growth factor receptor (tEGFR) reporter gene. tEGFR was used as a staining marker indicating the BCAR expression.

(B) FACS analysis of BCAR expression (identified as tEGFR^{+}) on ^{Allo}BCAR-iNKT at 72-hours post retrovector transduction. Healthy donor PBMC T cells transduced with the same Retro/BCAR-tEGFR vector (denoted as BCAR-T cells) were included as a staining control.
(C-F) *In vitro* killing of human multiple myeloma cells by ^{Allo}BCAR-iNKT cells. MM.1S-CD1d-FG, human MM.1S cell line engineered to overexpress human CD1d as well as FG dual-reporters. PBMC-T, BCAR-T, and ^{Allo}HSC-iNKT cells were included as effector cell controls. (C) Experimental design. (D) Diagram showing the tumor-targeting triple-mechanisms of ^{Allo}BCAR-iNKT cells, mediated by NK activating receptors, iNKT TCR, and BCAR. (E) Tumor cell killing by the indicated effector cells with/out the addition of αGC (n = 4). (F) Tumor cell killing by ^{Allo}BCAR-iNKT cells with/out the blockade of DNAM-1 (n = 4). Tumor cell killing was analyzed at 8-hours post co-culture (effector:tumor ratio 5:1).
(G-N) Studying the *in vivo* antitumor efficacy of ^{Allo}BCAR-iNKT cells in an MM.1S-CD1d-FG human multiple myeloma xenograft NSG mouse model. Tumor-bearing mice injected with BCAR-T cells or no cells (Vehicle) were included as controls. (G-J) Low tumor load condition. (G) Experimental design. (H) BLI images showing tumor loads in experimental mice over time. (I) Quantification of H (n = 5). (J) Kaplan-Meier survival curves of experimental mice over a period of 4 months post tumor challenge (n = 5). (K-N) High tumor load condition. (K) Experimental design. (L) BLI images showing tumor loads in experimental mice at day 38. (M) Quantification of tumor load in experimental mice over time (n = 5). (N) Kaplan-Meier survival curves of experimental mice over a period of 4 months post tumor challenge (n = 5).
Representative of 2 experiments (K-N) and 3 experiments (A-J). Data are presented as the mean ± SEM. ns, not significant, *P < 0.05, **P < 0.01, ***P < 0.001, ****P < 0.0001, by one-way ANOVA (E, F, I, and M), or by log rank (Mantel-Cox) test adjusted for multiple comparisons (J and N).

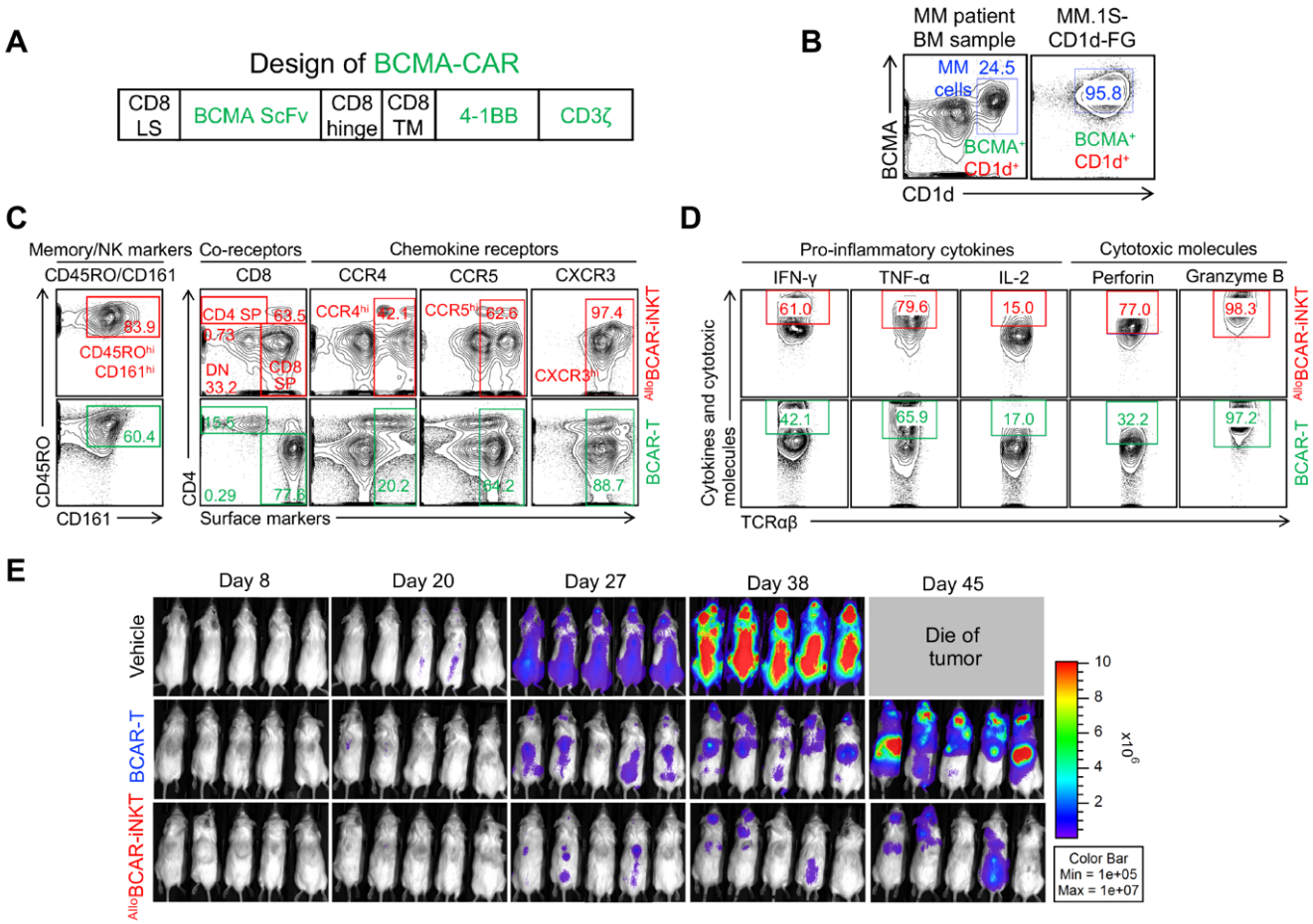

Figure 3-6. Tumor Targeting of ^{Allo}HSC-iNKT Cells Through Engineered Chimeric Antigen Receptors.

(A) Schematics showing the design of BCMA-CAR. LS, leader sequence; ScFv, single-chain variable fragment; TM, transmembrane domain.

(B) FACS analyses of BCMA and CD1d expression on MM.1S-CD1d-FG cells. A representative MM patient primary bone marrow (BM) sample was included as a control.

(C-D) FACS characterization of ^{Allo}BCAR-iNKT cells. (C) Surface marker expression. (D) Intracellular cytokine and cytotoxic molecule production. BCAR-T cells were included as a control.

(E) *In vivo* antitumor efficacy of ^{Allo}BCAR-iNKT cells in an MM.1S-CD1d-FG human multiple myeloma xenograft NSG mouse model. BLI images were presented showing tumor loads in experimental mice over time. Related to main Figures 4K-4N.

Representative of 2 (E) and 3 (A-D) experiments.

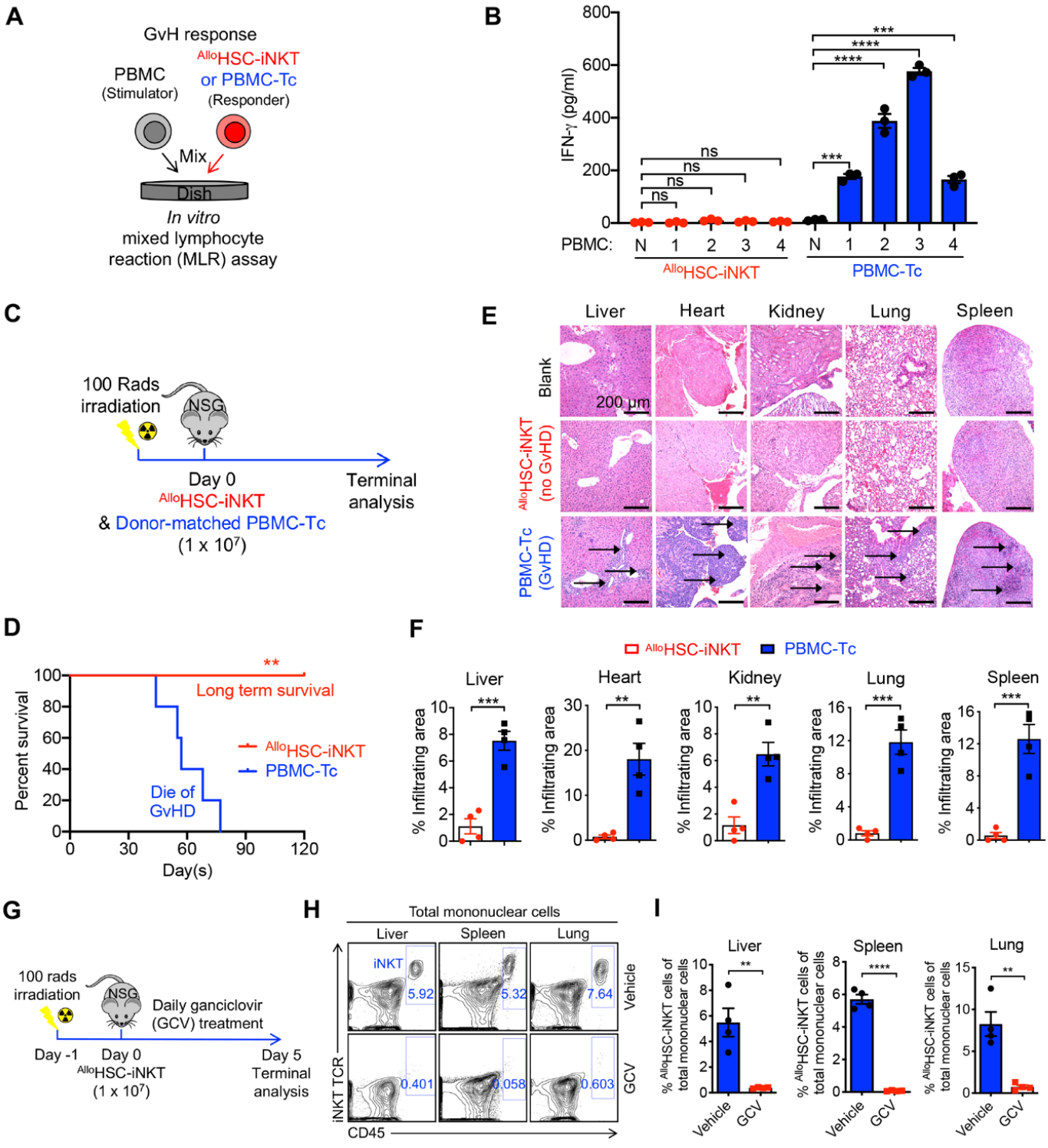

Figure 3-7. Safety Study of AlloHSC-iNKT Cells

(A-B) Studying the graft-verus-host (GvH) response of AlloHSC-iNKT cells using an *in vitro* mixed lymphocyte reaction (MLR) assay. PBMC-Tc cells were included as a responder cell control. (A) Experimental design. PBMCs from 4 different healthy donors were used as stimulator cells. (B) ELISA analyses of IFN-γ production at day 4 (n = 4). N, no stimulator cells.

(C-F) Studying the GvH response of AlloHSC-iNKT cells using an NSG mouse xenograft model. Donor-matched PBMC-Tc cells were included as a control. (C) Experimental design. (D)

Kaplan-Meier survival curves of experimental mice over time (n = 5). (E) H&E-stained tissue sections. Blank indicates tissue sections collected from control NSG mice receiving no adoptive cell transfer. Arrows point to mononuclear cell infiltrates. Scale bar: 200 μm. (F) Quantification of E (n = 4).
(G-I) *In vivo* controlled depletion of ^{Allo}HSC-iNKT cells via GCV treatment. GCV, ganciclovir. (G) Experimental design. (H) FACS detection of ^{Allo}HSC-iNKT cells in the liver, spleen, and lung of NSG mice at day 5. (I) Quantification of G (n = 4).
Representative of 2 experiments. Data are presented as the mean ± SEM. ns, not significant, *P < 0.05, **P < 0.01, ***P < 0.001, ****P < 0.0001, by one-way ANOVA (B), Student's *t* test (F and I), or by log rank (Mantel-Cox) test adjusted for multiple comparisons (D).

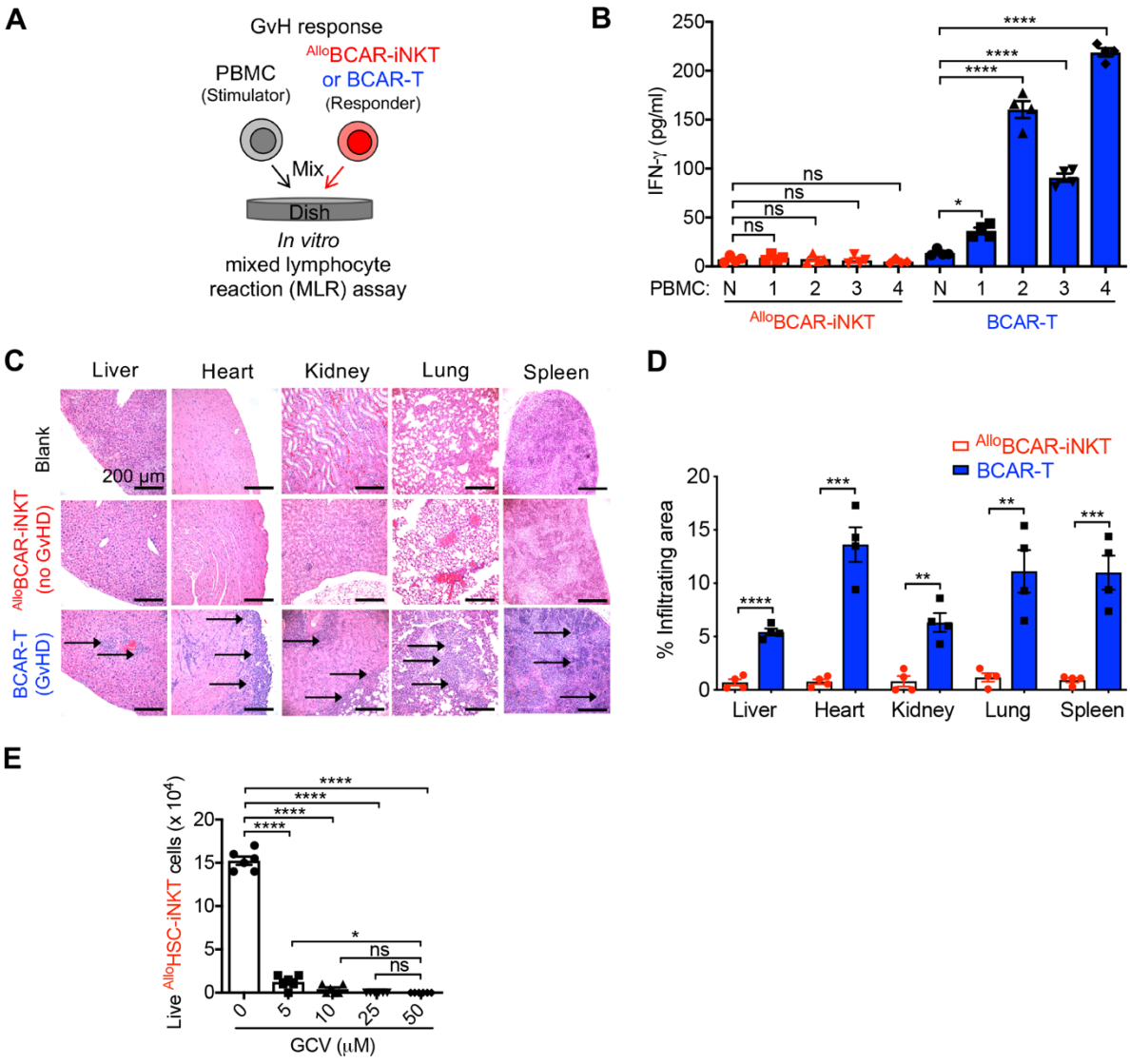

Figure 3-8. Safety study of ^{Allo}HSC-iNKT cells.

(A-B) Studying the graft-verus-host (GvH) response of ^{Allo}BCAR-iNKT cells using an *in vitro* mixed lymphocyte reaction (MLR) assay. BCAR-T cells were included as a responder cell control. (A) Experimental design. PBMCs from 4 different healthy donors were used as stimulator cells. (B) ELISA analyses of IFN-γ production at day 4 (n = 4).

(C-D) Histology analysis of tissue sections collected from experimental mice as described in Figures 4G-4J. (C) H&E-stained tissue sections. Blank indicates tissue sections collected from NSG mice receiving no adoptive cell transfer. Arrows point to mononuclear cell infiltrates. Scale bar: 200 μm. (D) Quantification of C (n = 4).

(E) *In vitro* GCV killing assay. ^{Allo}HSC-iNKT cells were cultured *in vitro* in the presence of gradient concentrations of GCV for 4 days, followed by quantification of live cells via cell counting (n = 6).

Representative of 2 experiments. Data are presented as the mean ± SEM. ns, not significant, *P<0.05, **P<0.01, ***P<0.001, ****P<0.0001, by Student's *t* test (D) or by 1-way ANOVA (B and E).

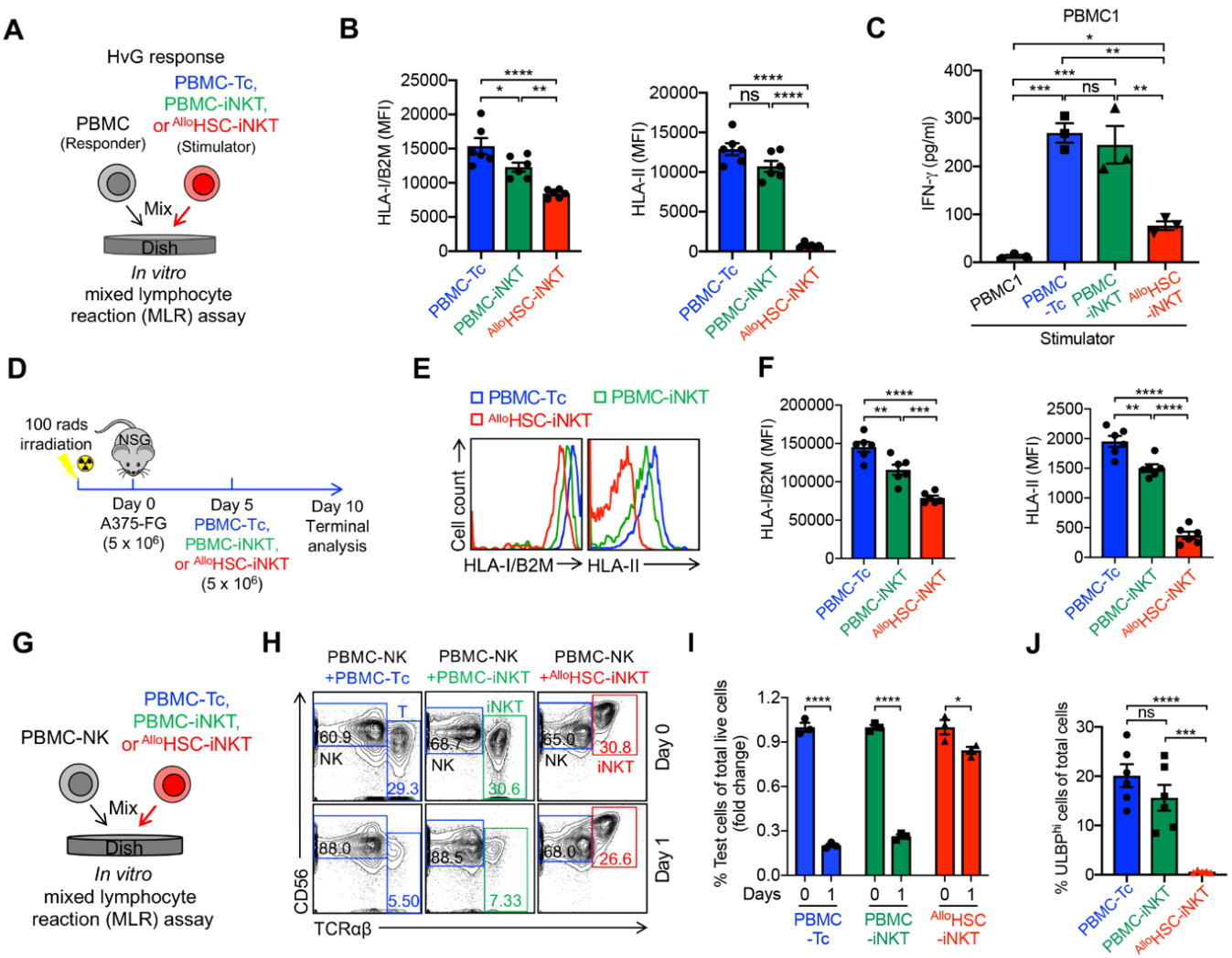

Figure 3-9. Immunogenicity Study of ^{Allo}HSC-iNKT Cells

(A-C) Studying allogenic T cell response against ^{Allo}HSC-iNKT cells using an *in vitro* MLR assay. Irradiated ^{Allo}HSC-iNKT cells (as stimulators) were co-cultured with donor-mismatched PBMC cells (as responders). Irradiated PBMC-iNKT and PBMC-Tc cells were included as stimulator cell controls. (A) Experimental design. PBMCs from 3 different healthy donors were used as responders. (B) FACS analyses of HLA-I and HLA-II expression on the indicated stimulator cells (n = 6). (C) ELISA analyses of IFN-γ production at day 4 (n = 3).

(D-F) Studying HLA-I/II expression on ^{Allo}HSC-iNKT cells *in vivo* in an A375-FG human melanoma xenograft NSG mouse model. PBMC-iNKT and PBMC-Tc cells were included as effector cell controls. (D) Experimental design. (E) FACS analyses of HLA-I/II expression on the indicated effector cells isolated from A375-FG solid tumors. (F) Quantification of E (n = 5).

(G-J) Studying allogenic NK cell response against ^{Allo}HSC-iNKT cells using an *in vitro* MLR assay. ^{Allo}HSC-iNKT cells were co-cultured with donor-mismatched PBMC-NK cells. PBMC-iNKT and PBMC-Tc cells were included as controls. (G) Experimental design. (H) FACS analyses of the indicated cells at day 0 and 1. (I) Quantification of H (n = 3). (J) FACS analyses of ULBP expression on the indicated cells (n = 5-6).

Representative of 2 (D-F) and 3 (A-C, and G-J) experiments. Data are presented as the mean ± SEM. ns, not significant, *P < 0.05, **P < 0.01, ***P < 0.001, ****P < 0.0001, by Student's *t* test (I) or by one-way ANOVA (B, C, F, and G).

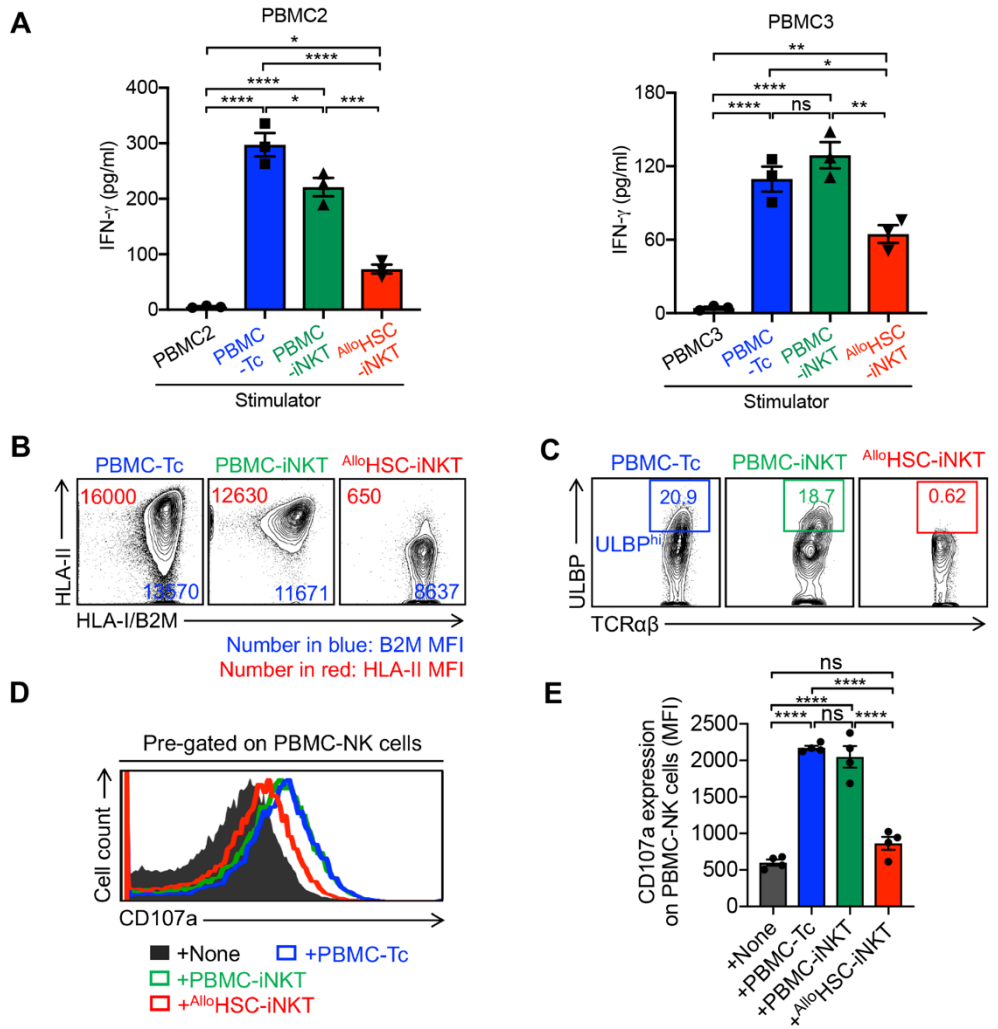

Figure 3-10. Immunogenicity Study of ^{Allo}HSC-iNKT Cells.
(A) ELISA analyses of IFN-γ production at day 4 in an *in vitro* MLR assay (n = 3). Data of PBMC2 and PBMC3 responders were presented. Related to main Figures 6A and 6C.
(B) FACS analyses of HLA-I/II expression on PBMC-Tc, PBMC-iNKT, and ^{Allo}HSC-iNKT cells. Representative FACS plots were presented. Related to main Figure 6B.
(C) FACS analyses of ULBP expression on PBMC-Tc, PBMC-iNKT, and ^{Allo}HSC-iNKT cells. Representative FACS plots were presented. Related to main Figure 6F.
(D-E) Studying CD107a expressions on PBMC-NK cells using an *in vitro* MLR assay. PBMC-NK cells were co-cultured with ^{Allo}HSC-iNKT, PBMC-iNKT, and PBMC-Tc cells for 24 hours. CD107a antibody was added into the cell cultures and incubated for 2 hours prior to flow cytometry. (D) FACS analyses of CD107a expression on PBMC-NK cells. (E) Quantification of D (n = 4).
Representative of 3 experiments. Data are presented as the mean ± SEM. ns, not significant, *P < 0.05, **P < 0.01, ***P < 0.001, ****P < 0.0001, by one-way ANOVA.

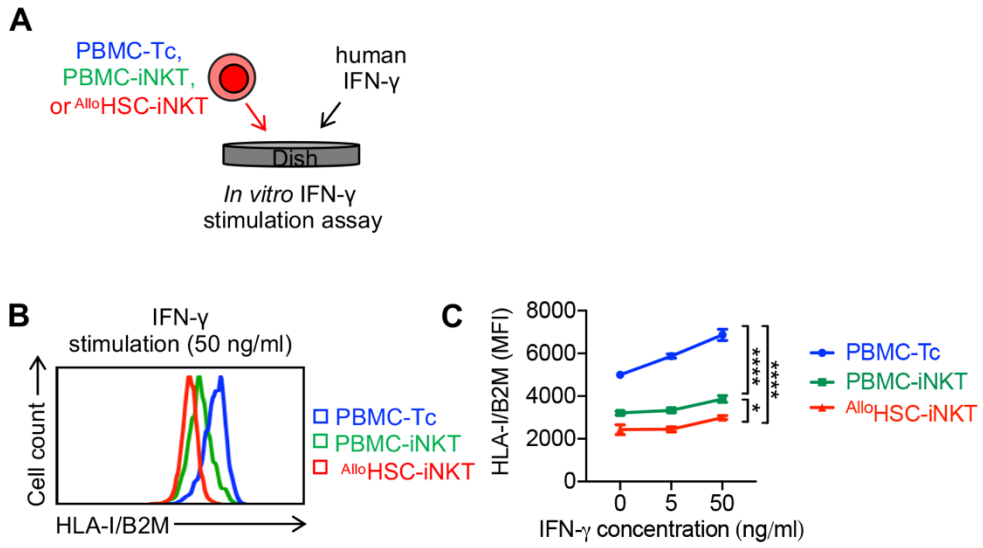

Figure 3-11. HLA-I Expression Study on ^{Allo}HSC-iNKT Cells Under IFN-γ Stimulation.
(A) Experimental design. ^{Allo}HSC-iNKT cells were stimulated with a range of IFN-γ (0, 5, and 50 ng/ml) for 3 days. PBMC-iNKT and PBMC-Tc cells were included as controls.
(B) FACS analyses of HLA-I expression on the indicated cells.
(C) Quantification of HLA-I expression on the indicated cells stimulated with IFN-γ of indicated concentrations (n = 3).
Representative of 3 experiments. Data are presented as the mean ± SEM. *P < 0.05, ***P < 0.001, ****P < 0.0001, by 1-way ANOVA.

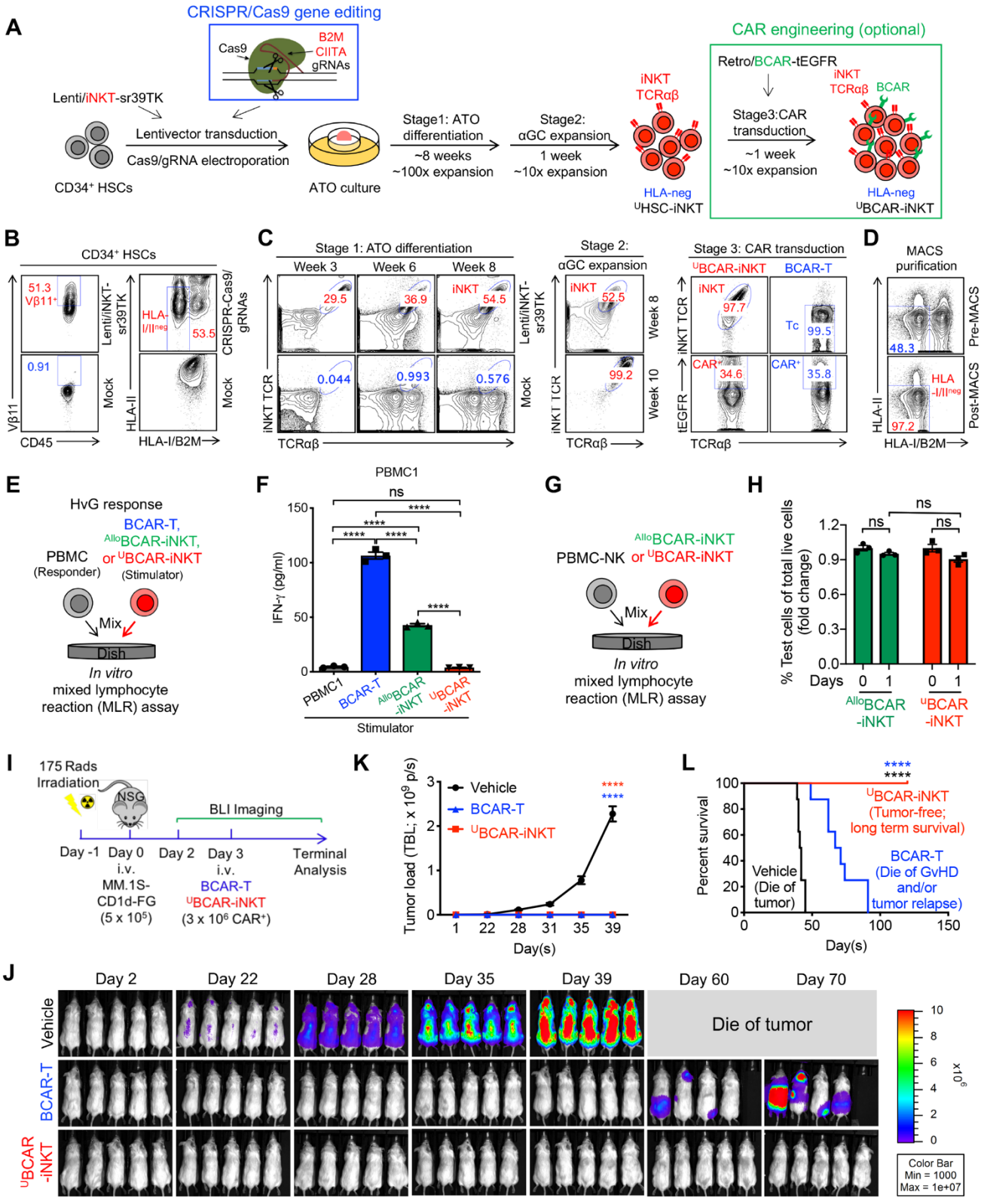

Figure 3-12. Development of HLA-Ablated Universal HSC-iNKT (^{U}HSC-iNKT) Cells and Derivatives

(A) Experimental design to generate ^{U}HSC-iNKT and BCMA CAR-engineered ^{U}HSC-iNKT (^{U}BCAR-iNKT) cells. CRISPR, clusters of regularly interspaced short palindromic repeats;

Cas 9, CRISPR associated protein 9; gRNA, guide RNA; B2M, beta-2-microglobulin; CIITA, class II major histocompatibility complex transactivator.
(B-D) FACS monitoring of ^{U}HSC-iNKT and ^{U}BCAR-iNKT cell generation. (B) Intracellular expression of iNKT TCR (identified as Vβ11^{+}) and surface ablation of HLA-I/II (identified as HLA-I/B2M^{-}HLA-II^{-}) in CD34^{+} HSCs cells at day 5 (72 hours post lentivector transduction and 48 hours post CRISPR/Cas9 gene editing). (C) Generation of iNKT cells (identified as iNKT TCR^{+}TCRαβ^{+} cells) during Stage 1 ATO differentiation culture, Stage 2 αGC expansion, and Stage 3 CAR transduction. Healthy donor PBMC T cells transduced with the same Retro/BCAR-tEGFR vector was included as a staining control (denoted as BCAR-T cells). (D) Purification of HLA-I/II-negative ^{U}HSC-iNKT cells using MACS sorting.
(E-F) Studying allogenic T cell response against ^{U}BCAR-iNKT cells using an *in vitro* MLR assay. Irradiated ^{U}BCAR-iNKT cells (as stimulators) were co-cultured with donor-mismatched PBMC cells (as responders). Irradiated ^{Allo}BCAR-iNKT and conventional BCAR-T cells were included as stimulator cell controls. (E) Experimental design. PBMCs from 3 different healthy donors were used as responders. (F) ELISA analyses of IFN-γ production at day 4 (n = 3).
(G-H) Studying allogenic NK cell response against ^{U}HSC-iNKT cells using an *in vitro* MLR assay. ^{U}HSC-iNKT cells were co-cultured with donor-mismatched PBMC-NK cells. ^{Allo}HSC-iNKT cells were included as a control. (G) Experimental design. (H) FACS quantification of the indicated cells (n = 3).
(I-L) Studying the *in vivo* antitumor efficacy of ^{U}BCAR-iNKT cells in an MM.1S-CD1d-FG human multiple myeloma xenograft NSG mouse model. (I) Experimental design. (J) BLI images showing tumor loads in experimental mice over time. (K) Quantification of J (n = 5). (L) Kaplan-Meier survival curves of experimental mice over a period of 4 months post tumor challenge (n = 8). Mice were combined from 2 independent experiments.
Representative of 2 (I-L) and 3 (B-H) experiments. Data are presented as the mean ± SEM. ns, not significant, ****P < 0.0001, by Student's *t* test (H), one-way ANOVA (F and K), or by log rank (Mantel-Cox) test adjusted for multiple comparisons (L).

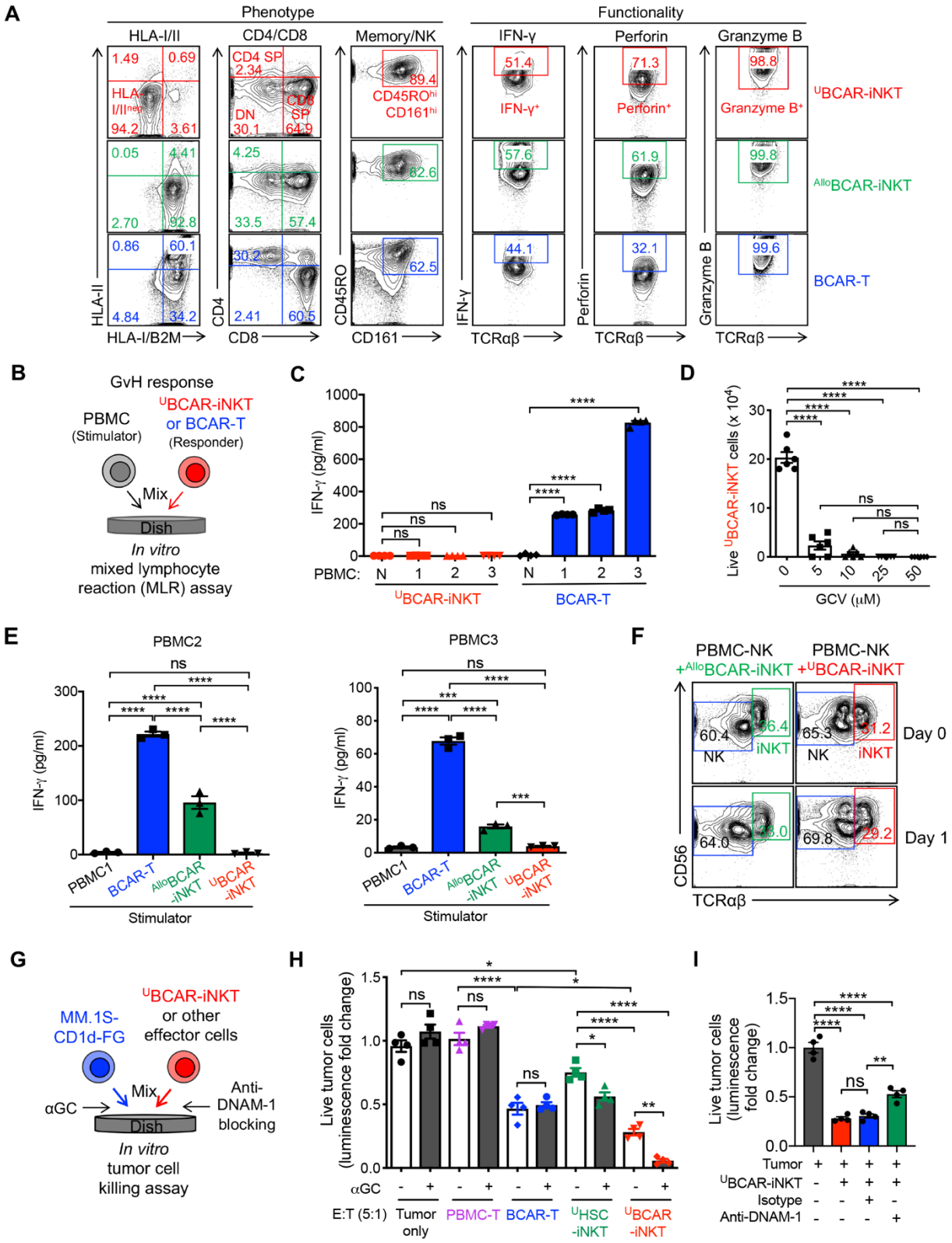

Figure 3-13. Development of HLA-Ablated Universal HSC-iNKT ([U]HSC-iNKT) Cells and Derivatives.

(A) FACS analyses of surface marker expression, and Intracellular cytokine and cytotoxic molecule production by [U]BCAR-iNKT cells. [Allo]BCAR-iNKT and BCAR-T cells were included as controls.

(B-C) Studying the GvH response of ^{u}BCAR-iNKT cells using an *in vitro* MLR assay. BCAR-T cells were included as a responder cell control. (B) Experimental design. PBMCs from 3 different healthy donors were used as stimulator cells. (C) ELISA analyses of IFN-γ production at day 4 (n = 4).
(D) *In vitro* GCV killing assay. ^{U}BCAR-iNKT cells were cultured *in vitro* in the presence of gradient concentrations of GCV for 4 days, followed by quantification of live cells via cell counting (n = 6).
(E) Studying allogenic T cell response against ^{U}BCAR-iNKT cells using an *in vitro* MLR assay. ELISA analyses of IFN-γ production at day 4 were presented (n = 3). Related to main Figures 7E and 7F.
(F) Studying allogenic NK cell response against ^{U}BCAR-iNKT cells using an *in vitro* MLR assay. ^{Allo}BCAR-iNKT cells were included as a control. Representative FACS plots were presented, showing the quantification of the indicated cells at day 0 and day 1. Related to main Figures 7G and 7H.
(G-I) *In vitro* killing of MM.1S-CD1d-FG human multiple myeloma cells by ^{U}BCAR-iNKT cells. PBMC-T, BCAR-T, and ^{U}HSC-iNKT cells were included as effector cell controls. (G) Experimental design. (H) Tumor cell killing by the indicated effector cells with/out the addition of αGC (n = 4). (I) Tumor cell killing by ^{Allo}BCAR-iNKT cells with/out the blockade of DNAM-1 (n = 4). Tumor cell killing was analyzed at 8-hours post co-culture (effector:tumor ratio 5:1).
Representative of 3 experiments. Data are presented as the mean ± SEM. ns, not significant, *P<0.05, **P<0.01, ***P<0.001, ****P<0.0001, by 1-way ANOVA.

Chapter 4 - Combating Ovarian Cancer Using Stem Cell-Engineered Off-The-Shelf CAR-iNKT Cells

Abstract

Adoptive cellular therapy has recently transformed the field of cancer immunotherapy, specifically the treatment of hematological malignancies, through the application of chimeric antigen receptor (CAR) T cells. While a tremendous step forward for cell therapy, current CAR T products face barriers to patient accessibility and clinical benefit. Their autologous nature renders the therapies patient selective and costly, and mechanisms of resistance to CAR T cells, including antigen downregulation/antigen-negative relapse, limit long-term therapeutic efficacy. In this letter, we report novel *ex vivo* HSC-derived mesothelin-CAR engineered NKT (^{Allo}MCAR-iNKT) cell products that are pure, potent, and safe allogeneic cell therapies. ^{Allo}MCAR-iNKT cells execute ovarian cancer killing through a CAR-TCR-NK triple-mechanism, do not cause GvHD, and are resistant to allorejection. Our feeder-free, serum-free culture method promotes the speedy clinical translationof HSC engineered cells, and here we validate our system as a versatility platform for the development of designer "off-the-shelf" cellular products with high therapeutic potential to ovarian cancer patients.

Introduction

Ovarian cancer (OC) is the leading cause of death among women with gynecological malignancies[1]. In the USA, California is the state with the highest incidences and deaths of ovarian cancer. In 2021, it is estimated that 2,550 women will be diagnosed with OC and 1,640 women will die from this disease at California[140]. Despite surgery and chemotherapy, 5-years survival rates for advanced stage disease have been improved only modestly over the past few decades remaining at about 45%, and majority of patients relapse within 10-18 months[141]. Therefore, novel therapies are urgently needed.

Adoptive T cell therapy is emerging as an attractive immunotherapy approach for OC. In particular, early clinical studies testing a mesothelin (MSLN)-targeting CAR-T (MCAR-T) cell therapy have generated encouraging results: the therapy was feasible and safe; the CAR-T cells engrafted and expanded in all subjects; and there was evidence of trafficking to tumor sites resulting in the clearance of pleural effusion in one patient and in stabilization of disease in all six patients[142]. Notably, MSLN is expressed at low levels in normal tissue but overexpressed in about 70% of OC tumors, making it an ideal CAR-T cell therapeutic target for treating OC[143]. Despite its promise, the current MCAR-T cell therapy has significant limitations: its efficacy needs to be improved; and importantly, it falls into the category of autologous cell therapy[142]. Such a conventional αβ T cell-based cell product risk inducing graft-versus-host disease (GvHD) when adoptively transferred into allogeneic hosts; therefore personalized MCAR-T cells need to be manufactured for each patient and can only be used to treat that single patient, making the therapy extremely costly and difficult to deliver to all OC patients in need[142]. In order to fully harness the potential of MCAR-directed cell therapy for OC, the development of a potent allogeneic "off-the-shelf" cell therapy is of great demand. Invariant natural killer T (iNKT) cells are a small population of unconventional αβ T cells[53]. These cells have several unique features, making them ideal cell carriers for developing allogeneic CAR-directed cell therapy for OC[53]. Compared to conventional CAR-T cells, CAR-engineered iNKT (CAR-iNKT) cells can attack tumor cells using multiple mechanisms and at higher efficacy; can more effectively traffic to and infiltrate solid tumors; can alter solid tumor immunosuppressive microenvironment; and most importantly, do not induce GvHD[37,136]. However, human blood contains extremely low numbers of iNKT cells (0.001-1%), making it very difficult to reliably grow large numbers of allogeneic iNKT cells for CAR-engineering[53]. Moreover, allogeneic iNKT cell products expanded from blood may contain bystander allogeneic conventional αβ T cells and thus risk inducing GvHD. Recently, we have

successfully overcome this critical hurdle by establishing a novel *Ex Vivo* Hematopoietic Stem Cell (HSC)-Derived CAR-iNKT Cell Culture Method, that can produce therapeutic levels of pure and potent CAR-iNKT cells suitable for allogeneic cell therapy. Based on this method, in this project we propose to develop a next-generation, off-the-shelf cell therapy for OC by generating potent allogeneic MCAR-iNKT (^{Allo}MCAR-iNKT) cells targeting OC.

Materials and Methods

Human CD34$^+$ Hematopoietic Stem Cells (HSCs) and Periphery Blood Mononuclear Cells (PBMCs)

Human CD34$^+$ HSCs from cord blood (CB) sources were purchased from HemaCare. For all CB HSCs aliquots, the purity of CD34$^+$ cells were more than 97%, as evaluated by flow cytometry. CB HSCs were cultured in X-VIVO 15 Serum-free Hematopoietic Cell Medium (Lonza). Healthy donor human PBMCs were obtained from the UCLA/CFAR Virology Core Laboratory without identification information under federal and state regulations. PBMCs were cultured in a complete lymphocyte culture medium (denoted as C10 medium) unless other specified. C10 was made of RPMI 1640 supplemented with FBS (10% vol/vol), P/S/G 40 (1% vol/vol), MEM NEAA (1% vol/vol), HEPES (10 mM), Sodium Pyruvate (1 mM), β-ME (50 mM), and Normocin (100 mg/ml).

Cell Lines

Human multiple myeloma cancer cell line MM.1S was purchased from American Type Culture Collection (ATCC), human ovarian carcinoma cell OVCAR8, human ovarian adenocarcinoma cell line OVCAR3, and human ovarian carcinoma cell line Skov3 were obtained from NIH. All cells were cultured in R10 medium, made of RPMI 1640 supplemented with FBS (10% vol/vol) and P/S/G (1% vol/vol). The parental tumor cell lines were transduced with lentiviral

vectors encoding the intended gene(s) as needed. Genes of interest include a human mesothelin (MSLN) and a dual reporter of firefly luciferase and enhanced green fluorescence protein (FG). 72h post lentivector transduction, cells were subjected to flow cytometry sorting to isolate gene-engineered cells for making stable cell lines. Six stable tumor cell lines were generated for this study, including MM.1S-FG, MM.1S-MSLN-FG, OVACR3-FG, OVCAR8-FG, and Skov3-FG.

Mice

All animal experiments used NOD.Cg-PrkdcSCIDIl2rgtm1Wjl/SzJ (NOD/SCID/IL-2Rγ-/-, NSG) mice were purchased from The Jackson Laboratory. All mice were 6- to 10-weeks old and maintained at the animal facilities of the University of California, Los Angeles (UCLA) under pathogen-free conditions. All mouse studies were conducted in accordance with national guidelines for the humane treatment of animals and were approved by the Institutional Animal Care and Use Committee of UCLA.

Lentiviral Vector Construction and Transduction

Lentiviral vectors used in this study were all constructed from a parental lentivector pMNDW as previously described. The Lenti/iNKT-sr39TK vector was constructed by inserting into pMNDW vector a synthetic tricistronic gene encoding human iNKT TCRα-F2A-TCRβ-P2A-sr39TK; The Lenti/iNKT-MCAR vector was constructed by inserting into pMNDW vector a synthetic tricistronic gene encoding human iNKT TCRα-F2A-TCRβ-P2A-mesothelin CAR; the Lenti/FG vector was constructed by inserting into pMNDW a synthetic bicistronic gene encoding Fluc-P2A-EGFP. The synthetic gene fragments were obtained from GenScript and IDT. Lentiviruses were produced using HEK 293T cells, following a standard lipofection with Trans-IT-Lenti Transfection reagent (Mirus Bio) and centrifugation concentration protocol as

previously described. Lentivector titers were measured by transducing HEK 293T-hCD3 (human CD3 expressing line, cloned in Lili Yang lab) with serial dilutions and performing flow cytometry following established protocols.

Antibodies and Flow Cytometry

Fluorochrome-conjugated antibodies specific for human CD45 (Clone H130), TCRαβ (Clone I26), CD3 (Clone HIT3a), CD4 (Clone OKT4), CD8 (Clone SK1), CD45RO (Clone UCHL1), CD45RA (Clone HI100), CD161 (Clone HP-3G10), CD25 (Clone BC96), CD69 (Clone FN50), CD56 (Clone HCD56), CD62L (Clone DREG-56), CTLA-4 (Clone BNI3), PD-1 (clone EH12.2H7), CD1d (Clone 51.1), CCR4 (Clone L291H4), CCR5 (Clone HEK/1/85a), CXCR3 (Clone G025H7), CXCR4 (Clone 12G5), NKG2D (Clone 1D11), DNAM-1 (Clone 11A8), CD158 (KIR2DL1/S1/S3/S5) (Clone HP-MA4), IFN-γ (Clone B27), granzyme B (Clone QA16A02), perforin (Clone dG9), TNF-α (Clone Mab11), IL-2 (Clone MQ1-17H12), HLAE (Clone 3D12), β2-microglobulin (B2M) (Clone 2M2), HLA-DR, DP, DQ (Clone Tü 39) were purchased from BioLegend. Fluorochrome-conjugated antibodies specific for human CD34 (Clone 581) and human iNKT TCR Vα24-Jβ18 (Clone 6B11) were purchased from BD Biosciences. Fluorochrome-conjugated antibodies specific for human iNKT TCR Vβ11 were purchased from Beckman-Coulter; Fluorochrome conjugated antibodies specific for human ULBP-2,5,6 (Clone 165903) was purchased from R&D Systems. Human Fc Receptor Blocking Solution (TrueStain FcX) was purchased from Biolegend, and Mouse Fc Block (anti-mouse CD16/32) was purchased from BD Biosciences. Fixable Viability Dye eFluor506 (e506) was purchased from Affymetrix eBioscience. All flow cytometry stains for surface markers were performed in PBS at 4°C for 15mins. Samples were stained with Fixable Viability Dye eFluor506 (e506) mixed with Mouse Fc Block (anti-mouse CD16/32) or Human Fc Receptor Blocking Solution (TrueStain FcX), followed by PBS wash. Antibody staining was then added

to all samples at specified dilutions according to the manufacturer's instructions. Intracellular cytokines were stained using a Cell Fixation/Permeabilization Kit (BD Biosciences). Flow cytometry was performed using a MACSQuant Analyzer 10 flow cytometer (Miltenyi Biotech), and FlowJo software version 9 and 10 was used for data analysis.

Ex Vivo Allogeneic HSC-Derived CAR-Engineered NKT (^{Allo}MCAR-NKT) Cell Culture

Non-tissue culture-treated 24-well plates were coated with StemSpan lymphoid differentiation coating material (LDCM, 500µl/well, StemCell Technologies) for 2 hours at room temperature or alternatively, overnight at 4^{o}C. Coating supernatants were removed, and plates were washed with a D-PBS buffer. Transduced CD34+ human stem cells (HSCs) at 2 x 10^4/well were suspended in 500 µl of StemSpan lymphoid progenitor expansion medium (LPEM, StemCell Technologies) and seeded into coated wells of the 24-well plate on day 0. Cells were cultured for 3 days at 5% CO2 and 37^{o}C. On day 4, another 500 µL LPEM was added to each well, and cells were cultured for additional 4 days. On days 7 and 11, half of the medium was removed and replenished with 500 µl fresh LPEM. On day 14, cells were harvested, counted, and reseeded into an LDCM-coated 12-well plate in 1mL of T cell progenitor maturation medium per well (TPMM, StemCell Technologies) (5 x 10^5 - 1 x 10^6 cells/well). On day 18, 1mL of fresh TPMM was added to each well. On days 21 and 24, half of the medium in each well was discarded and replaced with 1mL of TPMM. On day 28, cells were harvested, counted, and re-seeded into a new coated 12-well plate in 1mL of TPMM (1 x 10^6 cells/mL/well) with 12.5 µL/well CD3/CD28/CD2 T Cell Activator (StemCell Technologies) and 10 ng/mL Human Recombinant IL-15 (PeproTech). On Day 31, 1mL of fresh TPMM containing 10 ng/mL Human Recombinant IL-15 was added into the culture. On day 35, cells were harvested and analyzed by flow cytometry for double-positive (DP) and single-CD8 (SP) cells. Usually, over 50% DP/ SP CD8 cells could be reliably generated after 5 weeks of differentiation.

Feeder-Free Expansion of ^{Allo}MCAR-iNKT Cells

One day before the expansion, 24-well plates were coated with 1ug/ml anti-human CD3 antibody (OKT3, Biolegend) at 4°C overnight. Freshly collected ^{Allo}MCAR-iNKT cells were seeded at $5x10^5$/ml in OpTmizer™ CTS™ T-Cell Expansion serum-free medium (Gibco, Thermo Fisher Scientific) with IL-7 (10ng/ml), IL-15 (10ng/ml) and IL-21 (30ng/ml) for 3 days. The cultures were then collected, washed, and reseeded into new plates without Ab coating at $1x10^6$/ml with 10ng/ml IL-7 and 10ng/ml IL-15. Medium change was performed every 2-3 days. ^{Allo}MCAR-iNKT cells were allowed to expand for 7-14 days, then were aliquoted and frozen in liquid nitrogen storage tanks for future use.

On-Feeder Expansion of ^{Allo}MCAR-iNKT Cells

Healthy donor PBMCs were loaded with α-Galactosylceramide (αGC, Avanti Polar Lipids). Culture 107 - 108 PBMCs with 5 μg/ml αGC in 10ml culture medium for 1 hour. PBMCs were then irradiated at 6,000 rads (denoted as αGC/PBMCs). Freshly generated ^{Allo}MCAR-iNKT cells were mixed with αGC /PBMCs (at 1:3 or 1:5 ratios) and cultured in C10 medium with IL-7 (10ng/ml) and IL-15 (10ng/ml). Alternatively, expansion can be achieved with K562-based artificial antigen-presenting cells expression CD80, CD86, and CD137L (K562-aAPC) as previously described. K562-aAPC were engineered to express mesothelin for the expansion of corresponding ^{Allo}MCAR-iNKT cells. Prior to expansion, K562-aAPC was irradiated at 10,000 rads. Freshly generated ^{Allo}MCAR-iNKT cells were mixed irradiated K562-aAPC at 4:1 ratio with 10 ng/ml IL-7 and 10 ng/ml IL-15. ^{Allo}MCAR-iNKT cells were allowed to expand for 7-14 days, then were aliquoted and frozen in liquid nitrogen storage tanks for future use. All cultures described here were carried out in OpTmizer™ CTS™ T-Cell Expansion serum-free medium (Gibco, Thermo Fisher Scientific).

Generation of PBMC-Derived Conventional αβT, iNKT, γδT, and NK Cells

Healthy donor PBMCs were obtained from the UCLA/CFAR Virology Core Laboratory and were used to generate the PBMC-Tc, PBMC-iNKT, PBMC-γδT, and PBMC-NK cells. To generate PBMC-Tc cells, PBMCs were stimulated with CD3/CD28 T-activator beads (Thermo Fisher Scientific) and cultured in a C10 medium supplemented with human IL-2 (20 ng/mL) for 2-3 weeks, following the manufacturer's instructions. To generate PBMC-iNKT cells, PBMCs were MACS-sorted via anti-iNKT microbeads (Miltenyi Biotech) labeling to enrich iNKT cells, which were then stimulated with donor-matched irradiated αGC-PBMCs at the ratio of 1:1 and cultured in C10 medium supplemented with human IL-7 (10 ng/ml) and IL-15 (10 ng/ml) for 2-3 weeks. If needed, the resulting PBMC-iNKT cells could be further purified using Fluorescence-Activated Cell Sorting (FACS) via human iNKT TCR antibody (Clone 6B11; BD Biosciences) staining. To generate PBMC-γδT cells, PBMCs were stimulated with Zoledronate (5 μM; Sigma-Aldrich) and cultured in C10 medium supplemented with human IL-2 (20 ng/ml) for 2 weeks. If needed, the resulting PBMC-γδT cells could be further purified using FACS via human TCR Vδ2 antibody (Clone B6; Biolegend) staining or via MACS using a human TCRγ/δ T Cell Isolation Kit (Miltenyi Biotech). To generate PBMC-NK cells, PBMCs were FACS-sorted via human CD56 antibody (Clone HCD56; Biolegend) labeling or MACS-sorted using a human NK Cell Isolation Kit (Miltenyi Biotech).

Generation of Mesothelin CAR-Engineered PBMC T (MCAR-T) Cells

Healthy donor PBMCs were stimulated with CD3/CD28 T-activator beads (Thermo Fisher Scientific) in the presence of recombinant human IL-2 (30 ng/ml), following the manufacturer's instructions. On day 3, cells were infected with lentivector encoding mesothelin CAR. The

resulting MCAR-T cells were expanded for another 7-10 days and then were cryopreserved for future use.

Single-Cell TCR Sequencing

^{Allo}MCAR-iNKT (6B11^{+}TCRαβ^{+}), PBMC-iNKT (6B11^{+}TCRαβ^{+}), and PBMC-αβTc (6B11^{-} TCRαβ^{+}) cells were sorted using a FACSAria II flow cytometer. Sorted cells were immediately delivered to the UCLA TCGB (Technology Center for Genomics and Bioinformatics) Core to perform single cell TCR sequencing using a 10X Genomics ChromiumTM Controller Single Cell Sequencing System (10X Genomics), following the manufacturer's instructions and the TCGB Core's standard protocol. Libraries were constructed using an Illumina TruSeq RNA Sample Prep Kit (Cat #FC-122-1001) and sequenced with 150 bp paired-end reads (5,000 reads/cell) on an Illumina NovaSeq. The reads were mapped to the human T cell receptor reference genome (hg38) using Cell Ranger VDJ. The frequencies of the α or β chain recombination were plotted.

Cell Phenotype and Function Assay

^{Allo}MCAR-iNKT cells were analyzed in comparison with PBMC-Tc, PBMC-NK, PBMC-iNKT, or/and MCAR-T cells. The phenotype of these cells was studied using flow cytometry by analyzing cell surface markers including co-receptors (i.e., CD4 and CD8), NK cell receptors (i.e., CD161, NKG2D, DNAM-1, and KIR), memory T cell markers (i.e., CD45RO), and inflammatory tissue/tumor homing markers (i.e., CCR4, CCR5, and CXCR3). The capacity of these cells to produce cytokines (i.e., IFN-γ, TNF-α, and IL-2) and cytotoxic molecules (i.e., perforin and granzyme B) were studied using flow cytometry via intracellular staining. Response of ^{Allo}MCAR-iNKT cells to antigen stimulation was studied by culturing ^{Allo}MCAR-iNKT cells in vitro in C10 medium for 7 days, in the presence or absence of αGC

(100 ng/ml). The proliferation of ^{Allo}MCAR-iNKT cells was measured by cell counting and flow cytometry (identified as 6B11^{+}TCRαβ^{+}) over time. Cytokine production was assessed by ELISA analysis of cell culture supernatants collected on day 3 (for human IFN-γ. TNF-α, IL-2, IL-4, and IL-17).

In Vitro Tumor Cell Killing Assay

Tumor cells (1 x 10^4 cells per well) were co-cultured with effector cells (at ratios indicated in figure legends) in Corning 96-well clear bottom black plates for 8-24 hours, in C10 medium with or without the addition of αGC (100 ng/ml). At the end of culture, live tumor cells were quantified by adding D-luciferin (150 μg/ml; Caliper Life Science) to cell cultures and reading out luciferase activities using an Infinite M1000 microplate reader (Tecan). In experiments for tumor killing mechanism studies, 10 μg/ml of LEAFTM purified anti-human CD1d (Clone 51.1, Biolegend), anti-human DNAM-1 antibody (Clone 11A8, Biolegend), or LEAFTM purified mouse lgG2bk isotype control antibody (Clone MG2B-57, Biolegend) was added.

In Vitro Mixed Lymphocyte Reaction (MLR) Assay: Studying Graft-Versus-Host (GvH) Response

PBMCs of multiple healthy donors were irradiated at 2,500 rads and used as stimulators to study the GvH response of ^{Allo}MCAR-iNKT cells as responders. PBMC derived MCAR-T cells were included as responder controls. Stimulators (5 x 10^5 cells/well) and responders (2 x 10^4 cells/well) were co-cultured in 96-well round-bottom plates in C10 medium for 4 days; the cell culture supernatants were then collected to measure IFN-γ production using ELISA.

In Vitro MLR Assay: Studying Host-Versus-Graft (HvG) Response

PBMCs of multiple healthy donors were used as responders to study the HvG response of ^{Allo}MCAR-iNKT cells as stimulators (irradiated at 2,500 rads). PBMC derived MCAR-T cells were included as stimulator controls. Stimulators (5 x 10^5 cells/well) and responders (2 x 10^4 cells/well) were co-cultured in 96-well round-bottom plates in C10 medium for 4 days; the cell culture supernatants were then collected to measure IFN-γ production using ELISA.

In Vitro MLR Assay: Studying NK Cell-Mediated Allorejection

PBMC-NK cells isolated from PBMCs of multiple healthy donors were used to study the NK cell-mediated allorejection of ^{Allo}MCAR-iNKT cells. Allogeneic MCAR-T were included as controls. PBMC-NK cells (2 x 10^4 cells/well) and the corresponding allogeneic cells (2 x 10^4 cells/well) were co-cultured in 96-well round-bottom plates in C10 medium for 24 hours; the cell cultures were then collected to quantify live cells using flow cytometry.

In Vivo Antitumor Efficacy and Biodistribution Study of ^{Allo}MCAR-iNKT: human OVCAR3 xenograft NSG mouse model.

NSG mice were i.p. inoculated with 5 x 10^5 OVCAR3-FG cells as indicated on experimental design figure (day 0). To study antitumor efficacy with a single administration of effector cells, on day 4 or 40, the tumor-bearing experimental mice received i.p. injection of vehicle (PBS), ^{Allo}MCAR-iNKT cells (1 x 10^7 CAR^+ cells), or conventional MCAR-T cells (1 x 10^7 CAR^+ cells). Over time, experimental mice were monitored for survival, and their tumor loads were measured using BLI. Bleeding was performed if needed through the retro-orbital route.

Ganciclovir (GCV) In Vitro and In Vivo Killing Assay

For GCV in vitro killing assay, ^{Allo}MCAR-iNKT cells were cultured in C10 medium in the presence of the titrated amount of GCV (0-50 μM) for 4 days; live ^{Allo}MCAR-iNKT cells were then counted using flow cytometry with viability staining.

Histopathologic Analysis

Heart, liver, kidney, and lung tissues were taken from all experimental mice. Tissue samples were fixed in 10% Neutral Buffered Formalin for up to 36 hours and embedded in paraffin for sectioning (3 μm thickness). After sectioning, tissues were stained either with Hematoxylin and Eosin or anti-human CD3 primary antibodies following standard procedures (UCLA Translational Pathology Core Laboratory, Los Angeles, CA). Stained sections were imaged using an Olympus BX51 upright microscope equipped with an Optronics Macrofire CCD camera (AU Optronics) at 20 x and 40 x magnifications. All images were analyzed using Optronics PictureFrame software (AU Optronics).

Statistics

Statistical analysis using Graphpad Prism 8 software (Graphpad). Pairwise comparisons were made using a 2-tailed Student's T test. Multiple comparisons were performed using an ordinary 1-way ANOVA, followed by Tukey's multiple comparisons test. Kaplan- Meier survival curves were analyzed by log rank (Mantel-Cox) test adjusted for multiple comparisons. Data are presented as the mean ± SEM unless otherwise indicated. In all figures and figure legends, "n" represents the number of samples or animals utilized in the indicated experiments. P values less than 0.05 were considered significant. “ns” denotes not significant; * denotes $P < 0.05$; ** denotes $P < 0.01$; *** denotes $P < 0.001$; **** denotes $P < 0.0001$.

Results

Generation of Allogeneic MSLN-Targeting CAR-iNKT (^{Allo}MCAR-iNKT) Cells

Based on an established clinical lentivector and design [41], we have constructed a Lenti/iNKT-MCAR vector for the efficient co-delivery of an iNKT TCR gene and a MCAR gene into HSCs (**Figure 4-1A**). The MCAR construct is adapted from a clinically proven design that has been previously confirmed for safety and MSLN-targeting function [142,144]. This study collected human cord blood $CD34^+$ hematopoietic stem and progenitor cells (referred to as HSCs) through CliniMACS selection and cryopreserved. Thawed HSCs were transduced with Lenti/iNKT-MCAR vector and then differentiate and expand in the *ex vivo* ^{Allo}MCAR-iNKT cell culture over 6 weeks with ~10^6 folds of expansion (tested from 10 cord blood donors) (**Figure 4-1A**). Over 50% of the transduction rate was routinely achieved with lentivectors described (**Figure 4-1B**). We adopted an *in vitro* system of plate-bound delta-like 4 (DLL4) and vascular cell adhesion protein 1 (VCAM-1) to enable lymphoid differentiation as previously described [145–148]. Notch signaling through DLL1 or DLL4 is pivotal to thymocyte commitment [145,149,150], while VCAM-1 enhances pro-T cell mobility [145]. DLL4 and VCAM-1 synergistically enables T cell development from HSCs [145]. One week into the culture, HSCs gave rise to T-cell progenitors with iNKT TCR presented on the cell surface. At week 4, more mature $CD4^+CD8^+$ double-positive (DP) population emerges. By the end of culture at week 6, the final cell product can reach a purity of more than 99% iNKT TCR^+CD3^+ DP without any detectable endogenously rearranged TCR, suggesting the induction of allelic exclusion through the transgenic iNKT TCR (**Figure 4-1C**). The *ex vivo* generated ^{Allo}MCAR-iNKT cells presented a $CD8^+$ single-positive (SP) or $CD4^-CD8^-$ double-negative (DN) phenotype (**Figure 4-1C**). The introduction of CAR at the HSCs stage did not interfere with the *ex vivo* development of ^{Allo}MCAR-iNKT cells, and the product expresses MCAR and iNKT TCR (**Figure 4-1C**). Our approach saves the additional CAR transducing process upon mature T or NK cells required for all current allogeneic products, including many with the iPSC approach

[146,148,151]. Single-cell TCR sequencing analysis confirmed that these ^{Allo}MCAR-iNKT cells uniformly expressed the transgenic iNKT TCRs with nearly undetectable randomly rearranged endogenous αβ TCR pairs (**Figure 4-1D**). In contrast, healthy donor periphery blood mononuclear cells (PBMCs) derived conventional αβ T (PBMC- αβTc) cells expressed highly diverse endogenously rearranged αβ TCRs (**Figure 4-1D**); PBMC derived iNKT (PBMC-iNKT) cells expressed a conserved invariant TCR α chain (Vα24-Jα18) and limited diverse TCR β chains (dominantly Vβ11) (**Figure 4-1D**). We started from 1 x 10^5 HSCs and produced ~4 x 10^9 ^{Allo}MCAR-iNKT cells; based on this yield, it was estimated that from a single quality CB donor (~5 x 10^6 $CD34^+$ HSCs), ~10^{11} therapeutic ^{Allo}MCAR-iNKT cells could be generated that could potentially be formulated into ~1,000 doses (~10^8 cell per dose) (**Figure 4-1E**).

Characterization of ^{Allo}MCAR-iNKT Cells

The phenotype and functionality of the ^{Allo}MCAR-iNKT cells were studied using flow cytometry. ^{Allo}MCAR-iNKT cells displayed typical iNKT cell phenotype and functionality similar to that of the endogenous PBMC-derived iNKT cells: they expressed high levels of memory T cell marker CD45RO and NK cell marker CD161; they expressed high levels of NK activating receptors (i.e., NKG2D and DNAM-1); and they produced exceedingly high levels of effector cytokines (i.e., IFN-γ, TNF-α, and IL-2) and cytotoxic molecules (i.e., Perforin and Granzyme B) compared to that of the conventional MCAR-T cells (**Figure 4-1F**).

In Vitro Killing and Mechanism of ^{Allo}MCAR-iNKT Cells

To study the OC-targeting efficacy and mechanism of action (MOA) of ^{Allo}MCAR-iNKT cells, we used a pair of human OC tumor cell lines: OVCAR3 ($MSLN^+$; from ATCC) and SKOV3 ($MSLN^-$; from ATCC); both are human OC adenocarcinoma cell lines that have been proved suitable for studying CAR-directed tumor targeting in cell culture and in xenograft mouse

models (**Figure 4-2A**) [49,144,152]. We also included a pair of human MM cell lines as non-OC controls: a parental MM.1S cell line (MSLN$^-$; from ATCC) and an MM.1S-MSLN derivative engineered to overexpress MSLN (MSLN$^+$) (**Figure 4-2A**). All 4 cell lines were further engineered to express firefly luciferase (Fluc) and enhanced green fluorescence protein (EGFP) dual-reporters; that allows the sensitive measurement of tumor cell killing using luciferase activity assay or flow cytometry (**Figure 4-2B**). The 4 resulting cell lines (MSLN$^-$ MM.1S-FG, MSLN$^+$ MM.1S-MSLN-FG, MSLN$^-$ SKOV3-FG, and MSLN$^+$ OVCAR3-FG) were then used for in vitro efficacy/MOA study, in a pre-established *In Vitro* Tumor Cell Killing Assay (**Figure 4-2C**) [41]. Both MCAR-T and ^{Allo}MCAR-iNKT cells effectively killed the MM.1S-MSLN-FG cells but not MM.1S-FG cells, indicating an MCAR-mediated MSLN-dependent killing mechanism; ^{Allo}MCAR-iNKT cells showed highly tumor killing efficacy (**Figure 4-2D**). Similarly, both MCAR-T and ^{Allo}MCAR-iNKT cells effectively killed the MSLN$^+$ OVCAR3-FG cells, with ^{Allo}MCAR-iNKT showing a higher efficacy (**Figure 4-2D**). Interestingly, unlike MCAR-T cells that did not kill the MSLN$^-$ SKOV3-FG cells, ^{Allo}MCAR-iNKT cells could still kill SKOV3-FG cells effectively, albeit at a lower efficacy compared to their killing of the MSLN$^+$ OVCAR3 cells (**Figure 4-2D**). Therefore, ^{Allo}MCAR-iNKT cells may target OC using both MSLN/MCAR-dependent and independent mechanisms, such as the NK tumor-targeting mechanisms mediated by the highly-expressed NK activating receptors on these cells (i.e., NKG2D and DNAM-1) (**Figure 4-2G**). Indeed, blocking of NKG2D and DNAM-1 dampened the killing of OVCAR3-FG tumor cells by ^{Allo}MCAR-iNKT cells, confirming the presence of an NK-targeting mechanism for ^{Allo}MCAR-iNKT cells to attack both MSLN-positive and MSLN-negative OC tumor cells (**Figure 4-2H**). The capacity to deploy multiple OC-targeting mechanisms and thereby overcoming OC immune escape can be a very attractive feature of an HSC-engineered allogeneic MCAR-iNKT cell product. Corresponding to their higher tumor-killing efficacy, ^{Allo}MCAR-iNKT cells outperformed MCAR-T cells in upregulating the

production effector molecules (e.g., Granzyme B) when co-cultured with OC tumor cells (**Figures 4-2E and F**).

In Vivo Antitumor Capacity and Biodistribution of ^{Allo}MCAR-iNKT Cells

Using an OVCAR3-FG xenograft NSG (NOD/SCID$^{/\gamma c-/-}$) mouse model, we studied the *in vivo* efficacy of ^{Allo}MCAR-iNKT cells in comparison with MCAR-T cells. In a low tumor load model, with single administration of effector cells, ^{Allo}MCAR-iNKT cells effectively eliminated the development of OVCAR3 tumor cells (**Figures 4-3A, B, and C**). Nevertheless, MCAR-T cells could not eradicate OVCAR3-FG with this regimen (**Figures 4-3 B and C**). Under this condition, mice receiving the conventional MCAR-T cells, despite low tumor burdern, eventually die of GvHD due to xenoreactivity (**Figure 4-3D**). On the contrary, mice receiving ^{Allo}MCAR-iNKT cells remained tumor-free and survived long-term without GvHD (**Figure 4-3D**). Impressively, at a high tumor load condition, ^{Allo}MCAR-iNKT cells still managed to suppress tumor growth effectively and achieved tumor clearance in a fraction of experimental mice (2 out of 6 mice); conventional MCAR-T cells suppressed tumor growth less well and could not achieve tumor clearance (**Figures 4-3E-H**).

In the OVCAR3-FG xenograft mouse model, a single injection of ^{Allo}MCAR-iNKT cells can suppress the tumor progression better than MCAR-T cells (**Figures 4-3E-H**). Under the heavy tumor load, ^{Allo}MCAR-iNKT cells mounted an impressive *in vivo* expansion at an even higher magnitude than that of MCAR-T cells (**Figures 4-3I-K**). Biodistribution analysis showed that ^{Allo}MCAR-iNKT cells distribute across tissues similarly to the BCAR-T cells (**Figures 4-3I-K**). Although with the significant expansion, the proinflammatory cytokine IFN-γ produced by ^{Allo}MCAR-iNKT cells in the peripheral blood of experimental mice does not differ from that of MCAR-T (**Figure 4-3L**). Importantly, combined with traditional chemotherapy, ^{Allo}MCAR-iNKT cells displayed an extremely potent antitumor capacity in

OVCAR3-FG xenograft mouse model (**Figures 4-3M-P**), indicating their potential in the treatment of ovarian cancer.

Safety and Immunogenicity of ^{Allo}MCAR-iNKT Cells

For allogeneic immune cell therapy, GvHD is a major safety concern. We evaluated the GvHD risk of ^{Allo}MCAR-iNKT cells using an *In Vitro* Mixed Lymphocyte Reaction (MLR) Assay designated to study GvH response (**Figure 4-4A**). ^{Allo}MCAR-iNKT cells did not react to donor-mismatched PBMCs (**Figure 4-4B**), confirming that ^{Allo}MCAR-iNKT cells are free of GvHD risk. Meanwhile, for allogeneic cell therapies, a significant efficacy concern is the host-versus-graft (HvG) risk that may lead to the depletion of allogeneic therapeutic cells by host immune cells, in particular by host CD8 and CD4 T cells through their recognition of mismatched HLA-I/II molecules present on allogeneic therapeutic cells. Interestingly, study of ^{Allo}MCAR-iNKT cells revealed that these cells expressed on their cell surface significantly reduced HLA-I and nearly undetectable HLA-II molecules, compared to conventional MCAR-T cells. This unique feature render ^{Allo}MCAR-iNKT cells low immunogenicity and may enable these cells to persist in an allogeneic host long enough for delivering therapeutic benefits, without the need to ablate their surface HLA-I/II molecules through gene editing [136]. Indeed, in an *in vitro* MLR Assay designated to study HvG response (**Figure 4-4C**), compared to MCAR-T cells, ^{Allo}MCAR-iNKT cells triggered significantly reduced responses from PBMC T cells of multiple mismatched donors (**Figure 4-4D**). Because an inflammatory tumor microenvironment can upregulate surface HLA expression on many immune cells (e.g., via IFN-γ stimulation), we examined ^{Allo}MCAR-iNKT cells isolated from *in vivo* tumor site or stimulated with IFN-γ in vitro, and interestingly, found that these cells still maintained significantly lower surface HLA-I/II expression compared to MCAR-T cells (**Figures 4-4E and F**). Taken together, these

studies suggest ^{Allo}MCAR-iNKT cells to be GvHD-free and HvG-resistant, strongly supporting an off-the-shelf therapeutic application of these cells.

Antitumor Efficacy of ^{Allo}MCAR-iNKT cells Using an In Vivo OC-PDX Model and a Collection of Primary OC Patient Tumor Samples

Besides the OC xenograft models based on human OC tumor cell lines (i.e., OVCAR3 and SKOV3), we have successfully established a MSLN-positive OC patient-derived xenograft (OC-PDX) model, as a more physiologically relevant model for studying MCAR-directed OC-targeting efficacy (**Figure 4-5A**) [153]. Tumor cells were collected from a patient with advanced, therapy resistant ovarian cancer through IRB-approved protocols and viably cryopreserved. Tumor cells were thawed, injected into the peritoneal space of NSG mice, and serially passaged *in vivo*. A portion of passage 2 PDX cells harvested from mice were cryopreserved for future experimental use. Remaining cells were histologically analyzed by immunohistochemistry. Results demonstrate that Pax8$^+$ PDX cells (marker of gynecologic tumors) are MSLN$^+$ and may be targeted by ^{Allo}MCAR-iNKT cells (**Figure 4-5A**). We also have generated a collection of primary OC patient tumor samples expressing varied levels of surface mesothelin, that can be used in an *in vitro* tumor cell killing assay to study the antitumor efficacy of ^{Allo}MCAR-iNKT cells against primary OC tumor cells (**Figure 4-5B**). Impressively, our ^{Allo}MCAR-iNKT cells exhibited a tumor-killing efficacy significantly higher than that of conventional MCAR-T cells across multiple primary OC tumor samples (**Figure 4-5C**). In particular, some MSLN^{lo} primary OC patient tumor samples were not susceptible to MCAR-T killing but were still effectively killed by ^{Allo}MCAR-iNKT cells, likely due to the multiple tumor-targeting mechanisms of these cells which can be very attractive for their therapeutic applications.

Discussion

Epithelial ovarian cancers are aggressive tumors characterized by metastatic disease at the time of diagnoses and frequent recurrence despite standard treatment approaches with surgery and chemotherapy. Unfortunately, at this time the outcomes of this cancer are even more unfavorable for women from underserved communities, particularly Black women. Even after controlling for access to care, significant and disparate outcomes are evident in Black vs White patients. These epidemiologic and scientific data suggest existence of more aggressive and therapy resistant subtypes of ovarian cancer in Black women. Therefore, to close disparities in cancer care outcomes, and to deliver more effective therapies for these women, innovative research approaches as outlined in this proposal targeting these specific tumors is critical.

Even with equal access to care, Black women diagnosed with ovarian cancer have 1.3 times higher risk of death from ovarian cancer compared to white women [154–156]. The underlying cause of this health disparity is likely multifactorial. Contributing factors include some modifiable factors such as lifestyle and nutrition, but also inherent factors such as genetics and also epigenetic differences [13] . The genetic underpinning of this disease may also vary between Black vs White women based on discovery of distinct epithelial ovarian cancer risk foci in Black patients [158]. Beyond these inherent biologic differences, access to care based on geographic location is a clear barrier for cancer therapy and impacts outcome of women diagnosed with ovarian cancer [159]. This becomes particularly challenging for women of underserved communities who are diagnosed with aggressive ovarian tumors that invariably recur, necessitating repeated visits to care facilities.

Our proposed cell-based therapeutic, ^{Allo}MCAR-iNKT cells, is uniquely poised to help advance the care of women in underserved communities. ^{Allo}MCAR-iNKT cells can provide a new treatment option that eradicates the cancer with initial treatment, avoiding the need for repeated visits to the clinic-a barrier to care of underserved women. Additionally, given that

^{Allo}MCAR-iNKT cells do not require HLA haplotype matching, this cell-based therapy can be provided widely, irrespective of race and ethnicity.

There is a strong interest in finding a robust and scalable allogeneic cell source for "off-the-shelf" therapy with the advancement in cancer immunotherapy. Safety and tumor targeting capacity are two keys to successful cell therapy for cancer. In the ^{Allo}MCAR-iNKT cell culture platform that we developed, iNKT TCR directed the *ex vivo* development of NKT cells from HSCs giving the clonal expression of iNKT TCR, which significantly reduces the GvHD risks while bringing in the unique tumor-targeting capacity of iNKT TCR. This iNKT cell culture platform was scalable, high yield and purity, and highly editable with compatibility with CARs, suicide genes, and other enhancement genes like IL-15. ^{Allo}MCAR-iNKT cells generated from the platform targeted tumor through an effective CAR/TCR/NK triple-targeting mechanism. In addition, they are of low immunogenicity resistant to T cell-mediated allorejection. Have established an iNKT generation platform, in future work, we will study the development of NKT cells and evaluate ration combinations with genes and agents that affect persistence, exhaustion, and tumor targeting under the context of "off-the-shelf" cancer immunotherapy.

Acknowledgements

We thank the University of California, Los Angeles (UCLA) animal facility for providing animal support; the UCLA Translational Pathology Core Laboratory (TPCL) for providing histology support; the UCLA Technology Center for Genomics & Bioinformatics (TCGB) facility for providing RNAseq services; the UCLA CFAR Virology Core for providing human cells; and the UCLA BSCRC Flow Cytometry Core Facility for cell sorting support. This work was supported by a Director's New Innovator Award from the NIH (DP2 CA196335, to L.Y.), a Partnering Opportunity for Translational Research Projects Award and a Partnering

Opportunity for Discovery Stage Award from the California Institute for Regenerative Medicine (CIRM TRAN1-08533 and DISC2-11157, to L.Y.), a Stem Cell Research Award from the Concern Foundation (to L.Y.), a Research Career Development Award from the STOP CANCER Foundation (to L.Y.), a BSCRC-RHF Research Award from the Rose Hills Research Foundation (to L.Y.), and an Ablon Scholars Award (to L.Y.). Y-R.L. is a predoctoral fellow supported by the UCLA Whitcome Predoctoral Fellowship in Molecular Biology. Z.L. is a postdoctoral fellow supported by the UCLA Tumor Immunology Training Grant (USHHS Ruth L. Kirschstein Institutional National Research Service Award, T32-CA009120). D.L. is a predoctoral fellow supported by T32 Microbial Pathogenesis Training Grant (Ruth L. Kirschstein National Research Service Award, T32-AI007323).

Author contributions

Y-R.L. and L.Y. designed the experiments, analyzed the data, and wrote the manuscript. L.Y. conceived and oversaw the study, with assistance from Y-R.L., and with suggestions from S.M.L., A.R., D.B.K., O.N.W., and P.W. Y-R.L. performed all experiments, with assistance from Z.L., F.M., J.Y., D.L., and J.H. D.C. performed cell sorting. S.M. provided OC patient tumor samples. F.M. helped with analysis of RNAseq data.

Figures

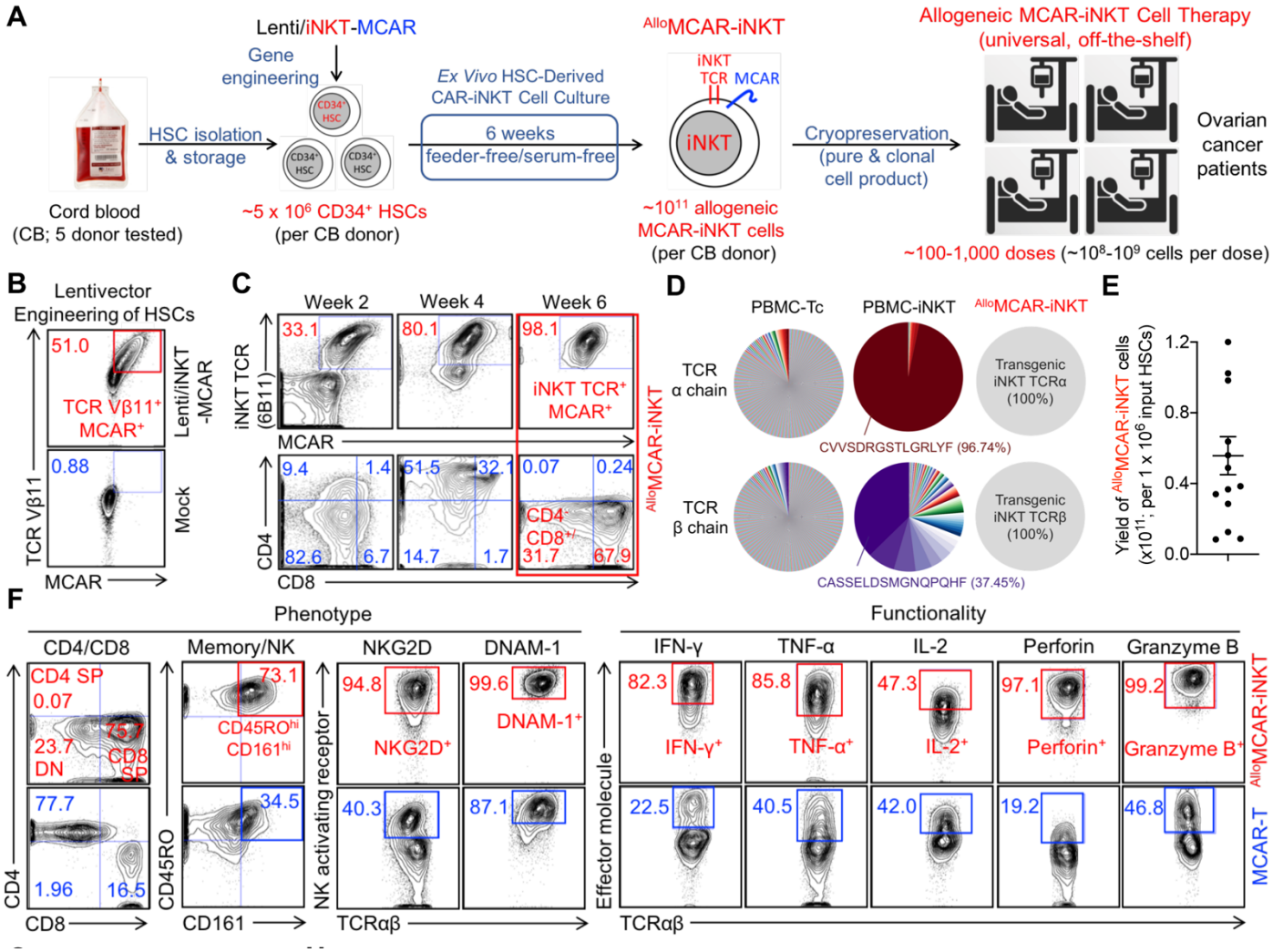

Figure 4-1. Generation of ^{Allo}MCAR-iNKT Cells

(A) Experimental design to generate ^{Allo}MCAR-iNKT cells *in vitro*.

(B-C) FACS monitoring of ^{Allo}MCAR-iNKT cell generation. (B) Intracellular expression of iNKT TCR (identified as Vβ11$^+$) in CD34$^+$ HSCs at 72 hours post lentivector transduction. (C) FACS monitoring of the generation of ^{Allo}MCAR-iNKT cells over 6 weeks.

(D) Single cell TCR sequencing analysis of ^{Allo}MCAR-iNKT cells. Healthy donor periphery blood mononuclear cell (PBMC)-derived conventional αβ T (PBMC-Tc) and iNKT (PBMC-iNKT) cells were included as controls. The relative abundance of each unique T cell receptor sequence among the total unique sequences identified for individual cells was represented by a pie slice.

(E) Yield of ^{Allo}MCAR-iNKT cells.

(F) FACS detection of surface markers, intracellular cytokines and cytotoxic molecules of ^{Allo}MCAR-iNKT cells. MCAR-T cells were included as a control.

Representative of 1 (E) and over 10 experiments (A-D, F).

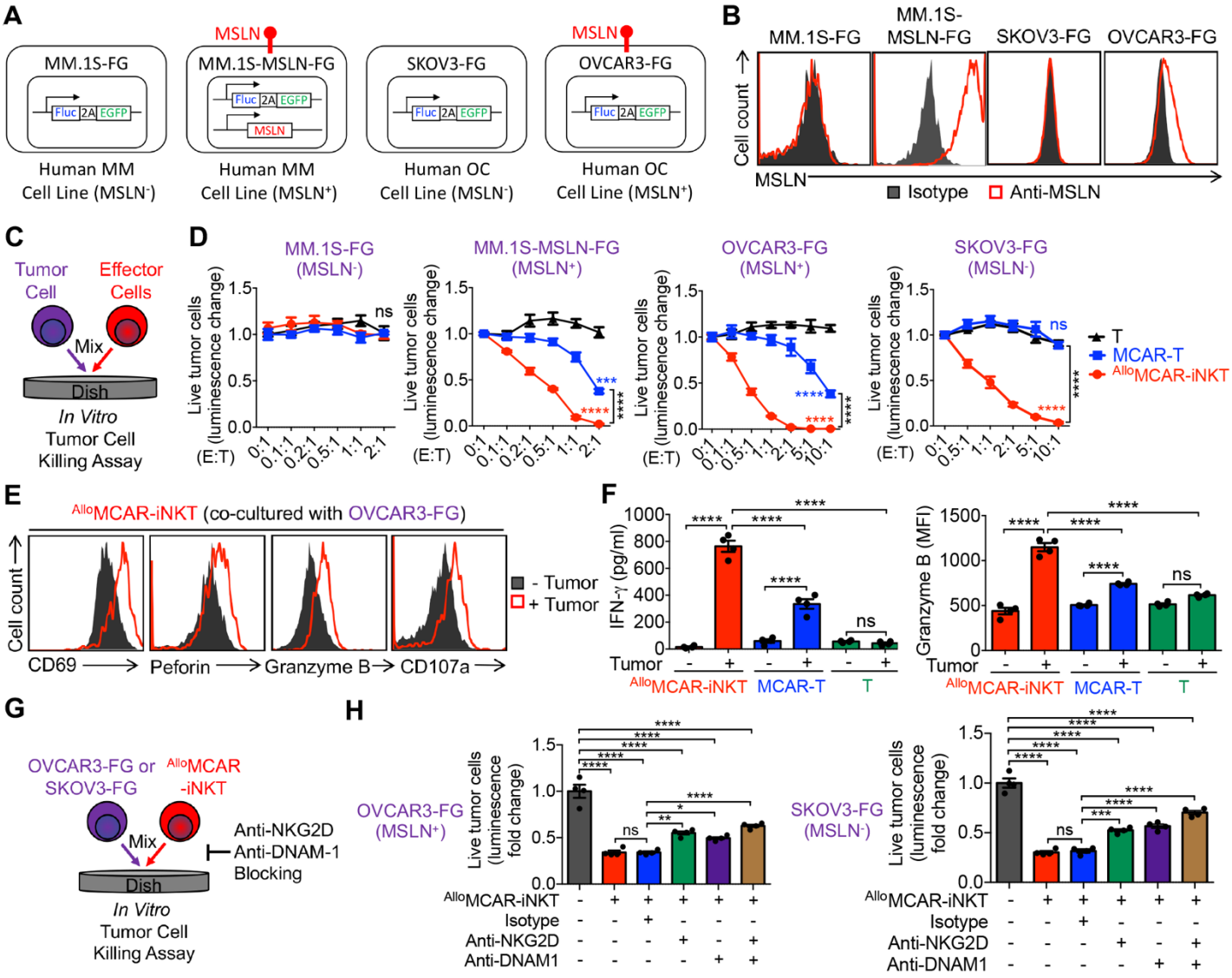

Figure 4-2. *In vitro* efficacy/MOA study of ^{Allo}MCAR-iNKT Cells

(A) Schematics of the 4 human tumor cell lines engineered and used for the study.

(B) FACS detection of MSLN expression on the 4 human tumor cell lines.

(C-F) *In vitro* tumor cell killing assay. Data were collected at 24-hours post setting up the assay. (C) Experimental design. (D) Tumor cell killing measured by luciferase activity assay (n = 4). (E) FACS detection of surface CD69, intracellular Peforin, Granzyme B, and CD107a of ^{Allo}MCAR-iNKT cells co-cultured with OVCAR3-FG cells. (F) FACS analysis of Granzyme B and IFN-γ production in ^{Allo}MCAR-iNKT cells co-cultured with OVCAR3-FG cells (n = 4). (G-H) Modified *in vitro* tumor cell killing assay to study NK activating receptor-mediated killing mechanism. Data were collected at 24-hours post setting up the assay. (G) Experimental design. (H) OVCAR3-FG and Skov3-FG tumor cell killing data (n = 4).

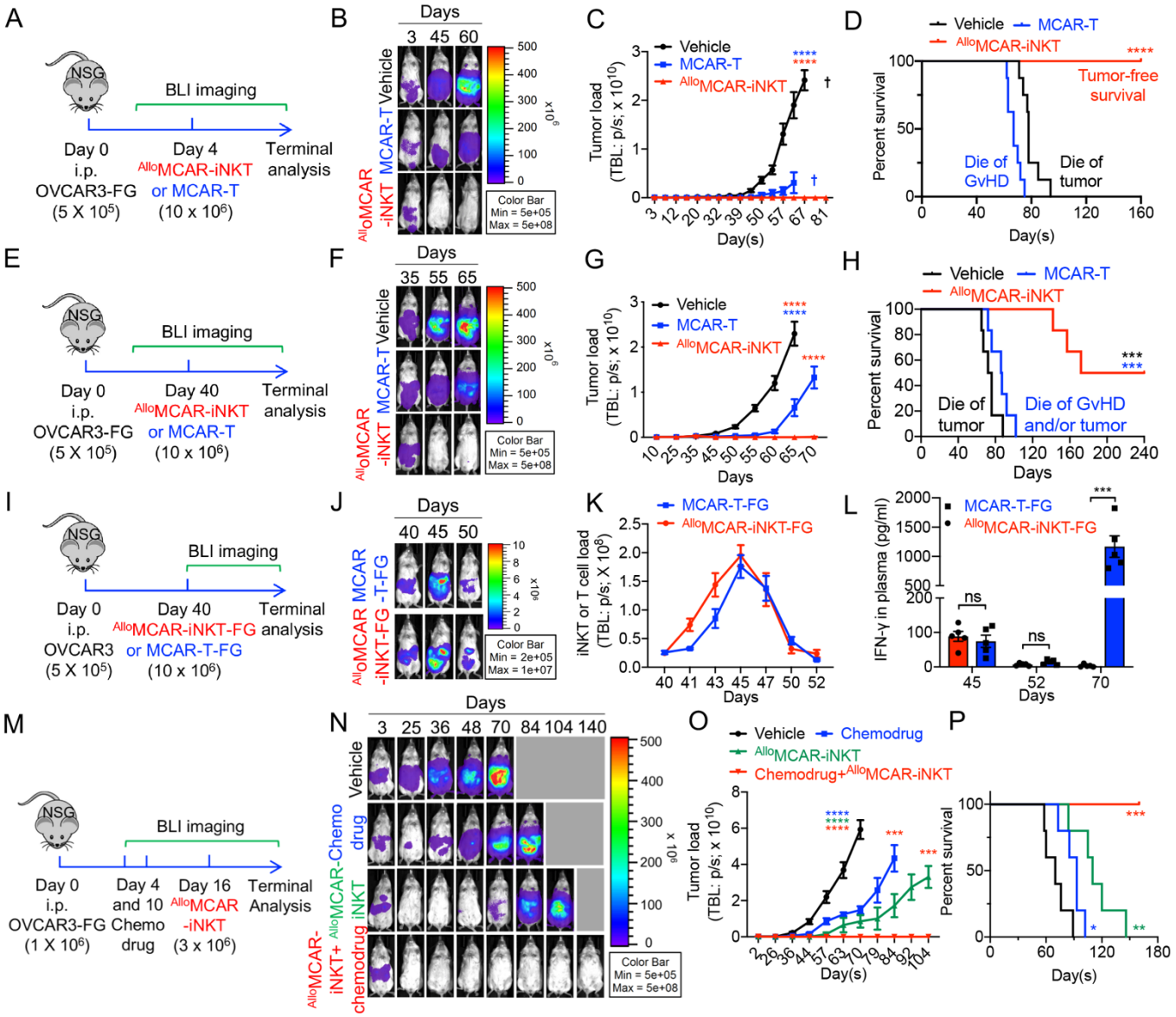

Figure 4-3. *In Vivo* Efficacy and Biodistribution Study of ^{Allo}MCAR-iNKT Cells

(A-D) Low tumor load of OVCAR3-FG i.p. xenograft model is presented (n = 8-10). (A) Experimental design. (B) Representative BLI images over time. (C) Quantification of B. (D) Kaplan-Meier survival curves. BLI, live animal bioluminescence imaging; TBL, total body luminescence.

(E-H) Heavy tumor load of OVCAR3-FG i.p. xenograft model is presented (n = 6). (E) Experimental design. (F) Representative BLI images over time. (G) Quantification of F. (H) Kaplan-Meier survival curves.

(I-L) *In vivo* biodistribution of ^{Allo}MCAR-iNKT cells in the heavy tumor load of OVCAR3-FG i.p. xenograft model (n = 5). FG labeled ^{Allo}MCAR-iNKTand MCAR-T cells were injected to experimental mice (I) Experimental design. (F) Representative BLI images over time. (K) Quantification of J. (L) Detection of plasma IFN-γ in the experimental mice.

(M-P) Combination therapy study using OVCAR3-FG i.p. xenograft model (n = 5). Traditional chemotherapy and ^{Allo}MCAR-iNKT cell therapy were studied. (M) Experimental design. (N) Representative BLI images over time. (O) Quantification of N. (P) Kaplan-Meier survival curves.

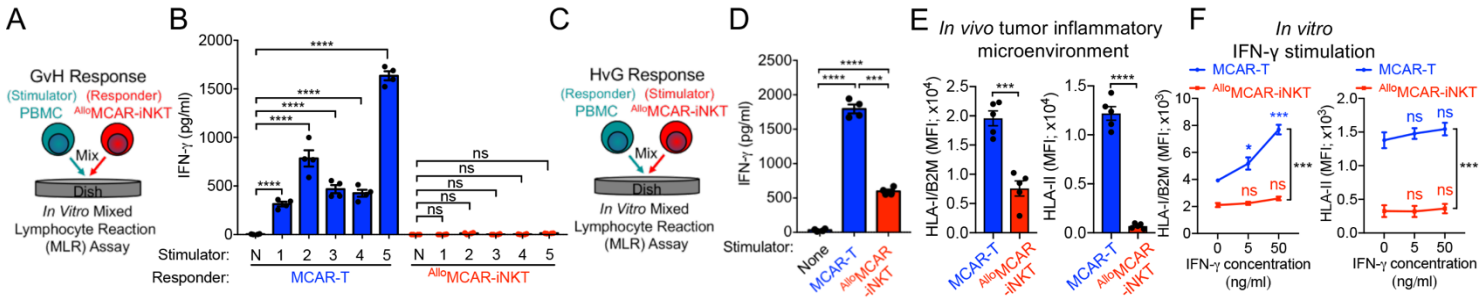

Figure 4-4. Safety and Immunogenicity Study of ^{Allo}MCAR-iNKT Cells

(A) An *In Vitro* Mixed Lymphocyte Reaction (MLR) Assay designated to study graft-versus-host (GvH) response.

(B) IFN-γ production from A showing no GvH responses induced by ^{Allo}MCAR-iNKT cells (n = 4). PBMCs from 5 random healthy donors were included as stimulators. N, no PBMC stimulator.

(C) An *In Vitro* Mixed Lymphocyte Reaction (MLR) Assay designated to study host-versus-graft (HvG) response.

(D) IFN-γ production from C showing low HvG responses induced by ^{Allo}MCAR-iNKT cells. PBMCs from 3 random healthy donors were tested as responders; data from one representative donor were shown (n = 4).

(E) FACS analyses of surface HLA-I/II expression on showing that ^{Allo}MCAR-iNKT cells isolated from OVCAR3-FG tumor bearing mice ascites 7 days post therapeutic cell transfer maintained low surface HLA-I/II expression (n = 5).

(F) FACS analyses showing that ^{Allo}MCAR-iNKT cells stimulated with IFN-γ *in vitro* maintained low surface HLA-I/II expression (n = 3).

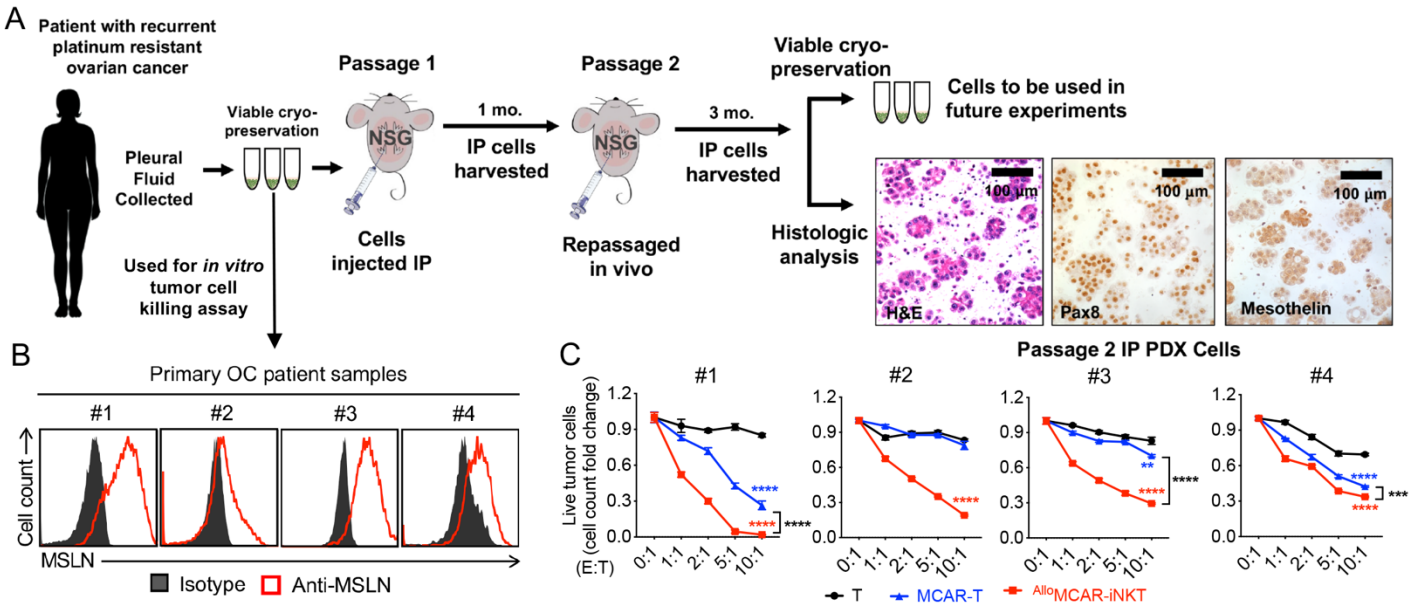

Figure 4-5. Studying the antitumor efficacy of ^{Allo}MCAR-iNKT cells using an *in vivo* OC-PDX model and a collection of primary OC patient tumor samples.

(A) An in vivo OC-PDX (patient-derived xenograft) model.

(B-C) A collection of primary OC patient tumor samples. (B) FACS analyses of these primary OC patient tumor samples, showing their varied expression of surface mesothelin (MSLN). (C) *In vitro* primary OC patient tumor cell killing assay, showing a higher antitumor efficacy of ^{Allo}MCAR-iNKT cells compared to conventional MCAR-T cells across multiple samples (n = 4).

Chapter 5 - Conclusions

Autologous cell therapy has transformed the treatment of hematological malignancies. Patients with relapsed and refractory B cell cancers experience response rates of up to 90% with CAR-T cell treatment, and durable clinical benefit occurs in about 30-40% of patients [160]. Tumor infiltrating lymphocyte (TIL) therapy continues to show clinical promise, with durable responses in some patients with refractory melanoma and cervical squamous cell carcinoma [161,162], and recombinant TCR-transduced T cells have shown encouraging clinical activity in multiple myeloma and melanoma [163]. These autologous therapies are by nature one of one, which hinders their manufacturability, accessibility, and affordability. Current CAR-T cell therapies are priced over $300,000 per treatment, not including additional costs associated with adverse events, and typically require over two weeks for production and administration [164]. Patients with rapidly progressing disease may not qualify for CAR-T cell therapy, and patient-derived cell starting material results in highly variable final products [165]. Allogeneic cell sources enable "off-the-shelf" cell therapies that can be produced at scale and administered on demand but face severe challenges of their own [166]. Graft-versus-host responses of conventional αβ T cells require efficient gene-editing of T cells or the use of non-alloreactive cell populations. Allogeneic cells also confront the host immune system, which can limit the persistence and efficacy of donor-derived cells. Various cell populations have been studied to achieve the holy grail of allogeneic cell therapy: maximizing the cancer-fighting ability of allogeneic cells while minimizing GvHD and allorejection. In this study, we highlighted the potential of hematopoietic stem cell-engineered iNKT cells to achieve this aim.

The HSC-iNKT cell production platform is robust and versatile, allowing the plug-in of additional engineering approaches. In our studies, we demonstrated the success to generate CAR-engineered or/and HLA-I/II-ablated ^{Allo}HSC-iNKT cells by incorporating additional CAR gene engineering and CRISPR-Cas9/B2M-CIITA-gRNAs gene editing steps. These

additional engineering approaches did not interfere with the production and antitumor function of ^{Allo}HSC-iNKT cells, opening up the possibility of developing more advanced ^{Allo}HSC-iNKT cell products. For example, incorporation of multiple tumor targeting molecules (e.g., CARs and TCRs) and functional enhancement factors (e.g., overexpression of immune enhancement genes like IL-15, and ablation of immune inhibitory genes like PD-1) may improve the cancer therapy potential of ^{Allo}HSC-iNKT cell products [167,168].

The intrinsic genomic instability of cancer cells coupled with the Darwinian process of immunoediting precipitates cancer cells that can avoid immune destruction [169,170]. Antigen negative relapse has been documented in CAR-T cell therapy [171], as well as the loss of an immunogenic epitope following TIL therapy [172]. We propose that multiple tumor-killing mechanisms are vital for adoptively transferred cells to contend with a cancer's plasticity and heterogeneity. iNKT cells possess intrinsic cancer killing ability. Using these cellular populations as carriers for CARs thus enables the killing of CAR-antigen positive and negative tumor cells.

The *ex vivo* activation, genetic manipulation, and expansion of patient or healthy donor lymphocytes leads to the differentiation of effector cells to achieve necessary cell numbers for dosing. This can result in cell products with limited self-renewal potential and diminished persistence upon infusion [173,174]. Telomere, differentiation, and CDKN2a mRNA analysis revealed that 15 days of T cell expansion aged cells the equivalent of 30 years [175]. Initiating genetic engineering and immune cell development at the stem cell level gives researchers control over the differentiation status of the final cell product while maintaining production of sufficient cell numbers. The massive expansion of stem cells can make multi-, high-dose strategies possible for all patients.

The number of genetic alterations that can be successfully applied to stem cells is continuing to grow. Wang et al. recently reported the generation of hypoimmunogenic T cells from genetically engineered allogeneic human iPSCs, in which iPSC lacking MHC Class I, MHC Class II, and NK cell-ligand poliovirus receptor CD155 were transduced to express single-chain MHC Class I antigen E [176]. Following iPSC to T cell differentiation, the resulting T cells were resistant to T, B and NK cell alloreactivity and, when further manipulated to express CAR, controlled preclinical tumor growth. The next steps are to incorporate modifications that allow the adoptively transferred cells to persistent autonomously, maintain proliferative potential, outmaneuver the immunosuppressive tumor microenvironment, infiltrate tumor beds, and stimulate endogenous antitumor immunity. Each of these goals has been addressed extensively in preclinical T and NK cell studies [177–179], such as through the exogenous expression of IL-15, immune checkpoint inhibitors, chemokine receptors, or immunomodulatory proteins, but are usually targeted individually or in pairs due to the limited genetic pliability of mature immune cells. Stem cell engineering opens the door for increasingly complex designer cell products, and future research will need to reveal if the accumulated changes hinder immune cell antitumor efficacy. By pursuing allogeneic therapies using stem cell-derived iNKT cells, we can take advantage of their natural tumor-targeting abilities and superior safety profiles to create ideal candidates for off-the-shelf cancer cell therapies.

In summary, here we report the pre-clinical development of autologous and allogeneic HSC-iNKT cell therapies that have the potential to treat a broad range of hematologic malignancies and solid tumors and that is ready to translate into clinical development. Three generations of HSC-iNKT cell products were reported here, including autologous HSC-iNKT cells generated in a humanized BLT-iNKT mouse model, and allogeneic HSC-iNKT cells generated in ATO and Ex Vivo Feeder-free culture systems. Further exploration of HSC-iNKT

cells as autologous and allogeneic cell carriers for developing cell therapy treating cancer especially solid tumors will certain be interesting directions for future study.

Bibliography

1. Restifo NP, Dudley ME, Rosenberg SA. Adoptive immunotherapy for cancer: Harnessing the T cell response. Nat Rev Immunol. 2012;12(4):269–81.
2. Sadelain M, Brentjens R, Rivière I. The basic principles of chimeric antigen receptor design. Cancer Discov. 2013;3(4):388–98.
3. Shimasaki N, Jain A, Campana D. NK cells for cancer immunotherapy. Nat Rev Drug Discov [Internet]. 2020;19(3):200–18. Available from: http://dx.doi.org/10.1038/s41573-019-0052-1
4. Brentjens RJ, Rivière I, Park JH, Davila ML, Wang X, Stefanski J, et al. Safety and persistence of adoptively transferred autologous CD19-targeted T cells in patients with relapsed or chemotherapy refractory B-cell leukemias. Blood. 2011;118(18):4817–28.
5. Lin Q, Zhao J, Song Y, Liu D. Recent updates on CAR T clinical trials for multiple myeloma. Mol Cancer. 2019;18(1):1–11.
6. Schaft N. The landscape of car-t cell clinical trials against solid tumors—a comprehensive overview. Cancers (Basel). 2020;12(9):1–36.
7. Brentjens RJ, Davila ML, Riviere I, Park J, Wang X, Cowell LG, et al. CD19-targeted T cells rapidly induce molecular remissions in adults with chemotherapy-refractory acute lymphoblastic leukemia. Sci Transl Med. 2013;5(177).
8. Kochenderfer JN, Dudley ME, Feldman SA, Wilson WH, Spaner DE, Maric I, et al. B-cell depletion and remissions of malignancy along with cytokine-associated toxicity in a clinical trial of anti-CD19 chimeric-antigen-receptor-transduced T cells. Blood. 2012;119(12):2709–20.
9. Kalos M, Levine BL, Porter DL, Katz S, Grupp SA, Bagg A, et al. T cells with chimeric antigen receptors have potent antitumor effects and can establish memory in patients with advanced leukemia. Sci Transl Med. 2011;3(95):1–13.
10. Rafiq S, Hackett CS, Brentjens RJ. Engineering strategies to overcome the current roadblocks in CAR T cell therapy. Nat Rev Clin Oncol [Internet]. 2020;17(3):147–67. Available from: http://dx.doi.org/10.1038/s41571-019-0297-y
11. Aftab BT, Sasu B, Krishnamurthy J, Gschweng E, Alcazer V, Depil S. Toward “off-the-shelf” allogeneic CAR T cells. Adv Cell Gene Ther. 2020;3(3):1–11.
12. Basar R, Daher M, Rezvani K. Next-generation cell therapies: The emerging role of CAR-NK cells.

Blood Adv. 2020;4(22):5868–76.

13. Lanza R, Russell DW, Nagy A. Engineering universal cells that evade immune detection. Nat Rev Immunol [Internet]. 2019;19(12):723–33. Available from: http://dx.doi.org/10.1038/s41577-019-0200-1

14. Ren J, Liu X, Fang C, Jiang S, June CH, Zhao Y. Multiplex genome editing to generate universal CAR T cells resistant to PD1 inhibition. Clin Cancer Res. 2017;23(9):2255–66.

15. Brudno JN, Somerville RPT, Shi V, Rose JJ, Halverson DC, Fowler DH, et al. Allogeneic T cells that express an anti-CD19 chimeric antigen receptor induce remissions of B-cell malignancies that progress after allogeneic hematopoietic stem-cell transplantation without causing graft-versus-host disease. J Clin Oncol. 2016;34(10):1112–21.

16. Kebriaei P, Singh H, Huls MH, Figliola MJ, Bassett R, Olivares S, et al. Phase i trials using sleeping beauty to generate CD19-specific CAR T cells. J Clin Invest. 2016;126(9):3363–76.

17. Kochenderfer JN, Dudley ME, Carpenter RO, Kassim SH, Rose JJ, Telford WG, et al. Donor-derived CD19-targeted T cells cause regression of malignancy persisting after allogeneic hematopoietic stem cell transplantation. Blood. 2013;122(25):4129–39.

18. Benjamin R, Graham C, Yallop D, Jozwik A, Ciocarlie O, Jain N, et al. Preliminary Data on Safety, Cellular Kinetics and Anti-Leukemic Activity of UCART19, an Allogeneic Anti-CD19 CAR T-Cell Product, in a Pool of Adult and Pediatric Patients with High-Risk CD19+ Relapsed/Refractory B-Cell Acute Lymphoblastic Leukemia. Blood. 2018;132(Supplement 1):896–896.

19. Benjamin R, Graham C, Yallop D, Jozwik A, Mirci-Danicar OC, Lucchini G, et al. Genome-edited, donor-derived allogeneic anti-CD19 chimeric antigen receptor T cells in paediatric and adult B-cell acute lymphoblastic leukaemia: results of two phase 1 studies. Lancet. 2020;396(10266):1885–94.

20. Qasim W, Zhan H, Samarasinghe S, Adams S, Amrolia P, Stafford S, et al. Molecular remission of infant B-ALL after infusion of universal TALEN gene-edited CAR T cells. Sci Transl Med. 2017;9(374):1–9.

21. Stadtmauer EA, Fraietta JA, Davis MM, Cohen AD, Weber KL, Lancaster E, et al. CRISPR-engineered T cells in patients with refractory cancer. Science (80-). 2020;367(6481):1–20.

22. Graham C, Jozwik A, Pepper A, Benjamin R. Allogeneic CAR-T Cells: More than Ease of Access? Cells. 2018;7(10):155.

23. Liu E, Marin D, Banerjee P, Macapinlac HA, Thompson P, Basar R, et al. Use of CAR-Transduced Natural Killer Cells in CD19-Positive Lymphoid Tumors. N Engl J Med. 2020;382(6):545–53.

24. Roberts MR, Cooke KS, Tran AC, Smith KA, Lin WY, Wang M, et al. Antigen-specific cytolysis by neutrophils and NK cells expressing chimeric immune receptors bearing zeta or gamma signaling domains. J Immunol [Internet]. 1998;161(1):375–84. Available from: http://www.ncbi.nlm.nih.gov/pubmed/9647246

25. Adair JE, Kubek SP, Kiem HP. Hematopoietic Stem Cell Approaches to Cancer. Hematol Oncol Clin North Am. 2017;31(5):897–912.

26. Bae EA, Seo H, Kim IK, Jeon I, Kang CY. Roles of NKT cells in cancer immunotherapy. Arch Pharm Res [Internet]. 2019;42(7):543–8. Available from: https://doi.org/10.1007/s12272-019-01139-8

27. Zhou Y, Li Y-R, Zeng S, Yang L. Methods for Studying Mouse and Human Invariant Natural Killer T Cells. Methods Mol Biol. 2021;2388:35–57.

28. Fujii S ichiro, Shimizu K, Okamoto Y, Kunii N, Nakayama T, Motohashi S, et al. NKT cells as an ideal anti-tumor immunotherapeutic. Front Immunol. 2013;4(DEC):1–7.

29. Vivier E, Ugolini S, Blaise D, Chabannon C, Brossay L. Targeting natural killer cells and natural killer T cells in cancer. Nat Rev Immunol. 2012 Mar;12(4):239–52.

30. Haraguchi K, Takahashi T, Hiruma K, Kanda Y, Tanaka Y, Ogawa S, et al. Recovery of Vα24+ NKT cells after hematopoietic stem cell transplantation. Bone Marrow Transplant. 2004;34(7):595–602.

31. de Lalla C, Rinaldi A, Montagna D, Azzimonti L, Bernardo ME, Sangalli LM, et al. Invariant NKT Cell Reconstitution in Pediatric Leukemia Patients Given HLA-Haploidentical Stem Cell Transplantation Defines Distinct CD4 + and CD4 − Subset Dynamics and Correlates with Remission State . J Immunol. 2011;186(7):4490–9.

32. Steimle V, Siegrist CA, Mottet A, Lisowska-Grospierre B, Mach B. Regulation of MHC class II expression by interferon-γ mediated by the transactivator gene CIITA. Science (80-). 1994;265(5168):106–9.

33. Abrahimi P, Chang WG, Kluger MS, Qyang Y, Tellides G, Saltzman WM, et al. Efficient gene disruption in cultured primary human endothelial cells by CRISPR/Cas9. Circ Res. 2015;117(2):121–8.

34. Godfrey DI, Berzins SP. Control points in NKT-cell development. Nat Rev Immunol. 2007;7(7):505–18.

35. Yamasaki K, Horiguchi S, Kurosaki M, Kunii N, Nagato K, Hanaoka H, et al. Induction of NKT cell-specific immune responses in cancer tissues after NKT cell-targeted adoptive immunotherapy. Clin Immunol [Internet]. 2011;138(3):255–65. Available from: http://dx.doi.org/10.1016/j.clim.2010.11.014

36. Bendelac A, Savage PB, Teyton L. The Biology of NKT Cells. Annu Rev Immunol. 2007;25(1):297–336.

37. Rotolo A, Caputo VS, Holubova M, Baxan N, Dubois O, Chaudhry MS, et al. Enhanced Anti-lymphoma Activity of CAR19-iNKT Cells Underpinned by Dual CD19 and CD1d Targeting. Cancer Cell [Internet]. 2018;34(4):596-610.e11. Available from: https://doi.org/10.1016/j.ccell.2018.08.017

38. Exley MA, Friedlander P, Alatrakchi N, Vriend L, Yue S, Sasada T, et al. Adoptive transfer of invariant NKT cells as immunotherapy for advanced melanoma: A phase I clinical trial. Clin Cancer Res. 2017;23(14):3510–9.

39. Rubio MT, Bouillié M, Bouazza N, Coman T, Trebeden-Nègre H, Gomez A, et al. Pre-transplant donor CD4 - Invariant NKT cell expansion capacity predicts the occurrence of acute graft-versus-host disease. Leukemia. 2017;31(4):903–12.

40. Chaidos A, Patterson S, Szydlo R, Chaudhry MS, Dazzi F, Kanfer E, et al. Graft invariant natural killer T-cell dose predicts risk of acute graft-versus-host disease in allogeneic hematopoietic stem cell transplantation. Blood. 2012;119(21):5030–6.

41. Zhu Y, Smith DJ, Zhou Y, Li YR, Yu J, Lee D, et al. Development of Hematopoietic Stem Cell-Engineered Invariant Natural Killer T Cell Therapy for Cancer. Cell Stem Cell [Internet]. 2019;25(4):542-557.e9. Available from: https://doi.org/10.1016/j.stem.2019.08.004

42. Smith DJ, Liu S, Ji S, Li B, McLaughlin J, Cheng D, et al. Genetic engineering of hematopoietic stem cells to generate invariant natural killer T cells. Proc Natl Acad Sci U S A. 2015;112(5):1523–8.

43. Nagato K, Motohashi S, Ishibashi F, Okita K, Yamasaki K, Moriya Y, et al. Accumulation of activated invariant natural killer T cells in the tumor microenvironment after α-galactosylceramide-pulsed antigen presenting cells. J Clin Immunol. 2012;32(5):1071–81.

44. Vizcardo R, Masuda K, Yamada D, Ikawa T, Shimizu K, Fujii SI, et al. Regeneration of human tumor antigen-specific T cells from iPSCs derived from mature CD8+ T cells. Cell Stem Cell [Internet]. 2013;12(1):31–6. Available from: http://dx.doi.org/10.1016/j.stem.2012.12.006

45. Kitayama S, Zhang R, Liu TY, Ueda N, Iriguchi S, Yasui Y, et al. Cellular Adjuvant Properties, Direct Cytotoxicity of Re-differentiated Vα24 Invariant NKT-like Cells from Human Induced Pluripotent Stem Cells. Stem Cell Reports [Internet]. 2016;6(2):213–27. Available from: http://dx.doi.org/10.1016/j.stemcr.2016.01.005

46. Deniger DC, Moyes JS, Cooper LJN. Clinical applications of gamma delta T cells with multivalent

immunity. Front Immunol. 2014;5(DEC):1–10.

47. Heczey A, Liu D, Tian G, Courtney AN, Wei J, Marinova E, et al. Invariant NKT cells with chimeric antigen receptor provide a novel platform for safe and effective cancer immunotherapy. Blood. 2014;124(18):2824–33.

48. Heczey A, Courtney AN, Montalbano A, Robinson S, Liu K, Li M, et al. Anti-GD2 CAR-NKT cells in patients with relapsed or refractory neuroblastoma: an interim analysis. Nat Med [Internet]. 2020;26(11):1686–90. Available from: http://dx.doi.org/10.1038/s41591-020-1074-2

49. Kronenberg M, Gapin L. The unconventional lifestyle of NKT cells. Nat Rev Immunol. 2002 Aug;2(8):557–68.

50. King LA, Lameris R, de Gruijl TD, van der Vliet HJ. CD1d-Invariant Natural Killer T Cell-Based Cancer Immunotherapy: α-Galactosylceramide and Beyond. Front Immunol. 2018;9(July).

51. Krijgsman D, Hokland M, Kuppen PJK. The role of natural killer T cells in cancer-A phenotypical and functional approach. Front Immunol. 2018;9(FEB).

52. Lam PY, Nissen MD, Mattarollo SR. Invariant natural killer T cells in immune regulation of blood cancers: Harnessing their potential in immunotherapies. Front Immunol. 2017;8(OCT):1–12.

53. Vivier E, Ugolini S, Blaise D, Chabannon C, Brossay L. Targeting natural killer cells and natural killer T cells in cancer. Nat Rev Immunol. 2012;12(4):239–52.

54. Krijgsman D, Hokland M, Kuppen PJK. The Role of Natural Killer T Cells in Cancer-A Phenotypical and Functional Approach. Front Immunol. 2018;9:367.

55. Waldowska M, Bojarska-Junak A, Roliński J. A brief review of clinical trials involving manipulation of invariant NKT cells as a promising approach in future cancer therapies. Cent J Immunol. 2017;42(2):181–95.

56. Nair S, Dhodapkar M V. Natural Killer T Cells in Cancer Immunotherapy. Front Immunol. 2017;8:1178.

57. Kunii N, Horiguchi S, Motohashi S, Yamamoto H, Ueno N, Yamamoto S, et al. Combination therapy of in vitro-expanded natural killer T cells and α-galactosylceramide-pulsed antigen-presenting cells in patients with recurrent head and neck carcinoma. Cancer Sci. 2009;100(6):1092–8.

58. Motohashi S, Ishikawa A, Ishikawa E, Otsuji M, Iizasa T, Hanaoka H, et al. A phase I study of in vitro expanded natural killer T cells in patients with advanced and recurrent non-small cell lung cancer. Clin cancer Res an Off J Am Assoc Cancer Res. 2006 Oct;12(20 Pt 1):6079–86.

59. Morrison SJ, Uchida N, Weissman IL. The biology of hematopoietic stem cells. Annu Rev Cell Dev Biol. 1995;11:35–71.

60. Yang L, Baltimore D. Long-term in vivo provision of antigen-specific T cell immunity by programming hematopoietic stem cells. Proc Natl Acad Sci U S A. 2005;102(12):4518–23.

61. Giannoni F, Hardee CL, Wherley J, Gschweng E, Senadheera S, Kaufman ML, et al. Allelic exclusion and peripheral reconstitution by TCR transgenic T cells arising from transduced human hematopoietic stem/progenitor cells. Mol Ther [Internet]. 2013;21(5):1044–54. Available from: http://dx.doi.org/10.1038/mt.2013.8

62. Vatakis DN, Arumugam B, Kim SG, Bristol G, Yang O, Zack JA. Introduction of exogenous T-cell receptors into human hematopoietic progenitors results in exclusion of endogenous T-cell receptor expression. Mol Ther. 2013;21(5):1055–63.

63. Baltimore D, Witte ON, Yang L, Economou J, Ribas A. Overcoming barriers to programming a therapeutic cellular immune response to fight melanoma. Vol. 23, Pigment cell & melanoma research. England; 2010. p. 288–9.

64. Puig-Saus C, Parisi G, Garcia-Diaz A, Krystofinski PE, Sandoval S, Zhang R, et al. IND-Enabling Studies for a Clinical Trial to Genetically Program a Persistent Cancer-Targeted Immune System. Clin cancer Res an Off J Am Assoc Cancer Res. 2019 Feb;25(3):1000–11.

65. Lan P, Tonomura N, Shimizu A, Wang S, Yang YG. Reconstitution of a functional human immune system in immunodeficient mice through combined human fetal thymus/liver and CD34+ cell transplantation. Blood. 2006;108(2):487–92.

66. Melkus MW, Estes JD, Padgett-Thomas A, Gatlin J, Denton PW, Othieno FA, et al. Humanized mice mount specific adaptive and innate immune responses to EBV and TSST-1. Nat Med. 2006;12(11):1316–22.

67. Montoya CJ, Pollard D, Martinson J, Kumari K, Wasserfall C, Mulder CB, et al. Characterization of human invariant natural killer T subsets in health and disease using a novel invariant natural killer T cell-clonotypic monoclonal antibody, 6B11. Immunology. 2007 Sep;122(1):1–14.

68. Cartier N, Hacein-Bey-Abina S, Bartholomae CC, Veres G, Schmidt M, Kutschera I, et al. Hematopoietic stem cell gene therapy with a lentiviral vector in X-linked adrenoleukodystrophy. Science. 2009 Nov;326(5954):818–23.

69. Larson S, De Oliveira SN. Gene-modified hematopoietic stem cells for cancer immunotherapy. Hum

Vaccines Immunother. 2014;10(4):982–5.

70. Kovalovsky D, Uche OU, Eladad S, Hobbs RM, Yi W, Alonzo E, et al. The BTB-zinc finger transcriptional regulator PLZF controls the development of invariant natural killer T cell effector functions. Nat Immunol. 2008;9(9):1055–64.

71. Bendelac A, Savage PB, Teyton L. The biology of NKT cells. Annu Rev Immunol. 2007;25:297–336.

72. Juno JA, Keynan Y, Fowke KR. Invariant NKT Cells: Regulation and Function during Viral Infection. PLoS Pathog. 2012;8(8).

73. Dhodapkar M V., Geller MD, Chang DH, Shimizu K, Fujii SI, Dhodapkar KM, et al. A reversible defect in natural killer T cell function characterizes the progression of premalignant to malignant multiple myeloma. J Exp Med. 2003;197(12):1667–76.

74. Dhodapkar M V., Richter J. Harnessing natural killer T (NKT) cells in human myeloma: Progress and challenges. Clin Immunol [Internet]. 2011;140(2):160–6. Available from: http://dx.doi.org/10.1016/j.clim.2010.12.010

75. Matsuda JL, Gapin L, Sidobre S, Kieper WC, Tan JT, Ceredig R, et al. Homeostasis of Vα14i NKT cells. Nat Immunol. 2002;3(10):966–74.

76. Bethune MT, Li XH, Yu J, McLaughlin J, Cheng D, Mathis C, et al. Isolation and characterization of NY-ESO-1-specific T cell receptors restricted on various MHC molecules. Proc Natl Acad Sci U S A. 2018;115(45):E10702–11.

77. Seet CS, He C, Bethune MT, Li S, Chick B, Gschweng EH, et al. Generation of mature T cells from human hematopoietic stem and progenitor cells in artificial thymic organoids. Nat Methods. 2017;14(5):521–30.

78. Chabannon C, Kubal J, Bondanza A, Dazzi F, Pedrazzoli P, Toubert A, et al. Hematopoietic stem cell transplantation in its 60s: A platform for cellular therapies. Sci Transl Med. 2018;10(436):1–11.

79. Lynch HE, Goldberg GL, Chidgey A, Van den Brink MRM, Boyd R, Sempowski GD. Thymic involution and immune reconstitution. Trends Immunol. 2009;30(7):366–73.

80. Beziat V, Nguyen S, Exley M, Achour A, Simon T, Chevallier P, et al. Shaping of iNKT cell repertoire after unrelated cord blood transplantation. Clin Immunol [Internet]. 2010;135(3):364–73. Available from: http://dx.doi.org/10.1016/j.clim.2010.01.010

81. Kamata T, Suzuki A, Mise N, Ihara F, Takami M, Makita Y, et al. Blockade of programmed death-1/programmed death ligand pathway enhances the antitumor immunity of human invariant natural killer

T cells. Cancer Immunol Immunother. 2016;65(12):1477–89.

82. Durgan K, Ali M, Warner P, Latchman YE. Targeting NKT cells and PD-L1 pathway results in augmented anti-tumor responses in a melanoma model. Cancer Immunol Immunother. 2011;60(4):547–58.

83. Tian G, Courtney AN, Jena B, Heczey A, Liu D, Marinova E, et al. CD62L+ NKT cells have prolonged persistence and antitumor activity in vivo. J Clin Invest. 2016 Jun;126(6):2341–55.

84. Shultz LD, Brehm MA, Victor Garcia-Martinez J, Greiner DL. Humanized mice for immune system investigation: Progress, promise and challenges. Nat Rev Immunol [Internet]. 2012;12(11):786–98. Available from: http://dx.doi.org/10.1038/nri3311

85. Theocharides APA, Rongvaux A, Fritsch K, Flavell RA, Manz MG. Humanized hemato-lymphoid system mice. Haematologica. 2016;101(1):5–19.

86. Wingender G, Krebs P, Beutler B, Kronenberg M. Antigen-Specific Cytotoxicity by Invariant NKT Cells In Vivo Is CD95/CD178-Dependent and Is Correlated with Antigenic Potency. J Immunol. 2010;185(5):2721–9.

87. Kalos M, June CH. Adoptive T Cell Transfer for Cancer Immunotherapy in the Era of Synthetic Biology. Immunity [Internet]. 2013;39(1):49–60. Available from: http://dx.doi.org/10.1016/j.immuni.2013.07.002

88. Maus M V., Fraietta JA, Levine BL, Kalos M, Zhao Y, June CH. Adoptive Immunotherapy for Cancer or Viruses. Annu Rev Immunol. 2014;32(1):189–225.

89. Labanieh L, Majzner RG, Mackall CL. Programming CAR-T cells to kill cancer. Nat Biomed Eng [Internet]. 2018;2(6):377–91. Available from: http://dx.doi.org/10.1038/s41551-018-0235-9

90. Mikkilineni L, Kochenderfer JN. Chimeric antigen receptor T-cell therapies for multiple myeloma. Blood. 2017;130(24):2594–602.

91. June CH, Sadelain M. Chimeric antigen receptor therapy. N Engl J Med. 2018;379(1):64–73.

92. Leko V, Rosenberg SA. Identifying and Targeting Human Tumor Antigens for T Cell-Based Immunotherapy of Solid Tumors. Cancer Cell [Internet]. 2020;38(4):454–72. Available from: https://doi.org/10.1016/j.ccell.2020.07.013

93. Rosenberg SA, Restifo NP. Adoptive cell transfer as personalized immunotherapy for human cancer. Science (80-). 2015;348(6230):62–8.

94. Lim WA, June CH. The Principles of Engineering Immune Cells to Treat Cancer. Cell [Internet].

2017;168(4):724–40. Available from: http://dx.doi.org/10.1016/j.cell.2017.01.016

95. Becker PSA, Suck G, Nowakowska P, Ullrich E, Seifried E, Bader P, et al. Selection and expansion of natural killer cells for NK cell-based immunotherapy. Cancer Immunol Immunother. 2016;65(4):477–84.

96. Montel-Hagen A, Seet CS, Li S, Chick B, Zhu Y, Chang P, et al. Organoid-Induced Differentiation of Conventional T Cells from Human Pluripotent Stem Cells. Cell Stem Cell. 2019;24(3):376-389.e8.

97. Lee PT, Benlagha K, Teyton L, Bendelac A. Distinct functional lineages of human Vα24 natural killer T cells. J Exp Med. 2002;195(5):637–41.

98. Gumperz JE, Miyake S, Yamamura T, Brenner MB. Functionally distinct subsets of CD1d-restricted natural killer T cells revealed by CD1d tetramer staining. J Exp Med. 2002;195(5):625–36.

99. Fujii SI, Liu K, Smith C, Bonito AJ, Steinman RM. The linkage of innate to adaptive immunity via maturing dendritic cells in vivo requires CD40 ligation in addition to antigen presentation and CD80/86 costimulation. J Exp Med. 2004;199(12):1607–18.

100. Fujii SI, Shimizu K, Hemmi H, Steinman RM. Innate Vα14+ natural killer T cells mature dendritic cells, leading to strong adaptive immunity. Immunol Rev. 2007;220(1):183–98.

101. Menon V. Clustering single cells: A review of approaches on high-and low-depth single-cell RNA-seq data. Brief Funct Genomics. 2018;17(4):240–5.

102. Alonzo ES, Sant'Angelo DB. Development of PLZF-expressing innate T cells. Curr Opin Immunol [Internet]. 2011;23(2):220–7. Available from: http://dx.doi.org/10.1016/j.coi.2010.12.016

103. Zhang Y, Zhang Y, Gu W, Sun B. Th1/Th2 cell differentiation and molecular signals. Adv Exp Med Biol. 2014;841:15–44.

104. Gagliani N, Huber S. Basic aspects of T helper cell differentiation. Methods Mol Biol. 2017;1514:19–30.

105. Cartwright T, Perkins ND, L Wilson C. NFKB1: a suppressor of inflammation, ageing and cancer. FEBS J. 2016;283(10):1812–22.

106. Riera-Sans L, Behrens A. Regulation of αβ/γδ T Cell Development by the Activator Protein 1 Transcription Factor c-Jun. J Immunol. 2007;178(9):5690–700.

107. Park JY, DiPalma DT, Kwon J, Fink J, Park JH. Quantitative Difference in PLZF Protein Expression Determines iNKT Lineage Fate and Controls Innate CD8 T Cell Generation. Cell Rep [Internet]. 2019;27(9):2548-2557.e4. Available from: https://doi.org/10.1016/j.celrep.2019.05.012

108. Matsuda JL, Zhang Q, Ndonye R, Richardson SK, Howell AR, Gapin L. T-bet concomitantly controls migration, survival, and effector functions during the development of Vα14i NKT cells. Blood. 2006;107(7):2797–805.

109. Thomas SY, Hou R, Boyson JE, Means TK, Hess C, Olson DP, et al. CD1d-Restricted NKT Cells Express a Chemokine Receptor Profile Indicative of Th1-Type Inflammatory Homing Cells. J Immunol. 2003;171(5):2571–80.

110. Fürst D, Neuchel C, Tsamadou C, Schrezenmeier H, Mytilineos J. HLA Matching in Unrelated Stem Cell Transplantation up to Date. Transfus Med Hemotherapy. 2019;46(5):326–36.

111. Ozdemir ZN, Civriz Bozdağ S. Graft failure after allogeneic hematopoietic stem cell transplantation. Transfus Apher Sci. 2018;57(2):163–7.

112. Lee HH, Kang H, Cho H. Natural killer cells and tumor metastasis. Arch Pharm Res. 2017;40(9):1037–49.

113. Liu H, Wang S, Xin J, Wang J, Yao C, Zhang Z. Role of NKG2D and its ligands in cancer immunotherapy. Am J Cancer Res [Internet]. 2019;9(10):2064–78. Available from: http://www.ncbi.nlm.nih.gov/pubmed/31720075%0Ahttp://www.pubmedcentral.nih.gov/articlerender.fcgi?artid=PMC6834480

114. Paul S, Lal G. The molecular mechanism of natural killer cells function and its importance in cancer immunotherapy. Front Immunol. 2017;8(SEP).

115. Del Zotto G, Marcenaro E, Vacca P, Sivori S, Pende D, Della Chiesa M, et al. Markers and function of human NK cells in normal and pathological conditions. Cytom Part B - Clin Cytom. 2017;92(2):100–14.

116. Ewen EM, Pahl JHW, Miller M, Watzl C, Cerwenka A. KIR downregulation by IL-12/15/18 unleashes human NK cells from KIR/HLA-I inhibition and enhances killing of tumor cells. Eur J Immunol. 2018;48(2):355–65.

117. Dominguez E, Lowdell MW, Perez-Cruz I, Madrigal A, Cohen SBA. Natural killer cell function is altered by freezing in DMSO. Biochem Soc Trans. 1997;25(2):997.

118. LI RUI, JOHNSON R, YU G, MCKENNA DH, HUBEL A. Preservation of cell-based immunotherapies for clinical trials. Cytotherapy. 2019;21(9):943–57.

119. Luo Y, Wang P, Liu H, Zhu Z, Li C, Gao Y. The state of T cells before cryopreservation: Effects on post-thaw proliferation and function. Cryobiology [Internet]. 2017;79:65–70. Available from:

http://dx.doi.org/10.1016/j.cryobiol.2017.08.008

120. Timmers M, Roex G, Wang Y, Campillo-Davo D, Van Tendeloo VFI, Chu Y, et al. Chimeric antigen receptor-modified T cell therapy in multiple myeloma: Beyond B cell maturation antigen. Front Immunol. 2019;10(JULY):1–12.

121. Liu Y, Chen Z, Fang H, Wei R, Yu K, Jiang S, et al. Durable Remission Achieved from Bcma-Directed CAR-T Therapy Against Relapsed or Refractory Multiple Myeloma. Blood [Internet]. 2018 Nov 29;132(Supplement 1):956. Available from: https://doi.org/10.1182/blood-2018-99-112786

122. Cohen AD. CAR T Cells and Other Cellular Therapies for Multiple Myeloma: 2018 Update. Am Soc Clin Oncol Educ B. 2018;(38):e6–15.

123. Brudno JN, Maric I, Hartman SD, Rose JJ, Wang M, Lam N, et al. T cells genetically modified to express an anti–B-Cell maturation antigen chimeric antigen receptor cause remissions of poor-prognosis relapsed multiple myeloma. J Clin Oncol. 2018;36(22):2267–80.

124. Cohen AD, Garfall AL, Stadtmauer EA, Melenhorst JJ, Lacey SF, Lancaster E, et al. B cell maturation antigen–specific CAR T cells are clinically active in multiple myeloma. J Clin Invest. 2019;129(6):2210–21.

125. Neelapu SS, Tummala S, Kebriaei P, Wierda W, Gutierrez C, Locke FL, et al. Chimeric antigen receptor T-cell therapy-assessment and management of toxicities. Nat Rev Clin Oncol. 2018;15(1):47–62.

126. Candolfi M, Kroeger K, Muhammad A, Yagiz K, Farrokhi C, Pechnick R, et al. Gene Therapy for Brain Cancer: Combination Therapies Provide Enhanced Efficacy and Safety. Curr Gene Ther. 2009;9(5):409–21.

127. Straathof KC, Pulè MA, Yotnda P, Dotti G, Vanin EF, Brenner MK, et al. An inducible caspase 9 safety switch for T-cell therapy. Blood. 2005;105(11):4247–54.

128. Thomis DC, Marktel S, Bonini C, Traversari C, Gilman M, Bordignon C, et al. A Fas-based suicide switch in human T cells for the treatment of graft-versus-host disease. Blood. 2001;97(5):1249–57.

129. Watanabe K, Kuramitsu S, Posey AD, June CH. Expanding the therapeutic window for CAR T cell therapy in solid tumors: The knowns and unknowns of CAR T cell biology. Front Immunol. 2018;9(OCT):1–12.

130. Keskinen P, Ronni T, Matikainen S, Lehtonen A, Julkunen I. Regulation of HLA class I and II expression by interferons and influenza A virus in human peripheral blood mononuclear cells.

Immunology. 1997;91(3):421–9.

131. Axelrod ML, Cook RS, Johnson DB, Balko JM. Biological consequences of MHC-II expression by tumor cells in cancer. Clin Cancer Res. 2019;25(8):2392–402.

132. Castro F, Cardoso AP, Gonçalves RM, Serre K, Oliveira MJ. Interferon-gamma at the crossroads of tumor immune surveillance or evasion. Front Immunol. 2018;9(MAY):1–19.

133. Torikai H, Reik A, Soldner F, Warren EH, Yuen C, Zhou Y, et al. Toward eliminating HLA class i expression to generate universal cells from allogeneic donors. Blood. 2013;122(8):1341–9.

134. Braud V, Calan CAO, So K, Andrea AD, Ogg GS, Lazetic S, et al. HLA-E binds to natural killer cell receptors CD94/NKG2A, B and C. Nature [Internet]. 1998;391(February):795–9. Available from: https://www-nature-com.ep.fjernadgang.kb.dk/articles/35869.pdf%0Ahttps://www.nature.com/articles/35869.pdf

135. Cosman D, Müllberg J, Sutherland CL, Chin W, Armitage R, Fanslow W, et al. ULBPs, novel MHC class I-related molecules, bind to CMV glycoprotein UL16 and stimulate NK cytotoxicity through the NKG2D receptor. Immunity. 2001;14(2):123–33.

136. Heczey A, Liu D, Tian G, Courtney AN, Wei J, Marinova E, et al. Invariant NKT cells with chimeric antigen receptor provide a novel platform for safe and effective cancer immunotherapy. Blood. 2014;124(18):2824–33.

137. Motohashi S, Nagato K, Kunii N, Yamamoto H, Yamasaki K, Okita K, et al. A Phase I-II Study of α-Galactosylceramide-Pulsed IL-2/GM-CSF-Cultured Peripheral Blood Mononuclear Cells in Patients with Advanced and Recurrent Non-Small Cell Lung Cancer. J Immunol. 2009;182(4):2492–501.

138. Verzeletti S, Bonini C, Marktel S, Nobili N, Ciceri F, Traversari C, et al. Herpes Simplex Virus T h y m i d i n e Kinase G e n e T r a n s f e r for Controlled Graft-versus-Host Disease a n d L e u k e m i a : Clinical F o l l o w - u p N e w Vectors and Improved. 1998;2251:2243–51.

139. Lee N, Llano M, Carretero M, Akiko-Ishitani, Navarro F, López-Botet M, et al. HLA-E is a major ligand for the natural killer inhibitory receptor CD94/NKG2A. Proc Natl Acad Sci U S A. 1998;95(9):5199–204.

140. Siegel RL, Miller KD, Fuchs HE, Jemal A. Cancer Statistics, 2021. CA Cancer J Clin. 2021 Jan;71(1):7–33.

141. Burger RA, Brady MF, Bookman MA, Fleming GF, Monk BJ, Huang H, et al. Incorporation of bevacizumab in the primary treatment of ovarian cancer. N Engl J Med. 2011 Dec;365(26):2473–83.

142. Tanyi JL, Haas AR, Beatty GL, Stashwick CJ, O'Hara MH, Morgan MA, et al. Anti-mesothelin chimeric antigen receptor T cells in patients with epithelial ovarian cancer. J Clin Oncol [Internet]. 2016 May 20;34(15_suppl):5511. Available from: https://doi.org/10.1200/JCO.2016.34.15_suppl.5511

143. Hassan R, Thomas A, Alewine C, Le DT, Jaffee EM, Pastan I. Mesothelin Immunotherapy for Cancer: Ready for Prime Time? J Clin Oncol Off J Am Soc Clin Oncol. 2016 Dec;34(34):4171–9.

144. Qu Y, Siegler E, Cheng C, Liu J, Cinay G, Bagrodia N, et al. Engineering CAR-expressing natural killer cells with cytokine signaling and synthetic switch for an off-the-shelf cell-based cancer immunotherapy. MRS Commun [Internet]. 2019;9(2):433–40. Available from: https://doi.org/10.1557/mrc.2019.31

145. Shukla S, Langley MA, Singh J, Edgar JM, Mohtashami M, Zúñiga-Pflücker JC, et al. Progenitor T-cell differentiation from hematopoietic stem cells using Delta-like-4 and VCAM-1. Nat Methods. 2017 May;14(5):531–8.

146. Iriguchi S, Kaneko S. Toward the development of true "off-the-shelf" synthetic T-cell immunotherapy. Cancer Sci. 2019;110(1):16–22.

147. Huijskens MJAJ, Walczak M, Koller N, Briedé JJ, Senden-Gijsbers BLMG, Schnijderberg MC, et al. Technical advance: ascorbic acid induces development of double-positive T cells from human hematopoietic stem cells in the absence of stromal cells. J Leukoc Biol. 2014 Dec;96(6):1165–75.

148. Themeli M, Kloss CC, Ciriello G, Fedorov VD, Perna F, Gonen M, et al. Generation of tumor-targeted human T lymphocytes from induced pluripotent stem cells for cancer therapy. Nat Biotechnol. 2013 Oct;31(10):928–33.

149. La Motte-Mohs RN, Herer E, Zúñiga-Pflücker JC. Induction of T-cell development from human cord blood hematopoietic stem cells by Delta-like 1 in vitro. Blood. 2005 Feb;105(4):1431–9.

150. Reimann C, Six E, Dal-Cortivo L, Schiavo A, Appourchaux K, Lagresle-Peyrou C, et al. Human T-lymphoid progenitors generated in a feeder-cell-free Delta-like-4 culture system promote T-cell reconstitution in NOD/SCID/γc(-/-) mice. Stem Cells. 2012 Aug;30(8):1771–80.

151. Li Y, Hermanson DL, Moriarity BS, Kaufman DS. Human iPSC-Derived Natural Killer Cells Engineered with Chimeric Antigen Receptors Enhance Anti-tumor Activity. Cell Stem Cell. 2018 Aug;23(2):181-192.e5.

152. Owens GL, Sheard VE, Kalaitsidou M, Blount D, Lad Y, Cheadle EJ, et al. Preclinical Assessment of CAR T-Cell Therapy Targeting the Tumor Antigen 5T4 in Ovarian Cancer. J Immunother. 2018 Apr;41(3):130–40.

153. Phan N, Hong JJ, Tofig B, Mapua M, Elashoff D, Moatamed NA, et al. A simple high-throughput approach identifies actionable drug sensitivities in patient-derived tumor organoids. Commun Biol. 2019;2:78.

154. Collins Y, Holcomb K, Chapman-Davis E, Khabele D, Farley JH. Gynecologic cancer disparities: a report from the Health Disparities Taskforce of the Society of Gynecologic Oncology. Gynecol Oncol. 2014 May;133(2):353–61.

155. McElvaney OJ, McEvoy NL, McElvaney OF, Carroll TP, Murphy MP, Dunlea DM, et al. Characterization of the inflammatory response to severe COVID-19 Illness. Am J Respir Crit Care Med. 2020;202(6):812–21.

156. Srivastava SK, Ahmad A, Miree O, Patel GK, Singh S, Rocconi RP, et al. Racial health disparities in ovarian cancer: not just black and white. J Ovarian Res. 2017 Sep;10(1):58.

157. Pinheiro PS, Medina HN, Koru-Sengul T, Qiao B, Schymura M, Kobetz EN, et al. Endometrial Cancer Type 2 Incidence and Survival Disparities Within Subsets of the US Black Population. Front Oncol. 2021;11:699577.

158. Manichaikul A, Peres LC, Wang X-Q, Barnard ME, Chyn D, Sheng X, et al. Identification of novel epithelial ovarian cancer loci in women of African ancestry. Int J cancer. 2020 Jun;146(11):2987–98.

159. Villanueva C, Chang J, Ziogas A, Bristow RE, Vieira VM. Ovarian cancer in California: Guideline adherence, survival, and the impact of geographic location, 1996-2014. Cancer Epidemiol. 2020 Dec;69:101825.

160. Bansal R, Reshef R. Revving the CAR - Combination strategies to enhance CAR T cell effectiveness. Blood Rev. 2021 Jan;45:100695.

161. Wu R, Forget M-A, Chacon J, Bernatchez C, Haymaker C, Chen JQ, et al. Adoptive T-cell therapy using autologous tumor-infiltrating lymphocytes for metastatic melanoma: current status and future outlook. Cancer J. 2012;18(2):160–75.

162. Kumar A, Watkins R, Vilgelm AE. Cell Therapy With TILs: Training and Taming T Cells to Fight Cancer. Front Immunol. 2021;12:690499.

163. Robbins PF, Kassim SH, Tran TLN, Crystal JS, Morgan RA, Feldman SA, et al. A pilot trial using lymphocytes genetically engineered with an NY-ESO-1-reactive T-cell receptor: long-term follow-up and correlates with response. Clin cancer Res an Off J Am Assoc Cancer Res. 2015 Mar;21(5):1019–27.

164. Hay AE, Cheung MC. CAR T-cells: costs, comparisons, and commentary. J Med Econ. 2019 Jul;22(7):613–5.

165. Hartmann J, Schüßler-Lenz M, Bondanza A, Buchholz CJ. Clinical development of CAR T cells-challenges and opportunities in translating innovative treatment concepts. EMBO Mol Med. 2017 Sep;9(9):1183–97.

166. Ruella M, Kenderian SS. Next-Generation Chimeric Antigen Receptor T-Cell Therapy: Going off the Shelf. BioDrugs. 2017 Dec;31(6):473–81.

167. Gordy LE, Bezbradica JS, Flyak AI, Spencer CT, Dunkle A, Sun J, et al. IL-15 Regulates Homeostasis and Terminal Maturation of NKT Cells. J Immunol. 2011;187(12):6335–45.

168. Bae EA, Seo H, Kim BS, Choi J, Jeon I, Shin KS, et al. Activation of NKT cells in an anti-PD-1–resistant tumor model enhances antitumor immunity by reinvigorating exhausted CD8 T cells. Cancer Res. 2018;78(18):5315–26.

169. Hanahan D, Weinberg RA. Hallmarks of cancer: the next generation. Cell. 2011 Mar;144(5):646–74.

170. Schreiber RD, Old LJ, Smyth MJ. Cancer immunoediting: integrating immunity's roles in cancer suppression and promotion. Science. 2011 Mar;331(6024):1565–70.

171. Majzner RG, Mackall CL. Tumor Antigen Escape from CAR T-cell Therapy. Cancer Discov. 2018 Oct;8(10):1219–26.

172. Tran E, Turcotte S, Gros A, Robbins PF, Lu Y-C, Dudley ME, et al. Cancer immunotherapy based on mutation-specific CD4+ T cells in a patient with epithelial cancer. Science. 2014 May;344(6184):641–5.

173. Fraietta JA, Lacey SF, Orlando EJ, Pruteanu-Malinici I, Gohil M, Lundh S, et al. Determinants of response and resistance to CD19 chimeric antigen receptor (CAR) T cell therapy of chronic lymphocytic leukemia. Nat Med. 2018 May;24(5):563–71.

174. Ghassemi S, Nunez-Cruz S, O'Connor RS, Fraietta JA, Patel PR, Scholler J, et al. Reducing Ex Vivo Culture Improves the Antileukemic Activity of Chimeric Antigen Receptor (CAR) T Cells. Cancer Immunol Res. 2018 Sep;6(9):1100–9.

175. Bankoti R, Akbal HP, Adorno M, Robilant B Di. 830 Targeting cellular senescence to increase CAR-T cell fitness. J Immunother Cancer [Internet]. 2020;8(Suppl 3):A497--A497. Available from: https://jitc.bmj.com/content/8/Suppl_3/A497.1

176. Wang B, Iriguchi S, Waseda M, Ueda N, Ueda T, Xu H, et al. Generation of hypoimmunogenic T cells

from genetically engineered allogeneic human induced pluripotent stem cells. Nat Biomed Eng. 2021 May;5(5):429–40.

177. Yeku OO, Brentjens RJ. Armored CAR T-cells: utilizing cytokines and pro-inflammatory ligands to enhance CAR T-cell anti-tumour efficacy. Biochem Soc Trans. 2016 Apr;44(2):412–8.

178. Rezvani K. Adoptive cell therapy using engineered natural killer cells. Bone Marrow Transplant. 2019 Aug;54(Suppl 2):785–8.

179. Hawkins ER, D'Souza RR, Klampatsa A. Armored CAR T-Cells: The Next Chapter in T-Cell Cancer Immunotherapy. Biologics. 2021;15:95–105.